STRINGQFT

String-Theoretic Construction
of Quantum Field Theory

VOLUME IX

Hanany–Witten Constructions and Brane Dynamics

Xingyang Yu

StringQFT v1.0

Drafted with AI assistance under the supervision of the author.
Manuscript free to read. All rights reserved.

Contents

IX.1 The Hanany–Witten setup **1**

IX.1.1 A gauge theory on a finite interval . . . 1
IX.1.2 The branes and eight real supercharges . . . 2
IX.1.3 Fields that survive the endpoints . . . 4
IX.1.4 Flavor branes and physical masses . . . 6
IX.1.5 The interval coupling and the three-dimensional limit . . . 8
IX.1.6 FI displacement and the charged center . . . 10
IX.1.7 Fivebrane charge and linking number . . . 12
IX.1.8 Crossing and reconnection are different problems . . . 13
IX.1.9 The local s-rule and its consequences . . . 16
IX.1.10 From one interval to a framed two-node theory . . . 17
IX.1.11 What the construction establishes . . . 19
Status and sources . . . 21
References . . . 23

IX.2 Mirror symmetry from IIB S-duality **24**

IX.2.1 Two descriptions of the same infrared physics . . . 24
IX.2.2 Exchanging species and restoring the axes . . . 25
IX.2.3 Conserved charges determine the crossing . . . 27
IX.2.4 One charged hypermultiplet and a free mirror . . . 28
IX.2.5 Two flavors and self-mirror symmetry . . . 30
IX.2.6 Three flavors and a two-node mirror . . . 32
IX.2.7 Gauge lattices and branch dimensions . . . 34
IX.2.8 Relative masses and FI parameters . . . 36
IX.2.9 A deformed branch from elementary mirror fields . . . 38
IX.2.10 What the mirror construction establishes . . . 42
Status and sources . . . 43

IX.3 Higgs, Coulomb and mixed branches **45**

IX.3.1 From movable branes to a space of vacua . . . 45
IX.3.2 Which positions are fields? . . . 46
IX.3.3 A quotient before a dimension count . . . 48
IX.3.4 Invariant matrices, resolutions and deformations . . . 50
IX.3.5 The photon as a compact scalar . . . 52
IX.3.6 Circle fibers and the Coulomb metric . . . 53

IX.3.7 Quantum functions and integer magnetic flux 56
IX.3.8 An asymmetric mirror in an integral charge basis 57
IX.3.9 A mixed stratum with an unbroken photon 60
IX.3.10 What monopole dimensions diagnose 62
IX.3.11 Reading a branch without losing its conditions 64

IX.4 Boundary conditions and Nahm poles 69
IX.4.1 What an endpoint must remember 69
IX.4.2 From the brane frame to the surface variation 70
IX.4.3 The cubic boundary action and Nahm's equation 72
IX.4.4 Noncommuting poles at small rank 74
IX.4.5 Partitions and the symmetry of the full residue 77
IX.4.6 Boundary S-duality and the rank-two theory 80
IX.4.7 Quiver matter and nilpotent moment maps 82
IX.4.8 Faithful flavor symmetry and one anomaly probe 85
IX.4.9 What the boundary construction establishes 87
Status and sources 88

IX.5 D4–NS5 constructions and the M-theory lift 91
IX.5.1 From an interval to a quantum curve 91
IX.5.2 The interval spectrum and full hypermultiplets 92
IX.5.3 Coupling normalization and the field-theory limit 94
IX.5.4 Logarithmic bending and the matter coefficient 96
IX.5.5 Normalizability selects the dynamical algebra 98
IX.5.6 The M5 surface and its two sheets 99
IX.5.7 Membrane masses and the normalized differential 101
IX.5.8 Two elliptic curves and a degree-two map 103
IX.5.9 Cycles, contour integrals and a numerical vacuum 104
IX.5.10 Weak coupling and a vanishing monopole period 107
IX.5.11 The particle lattice and based monodromies 108
IX.5.12 Pure SU(3): trace coordinates, a node and a cusp 110
IX.5.13 Exercises on curves, charges and periods 112
IX.5.14 What the construction determines 113
Status and sources 114
References 116

IX.6 Rotated branes and Seiberg duality 117
IX.6.1 The rotation and its four supercharges 117
IX.6.2 Which interval modes disappear? 120
IX.6.3 Eliminating the adjoint 121
IX.6.4 A complete electric-to-magnetic brane move 123
IX.6.5 Magnetic matter and the charged center 126
IX.6.6 Anomalies of the undeformed SQCD comparison 127
IX.6.7 The pure-gauge lift and its two fixed ends 130
IX.6.8 Winding and relative membrane charge 133
IX.6.9 A rational degeneration of the parent curve 134

IX.6.10 The extra circle scale in MQCD . . . 135
IX.6.11 Exercises . . . 137
Status and sources . . . 138

IX.7 Three-dimensional dualities from branes 141
IX.7.1 What survives a compactification? . . . 141
IX.7.2 A spacetime circle and its T-dual interval . . . 142
IX.7.3 D1 instantons and the affine monopole . . . 143
IX.7.4 Seven flavors and a separated magnetic vacuum . . . 146
IX.7.5 Remote theories and surviving singlets . . . 148
IX.7.6 Monopole charges and the singlet equations . . . 150
IX.7.7 Signed masses, Chern–Simons terms and BF couplings . . . 152
IX.7.8 The resolved fivebrane move and the GK rank . . . 154
IX.7.9 The central level and the primitive magnetic flux . . . 157
IX.7.10 The suspension circle and its supercharges . . . 158
IX.7.11 Primitive cycles and the finite quotient . . . 160
IX.7.12 What the construction determines . . . 161
IX.7.13 Three calculations to carry out . . . 162
Status and sources . . . 164
References . . . 166

IX.8 Atlas of Hanany–Witten constructions 167
IX.8.1 Choosing a construction . . . 167
IX.8.2 Eight supercharges on an interval . . . 168
IX.8.2.1 Setups and their mirror views . . . 169
IX.8.2.2 Reconstructing the asymmetric surface . . . 170
IX.8.2.3 A framed interval is not a dimension subtraction . . . 171
IX.8.3 Half-BPS boundaries and T theories . . . 172
IX.8.3.1 The rank-two pole . . . 172
IX.8.3.2 Reading the two T theories . . . 173
IX.8.4 From the M5 equation to periods and particles . . . 174
IX.8.4.1 Eliminating the exponential coordinate . . . 174
IX.8.4.2 The factor of two in the SU(2) readout . . . 175
IX.8.4.3 What the SU(3) extension adds . . . 176
IX.8.5 Rotating fivebranes and comparing interacting sectors . . . 177
IX.8.6 Fixed ends and the MQCD winding . . . 179
IX.8.7 Four-supercharge dualities in three dimensions . . . 180
IX.8.7.1 Why the remote sectors cannot be discarded first . . . 180
IX.8.7.2 Keeping the sign of the Chern–Simons level . . . 181
IX.8.8 Two suspension-circle interfaces . . . 182
IX.8.9 Carrying a result to the next calculation . . . 183
IX.8.10 Three reconstructions for the reader . . . 184
Status and sources . . . 185

Chapter IX.1

The Hanany–Witten setup

IX.1.1 A gauge theory on a finite interval

A D3-brane carries a gauge field in four worldvolume dimensions. To obtain a three-dimensional theory, we can make one of those directions finite. At wavelengths much longer than the interval, the fields cannot resolve their dependence on that coordinate. Their constant modes become three-dimensional fields. The ends of the interval then do more than confine the brane: they decide which constant modes are allowed.

In the Hanany–Witten construction, a D3 ends on two NS5-branes. A suitable relative orientation preserves eight real supercharges, so the surviving gauge field belongs to a three-dimensional $\mathcal{N} = 4$ vector multiplet. Additional D5-branes supply fundamental hypermultiplets through strings joining the D3s to the D5s. Lengths and positions acquire direct field-theory meanings. The interval length controls the gauge coupling; separations in one transverse three-plane give masses; displacement in the other gives a Fayet–Iliopoulos deformation.

There is also a question that cannot be answered by counting the branes in one drawing. What happens when a D5 and an NS5 exchange order along the interval direction? A connecting D3 may have to appear. We will identify the individual fivebrane charges that enforce this change, derive the unit creation term, and distinguish it from the extra physical condition that a specified mixed pair supports at most one supersymmetric D3.

Take-home message of this chapter

With the stated endpoint prescription and decoupling limit, a finite NS5-bounded stack of N_c D3s gives a $U(N_c)$ gauge theory. An interior D5 adds a fundamental hypermultiplet, so the gauge center acts on matter and must be retained. The interval and transverse separations determine the classical coupling and deformations. When unlike fivebranes cross, conservation of each fivebrane's linking number fixes the change of D3 endpoints. Supersymmetry imposes further restrictions; conserved charge by itself does not establish a duality.

We assume the elementary open-string spectrum, the leading D-brane action, and the

eight-supercharge multiplet language developed in Volumes III and 0. The applications to this interval will be derived explicitly. Throughout, the fivebranes are external sources and x^6 is noncompact. Our first worked gauge theory is $U(2)$ with three fundamentals. It is small enough to display every charge and mass, while retaining the distinction between the full matrix group and its center. Chapter 2 uses these ingredients to study mirror symmetry. Chapter 4 develops the boundary physics, and Chapter 5 changes the suspended-brane system to construct four-dimensional theories.

IX.1.2 The branes and eight real supercharges

Choose coordinates so that all three kinds of brane share x^0, x^1, x^2. The remaining directions separate into the interval coordinate x^6 and two transverse three-planes. The orientation table is

	012	345	6	789
NS5	×	×	–	–
D3	×	–	×	–
D5	×	–	–	×

. (IX.1.1)

An NS5 has fixed position t_i in x^6 and fixed position $\boldsymbol{w}_i$ in 789. A D5 has fixed x^6 position z_a and fixed 345 position $\boldsymbol{m}_{\text{geom},a}$. For the color D3s we use $\boldsymbol{x}_i$ for their 345 positions. In particular,

$$t_L < x^6 < t_R, \qquad L = t_R - t_L > 0, \qquad t_L < z_a < t_R \quad (a = 1, \ldots, N_f). \tag{IX.1.2}$$

The color branes end on the NS5s. A D5 in the interior intersects their projection without necessarily being a D3 endpoint. Figure IX.1.1 shows this distinction for two color branes and three flavor branes.

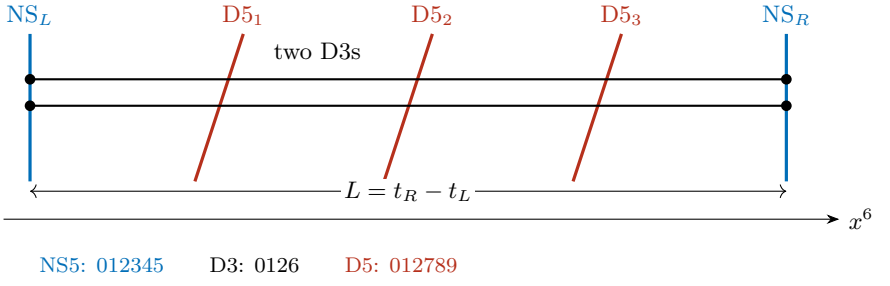


Figure IX.1.1: Two NS5-bounded D3s and three interior D5s. The filled dots are actual endpoints on the NS5s. The intersections with the D5 strokes are not endpoints, so this arrangement has one gauge interval. Blue and red strokes denote fivebranes in a schematic projection; neither represents a literal one-dimensional fivebrane. Vertical offsets distinguish color strands, not transverse vevs. Common 012 directions are suppressed.

The compatible brane configuration preserves eight real supercharges. To see how a compatible set of spinor conditions gives this number, we now specify one complete local

gamma-matrix frame. This calculation establishes consistency of the stated orientations. Its signs are not being identified with every spinor or Ramond–Ramond orientation convention used to describe the same physical branes.

Take upper-index gamma matrices in mostly-plus signature and positive IIB chirality for both supersymmetry parameters:

$$\{\Gamma^\mu,\Gamma^\nu\}=2\eta^{\mu\nu},\qquad \eta=\mathrm{diag}(-1,1,\dots,1),\qquad \chi=\Gamma^0\Gamma^1\cdots\Gamma^9,\quad \chi\epsilon_{L,R}=\epsilon_{L,R}. \tag{IX.1.3}$$

Here L,R label the two IIB parameters. Let X,Y,Z be the Pauli matrices, and define thirty-two-dimensional matrices by tensor products,

$$\begin{gathered} e_{2j}=Z^{\otimes j}\otimes X\otimes 1^{\otimes(4-j)},\qquad e_{2j+1}=Z^{\otimes j}\otimes Y\otimes 1^{\otimes(4-j)},\\ j=0,\dots,4,\qquad \Gamma^0=ie_0,\qquad \Gamma^a=e_a\quad(a>0). \end{gathered} \tag{IX.1.4}$$

The first differing tensor factor in two different generators gives one anticommutation sign. Each e_a squares to one; multiplying e_0 by i gives the negative timelike square. Thus this representation realizes (IX.1.3), rather than only a Euclidean Clifford algebra.

Within this spinor calculation, name the ordered worldvolume products A,B,C. Our compatible orientation choices are

$$\begin{gathered} A=\Gamma^{012345},\qquad B=\Gamma^{012789},\qquad C=\Gamma^{0126},\\ A\epsilon_L=+\epsilon_L,\qquad A\epsilon_R=-\epsilon_R,\qquad \epsilon_L=+B\epsilon_R=-C\epsilon_R. \end{gathered} \tag{IX.1.5}$$

Both NS5 ends use the same NS5 orientation. For an ordered product of p distinct gammas, moving a second copy into reverse order gives

$$(\Gamma^{i_1}\cdots\Gamma^{i_p})^2=(-1)^{p(p-1)/2}\prod_{r=1}^{p}\eta^{i_ri_r},\qquad A^2=B^2=\chi^2=1,\quad C^2=-1. \tag{IX.1.6}$$

The same contractions give the relation that makes the D3 condition compatible with the two fivebrane conditions:

$$AB=-BA,\qquad CA=\Gamma^{3456},\qquad \Gamma^{3456}\chi=\Gamma^{012789},\qquad B=CA\chi. \tag{IX.1.7}$$

All three even worldvolume products commute with χ. The right spinor can therefore be selected by the commuting projections

$$P=\frac{(1+\chi)(1-A)}{4},\qquad P^2=P,\qquad \mathrm{tr}\,P=\frac{32+0-0-0}{4}=8. \tag{IX.1.8}$$

The three zero traces are those of χ, A and $\chi A=\Gamma^{6789}$. Each is a nonempty even blade that anticommutes with an invertible generator, hence has zero trace. Since P is idempotent, its trace equals its complex rank. On its image,

$$BP=CA\chi P=-CP,\qquad (A-1)BP=0,\qquad (\chi-1)BP=0. \tag{IX.1.9}$$

Consequently $\epsilon_L=B\epsilon_R$ obeys the left NS5 and chirality conditions, and the chosen D3 condition removes no further components.

A complex rank of eight is not yet a count of real supercharges. In (IX.1.4), precisely the generators with indices $0, 1, 3, 5, 7, 9$ are imaginary. With K denoting componentwise complex conjugation, choose

$$R = \Gamma^{013579}, \qquad J = RK, \qquad R\overline{R} = 1, \qquad R\overline{\Gamma^{\mu}} = \Gamma^{\mu}R, \qquad J^2 = 1. \tag{IX.1.10}$$

The product R is real, anticommutes with the six imaginary generators and commutes with the four real ones. These facts give the displayed identities and show that J preserves $\operatorname{im} P$. Any vector in that image decomposes into two vectors fixed by J:

$$v = \frac{v + Jv}{2} + i\frac{v - Jv}{2i}, \qquad \dim_{\mathbb{R}}(\operatorname{im} P)^{J=1} = \dim_{\mathbb{C}} \operatorname{im} P = 8. \tag{IX.1.11}$$

Imposing $J\epsilon_R = \epsilon_R$ gives eight real parameters, and J commuting with B imposes the same reality on ϵ_L.

Relative orientation matters. Hold the two fivebrane conditions fixed and replace the D3 condition by $\epsilon_L = +C\epsilon_R$. Then

$$(B - C)P = -2CP, \qquad \ker\big((B - C)|_{\operatorname{im} P}\big) = 0, \tag{IX.1.12}$$

because C is invertible. No common supersymmetry survives this relative reversal. Reversing the NS5 signs as well instead selects $(1 + \chi)(1 + A)/4$, on which $B = +C$, and restores eight real parameters. The isolated sign of a gamma equation therefore does not specify a signed D3 charge. The magnetic-charge orientation used later will be stated separately.

The two transverse rotation groups act as the R-symmetry factors of the undeformed three-dimensional theory,

$$SU(2)_C \longrightarrow SO(3)_{345}, \qquad SU(2)_H \longrightarrow SO(3)_{789}. \tag{IX.1.13}$$

These are double covers on spinors. Fixed nonzero mass and FI triplets can break the corresponding rotations. We next identify which D3 fluctuations transform as the vector-multiplet triplet.

IX.1.3 Fields that survive the endpoints

A constant function on an interval need not be an allowed mode. Its endpoint values must satisfy the boundary conditions supplied by the fivebranes. We first take that physical prescription as given, and then solve its linear fluctuation problem. At an NS5 end, the D3 endpoint can move in 345 but its 789 position is fixed. For small abelian fluctuations, this gives

$$\partial_6 X^{3,4,5} = 0, \qquad \delta X^{7,8,9} = 0 \qquad \text{at an NS5 end.} \tag{IX.1.14}$$

At a D5 end, the movable and fixed triples are exchanged. We use these physical endpoint conditions to solve the scalar problem; a general nonabelian boundary condition is a further problem for Chapter 4.

Let $s = x^6 - t_L$ and separate a fluctuation into a three-dimensional field and an interval wavefunction. The mass eigenvalue equation is

$$X(x^\mu, s) = \varphi(x^\mu) f(s), \qquad -f''(s) = m^2 f(s), \qquad 0 \le s \le L. \tag{IX.1.15}$$

For a massless mode, integration twice gives $f = c_0 + c_1 s$. Neumann conditions constrain f' and Dirichlet conditions constrain f, so

ends	constraints	zero-mode space
NN	$c_1 = 0$	span$\{1\}$
DD	$c_0 = 0, \quad c_0 + Lc_1 = 0$	0
ND	$c_1 = 0, \quad c_0 + Lc_1 = 0$	0
DN	$c_0 = 0, \quad c_1 = 0$	0

. (IX.1.16)

The condition $L > 0$ is essential in the DD row. For two NS5 ends, the three 345 scalars have the NN constant mode; all three 789 scalar fluctuations vanish. A mixed pair has no transverse scalar zero mode.

The first excitations also display the energy scale being removed. The NN eigenfunctions and their masses are

$$f_0 = L^{-1/2}, \qquad f_n = \sqrt{\frac{2}{L}} \cos \frac{n\pi s}{L}, \qquad m_n = \frac{n\pi}{L}, \quad n \ge 1. \tag{IX.1.17}$$

For instance, $\int_0^L f_0 f_1 \, ds = 0$ and $\int_0^L f_1^2 \, ds = 1$. A D condition at the right end instead requires the cosine to vanish there:

$$f_n^{ND} = \sqrt{\frac{2}{L}} \cos \frac{(n + \frac{1}{2})\pi s}{L}, \qquad m_n^{ND} = \frac{(n + \frac{1}{2})\pi}{L}, \quad n \ge 0. \tag{IX.1.18}$$

There is a gap $\pi/(2L)$ and no constant mode. Setting $m = 0$ before imposing the endpoints would have missed this distinction.

The gauge field has complementary boundary behavior. Its abelian conditions, with $\mu, \nu = 0, 1, 2$, are

$$\text{NS5}: \ F_{6\mu} = 0, \qquad \text{D5}: \ F_{\mu\nu} = 0. \tag{IX.1.19}$$

Two NS5s admit a three-dimensional vector a_μ. Two D5s instead admit the scalar described locally by $\partial_\mu b = F_{\mu 6}$, with the complementary boundary behavior. In particular, one cannot count A_6 as an additional unconstrained Wilson-line scalar on every interval. The endpoint gauge transformations and Maxwell conditions matter. The abelian massless content is

ends	position modes	gauge mode	multiplet
NS5, NS5	$X^{3,4,5}$	a_μ	$\mathcal{N} = 4$ vector
D5, D5	$X^{7,8,9}$	b	$\mathcal{N} = 4$ hyper
NS5, D5	0	0	none

. (IX.1.20)

The Maxwell boundary prescription and its supersymmetric completion are physical input here. The explicit scalar solution establishes the position-mode part of the table; it does not construct the microscopic NS5 boundary theory.

For N_c coincident D3s, a string can begin on color i and end on color j. Let e_i be a basis of $\mathbb{C}^{N_c}$. The Chan–Paton matrix for such an oriented string is

$$E_{ij} = e_i e_j^T, \qquad E_{ij}E_{kl} = e_i(e_j^T e_k)e_l^T = \delta_{jk}E_{il}, \qquad [E_{ij}, E_{kl}] = \delta_{jk}E_{il} - \delta_{li}E_{kj}. \tag{IX.1.21}$$

This supplies the full matrix algebra, including off-diagonal strings. Hermitian gauge fields have N_c real diagonal entries and one complex entry for every unordered pair:

$$A_\mu = \sum_{i,j}(A_\mu)_{ij}E_{ij}, \qquad (A_\mu)_{ji} = (A_\mu)_{ij}^*, \qquad N_c + 2\binom{N_c}{2} = N_c^2. \tag{IX.1.22}$$

For two branes, $E_{11}, E_{12}, E_{21}, E_{22}$ span the complexified algebra. Four independent Hermitian generators are

$$E_{11}, \qquad E_{22}, \qquad E_{12} + E_{21}, \qquad -i(E_{12} - E_{21}). \tag{IX.1.23}$$

At coincidence the resulting group is $U(2)$. More generally, the gauge group is $U(N_c)$ and the three surviving position scalars are adjoint matrices. A massless vector in three dimensions has one physical polarization, giving

$$1\ (a_\mu) + 3\ (X^{3,4,5}) = 4 \quad \text{bosonic states per generator.} \tag{IX.1.24}$$

The eight supercharges supply their fermionic partners. In $\mathcal{N} = 2$ language this is a vector plus an adjoint chiral multiplet, the gauge sector to which the D5 matter will couple.

IX.1.4 Flavor branes and physical masses

An interior D5 adds strings whose second endpoint carries a flavor label. The relative orientation first determines whether these strings can be massless. For a D3 in 0126 and a D5 in 012789, the shared Neumann, shared Dirichlet and mixed directions are

$$NN = \{0, 1, 2\}, \qquad DD = \{3, 4, 5\}, \qquad ND = \{6, 7, 8, 9\}. \tag{IX.1.25}$$

The open-superstring NS vacuum energy with ν mixed directions is $a_{\mathrm{NS}} = -\frac{1}{2} + \nu/8$. Thus this sector has

$$\nu = 4, \qquad a_{\mathrm{NS}} = 0, \tag{IX.1.26}$$

and the GSO-projected massless spectrum, together with its fermions, forms an $\mathcal{N} = 4$ hypermultiplet. This uses the perturbative D3–D5 open-string spectrum. It is not a calculation of strings ending on an NS5. Applying the same coordinate-set operations to an NS5 can classify intersections of worldvolumes, but cannot assign a perturbative fundamental-string vacuum energy to a D3–NS5 sector. For comparison, rotating the D5 to give two mixed directions would give $a_{\mathrm{NS}} = -1/4$, outside the present construction.

With N_f D5s, arrange the two string orientations as rectangular matrices Q and $\widetilde{Q}$. Under color and flavor transformations,

$$Q \in \mathrm{Hom}(\mathbb{C}^{N_f}, \mathbb{C}^{N_c}), \quad \widetilde{Q} \in \mathrm{Hom}(\mathbb{C}^{N_c}, \mathbb{C}^{N_f}), \qquad Q \mapsto gQh^{-1}, \quad \widetilde{Q} \mapsto h\widetilde{Q}g^{-1}. \tag{IX.1.27}$$

Here $g \in U(N_c)$ is gauged and $h \in U(N_f)$ is a flavor transformation. If e_i and f_a now denote unit Cartan weights, each matrix entry has the charges

$$w(Q_{ia}) = (e_i, -f_a), \qquad w(\widetilde{Q}_{ai}) = (-e_i, +f_a), \qquad \dim_{\mathbb{C}}(Q, \widetilde{Q}) = 2N_c N_f. \quad \text{(IX.1.28)}$$

There are N_f fundamental hypermultiplets, not $N_c N_f$ flavors. Each flavor has N_c color components. For $U(2)$ with three flavors, Q is 2×3 and $\widetilde{Q}$ is 3×2, giving twelve complex or twenty-four real scalar components.

The trace part of the gauge field acts on these strings. Taking $g = e^{i\theta} 1_{N_c}$ with the flavor transformation held fixed gives

$$Q \mapsto e^{i\theta} Q, \qquad \widetilde{Q} \mapsto e^{-i\theta} \widetilde{Q}. \quad \text{(IX.1.29)}$$

These are charges $+1$ and -1. The simultaneous color and flavor phase can cancel in (IX.1.27), but a flavor transformation is not another gauge transformation that allows us to remove the gauge center. Indeed a color matrix that acts as the identity on every fundamental vector is itself the identity. With fundamentals, the full matrix group has a faithful action.

Displacing a D5 in 345 stretches these strings. All geometric coordinates below are physical lengths. The fundamental-string tension and mass are

$$T_{\mathrm{F1}} = \frac{1}{2\pi\alpha'}, \qquad M_{ia} = T_{\mathrm{F1}} |\boldsymbol{x}_i - \boldsymbol{m}_{\mathrm{geom},a}|. \quad \text{(IX.1.30)}$$

Define field-theory scalar eigenvalues and bare masses by dividing positions by $2\pi\alpha'$:

$$\boldsymbol{\phi}_i = \frac{\boldsymbol{x}_i}{2\pi\alpha'}, \qquad \boldsymbol{m}_a = \frac{\boldsymbol{m}_{\mathrm{geom},a}}{2\pi\alpha'}, \qquad M_{ia}^2 = |\boldsymbol{\phi}_i - \boldsymbol{m}_a|^2. \quad \text{(IX.1.31)}$$

Figure IX.1.2(a) depicts a single component of this separation. Moving the D5 only in x^6 within the interval does not create the 345 separation in (IX.1.31).

For a concrete Coulomb background of the ultraviolet $U(2)$ theory, choose a mass unit $\mu_* > 0$ and take

$$\frac{\boldsymbol{\phi}_1}{\mu_*} = (0,0,0), \quad \frac{\boldsymbol{\phi}_2}{\mu_*} = (1,2,2), \qquad \frac{(\boldsymbol{m}_1, \boldsymbol{m}_2, \boldsymbol{m}_3)}{\mu_*} = \big((0,0,0), (3,0,0), (0,4,0)\big). \quad \text{(IX.1.32)}$$

The color scalars are commuting diagonal matrices, the FI level and hyper vevs are zero, and the separated color positions break $U(2)$ to its Cartan at this point. Applying the Euclidean norm gives

$$\frac{M_{ia}^2}{\mu_*^2} = \begin{pmatrix} 0 & 9 & 16 \\ 9 & 12 & 9 \end{pmatrix}, \qquad \frac{M_{22}^2}{\mu_*^2} = (-2)^2 + 2^2 + 2^2 = 12. \quad \text{(IX.1.33)}$$

This is a mass matrix at a chosen Coulomb background, not a change of the ultraviolet gauge-group definition. In particular, the massless entry arises from one coincident color/flavor pair, not from removal of that color's gauge charge.

The adjoint scalar action gives a second way to read the color-string masses. For $\Phi^A = \mathrm{diag}(\phi_1^A, \ldots, \phi_{N_c}^A)$,

$$[\Phi^A, E_{ij}] = (\phi_i^A - \phi_j^A) E_{ij}, \qquad M_{W,ij}^2 = \sum_{A=3}^{5} (\phi_i^A - \phi_j^A)^2. \quad \text{(IX.1.34)}$$

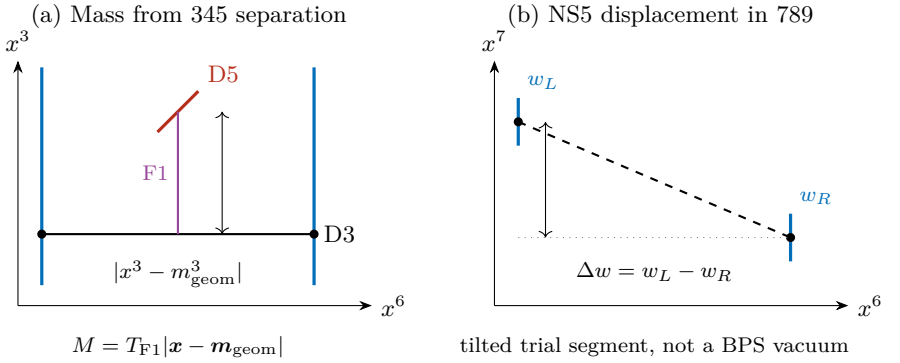


Figure IX.1.2: Two different readings of brane displacement. (a) A string between a color D3 and a flavor D5 has a mass proportional to their 345 separation; a one-component slice is drawn. (b) Separating the NS5s in 789 changes the FI deformation. The dashed tilted D3 is a trial configuration for its tension cost, not a supersymmetric vacuum. The two panels describe different choices of background.

The off-diagonal kinetic term becomes a mass term with exactly the squared separation of the color branes. In the preceding example the off-diagonal W has mass $3\mu_*$. At color coincidence it becomes massless and restores the nonabelian enhancement.

Only relative positions enter these expressions. A common translation of all color and flavor positions acts as

$$\boldsymbol{\phi}_i \mapsto \boldsymbol{\phi}_i + \boldsymbol{c}, \qquad \boldsymbol{m}_a \mapsto \boldsymbol{m}_a + \boldsymbol{c}, \qquad M_{ia}^2 \mapsto M_{ia}^2. \tag{IX.1.35}$$

For $N_f \geq 1$, one may choose a mass origin and keep $N_f - 1$ independent relative bare mass triplets. This freedom to shift a scalar origin is distinct from an ineffective gauge-center action.

IX.1.5 The interval coupling and the three-dimensional limit

The constant gauge mode samples the whole D3 length. Its kinetic coefficient must therefore be proportional to that length. To determine the normalization, start with the D3 tension and the quadratic term in the Dirac–Born–Infeld action,

$$\tau_3 = \frac{1}{(2\pi)^3 g_s \alpha'^2}, \qquad S_{F^2} = -\frac{\tau_3 (2\pi\alpha')^2}{4} \int d^4x \ \mathrm{Tr}_f \, F_{mn} F^{mn}. \tag{IX.1.36}$$

For example, a magnetic field $F_{12} = B$ occupies a two-by-two block. Expanding that block and remembering the two antisymmetric tensor entries gives

$$\det \begin{pmatrix} 1 & 2\pi\alpha' B \\ -2\pi\alpha' B & 1 \end{pmatrix} = 1 + (2\pi\alpha' B)^2, \qquad \sqrt{\det} = 1 + \frac{(2\pi\alpha')^2 B^2}{2} + O(B^4), \tag{IX.1.37}$$

with $F_{mn}F^{mn} = 2B^2$. This accounts for the factor 1/4 in (IX.1.36). Use Hermitian generators with $\mathrm{Tr}_f(T^aT^b) = \delta^{ab}/2$. Matching the two ways of writing the action gives

$$\frac{\tau_3(2\pi\alpha')^2}{4} = \frac{1}{8\pi g_s} = \frac{1}{2g_{4,\mathrm{YM}}^2}, \qquad g_{4,\mathrm{YM}}^2 = 4\pi g_s, \tag{IX.1.38}$$

since the component action is $-F^a_{mn}F^{a\,mn}/(4g_{4,\mathrm{YM}}^2)$. The trace factor and the antisymmetric tensor factor have different origins; losing either one changes the coupling.

Keep the matrix gauge field independent of s without rescaling its charge-one covariant derivative. Integrating the component action yields

$$S_3 = -\frac{1}{4g_{4,\mathrm{YM}}^2}\int d^3x \int_0^L ds\, F^a_{\mu\nu}F^{a\,\mu\nu} = -\frac{L}{4g_{4,\mathrm{YM}}^2}\int d^3x\, F^a_{\mu\nu}F^{a\,\mu\nu}. \tag{IX.1.39}$$

Thus the finite interval determines

$$\frac{1}{g_{3,\mathrm{YM}}^2} = \frac{L}{g_{4,\mathrm{YM}}^2}, \qquad g_{3,\mathrm{YM}}^2 = \frac{4\pi g_s}{L}, \qquad [g_{3,\mathrm{YM}}^2] = \text{mass}. \tag{IX.1.40}$$

The normalized wavefunction $f_0 = L^{-1/2}$ used for the spectral problem would instead rescale the three-dimensional field. Either choice gives the same coupling after the covariant derivative is put in the same normalization. A longer interval has a larger inverse kinetic coefficient and a weaker classical gauge coupling.

For an abelian field whose fundamental has unit charge, a second normalization distinction matters. Set the matrix field equal to $a_\mu 1_N$, with field strength $f_{\mu\nu}1_N$. Then

$$-\frac{1}{2g_{3,\mathrm{YM}}^2}\,\mathrm{Tr}_f(f^2 1_N) = -\frac{N}{2g_{3,\mathrm{YM}}^2}f^2 = -\frac{1}{4e_{\mathrm{center}}^2}f^2, \qquad e_{\mathrm{center}}^2 = \frac{g_{3,\mathrm{YM}}^2}{2N}. \tag{IX.1.41}$$

For one D3 the charge-one coupling is therefore

$$e_3^2 = \frac{g_{3,\mathrm{YM}}^2}{2} = \frac{2\pi g_s}{L}. \tag{IX.1.42}$$

The normalized generator $T^0 = 1_N/\sqrt{2N}$ and the charge-one matrix field $a1_N$ are different gauge-field variables. The expression $2\pi g_s/L$ in (IX.1.42) does not replace $4\pi g_s/L$ in (IX.1.40). The former will be the convenient variable for the abelian FI potential.

To interpret the result as a three-dimensional theory, work below both the string scale and the interval excitation scale:

$$M_s = \alpha'^{-1/2}, \qquad M_{\mathrm{KK}} = \frac{\pi}{L}, \qquad E\sqrt{\alpha'} \ll 1, \qquad EL \ll 1. \tag{IX.1.43}$$

There is a controlled family in which both cutoffs become large while the dimensionful gauge coupling stays fixed. Let G and Λ be fixed positive mass scales, l_0 a positive dimensionless number, and ε approach zero through positive values. Choose

$$\alpha' = \frac{\varepsilon^2}{\Lambda^2}, \qquad L = \frac{\varepsilon l_0}{\Lambda}, \qquad g_s = \frac{G\varepsilon l_0}{4\pi\Lambda}. \tag{IX.1.44}$$

Substitution, rather than simply shrinking the drawing, determines the scales:

$$g^2_{3,\mathrm{YM}} = G, \qquad M_s = \frac{\Lambda}{\varepsilon}, \qquad M_{\mathrm{KK}} = \frac{\pi\Lambda}{\varepsilon l_0}, \qquad g_s^2\alpha'^4 = \frac{G^2 l_0^2 \varepsilon^{10}}{16\pi^2\Lambda^{10}}. \tag{IX.1.45}$$

The last expression measures the vanishing bulk gravitational coupling up to its fixed numerical factor. At fixed g_s, by contrast, shrinking L would send $g^2_{3,\mathrm{YM}}$ to infinity. Equation (IX.1.44) makes the fixed-coupling choice explicit.

The fivebranes extend over noncompact spatial directions, so a uniform change of their transverse position has infinite norm. Their positions are treated as external parameters, whereas the finite D3 modes are dynamical. The bulk hierarchy just derived does not control every localized NS5-core sector. The decoupled three-dimensional description assumes that these sectors do not add light dynamical fields beyond the stated endpoint prescription. Nor does the classical kinetic coefficient determine an exact quantum Coulomb-branch metric; that question belongs to Chapter 3.

IX.1.6 FI displacement and the charged center

Moving the NS5s in 789 changes a different part of the gauge theory from moving the D5s in 345. A straight D3 at fixed 789 position can end on both NS5s only if their positions agree. Define

$$\Delta\boldsymbol{w} = \boldsymbol{w}_L - \boldsymbol{w}_R, \qquad \text{straight unbroken NS5–NS5 D3}: \quad \Delta\boldsymbol{w} = 0. \tag{IX.1.46}$$

The field-theory deformation associated with $\Delta\boldsymbol{w}$ is an FI triplet for the central $U(1)$. Nonzero FI need not eliminate supersymmetric vacua. It instead excludes the straight unbroken configuration and can force hypermultiplet expectation values.

First fix the action normalization. For one color take canonical charge-one hypers and one real FI component. With D the auxiliary field and μ_R the real moment map, use

$$\mu_R = |Q|^2 - |\widetilde{Q}|^2, \qquad \mathcal{L}_D = \frac{D^2}{2e_3^2} + D(\mu_R - \zeta_R). \tag{IX.1.47}$$

The stationary value of D and the resulting potential follow by completing the square:

$$\mathcal{L}_D = \frac{[D + e_3^2(\mu_R - \zeta_R)]^2}{2e_3^2} - \frac{e_3^2}{2}(\mu_R - \zeta_R)^2, \qquad V_D = \frac{e_3^2}{2}(\mu_R - \zeta_R)^2. \tag{IX.1.48}$$

Thus positive ζ_R favors the fundamental bilinear relative to the antifundamental one. We take the signed geometric displacement to be left minus right as in (IX.1.46). This sign choice for the moment map is independent of the local gamma equations.

We can determine a candidate magnitude by matching leading classical energies. Set the hypers to zero and consider the tilted D3 in Figure IX.1.2(b). Its extra tension energy per unit common spatial area is

$$\Delta\mathcal{E} = \tau_3\left(\sqrt{L^2 + |\Delta\boldsymbol{w}|^2} - L\right) = \frac{\tau_3|\Delta\boldsymbol{w}|^2}{2L} - \frac{\tau_3|\Delta\boldsymbol{w}|^4}{8L^3} + O\!\left(\frac{\tau_3|\Delta\boldsymbol{w}|^6}{L^5}\right). \tag{IX.1.49}$$

This is a trial energy, not a claim that the tilted segment is a BPS vacuum. Assume that its leading small-slope term matches the canonical FI potential at zero hypers. For one real component this gives

$$\frac{e_3^2\zeta_R^2}{2}=\frac{\tau_3(\Delta w)^2}{2L},\qquad |\zeta_R|=\sqrt{\frac{\tau_3}{Le_3^2}}\,|\Delta w|=\frac{|\Delta w|}{4\pi^2 g_s\alpha'}. \tag{IX.1.50}$$

Using the signed triplet direction, the candidate identification in this normalization is

$$\boldsymbol{\zeta}=\frac{\Delta \boldsymbol{w}}{4\pi^2 g_s\alpha'}\qquad \text{under leading small-slope classical matching.} \tag{IX.1.51}$$

The energy determines a magnitude, not a sign. Its quartic term shows why the matching is not an unrestricted finite-slope equality. The coefficient also depends on the canonical matter and auxiliary-field normalization; it is not an exact quantum dictionary. Since $[Q]=\frac{1}{2}$ in mass units, $[\mu_R]=[\zeta_R]=1$, consistent with physical length divided by α'. At fixed FI in the scaling family (IX.1.44), the slope behaves as

$$\frac{\Delta w}{L}=\pi G\zeta_R\frac{\varepsilon^2}{\Lambda^2}\longrightarrow 0. \tag{IX.1.52}$$

Thus the small-slope regime can be maintained in the same field-theory limit, rather than imposed at a conflicting scale.

For several colors, work in a real FI direction with the other two components zero. With commuting vector scalars, the hypermultiplet equations are

$$QQ^\dagger-\widetilde{Q}^\dagger\widetilde{Q}=\zeta_R 1_{N_c},\qquad Q\widetilde{Q}=0. \tag{IX.1.53}$$

The second equation sets the complex moment map to zero; no additional complex-coordinate normalization will be needed. Taking the trace of the first equation gives

$$\|Q\|^2-\|\widetilde{Q}\|^2=N_c\zeta_R. \tag{IX.1.54}$$

Fundamentals contribute to this trace. It does not say $N_c\zeta_R=0$. For $U(1)$ with one flavor and $\zeta_R=z>0$, an immediate solution is

$$Q=\sqrt{z},\qquad \widetilde{Q}=0,\qquad \boldsymbol{\phi}=\boldsymbol{m}=0. \tag{IX.1.55}$$

The nonzero moment-map level is possible because the gauge $U(1)$ acts on the hypermultiplet.

The same point survives a nonzero antifundamental expectation value. For $U(2)$ with three flavors, set all vector and bare mass triplets to zero and let t be real. The matrices

$$Q=\begin{pmatrix}\sqrt{z+t^2} & 0 & 0\\ 0 & \sqrt{z} & 0\end{pmatrix},\qquad \widetilde{Q}=\begin{pmatrix}0 & 0\\ 0 & 0\\ t & 0\end{pmatrix}\qquad (z>0) \tag{IX.1.56}$$

solve both equations because

$$QQ^\dagger=\begin{pmatrix}z+t^2 & 0\\ 0 & z\end{pmatrix},\quad \widetilde{Q}^\dagger\widetilde{Q}=\begin{pmatrix}t^2 & 0\\ 0 & 0\end{pmatrix},\quad Q\widetilde{Q}=0. \tag{IX.1.57}$$

At $t = 0$ this reduces to two orthogonal fundamental vevs. For $t \neq 0$ the antifundamental contribution subtracts only the added t^2 term. Interchanging Q with $\widetilde{Q}^\dagger$ and $\widetilde{Q}$ with $Q^\dagger$ reverses the real FI level. These backgrounds use zero vector and mass data; they are not being combined with the separated Coulomb background of (IX.1.32).

For N identical branes, the normalization also accounts for their total tension. The matrix moment-map level is $\zeta_R 1_N$, but tracing its coupling to the central auxiliary field gives a source $N\zeta_R$. Therefore

$$\frac{e^2_{\text{center}}}{2}(N\zeta_R)^2 = N\frac{g^2_{3,\text{YM}}\zeta_R^2}{4} = N\frac{\tau_3(\Delta w)^2}{2L} \tag{IX.1.58}$$

at the same leading match. Both the gauge coupling and the source must be converted when passing to a charge-one central field.

An unframed bifundamental quiver behaves differently. Each bifundamental contributes with opposite signs to the two node traces. Summing all node equations then gives

$$\sum_i \operatorname{Tr}\mu_i = 0 \quad \Longrightarrow \quad \sum_i N_i\zeta_i = 0. \tag{IX.1.59}$$

The fundamental terms in (IX.1.54) do not cancel this way. Removing a diagonal $U(1)$, or imposing the last sum rule, requires examining the actual matter representation. We will do this again for a two-node framed example.

IX.1.7 Fivebrane charge and linking number

An endpoint on a fivebrane carries magnetic charge in its worldvolume description. The total charge also receives a contribution from the bulk flux of fivebranes of the other species. When their ordering changes, the bulk contribution changes; actual D3 endpoints can compensate it. This is the physical origin of the linking number. We take the unit fivebrane flux, the D3 endpoint charge and conservation at infinity as the charge inputs. They are not consequences of the spinor count.

The half-unit contribution has a simple geometric explanation. A unit radial flux in four transverse dimensions has flux density normalized by the area $2\pi^2$ of the unit three-sphere. Restrict it to a three-plane a signed distance d from the source. Its normal component and integral, with the chosen plane orientation, are

$$j_\perp(r;d) = \frac{d}{2\pi^2(r^2+d^2)^2}, \qquad \Phi(d) = \frac{4\pi d}{2\pi^2}\int_0^\infty \frac{r^2\,dr}{(r^2+d^2)^2}. \tag{IX.1.60}$$

For $d > 0$, substitute $r = d\tan\theta$. The remaining integral is

$$\int_0^\infty \frac{r^2\,dr}{(r^2+d^2)^2} = \frac{1}{d}\int_0^{\pi/2}\sin^2\theta\,d\theta = \frac{\pi}{4d}, \qquad \Phi(d) = \frac{1}{2}. \tag{IX.1.61}$$

For negative d the denominator is unchanged and the numerator reverses sign. Hence

$$\Phi(d) = \frac{1}{2}\operatorname{sgn} d \quad (d \neq 0), \qquad \Phi(0^+) - \Phi(0^-) = 1. \tag{IX.1.62}$$

The plane at $d = 0$ crosses the source, so it is not a regular member of this flux calculation. The half-unit is a flux through a noncompact plane, not a fractional number of D3s. The integral fixes its magnitude and jump; the charge orientation is specified next.

Order fivebranes by increasing x^6. At a specified fivebrane B, let $n_{\mathrm{opp},R}$ and $n_{\mathrm{opp},L}$ count fivebranes of the opposite species to its right and left. Let $n_{3,R}$ and $n_{3,L}$ count actual D3 endpoints whose segments extend right and left. Use the same convention for both species:

$$\ell_B = \frac{1}{2}(n_{\mathrm{opp},R} - n_{\mathrm{opp},L}) + n_{3,L} - n_{3,R}. \tag{IX.1.63}$$

A D3 passing through the projected position of an interior D5 has no endpoint contribution there. The signs in (IX.1.63) express the chosen flux and endpoint-charge orientation, independently of the local gamma signs. For a pair of unlike fivebranes and for a finite D3 segment the contributions are, respectively,

$$(\delta\ell_{\mathrm{left}}, \delta\ell_{\mathrm{right}})_{\text{unlike pair}} = \left(\frac{1}{2}, -\frac{1}{2}\right), \qquad (\delta\ell_{\mathrm{left}}, \delta\ell_{\mathrm{right}})_{n\,\mathrm{D3}} = (-n, +n). \tag{IX.1.64}$$

Every contribution cancels in the sum over a finite system with both ends of each D3 included. Thus

$$\sum_B \ell_B = 0. \tag{IX.1.65}$$

Semi-infinite D3s require additional boundary charges and are outside this assertion. Even for a finite system, zero total charge is weaker than conservation of the individual ℓ_B.

Apply the definition to N_c unbroken D3s between two NS5s with N_f D5s inside. The left NS5 sees N_f D5s to its right and N_c D3s extending right. The right NS5 sees the opposite. Each D5 sees one NS5 on each side and no D3 endpoint. Therefore

$$\ell_{\mathrm{NS}_L} = \frac{N_f}{2} - N_c, \qquad \ell_{\mathrm{NS}_R} = N_c - \frac{N_f}{2}, \qquad \ell_{\mathrm{D5}_a} = 0. \tag{IX.1.66}$$

For Figure IX.1.1, in spatial order this is

$$(\ell_{\mathrm{NS}_L}, \ell_{\mathrm{D5}_1}, \ell_{\mathrm{D5}_2}, \ell_{\mathrm{D5}_3}, \ell_{\mathrm{NS}_R}) = \left(-\frac{1}{2}, 0, 0, 0, \frac{1}{2}\right). \tag{IX.1.67}$$

With no flavor branes the NS5 charges instead become $(-N_c, +N_c)$; with one color and two flavors all four fivebrane charges vanish. These different endpoint systems can share a zero total while having different individual charges. To determine what a crossing creates, we must preserve the full list, not only its sum.

IX.1.8 Crossing and reconnection are different problems

Consider an adjacent NS5, denoted N, to the left of a D5, denoted D. Exchange their order without introducing a new source at infinity. There are two useful ways to specify

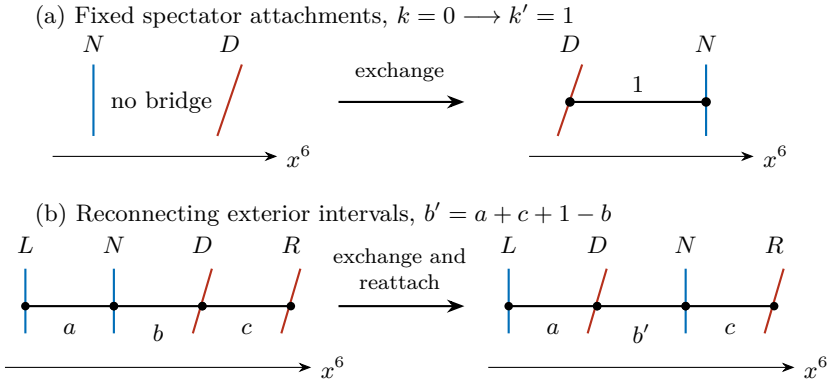


Figure IX.1.3: Two charge-conservation problems. (a) The elementary bridge move with unchanged spectator attachments, illustrated for no initial bridge. Exchanging N and D requires one final bridge. (b) An adjacent-interval presentation with exterior ranks a, c fixed. The exterior endpoints change from L–N and D–R to L–D and N–R, so the middle rank obeys a different formula. Blue strokes are NS5s, red strokes D5s, and filled dots are actual endpoints. These are before/after incidence diagrams; no transverse trajectory is specified.

what else stays fixed. In the first, every spectator segment remains attached to the same named fivebranes. In the second, exterior interval ranks stay fixed but their endpoints reconnect. Figure IX.1.3 separates the two operations. Confusing their fixed quantities gives different answers for the same symbol called a rank.

Let k be the number of initial D3 bridges from N to D. In the fixed-attachment problem, collect the spectator endpoint charges into two integers and the initial fivebrane half-counts into two numbers:

$$S_N = n^{\text{spect}}_{3,L,N} - n^{\text{spect}}_{3,R,N}, \qquad S_D = n^{\text{spect}}_{3,L,D} - n^{\text{spect}}_{3,R,D}, \qquad h_B = \tfrac{1}{2}(n_{\text{opp},R,B} - n_{\text{opp},L,B}). \tag{IX.1.68}$$

The bridge extends right from N and left from D, so the initial charges are

$$\ell_N = h_N + S_N - k, \qquad \ell_D = h_D + S_D + k. \tag{IX.1.69}$$

After exchanging the adjacent pair, D has gone from the right to the left of N, lowering h_N by one. Conversely h_D increases by one. Let k' be the final bridge multiplicity. The bridge now extends left from N and right from D, giving

$$\ell'_N = h_N - 1 + S_N + k', \qquad \ell'_D = h_D + 1 + S_D - k'. \tag{IX.1.70}$$

Subtract the two initial charges separately:

$$\ell'_N - \ell_N = k + k' - 1, \qquad \ell'_D - \ell_D = 1 - k - k'. \tag{IX.1.71}$$

Conservation of both is equivalent to

$$k + k' = 1, \qquad k' = 1 - k. \tag{IX.1.72}$$

The spectator charges canceled without being set to zero. Other fivebranes retain their charges because the exchanged pair are adjacent and cross no other fivebrane, while every spectator endpoint keeps its side relative to its own endpoint brane. This is why the argument applies to arbitrary spectator endpoint multiplicities.

With no initial bridge, the final bridge count must be one. With one initial bridge, the reversed arrangement has none. Suppressing creation at $k = 0$ would instead give

$$k = k' = 0 : \qquad (\Delta\ell_N, \Delta\ell_D) = (-1, +1), \qquad \Delta(\ell_N + \ell_D) = 0. \tag{IX.1.73}$$

The total sum still vanishes, but each fivebrane charge is wrong. This example identifies precisely what the conservation argument requires. For $k = 2$, the formal answer $k' = -1$ is outside a graph of positive D3 multiplicities with those fixed attachments. It is not, by itself, a theorem about all possible supersymmetric configurations.

Now change the fixed quantities. Begin with four ordered fivebranes L, N, D, R, where L, N are NS5s and D, R are D5s. Initially there are a, b, c D3s on the three adjacent intervals. After exchanging N, D, keep the exterior ranks a, c but attach them to the new neighbors:

order	left interval	middle interval	right interval
L, N, D, R	$(L, N) : a$	$(N, D) : b$	$(D, R) : c$
L, D, N, R	$(L, D) : a$	$(D, N) : b'$	$(N, R) : c$

. (IX.1.74)

The D3 of rank a no longer ends on N, and the D3 of rank c now does. In terms of the initial half-counts, the two relevant charges are therefore

$$\begin{aligned} \ell_N &= h_N + a - b, & \ell_D &= h_D + b - c, \\ \ell'_N &= h_N - 1 + b' - c, & \ell'_D &= h_D + 1 + a - b'. \end{aligned} \tag{IX.1.75}$$

Equating each pair gives the two opposite residuals

$$\Delta\ell_N = b + b' - a - c - 1 = -\Delta\ell_D, \qquad b' = a + c + 1 - b. \tag{IX.1.76}$$

The unit term again comes from the half-flux jump. The terms $a + c$ come from the changed attachments. Equation (IX.1.72) keeps those attachments fixed; equation (IX.1.76) does not. Neither formula can be substituted for the other while silently preserving its interpretation.

As a numerical example, take $a = 1, b = 1, c = 0$. The new middle rank is $b' = 1$; the left segment now ends on D rather than N. The more revealing example has $a = b = c = 2$, for which

$$(a, b, c) = (2, 2, 2), \quad b' = 3, \qquad (\ell_L, \ell_N, \ell_D, \ell_R) = (-1, 1, -1, 1) \quad \text{before and after.} \tag{IX.1.77}$$

The charges here are listed by brane name, not by final spatial order. For example, initially $\ell_N = 1 + 2 - 2 = 1$, while finally $\ell'_N = 0 + 3 - 2 = 1$. Every multiplicity is nonnegative, and every charge is conserved. Yet the central mixed pair has multiple D3 occupancy. The next section explains why that is excluded by a further supersymmetry input.

The charge argument is a necessary accounting of endpoints. The physical elementary creation process supplies a configuration realizing the unit change in its allowed domain. A table of before/after incidences does not establish a continuous BPS motion through all intermediate transverse geometries. Still less does it establish that two endpoint theories have identical infrared dynamics. Those are separate questions when Chapter 2 applies brane moves to mirror symmetry.

IX.1.9 The local s-rule and its consequences

The additional local physical input is the s-rule: at most one supersymmetric D3 may directly connect a specified ordinary resolved NS5–D5 pair in this flat noncompact setup. If n_{ND} counts that pair's occupancy, the rule is

$$n_{ND} \in \{0, 1\}. \tag{IX.1.78}$$

It concerns a specified mixed pair. It is not a bound on the number of color D3s between two NS5s or on the total number of D3s in a drawing. Its extension to unresolved stacks, winding sectors or other fivebrane species requires additional physics.

The example (IX.1.77) makes the logical separation concrete. The charge equations admit

$$b = 2, \quad b' = 3, \quad \Delta\ell_B = 0 \text{ for every } B, \qquad b, b' \notin \{0, 1\}. \tag{IX.1.79}$$

Thus charge conservation does not imply the s-rule. We impose the local quantum restriction, then compute its consequences. The mixed-endpoint zero-mode calculation also does not prove it: absence of a massless scalar on one segment is a different statement from the impossibility of a supersymmetric state with two segments.

A field-theory obstruction helps explain why such a restriction is needed. Suppose $\zeta_R > 0$ and $N_f < N_c$ in the moment-map equations (IX.1.53). The map $Q^\dagger$ then has a nonzero kernel vector v:

$$Q^\dagger \colon \mathbb{C}^{N_c} \longrightarrow \mathbb{C}^{N_f}, \qquad \operatorname{rank} Q^\dagger \leq N_f < N_c \quad \Longrightarrow \quad Q^\dagger v = 0, \quad v \neq 0. \tag{IX.1.80}$$

Evaluate the real moment-map equation between $v^\dagger$ and v. The fundamental term vanishes, leaving

$$v^\dagger (QQ^\dagger - \widetilde{Q}^\dagger \widetilde{Q}) v = -\|\widetilde{Q} v\|^2 = \zeta_R \|v\|^2 > 0. \tag{IX.1.81}$$

Its left side is nonpositive, so there is no solution. This argument allows a nonzero $\widetilde{Q}$; it is stronger than inspecting only the slice $\widetilde{Q} = 0$. For a concrete $N_c = 2, N_f = 1$ example,

$$Q = \begin{pmatrix} 1+i \\ 2-i \end{pmatrix}, \qquad v = \begin{pmatrix} -2-i \\ 1-i \end{pmatrix}, \qquad \widetilde{Q} = \begin{pmatrix} 2+i & 3 \end{pmatrix}, \qquad Q^\dagger v = 0. \tag{IX.1.82}$$

Here $\widetilde{Q} v = -7i$, so the two sides that would have to agree are

$$-\|\widetilde{Q} v\|^2 = -49, \qquad \|v\|^2 = 7, \qquad -49 = 7\zeta_R \quad \text{would be required.} \tag{IX.1.83}$$

This numerical vector illustrates the negative-semidefinite argument; it is not proposed as a solution of the other moment-map equation. For negative FI the conjugate representations exchange roles.

The hypothesis of nonzero FI cannot be dropped. At zero FI,

$$Q = 0, \qquad \widetilde{Q} = 0, \qquad \zeta_R = 0 \tag{IX.1.84}$$

solves both moment maps for any N_c, N_f, including $(2, 1)$. There is no universal $N_c \leq N_f$ restriction on the undeformed SQCD construction. The nonzero-FI obstruction gives a field-theory consistency argument for the local s-rule, not a microscopic derivation of that quantum brane input.

Its elementary combinatorial consequence can be seen without making a vacuum-count claim. Label two color endpoints and three resolved flavor slots. If no specified mixed pair may receive both endpoints, the allowed assignments are

$$(0,1),\ (0,2),\ (1,0),\ (1,2),\ (2,0),\ (2,1). \tag{IX.1.85}$$

There are three choices for the first endpoint and two for the second. Sequential choice for N_c labeled endpoints gives

$$\#\{\text{injective assignments}\} = \begin{cases} \dfrac{N_f!}{(N_f - N_c)!}, & N_c \leq N_f, \\ 0, & N_c > N_f. \end{cases} \tag{IX.1.86}$$

For two endpoints and one slot the set is empty. For no endpoints it contains the single empty assignment. Gauge and Weyl identifications have not been taken, and the assignments do not describe the full space of supersymmetric vacua. Chapter 3 will study branches as field-theory spaces rather than as labeled attachment lists.

IX.1.10 From one interval to a framed two-node theory

The single-node construction now has a definite recipe. Choose two NS5s, count the D3s ending on them, add the interior D5s, and then read the gauge group, fundamental representations and deformation parameters. For one color and $N_f = 1, 2$, it gives

$$U(1), \quad N_f = 1 :\ \dim_{\mathbb{R}}(Q, \widetilde{Q}) = 4; \qquad U(1), \quad N_f = 2 :\ \dim_{\mathbb{R}}(Q, \widetilde{Q}) = 8. \tag{IX.1.87}$$

The vector is present in both examples. For $N_f = 0$, the fundamental sector disappears; the trace vector of the pure $U(N_c)$ theory has no charged matter and is free. Adding even one fundamental changes that center action, as (IX.1.29) shows.

A third NS5 divides the color branes into neighboring gauge intervals. When D3 endpoints on the two intervals meet at the common NS5, the brane description supplies a bifundamental hypermultiplet. We use this as a physical dictionary statement. Its direct NS5 argument is nonperturbative and heuristic, unlike the four-ND D3–D5 calculation; the following representation calculation does not derive that localized matter sector microscopically.

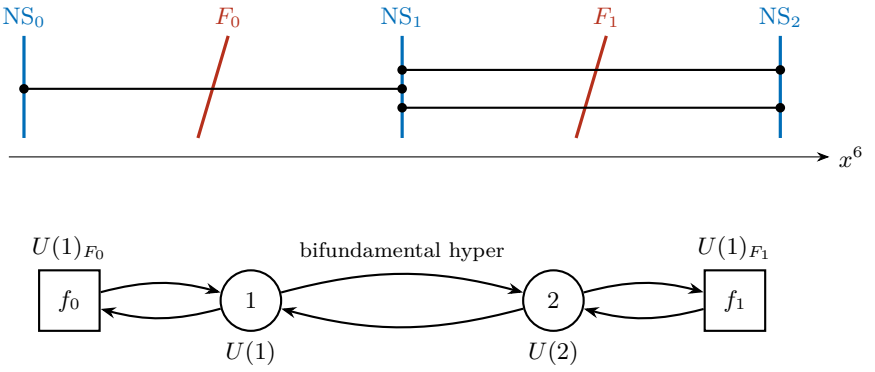


Figure IX.1.4: A framed $U(1)_1 \times U(2)_2$ theory. The upper drawing has one color D3 in the left interval and two in the right, with one D5 in each. In the lower quiver, circles are gauge nodes and squares are flavor nodes. Each pair of opposite arrows is one hypermultiplet; the pair between gauge nodes is the matter supplied at the common NS5. Vertical offsets display multiplicity, not transverse vevs. Gauge factors are written beside the nodes.

Take three NS5s at $t_0 < t_1 < t_2$, one D3 on the first interval, two on the second, and one interior D5 in each interval. At coincident appropriate endpoint positions, Figure IX.1.4 gives

$$G = U(1)_1 \times U(2)_2, \qquad L_1 = t_1 - t_0, \quad L_2 = t_2 - t_1, \qquad g_{3,i}^2 = \frac{4\pi g_s}{L_i}. \tag{IX.1.88}$$

There is one fundamental hyper at each node and one bifundamental hyper between the nodes. A hyper means both conjugate complex representations. The representation spaces may be listed as

	H_1	H_2	H_{12}
$U(1)_1$ charge q_1	1	0	1
$U(2)_2$ representation	$\mathbf{1}$	$\mathbf{2}$	$\overline{\mathbf{2}}$

. (IX.1.89)

Each column is accompanied by its conjugate representation. The fundamental H_1 has charge one at node 1 and is neutral under node 2; H_2 is neutral under node 1 and is a defining doublet of node 2.

The vector and unconstrained hypermultiplet dimensions are different counts, even though they coincide numerically in this example:

$$\dim_{\mathbb{R}} \mathfrak{g} = 1^2 + 2^2 = 5, \qquad \dim_{\mathbb{H}} \mathcal{H} = 1 + 2 + (1 \cdot 2) = 5. \tag{IX.1.90}$$

The second expression counts hyper components before moment maps and gauge identifications. It is not the dimension of a branch.

To test whether any common center is ineffective, give the two central phases

parameters θ_1, θ_2. The three hyper sectors have charge rows

$$C_{\text{matter}} = \begin{pmatrix} 1 & 0 \\ 0 & 1 \\ 1 & -1 \end{pmatrix}, \qquad C_{\text{matter}} \begin{pmatrix} \theta_1 \\ \theta_2 \end{pmatrix} = \begin{pmatrix} \theta_1 \\ \theta_2 \\ \theta_1 - \theta_2 \end{pmatrix}. \tag{IX.1.91}$$

The fundamental at each node requires its own phase to be identity,

$$e^{i\theta_1} = 1, \qquad e^{i\theta_2} = 1. \tag{IX.1.92}$$

There is no continuous or residual finite central kernel to remove. The defining fundamental at each node also detects any noncentral matrix transformation, so the full product group acts faithfully. Keeping only the bifundamental would instead leave

$$(1, -1) \begin{pmatrix} \theta_1 \\ \theta_2 \end{pmatrix} = 0, \qquad \ker(1, -1) = \text{span}\{(1, 1)\}. \tag{IX.1.93}$$

Framing is therefore a physical change in the representation, not a small notational adjustment to an unframed quiver. In particular the two FI triplets need not obey the unframed weighted sum restriction:

$$\boldsymbol{\zeta}_1 \;\propto\; \boldsymbol{w}_0 - \boldsymbol{w}_1, \qquad \boldsymbol{\zeta}_2 \;\propto\; \boldsymbol{w}_1 - \boldsymbol{w}_2. \tag{IX.1.94}$$

The proportionality has the same conditional leading-action normalization as (IX.1.51).

Finally, take the fivebranes in the displayed order $\text{NS}_0, F_0, \text{NS}_1, F_1, \text{NS}_2$ and count only the actual interval endpoints. Their linking numbers are

$$(\ell_{\text{NS}_0}, \ell_{F_0}, \ell_{\text{NS}_1}, \ell_{F_1}, \ell_{\text{NS}_2}) = \left(0, \frac{1}{2}, -1, -\frac{1}{2}, 1\right). \tag{IX.1.95}$$

For example, the middle NS5 has one D5 on each side, one color endpoint extending left and two extending right, giving $0 + 1 - 2 = -1$. The first flavor brane has two NS5s to its right and one to its left, giving $+1/2$, with no D3 endpoints there. These explicit charges are the quantities to preserve if one later changes the ordering.

IX.1.11 What the construction establishes

The interval provides a useful division between dynamical fields and external couplings. The D3 zero modes are the fields. Noncompact fivebrane positions are the parameters. Under the imported endpoint and decoupling assumptions, the endpoint conditions select the vector multiplet, the oriented D3–D5 strings supply fundamental hypers, and the normalized interval action determines the classical gauge coupling. The resulting group is $U(N_c)$; fundamentals give its center a physical action. A Coulomb background separates the color scalar eigenvalues without redefining that ultraviolet group.

This picture also distinguishes two different questions about moving branes. Charge conservation determines how the endpoint numbers must change. The local s-rule supplies an additional supersymmetry restriction. Neither statement alone proves continuity of an infrared theory across a fivebrane crossing. The fixed-spectator and

reconnecting calculations expose exactly which quantities were held fixed, so a subsequent physical application can state the extra assumptions it needs.

There are corresponding limits to what has been determined. The scalar boundary problem used homogeneous abelian endpoint conditions, while its Maxwell and fermionic completion was supplied by the brane description. The explicit gamma calculation counted real solutions of one compatible convention; it did not identify every source's spinor and Ramond–Ramond signs. The coupling came from the leading classical action, and the FI magnitude required a small-slope energy match. Quantum branch metrics and a microscopic proof of the local s-rule have not followed from these calculations.

Reading a suspended-brane configuration

Identify the common spacetime and interval direction. Count actual D3 endpoints to determine the gauge intervals, then read the matter representations and their center charges. Convert physical displacements to field units before interpreting masses or FI parameters. For an exchange of unlike fivebranes, conserve each linking number and specify whether spectator attachments or only exterior ranks are fixed. Apply the local s-rule separately; an admissible endpoint count is not yet a proof of infrared equivalence.

Chapter 2 uses this construction to compare theories related by IIB duality and brane rearrangement. Chapter 3 distinguishes Coulomb and Higgs branches by their multiplets and studies their quantum geometry. Chapter 4 replaces the elementary endpoint prescription by a richer boundary description. Chapter 5 turns to D4-based four-dimensional engineering, where the status of a trace mode must be reconsidered in that construction. The mass, coupling, FI and linking calculations here provide the starting quantities for those developments.

Status and sources

The source notes distinguish supplied physical premises from their mathematical consequences.

WS means a controlled physical-worldsheet derivation in the untwisted string. An imported spectrum, tension or worldvolume action, followed by algebra, does not by itself supply that derivation here. The endpoint fields, string masses and leading action are supplied physical inputs. Their algebraic consequences retain the stated hypotheses.

The principal source is Hanany and Witten (1997), specifically `arXiv:hep-th/9611230v3` (11 December 1996); all page numbers below refer to its printed pages, one less than the PDF viewer page. General open-string and D-brane machinery is inherited from Volumes III and V and the convention dictionary; the Clifford root is Polchinski Vol. 2, Appendix B (Polchinski 1998). The source's suppressed string-unit constants are not substituted for the book's action normalizations.

§IX.1.1, §IX.1.2 and §IX.1.5 Finite intervals and supersymmetry. [DEC]: the low-energy $U(N_c)$ SQCD construction is conditional on the endpoint, open-string and decoupling inputs. Equations (IX.1.1)–(IX.1.2), (IX.1.43)–(IX.1.45) specify the geometry and scale hierarchy. HW §2, (2.2)–(2.4), p. 2 and §3, pp. 4–7, Fig. 4(a), p. 11 support the physical axes, eight real supercharges and the external-fivebrane SQCD interpretation. The scale calculation does not prove complete NS5-core decoupling. Coverage is the finite check and the symbolic calculation, with known one-color and zero-flavor limits.

[MATH]: equations (IX.1.3)–(IX.1.12) give a native mostly-plus upper-index Clifford calculation, positive IIB chirality, an explicit Majorana involution, and an eight-real-parameter kernel. Opposite relative D3 orientation gives zero. This is internal convention consistency conditional on the declared projector prescription, not a microscopic derivation or an exact translation of HW's printed lower-index signs. The correlated HW spinor/chirality/brane/RR map remains unused source-interface debt. The native minus sign does not assign the integer D3 charge in (IX.1.63). Root normalization is Polchinski Vol. 2 (B.1.1), (B.1.11), with IIB chirality (10.6.12), inherited through spinor and supersymmetry counting. Coverage is the symbolic calculation, including a direct real simultaneous kernel; the separate object-level calculation also imposed both spinors' equations on 128 real variables. These calculations do not strengthen the physical source statement by consensus.

§IX.1.3 Boundary modes and matrix fields. [MATH]: the scalar kernels (IX.1.15)–(IX.1.18) solve the homogeneous linear endpoint problem for $L > 0$. HW §3, pp. 4–7 supplies the N/D prescription, Maxwell boundary conditions and vector/hyper interpretation in (IX.1.19)–(IX.1.20). The abelian completion is imported physical input, not an independent fermionic boundary derivation. the finite check and the symbolic calculation cover the scalar problem. General nonabelian boundaries are deferred to IX.4 under brane endpoint and projector foundations.

§IX.1.3 and §IX.1.4 Chan–Paton fields, flavor and masses. In the sourced spectrum, the four-ND D3–D5 hyper and charged color center use the perturbative spectrum in HW §3, Fig. 3(b), pp. 9–10 and Fig. 4(a), p. 11. Equations (IX.1.21)–(IX.1.24) and (IX.1.25)–(IX.1.29) display the matrix algebra, imported GSO consequence, complete representation weights and center action. the finite check validate finite representations, including all matrix-unit products and exact charge vectors. They are not a new worldsheet quantization or an all-rank certification of an arbitrary enumerator.

Q5 (physical primary classification unassigned; imported F1 tension): equations (IX.1.30)–(IX.1.35) apply the F1 tension to the mass dictionary. HW §3, pp. 10–11 supplies the positional dependence and common-mass shift; brane-action and trace normalization restores $2\pi\alpha'$. The

asymmetric squared masses and adjoint commutator are the finite check and the symbolic calculation; the consistency check covers dimensions and limits. The separated colors are a Coulomb background of the UV $U(2)$ theory, not a simultaneous nonzero-FI Higgs solution or a determination of an interacting quantum spectrum.

§IX.1.5 Kinetic normalization. Conditional on the leading DBI action, equations (IX.1.36)–(IX.1.42) derive, from the displayed tension and quadratic action, the coefficient, interval reduction and conversion to a charge-one center. HW (3.2), p. 7 gives the length-reduction law; brane-action and trace normalization gives the absolute D3 tension and trace normalization. The resulting $g^2_{3,\mathrm{YM}} = 4\pi g_s/L$ is a classical UV coefficient, not an exact quantum Coulomb metric. the finite check and the symbolic calculation cover tensor, trace and interval factors. General DBI machinery remains the DBI and Wess–Zumino action–gravity decoupling; no new Dp normalization is introduced.

§IX.1.6 FI deformation and framing. [GEO-E]: equation (IX.1.46) uses the left-minus-right direction of HW §3, p. 12. Its moment-map sign is pinned by HW §5.2, (5.11), p. 27 with the identification $A = Q$, $B = \widetilde{Q}$. The finite equations and explicit solutions (IX.1.53)–(IX.1.57) show that framed fundamentals permit nonzero FI. The normalization does not turn the positional dictionary into GEO-X. the finite check, the symbolic calculation and the consistency check cover the declared algebra and limits; the symbolic calculation is not source verification. The nonzero-antifundamental example was independently recomputed in the saved object-level calculation. All these FI vevs use compatible zero vector/mass data.

[MATH]: *assuming leading small-slope classical DBI/action matching and canonical charge-one hypers*, equations (IX.1.47)–(IX.1.51) give the candidate magnitude $|\zeta| = |\Delta w|/(4\pi^2 g_s \alpha')$. The sourced displacement dictionary supplies its sign. HW does not print this absolute coefficient; there is no finite-slope or exact quantum claim. The auxiliary elimination is the symbolic calculation and the defining energy-match implementation is the symbolic calculation. Equation (IX.1.58) converts both the central coupling and source. The local displacement and auxiliary-field calculation concerns the FI magnitude. Chapter 2 treats the complex mirror map separately.

§IX.1.7 Flux and endpoint charges. [SUGRA]: the tag covers only the bulk/worldvolume flux and D3 endpoint magnetic-charge argument in HW §5, (5.1)–(5.8), pp. 20–22. The common sign formula (IX.1.63) is HW (5.9)–(5.10), including the footnote, p. 23. Equations (IX.1.60)–(IX.1.62) evaluate a normalized radial-flux plane integral, independently derived in the saved object-level calculation. It gives the half-unit magnitude and jump, not the source orientation or the existence of a BPS crossing path. Fixed external sources and endpoint charge remain physical inputs.

[MATH]: the finite incidence system gives (IX.1.64)–(IX.1.67) and the arbitrary-spectator identity in (IX.1.69)–(IX.1.72). The single-node charge target is also HW §6.3, Fig. 19(a), p. 39. the finite check and the symbolic calculation cover individual charge conservation. The 512 finite graph samples test incidence arithmetic, not 512 continuous supersymmetric trajectories. the finite check compares two implementations without certifying independence.

§IX.1.8 Two crossing charts. [MATH]: changed exterior attachments in (IX.1.74)–(IX.1.76) give $b' = a + c + 1 - b$ under the same HW p. 23 charge convention. the finite check and the symbolic calculation derive the two residuals and the positive conserved counterexample (IX.1.77). Conservation is not sufficient for supersymmetry or IR equivalence. The local physical creation/s-rule input is A-001-HW-CREATION; A-002-HW-CONT is not invoked to prove an infrared equivalence here.

§IX.1.9 Conditional local restriction. [MATH]: given the adopted local s-rule, equations (IX.1.85)–(IX.1.86) count labeled injective assignments. Equations (IX.1.80)–(IX.1.84) give a

finite moment-map obstruction and its zero-FI limit. The general kernel argument includes nonzero antifundamental data; the complex numerical example is from the independent object-level calculation. HW §5.2, Fig. 10 and (5.11), pp. 26–28 motivates the s-rule and explicitly leaves a direct argument open on p. 28. the finite check, the symbolic calculation and the consistency check compute consequences, not a microscopic quantum s-rule or a vacuum count. The distinction is the conservation/supersymmetry distinction.

§IX.1.10 Neighboring intervals. [GEO-E]: HW §3, Fig. 1, pp. 7–9 supplies the common-NS5 bifundamental dictionary and explicitly qualifies its direct argument as nonperturbative/heuristic. Equations (IX.1.88)–(IX.1.95) compute the resulting representation, faithful framed center and endpoint charges. the finite check and the independent primitive-charge calculation support the arithmetic, not a WS upgrade of the physical dictionary. The unconstrained representation count is not a branch dimension. The distinction is why the unframed FI restriction does not apply.

Figures, conventions and deferred interfaces. All four figures are original local TikZ drawings. Figure IX.1.1 specializes HW Fig. 4(a), p. 11 and Fig. 19(a), p. 39 to $(N_c, N_f) = (2, 3)$. Figure IX.1.2 depicts the §3 pp. 10–12 mass/FI distinction, with the trial tension geometry of (IX.1.49). Figure IX.1.3 draws the two explicitly derived incidence problems, using HW (5.9)–(5.10) rather than asserting a transverse BPS path. Figure IX.1.4 specializes HW Fig. 1, pp. 7–9. The position, auxiliary-field and FI conventions used here apply to this local interval construction. Chapters 2–5 develop, respectively, the mirror map, branch geometry, boundary theories and D4-based engineering. The finite calculations assume the endpoint prescription and the decoupling and quantum s-rule premises. Together they give the scoped construction [DEC] of three-dimensional $\mathcal{N} = 4$ unitary gauge theories on NS5-bounded D3 intervals with D5 flavors.

References

Hanany, A. and E. Witten (1997). "Type IIB superstrings, BPS monopoles, and three-dimensional gauge dynamics". In: *Nucl. Phys. B* 492, pp. 152–190. DOI: 10.1016/S0550-3213(97)00157-0. arXiv: hep-th/9611230.

Polchinski, J. (1998). *String Theory. Vol. 2: Superstring Theory and Beyond*. Cambridge Monographs on Mathematical Physics. Cambridge University Press. DOI: 10.1017/CBO9780511618123.

Chapter IX.2

Mirror symmetry from IIB S-duality

IX.2.1 Two descriptions of the same infrared physics

A three-dimensional photon carries one propagating degree of freedom. Dualizing it to a periodic scalar makes the Coulomb branch of an $\mathcal{N} = 4$ gauge theory four-real-dimensional per abelian gauge factor: three vector-multiplet scalars and one dual photon. A hypermultiplet also contains four real scalars, but they transform under the other factor of the R-symmetry. This makes a particular possibility worth investigating. Could the quantum Coulomb branch of one gauge theory be the Higgs branch of another?

The branes of Chapter 1 give a physical way to ask this question. An NS5-bounded D3 interval carries a vector multiplet. A D5-bounded interval carries a hypermultiplet. Type IIB S-duality exchanges the two fivebrane species. A spatial rotation restores their original coordinate orientations, so that the same rules for reading the suspended theory can be applied again. The resulting gauge group need not resemble the original one. It is the low-energy physics, together with the exchange of the two R-symmetry factors, that is proposed to agree.

We will follow this operation for an abelian gauge theory with one, two, and three charge-one hypermultiplets. The first becomes a free hypermultiplet in the mirror description. The second returns a theory with the same gauge and matter content. The third becomes a theory with two abelian gauge factors, one hypermultiplet joining the nodes, and one flavor hypermultiplet at each end. This last example makes the exchange visible: a Higgs branch of quaternionic dimension two is paired with a Coulomb branch of quaternionic dimension two, while the other two branches have quaternionic dimension one.

Take-home message of this chapter

Exchanging fivebranes changes which D3 intervals carry gauge fields. Conserved fivebrane charges determine the allowed segment counts along the chosen motion. The transverse positions then turn relative masses into FI parameters. The resulting mirror proposal can be tested by calculating the mirror Higgs quotient with elementary fields and comparing it with independently known electric Coulomb data.

Our fivebranes are external sources, x^6 is noncompact, and all color ranks in the worked examples are one. We use the endpoint and decoupling assumptions of Chapter 1. Motion through a strongly coupled brane arrangement also requires infrared continuity; conservation of charge does not establish that dynamical assertion. The calculations below separate the actual conserved quantities from this physical premise. Chapter 3 develops the branch geometry, while Chapter 4 reinterprets S-duality through boundary conditions. Here the aim is to derive the finite brane moves and the parameter dictionary closely enough that a reader can reconstruct the three mirror descriptions.

IX.2.2 Exchanging species and restoring the axes

S-duality alone changes the kind of fivebrane without restoring the orientation used to read its worldvolume fields. We therefore need both the charge transformation and a spatial rotation. Keep the coordinate table of Chapter 1,

	012	345	6	789
NS5	×	×	–	–
D3	×	–	×	–
D5	×	–	–	×

, $\qquad \boldsymbol{v} = (x^3, x^4, x^5), \quad \boldsymbol{w} = (x^7, x^8, x^9).$ (IX.2.1)

We label the original description electric and the transformed description mirror. In either restored coordinate frame,

$$SU(2)_C \longleftrightarrow SO(3)_{345}, \qquad SU(2)_H \longleftrightarrow SO(3)_{789}. \tag{IX.2.2}$$

These are the spin covers acting on the supersymmetry multiplets. They specify which branch we mean when a geometric direction is exchanged.

Use an ordered charge column $(q_D, q_N)^T$ for the D5 and NS5 charges, including an oriented worldvolume in the definition of a charged brane. The S transformation is

$$S = \begin{pmatrix} 0 & 1 \\ -1 & 0 \end{pmatrix}, \qquad S\begin{pmatrix} 0 \\ 1 \end{pmatrix} = \begin{pmatrix} 1 \\ 0 \end{pmatrix}, \qquad S\begin{pmatrix} 1 \\ 0 \end{pmatrix} = \begin{pmatrix} 0 \\ -1 \end{pmatrix}. \tag{IX.2.3}$$

The minus sign in the second image cannot be discarded. To interpret it we must also transform the tangent orientation. Let e_j denote a coordinate basis vector and take the active rotation

$$Re_j = e_{j+4}, \qquad Re_{j+4} = -e_j \quad (j = 3, 4, 5), \qquad Re_\mu = e_\mu \quad (\mu = 0, 1, 2, 6). \tag{IX.2.4}$$

Each affected two-plane undergoes a right-angle rotation. On coordinate components this gives

$$(\boldsymbol{v}', \boldsymbol{w}') = (-\boldsymbol{w}, \boldsymbol{v}), \qquad R^T R = 1, \qquad \det R = 1. \tag{IX.2.5}$$

The operation is proper and leaves the D3 tangent directions 0126 fixed. It changes neither the ordering nor the distances along x^6. Figure IX.2.1 depicts the three identical rotation blocks.

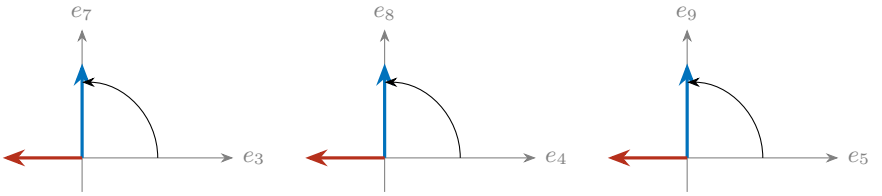


Figure IX.2.1: The active restoring rotation in each of the three transverse two-planes. A basis vector in 345 goes to the corresponding vector in 789; the latter goes to the negative of the former. The charge transformation and tangent orientation must both be included when identifying the resulting fivebrane. The common 0126 directions are fixed.

An NS5 starts with the oriented spatial triple $e_3 \wedge e_4 \wedge e_5$. The effect on the two fivebrane tangent triples is

$$\begin{aligned} R(e_3 \wedge e_4 \wedge e_5) &= e_7 \wedge e_8 \wedge e_9, \\ R(e_7 \wedge e_8 \wedge e_9) &= -e_3 \wedge e_4 \wedge e_5. \end{aligned} \tag{IX.2.6}$$

Thus the NS5 acquires D5 charge with the positive D5 orientation. The D5 acquires negative NS5 charge and a negative NS5 tangent orientation. Their product is again the ordinary positive NS5. In the returned coordinate table the net identification is consequently

$$(\text{NS5}, +012345) \xrightarrow{RS} (\text{D5}, +012789), \qquad (\text{D5}, +012789) \xrightarrow{RS} (\text{NS5}, +012345). \tag{IX.2.7}$$

This is a bosonic orientation calculation. We do not need a lift of R to fermionic spinors to perform the following segment calculations.

The same signs answer what happens on applying the transformation twice:

$$S^2 = -1, \qquad R^2(\boldsymbol{v}, \boldsymbol{w}) = (-\boldsymbol{v}, -\boldsymbol{w}), \qquad R^4 = 1. \tag{IX.2.8}$$

A diagram containing only the two species returns to its original labels. The full oriented data do not. Electric and magnetic charge labels undergo charge conjugation, and the transverse position triplets are inverted. Calling this a literal identity would lose information precisely where masses and FI signs are to be determined. One could choose a different identification for the inverse duality; we instead keep the same S on both applications.

There is also a field-theory reason for exchanging the branch names. The scalar obtained by dualizing the D3 gauge field is interchanged by electric-magnetic duality

with the scalar arising from its interval component. Along with the exchanged transverse triplets, this gives

$$\mathcal{C}(T) \longleftrightarrow \mathcal{H}(T^\vee), \qquad \mathcal{H}(T) \longleftrightarrow \mathcal{C}(T^\vee), \qquad SU(2)_C(T) \longleftrightarrow SU(2)_H(T^\vee). \quad \text{(IX.2.9)}$$

The symbols on each side refer to the named theory's own multiplets. They are not interchangeable labels for an unqualified moduli space.

IX.2.3 Conserved charges determine the crossing

After exchanging species, the fivebranes need not sit in a convenient order for reading a gauge theory. We must move them while retaining their conserved charges. The distinction between an endpoint and a crossing is essential. A D3 that passes through a flavor D5 contributes no endpoint charge on that D5; splitting it there produces a left and a right endpoint with canceling contributions.

For a labeled fivebrane b, let $n^{\text{opp}}_{L,R}$ count opposite-species fivebranes to its left and right. Let $n^3_{L,R}$ count actual D3 endpoints whose segments extend to the corresponding side. We use

$$\ell_b = \frac{n^{\text{opp}}_R - n^{\text{opp}}_L}{2} + n^3_L - n^3_R. \quad \text{(IX.2.10)}$$

The same expression applies to NS5s and D5s. The halves reflect the noncompact flux convention, not fractional D3 multiplicity. A finite graph without external D3s satisfies

$$\sum_b \ell_b = 0. \quad \text{(IX.2.11)}$$

Each opposite-species pair contributes opposite half-units, and every segment contributes opposite endpoint terms. This total cancellation is much weaker than conservation of each individual ℓ_b.

Consider adjacent branes N, D, initially in that order, with k D3s directly joining them. Hold all other segment attachments fixed. Write h_N, h_D for their original half-count terms and A_N, A_D for the net contributions of the spectator endpoints. Before the crossing,

$$\ell_N = h_N + A_N - k, \qquad \ell_D = h_D + A_D + k. \quad \text{(IX.2.12)}$$

Passing N through D lowers h_N by one and raises h_D by one. If the new bridge multiplicity is k', its endpoint signs reverse:

$$\ell'_N = h_N - 1 + A_N + k', \qquad \ell'_D = h_D + 1 + A_D - k'. \quad \text{(IX.2.13)}$$

The two conservation equations therefore agree on a unique answer,

$$\ell'_N - \ell_N = k + k' - 1 = 0, \qquad \ell'_D - \ell_D = 1 - k - k' = 0, \qquad k' = 1 - k. \quad \text{(IX.2.14)}$$

With no initial bridge, one must be created. With one initial bridge, it is annihilated. Suppressing creation when $k = 0$ changes the two charges by $-1, +1$, even though their sum is still zero. The labels of the fivebranes let us detect the loss of charge.

A different local question allows the exterior D3s to reconnect at the crossing. Denote the consecutive interval occupancies by a, b, c, with the exchanged fivebranes bounding the middle interval. Holding a, c fixed in this adjacent-endpoint description gives

$$b' = a + c + 1 - b. \tag{IX.2.15}$$

For example, if $(a, b, c) = (0, 1, 1)$, the new middle interval still has one D3. This does not contradict creation of a bridge in (IX.2.14): the two calculations hold different exterior attachments fixed. We will first display the actual created segments, then reconnect them at aligned transverse positions.

The ranks of a completely split graph can also be recovered by summing charge over a cut in the ordered chain. Suppose the cut lies between two neighboring fivebranes, and all segments end on neighbors. Internal endpoint contributions cancel. Only pairs of opposite species lying on opposite sides of the cut contribute to the half-count sum. Thus

$$\sum_{b \in L} \ell_b = \frac{1}{2} N_{\text{opp}}(L, R) - r_{\text{cut}}, \tag{IX.2.16}$$

where r_{cut} is the number of D3s across that interval. Solving,

$$r_{\text{cut}} = \frac{1}{2} N_{\text{opp}}(L, R) - \sum_{b \in L} \ell_b. \tag{IX.2.17}$$

This reconstruction requires the order, the adjacent-endpoint description, and zero external D3 charge. The list of linking numbers alone does not specify which transverse reconnections can occur.

In the resolved configurations used here, we impose the local s-rule: at most one supersymmetric D3 joins a specified NS5 and D5. In (IX.2.14), the formal continuation $k = 2$ would give $k' = -1$, outside the positive-D3 description. This arithmetic explains why the chosen single-bridge examples are compatible with the rule; it does not derive the microscopic rule. Interpreting a sequence of such motions as a mirror duality further assumes that the infrared theory is continuous along the chosen path. These two physical requirements will accompany the charge calculation in each example.

IX.2.4 One charged hypermultiplet and a free mirror

Begin with one D3 between two NS5s and one interior flavor D5. Name the outer branes L, R and the flavor brane F_1. These labels follow individual branes throughout the motion. The initial configuration is

$$N_L \; D_{F_1} \; N_R, \qquad E_3 = \{(L, R; 1)\}, \qquad (\ell_L, \ell_{F_1}, \ell_R) = (-\tfrac{1}{2}, 0, \tfrac{1}{2}). \tag{IX.2.18}$$

Here $(a, b; n)$ means n actual D3s joining the labeled branes a, b. For example, L sees one D5 to its right and one D3 endpoint extending right, giving $1/2 - 1 = -1/2$. The interior D5 has no endpoints and has one NS5 on either side. This is $U(1)$ gauge theory with one charge-one hypermultiplet.

After RS, the same segment joins the two D5s:

$$D_L \; N_{F_1} \; D_R, \qquad E_3 = \{(L, R; 1)\}. \tag{IX.2.19}$$

Move D_L to the right of N_{F_1}. Since there was no segment between these two branes, the crossing creates one. The result is

$$N_{F_1} \; D_L \; D_R, \qquad E_3 = \{(F_1, L; 1), (L, R; 1)\}. \tag{IX.2.20}$$

The charges remain those in (IX.2.18). In particular, F_1 now sees two D5s to its right but also a D3 endpoint extending right, giving $1 - 1 = 0$. There is no interval with two NS5 endpoints. The mixed F_1–L segment is rigid; the L–R segment has two D5 endpoints and carries one hypermultiplet.

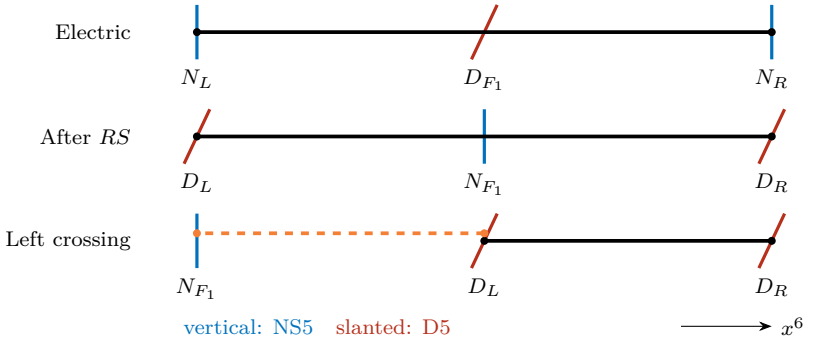


Figure IX.2.2: The one-flavor construction. Black lines are the original L–R D3, and the orange dashed line is the newly created D3. Dots mark actual endpoints; intersections without dots are not endpoints. The final mixed segment has no massless multiplet, while the D5-bounded segment carries a hypermultiplet. Vertical offsets separate strands in this schematic projection and do not specify vevs.

The brane picture predicts that the low-energy electric Coulomb degrees of freedom become those of a hypermultiplet. There is also a direct field-theory reason that the infrared theory is free. With unit magnetic flux, the $\mathcal{N} = 4$ abelian monopole charge formula gives

$$\frac{1}{2\pi} \int_{S^2} F = a \in \mathbb{Z}, \qquad \Delta(V_a) = \frac{1}{2} \sum_{i=1}^{N_f} |a| = \frac{N_f}{2} |a|. \tag{IX.2.21}$$

There are no nonabelian roots to subtract for $U(1)$. For one charge-one hyper, the two minimal monopoles have

$$\Delta(V_+) = \Delta(V_-) = \frac{1}{2}. \tag{IX.2.22}$$

At the infrared superconformal point these chiral scalars saturate the three-dimensional scalar unitarity bound and belong to a free hypermultiplet. They transform with the

electric Coulomb R-symmetry, so this is a *twisted* hypermultiplet in electric language. It is an ordinary hypermultiplet in the mirror's own labeling, as required by (IX.2.9). This argument is specific to the minimal charge-one theory and its infrared limit.

The electric Higgs branch is a useful contrasting calculation. At zero FI its single pair of hyper scalars obeys

$$q\widetilde{q} = 0, \qquad |q|^2 - |\widetilde{q}|^2 = 0 \quad \Longrightarrow \quad q = \widetilde{q} = 0. \tag{IX.2.23}$$

Thus the Higgs branch is a point, although the gauge action there is not free. In quaternionic dimensions, using each theory's own labels,

$$(\dim_{\mathbb{H}} \mathcal{H}, \dim_{\mathbb{H}} \mathcal{C})_T = (0,1), \qquad (\dim_{\mathbb{H}} \mathcal{H}, \dim_{\mathbb{H}} \mathcal{C})_{T^\vee} = (1,0). \tag{IX.2.24}$$

The finite-coupling electric Coulomb metric is not the flat free-field metric globally. The free interpretation concerns the infrared limit. Chapter 3 will distinguish this limit from the finite-coupling geometry.

IX.2.5 Two flavors and self-mirror symmetry

With two flavor branes, the electric starting point is

$$N_L \; D_{F_1} \; D_{F_2} \; N_R, \qquad E_3 = \{(L,R;1)\}, \qquad (\ell_L, \ell_{F_1}, \ell_{F_2}, \ell_R) = (0,0,0,0). \tag{IX.2.25}$$

The left NS5 now has half-count one and endpoint contribution minus one. All four conserved charges vanish. Apply RS and retain the same actual D3 attachment:

$$D_L \; N_{F_1} \; N_{F_2} \; D_R, \qquad E_3 = \{(L,R;1)\}. \tag{IX.2.26}$$

Move D_L through N_{F_1} and D_R through N_{F_2}. Both initial bridges are absent, so each move creates one D3. The intermediate endpoint graph is

$$N_{F_1} \; D_L \; D_R \; N_{F_2}, \qquad E_3 = \{(F_1,L;1), (L,R;1), (R,F_2;1)\}. \tag{IX.2.27}$$

Each fivebrane still has zero linking number. At D_L, for instance, the left and right D3 endpoints cancel; the two NS5s also contribute opposite half-counts.

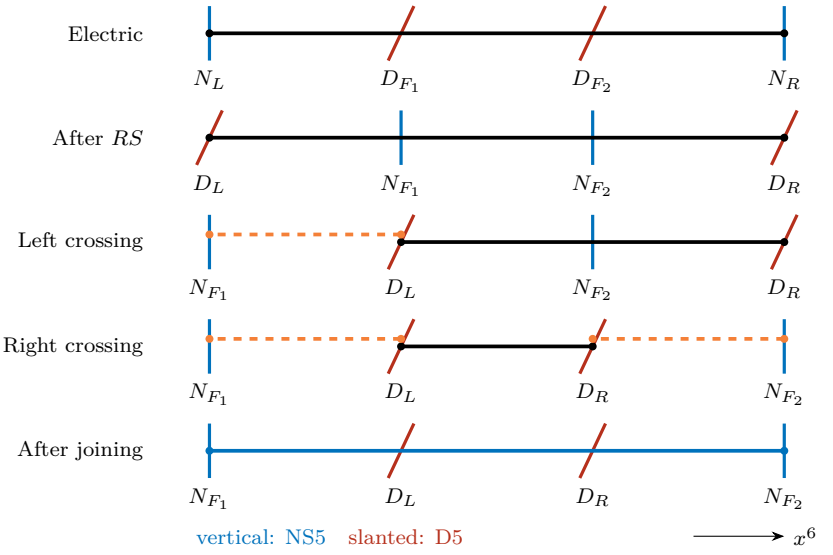


Figure IX.2.3: The two-flavor electric theory returns to the same gauge and matter content. The two orange dashed bridges are created by crossings. Only after aligning the transverse positions do the three pieces join into the blue D3, which passes through both D5s. The interior D5–D5 piece before joining is not an additional decoupled hypermultiplet of the joined gauge description.

At the undeformed common point, join the three segments at D_L, D_R. The joined graph is

$$E_3^{\text{joined}} = \{(F_1, F_2; 1)\}, \qquad G^\vee = U(1), \qquad N_f^\vee = 2. \tag{IX.2.28}$$

The two D5s are now interior flavor branes of an NS5-bounded interval. The joining requires equal transverse positions; the construction of this Lagrangian presentation is performed at the common zero-mass, zero-FI point. One subsequently restores the external deformations and identifies their map. This does not assert that the same pure branch survives at every deformation.

One orientation of the two mirror hyper charges is

$$Q^\vee = (-1, 1), \qquad (q_1, \widetilde{q}_1) \mapsto (\widetilde{q}_1, -q_1) \quad \Longrightarrow \quad Q^\vee = (1, 1). \tag{IX.2.29}$$

The transformation exchanges the two conjugate chiral representations of the first hyper and changes its signed complex moment map. Its mass marker must be transformed with it. The paired representation is the same in either notation; the explicit sign will matter in the self-mirror parameter map below.

For the undeformed branch dimensions the two descriptions agree:

$$\dim_{\mathbb{H}} \mathcal{H} = 2 - 1 = 1, \qquad \dim_{\mathbb{H}} \mathcal{C} = \operatorname{rank} U(1) = 1. \tag{IX.2.30}$$

This agreement is compatible with mirror symmetry, but the two equal numbers cannot tell us whether Higgs and Coulomb branches were actually exchanged. Nor does self-

mirror mean that the microscopic charged hypers are identical to the monopoles. The same abelian formula now gives

$$\Delta(V_\pm) = 1 \qquad (N_f = 2). \tag{IX.2.31}$$

The free-field argument of the preceding section no longer applies. The self-mirror statement concerns the infrared interacting theory; the brane exchange identifies its two distinct branch descriptions. To see rank and dimension exchange without this numerical coincidence, we next add a third flavor.

IX.2.6 Three flavors and a two-node mirror

The next example has an asymmetric answer. Start with one color D3 and three interior D5s,

$$N_L \; D_{F_1} \; D_{F_2} \; D_{F_3} \; N_R, \qquad E_3 = \{(L, R; 1)\}. \tag{IX.2.32}$$

The five individual linkings are

$$\ell_L = \frac{3}{2} - 1 = \frac{1}{2}, \qquad \ell_{F_i} = 0, \qquad \ell_R = -\frac{3}{2} + 1 = -\frac{1}{2}. \tag{IX.2.33}$$

All flavor D5s are spectators to the original endpoints. After RS,

$$D_L \; N_{F_1} \; N_{F_2} \; N_{F_3} \; D_R, \qquad E_3 = \{(L, R; 1)\}, \tag{IX.2.34}$$

with the same linkings attached to the same labels. Move the two outer D5s inward past the nearest NS5s. The first crossing gives

$$N_{F_1} \; D_L \; N_{F_2} \; N_{F_3} \; D_R, \qquad E_3 = \{(F_1, L; 1), (L, R; 1)\}. \tag{IX.2.35}$$

The second crossing gives

$$N_{F_1} \; D_L \; N_{F_2} \; D_R \; N_{F_3}, \qquad E_3 = \{(F_1, L; 1), (L, R; 1), (R, F_3; 1)\}. \tag{IX.2.36}$$

These are two actual creations with the old L–R attachment held fixed. For example, in the final order D_L sees one NS5 on the left and two on the right. Its two D3 endpoint contributions cancel, so its linking is still $(2 - 1)/2 = 1/2$.

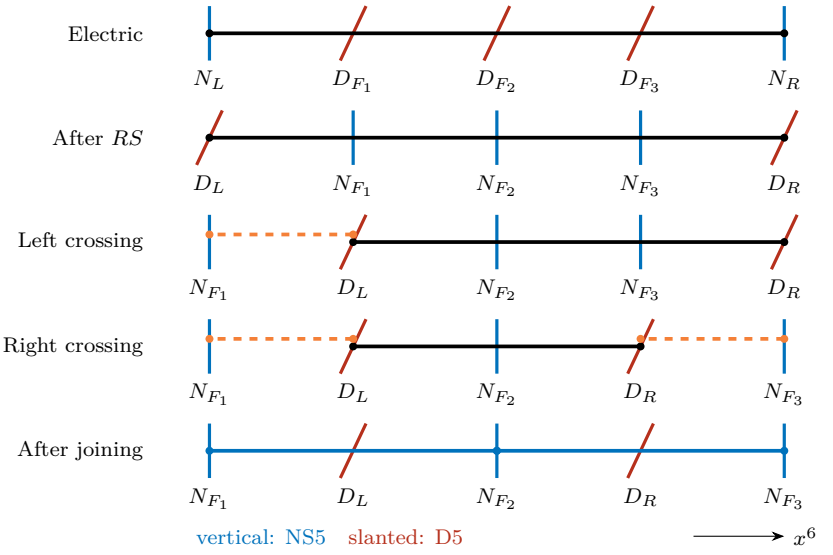


Figure IX.2.4: The finite three-flavor move. Crossings create the orange bridges while preserving the black L–R attachment. At the common transverse point, that attachment splits at N_{F_2}, and joining at D_L, D_R produces the two blue NS5-bounded intervals. Their common NS5 supplies the bifundamental; the two D5s supply the endpoint flavors. The through-line at an intermediate NS5 is separated from the reconnected description in the last panel.

To reach the gauge description, bring the pieces to coincident transverse positions. Split the L–R segment at N_{F_2}, then join at D_L and D_R. We obtain

$$E_3^{\text{joined}} = \{(F_1, F_2; 1), (F_2, F_3; 1)\}. \tag{IX.2.37}$$

At the central NS5 the two endpoints remain distinct ends of the two gauge intervals. At each D5 there is a through-going D3 and a flavor hypermultiplet. The two NS5 intervals give two gauge factors.

We can recover their ranks without anticipating the answer. Temporarily split at every fivebrane in the final order and apply (IX.2.17). For the four cuts, respectively after F_1, L, F_2, R, the required numbers are

cut after	F_1	L	F_2	R
$N_{\text{opp}}(L,R)$	2	3	3	2
$\sum_{b\in L}\ell_b$	0	$\frac{1}{2}$	$\frac{1}{2}$	0
r_{cut}	1	1	1	1

. (IX.2.38)

Equal occupancies on both sides of each interior D5 permit the pieces to join. Consequently the ranks between successive NS5s are

$$(r_1, r_2) = (1, 1), \qquad G^\vee = U(1)_1 \times U(1)_2. \tag{IX.2.39}$$

The rank count has followed from the chosen order and the individual conserved charges. It was not obtained by guessing a linear quiver.

Choose one chiral field from each hyper and order them as left flavor, bifundamental, right flavor. The charges are

$$\begin{array}{c|ccc} & q_1 & q_2 & q_3 \\ \hline U(1)_1 & -1 & 1 & 0 \\ U(1)_2 & 0 & -1 & 1 \end{array}, \qquad Q = \begin{pmatrix} -1 & 1 & 0 \\ 0 & -1 & 1 \end{pmatrix}. \tag{IX.2.40}$$

Each $\widetilde{q}_i$ has the opposite column. The central hyper couples both gauge intervals; either endpoint hyper couples just one. A drawing that retains only the central link therefore describes a different theory.

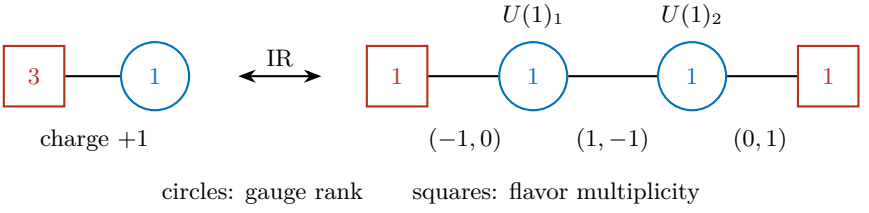


Figure IX.2.5: The electric three-flavor theory and its framed two-node mirror. Circles are dynamical $U(1)$ gauge factors and squares are flavor groups. Each edge denotes a full hypermultiplet, with one displayed charge column and its conjugate. The electric flavor square has multiplicity three; the mirror has one flavor at each end and the central $(1,-1)$ hypermultiplet.

The inverse motion reverses the crossings and the reconnections. Since each elementary crossing obeys the individual charge equations, it recovers the initial segment multiplicities. Applying the same RS again also returns the species, but retains the charge-conjugation and transverse-inversion action of (IX.2.8). These finite operations use aligned transverse positions and the resolved local s-rule. They do not specify a reconstruction for arbitrary nonabelian ranks, winding D3s, or physical circular arrangements.

IX.2.7 Gauge lattices and branch dimensions

The two-node theory has a second useful description. It can be written as an affine three-node abelian quiver with a redundant diagonal gauge factor removed. Showing the equivalence at the charge-lattice level prevents two common mistakes: losing an endpoint flavor and removing one gauge factor twice.

Use the affine incidence matrix

$$Q_{\mathrm{aff}} = \begin{pmatrix} -1 & 1 & 0 \\ 0 & -1 & 1 \\ 1 & 0 & -1 \end{pmatrix}, \qquad G_{\mathrm{aff}} = U(1)^3/U(1)_{\mathrm{diag}}. \tag{IX.2.41}$$

For phases (g_1, g_2, g_3), its action on the three hypers depends only on phase ratios. There is a global integral choice of representative,

$$[(g_1, g_2, g_3)] \longmapsto (g_1/g_3, g_2/g_3, 1). \tag{IX.2.42}$$

Deleting the redundant third row in this representative leaves (IX.2.40). No fractional phase or finite covering is involved. What were links to the third node become the two endpoint flavors. This algebraic presentation does not add a compact suspension circle to the brane construction.

The distinction between the redundant and faithful actions is explicit:

$$\ker Q_{\mathrm{aff}}^T = \mathbb{R}(1,1,1), \qquad \ker Q^T = 0, \qquad \det \begin{pmatrix} -1 & 1 \\ 0 & -1 \end{pmatrix} = 1. \tag{IX.2.43}$$

The determinant also rules out a finite ineffective subgroup of the two-node gauge torus. In elementary terms, a transformation acting trivially on the left endpoint hyper must have $g_1 = 1$, and the right endpoint similarly forces $g_2 = 1$. Hence there is no additional free diagonal gauge $U(1)$ to discard.

The FI count follows from the same charge matrix. The three affine moment maps sum to zero, whereas the two framed moment maps are independent:

$$\zeta_1^{\mathrm{aff}} + \zeta_2^{\mathrm{aff}} + \zeta_3^{\mathrm{aff}} = 0, \qquad (\zeta_1, \zeta_2) \text{ unrestricted}, \qquad \zeta_3^{\mathrm{aff}} = -\zeta_1 - \zeta_2. \tag{IX.2.44}$$

Imposing another sum-zero condition on the two remaining levels would remove a physical parameter. Framing has made the full two-node gauge action faithful.

We now count branch dimensions from the representations. On a regular moment-map level with free effective compact gauge action, the three real moment maps remove $3 \dim G$ real dimensions and the gauge quotient removes another $\dim G$. Therefore

$$\dim_{\mathbb{R}} \mathcal{H} = 4 \dim_{\mathbb{H}} V - 4 \dim_{\mathbb{R}} G, \qquad \dim_{\mathbb{H}} \mathcal{H} = \dim_{\mathbb{H}} V - \dim_{\mathbb{R}} G. \tag{IX.2.45}$$

For $U(1)$ with three charge-one hypers, $\dim_{\mathbb{H}} V = 3$ and $\dim G = 1$. For the mirror, each endpoint fundamental and the bifundamental has quaternionic dimension one. Thus

$$\dim_{\mathbb{H}} \mathcal{H}(T) = 3 - 1 = 2, \qquad \dim_{\mathbb{H}} \mathcal{H}(T^\vee) = (1+1+1) - (1+1) = 1. \tag{IX.2.46}$$

At an unlifted generic abelian Coulomb point, the vector scalar triplet and dual photon give four real coordinates per Cartan factor:

$$\dim_{\mathbb{H}} \mathcal{C}(T) = \operatorname{rank} U(1) = 1, \qquad \dim_{\mathbb{H}} \mathcal{C}(T^\vee) = \operatorname{rank} U(1)^2 = 2. \tag{IX.2.47}$$

The unequal pair $(2,1)$ is exchanged with $(1,2)$. A mere repetition of the electric dimensions would fail this comparison, unlike the two-flavor self-mirror example.

It is useful to exhibit a point where the quotient hypotheses hold. In the mirror at zero moment-map level take $q_i = \widetilde{q}_i = 1$ for all three hypers. If $q_i = x_i + iy_i$ and $\widetilde{q}_i = u_i + iv_i$, linearization at this point gives

$$\delta \boldsymbol{\mu}_R = 2Q(\delta x - \delta u), \qquad \delta \operatorname{Re} \boldsymbol{\mu}_C = Q(\delta x + \delta u), \qquad \delta \operatorname{Im} \boldsymbol{\mu}_C = Q(\delta y + \delta v). \tag{IX.2.48}$$

Since Q has rank two, the constraint derivative has real rank six. The gauge orbit has rank two and no discrete stabilizer at this point. The local dimension is indeed

$$12 - 6 - 2 = 4 \quad \text{real dimensions.} \tag{IX.2.49}$$

This explicit regular locus is different from the origin, where the stabilizer is nontrivial and the constraint derivative vanishes. The count concerns the top branch, not its singular tangent space. The one-flavor origin was instead solved directly in (IX.2.23).

Finally, deleting a single endpoint hyper changes the mirror count to $2 - 2 = 0$ for a fully Higgsed quotient. Deleting both endpoints is a different operation: the remaining bifundamental leaves a common gauge phase ineffective, so subtracting the original two-dimensional gauge group is no longer justified. Matter content and effective gauge action must be determined before applying the dimension formula.

IX.2.8 Relative masses and FI parameters

The rank map tells us which fields occur. Their external parameters follow from the same signed spatial transformation. A D5's position in 345 sets a hypermultiplet mass. An NS5 displacement in 789 sets an FI parameter. Exchanging the species and the two three-planes must therefore exchange these two kinds of deformation. To determine the independent parameters, we must also quotient out changes of scalar origin and retain the orientation of every hyper charge.

Use physical length coordinates and first write real triplets. The electric vector scalar and flavor masses are

$$\boldsymbol{\phi} = \frac{\boldsymbol{v}_{D3}}{2\pi\alpha'}, \qquad \boldsymbol{m}_i = \frac{\boldsymbol{v}_{F_i}}{2\pi\alpha'}, \qquad M_i^2 = |\boldsymbol{\phi} - \boldsymbol{m}_i|^2. \tag{IX.2.50}$$

A simultaneous translation of all masses and the vector scalar leaves every physical mass invariant:

$$\boldsymbol{m}_i \mapsto \boldsymbol{m}_i + \boldsymbol{c}, \quad \boldsymbol{\phi} \mapsto \boldsymbol{\phi} + \boldsymbol{c}, \qquad \overline{\boldsymbol{m}}_i = \boldsymbol{m}_i - \frac{1}{n}\sum_{a=1}^{n} \boldsymbol{m}_a. \tag{IX.2.51}$$

There are $n - 1$ independent mass triplets. This translation does not remove the gauge photon; a charge-one hyper still transforms under the electric $U(1)$. A useful basis is

$$\boldsymbol{d}_j = \boldsymbol{m}_j - \boldsymbol{m}_{j+1} \quad (j = 1, \ldots, n-1). \tag{IX.2.52}$$

The brane ordering fixes the left-minus-right sign in this definition. In the mirror, the new NS5 positions satisfy $\boldsymbol{w}'_{F_i} = \boldsymbol{v}_{F_i}$, so their adjacent displacements are precisely the electric differences before conversion to FI units.

We retain a specific restriction on the absolute conversion. Chapter 1 matched the leading small-slope classical D3 tension cost to the canonical auxiliary-field potential. In that approximation,

$$\begin{aligned} \Delta\mathcal{E} &= \frac{\tau_3}{2L_6}|\Delta\boldsymbol{w}|^2 + \cdots, \quad & V(0) &= \frac{e_3^2}{2}|\boldsymbol{\zeta}|^2, \\ \tau_3 &= \frac{1}{(2\pi)^3 g_s \alpha'^2}, & e_3^2 &= \frac{2\pi g_s}{L_6}. \end{aligned} \tag{IX.2.53}$$

The magnitude follows by equating the quadratic terms; the sign is chosen independently as the NS5 left-minus-right displacement:

$$\boldsymbol{\zeta} = \frac{\boldsymbol{w}_L - \boldsymbol{w}_R}{4\pi^2 g_s \alpha'}. \tag{IX.2.54}$$

Equation (IX.2.54) is conditional on that leading classical match. It is not an exact finite-slope or quantum normalization. For our absolute-unit mirror example take $C_0 = 0$, $g_s = 1$, hence $\tau = i$, where S leaves the asymptotic frame unchanged. Then

$$\boldsymbol{\zeta}'_j = \frac{\boldsymbol{v}_{F_j} - \boldsymbol{v}_{F_{j+1}}}{4\pi^2 \alpha'} = \frac{\boldsymbol{d}_j}{2\pi}, \qquad \boldsymbol{\eta}_j \equiv 2\pi \boldsymbol{\zeta}'_j = \boldsymbol{d}_j. \tag{IX.2.55}$$

The differences and their signs follow from positions. The factor 2π inherits the stated classical normalization premise. At generic g_s, S also changes the string-frame units and coupling; we do not extend this absolute formula to that case.

For the two-node mirror, assign mass markers $\boldsymbol{b}_i$ to its three oriented hyper columns. Their effective masses are $Q_i \cdot \boldsymbol{\phi}' - \boldsymbol{b}_i$. A shift of the two vector scalars changes the markers by an element of $\operatorname{im} Q^T$:

$$\boldsymbol{\phi}' \mapsto \boldsymbol{\phi}' + \boldsymbol{\delta}, \qquad \boldsymbol{b} \mapsto \boldsymbol{b} + Q^T \boldsymbol{\delta}, \qquad Q \begin{pmatrix} 1 \\ 1 \\ 1 \end{pmatrix} = 0. \tag{IX.2.56}$$

Consequently the primitive surviving mass triplet is

$$\boldsymbol{B} = \boldsymbol{b}_1 + \boldsymbol{b}_2 + \boldsymbol{b}_3. \tag{IX.2.57}$$

It is a sum, rather than a difference, because the endpoint and bifundamental charges have the orientation in (IX.2.40). The integer kernel vector has coprime entries; B is not a fractional or multiply covered mass coordinate.

Choose a representative with the internal hyper mass zero. If $\boldsymbol{m}'_L, \boldsymbol{m}'_R$ are the two new D5 positions in mass units, the endpoint charges give

$$\boldsymbol{b}_1 = -\boldsymbol{m}'_L, \qquad \boldsymbol{b}_2 = 0, \qquad \boldsymbol{b}_3 = \boldsymbol{m}'_R, \qquad \boldsymbol{m}'_{L,R} = -\frac{\boldsymbol{w}_{L,R}}{2\pi\alpha'}. \tag{IX.2.58}$$

The last minus sign is the active rotation, not a change in the FI definition. Substitution yields the reverse parameter map,

$$\boldsymbol{B} = \boldsymbol{m}'_R - \boldsymbol{m}'_L = \frac{\boldsymbol{w}_L - \boldsymbol{w}_R}{2\pi\alpha'} = 2\pi\boldsymbol{\zeta} \qquad (\tau = i). \tag{IX.2.59}$$

For one flavor the same expression is the free mirror hyper's mass. For two flavors it is the sum of the two oriented markers. After conjugating the left hyper to the two-positive-charge convention, the mirror mass difference is $-B$. Thus the oriented self-mirror map for one relative mass d and one FI level is

$$\begin{pmatrix} d' \\ \zeta' \end{pmatrix} = \begin{pmatrix} 0 & -2\pi \\ 1/(2\pi) & 0 \end{pmatrix} \begin{pmatrix} d \\ \zeta \end{pmatrix}, \qquad \begin{pmatrix} d'' \\ \zeta'' \end{pmatrix} = -\begin{pmatrix} d \\ \zeta \end{pmatrix}. \tag{IX.2.60}$$

This is the parameter version of the signed double operation, not an identity matrix hidden by the self-mirror gauge graph.

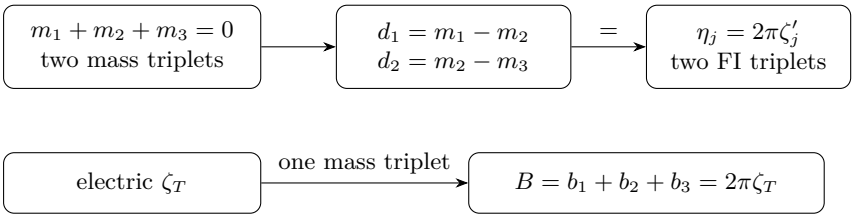


Figure IX.2.6: Independent parameter bases for the asymmetric pair. The common electric mass shift is removed. The two relative masses map to the two mirror FI levels, and the electric FI maps to the primitive sum of the mirror mass markers. The absolute 2π conversion is restricted to $\tau = i$ and the leading classical normalization stated in the text.

In counts of real triplets, the complete parameter correspondence for these examples is

N_f	$\#m_T$	$\#\zeta_T$	$\#m_{T^\vee}$	$\#\zeta_{T^\vee}$
1	0	1	1	0
2	1	1	1	1
3	2	1	1	2

. (IX.2.61)

These are parameters of the theories. Their existence does not imply that every branch survives when they are nonzero.

For a holomorphic calculation we must specify how triplets become complex scalars. Use the same projection for every triplet,

$$a_C = \frac{a_1 + ia_2}{2}, \qquad a_R = a_3, \qquad \boldsymbol{\mu} = (2\,\mathrm{Re}\, q\widetilde{q}, 2\,\mathrm{Im}\, q\widetilde{q}, |q|^2 - |\widetilde{q}|^2). \tag{IX.2.62}$$

It gives $\mu_C = q\widetilde{q}$ and $\mu_R = |q|^2 - |\widetilde{q}|^2$. For the canonical superpotential normalization $W = \sqrt{2}\widetilde{q}\Phi q$, the chiral scalar and physical triplet coordinate are related by $\Phi = \sqrt{2}\phi_C$. Hence

$$M_i^2 = (\phi_R - m_{i,R})^2 + 4|\phi_C - m_{i,C}|^2. \tag{IX.2.63}$$

The factor four is required by the common half-projection. Applying this projection to both sides of (IX.2.55) preserves its linear parameter map. We will suppress the subscript C only within the complex algebraic comparison in the next section.

IX.2.9 A deformed branch from elementary mirror fields

Branch dimensions cannot tell whether the two independent relative masses were mapped correctly. A more informative comparison keeps both complex deformations and follows the polynomial relation among branch coordinates. We can derive the

mirror side directly from its three elementary hypermultiplets. The electric side requires quantum Coulomb-branch information, which we will state as an input.

First specify the vacua being compared. We set the full electric FI triplet to zero and the primitive mirror mass to zero:

$$\boldsymbol{\zeta}_T = 0, \qquad \boldsymbol{B} = 0. \tag{IX.2.64}$$

These are corresponding conditions under the parameter map. For the affine complex quotient below we also set the real mirror FI components to zero and allow the two complex mirror FI components to vary. This last choice selects the complex deformation comparison; it is not a restriction on the existence of FI resolutions elsewhere.

The electric condition has a direct physical reason. A pure Coulomb vacuum has $q_i = \widetilde{q}_i = 0$. Eliminating the real and complex auxiliary fields with the normalization of Chapter 1 gives

$$V\big|_{q=\widetilde{q}=0} = \frac{e_3^2}{2}\zeta_R^2 + 2e_3^2|\zeta_C|^2 = \frac{e_3^2}{2}|\boldsymbol{\zeta}_T|^2. \tag{IX.2.65}$$

It vanishes only at zero FI triplet. A nonzero electric FI parameter therefore removes this pure supersymmetric Coulomb locus; it does not rule out Higgs vacua or isolated supersymmetric vacua.

There is an equally explicit mirror reason. On the dense Higgs patch where every hypermultiplet is nonzero, each effective mass must vanish. Using the three columns of (IX.2.40), the vector equations are

$$-\boldsymbol{\varphi}_1 - \boldsymbol{b}_1 = 0, \qquad \boldsymbol{\varphi}_1 - \boldsymbol{\varphi}_2 - \boldsymbol{b}_2 = 0, \qquad \boldsymbol{\varphi}_2 - \boldsymbol{b}_3 = 0. \tag{IX.2.66}$$

Their sum is $-\boldsymbol{B} = 0$. If $\boldsymbol{B}$ is nonzero, no choice of the two vector-multiplet scalars can make this patch supersymmetric. Conversely, when $\boldsymbol{B} = 0$, the first and last equations determine the two scalars and the middle one follows. Thus the restriction is tied to the branch under study. We will not extend the polynomial below to nonzero electric FI or nonzero primitive mirror mass.

Now take the complex quotient. Write the canonical mirror fields as $(q_i, \widetilde{q}_i)$, $i = 1, 2, 3$. The complex moment maps in the faithful charge basis are

$$-q_1\widetilde{q}_1 + q_2\widetilde{q}_2 = \zeta'_{1,C}, \qquad -q_2\widetilde{q}_2 + q_3\widetilde{q}_3 = \zeta'_{2,C}. \tag{IX.2.67}$$

The parameter correspondence was simplest in terms of $\eta_j = 2\pi\zeta'_{j,C}$. To use these coordinates in the algebra, define new variables

$$u_i = \sqrt{2\pi}\, q_i, \qquad v_i = \sqrt{2\pi}\, \widetilde{q}_i, \qquad s_i = u_i v_i. \tag{IX.2.68}$$

The u_i, v_i are algebraic coordinates, not canonically normalized fields. In particular, this rescaling alone is not a claim about a normalized metric or holomorphic symplectic form. It gives

$$-s_1 + s_2 = \eta_1, \qquad -s_2 + s_3 = \eta_2, \qquad z = \frac{s_1 + s_2 + s_3}{3}. \tag{IX.2.69}$$

Solving these three linear equations yields

$$s_1 = z - \frac{2\eta_1 + \eta_2}{3}, \qquad s_2 = z + \frac{\eta_1 - \eta_2}{3}, \qquad s_3 = z + \frac{\eta_1 + 2\eta_2}{3}. \tag{IX.2.70}$$

The centered coordinate z is convenient precisely because the common mass shift has already been removed on the electric side.

We must still find the gauge-invariant coordinates; solving moment maps is not by itself taking a quotient. The obvious invariants are s_i and

$$X = u_1u_2u_3, \qquad Y = v_1v_2v_3, \qquad XY = s_1s_2s_3. \tag{IX.2.71}$$

To see that these suffice, consider any invariant monomial $\prod_i u_i^{a_i} v_i^{c_i}$, with nonnegative integral exponents. Its charge vanishes if and only if

$$Q(\boldsymbol{a}-\boldsymbol{c}) = 0 \quad \Longleftrightarrow \quad \boldsymbol{a}-\boldsymbol{c} = k(1,1,1), \qquad k \in \mathbb{Z}. \tag{IX.2.72}$$

For $k \geq 0$ the monomial is $X^k \prod_i s_i^{c_i}$; for $k < 0$ it is $Y^{-k} \prod_i s_i^{a_i}$. Every invariant polynomial is a sum of such monomials. Products containing both X and Y reduce by $XY = s_1s_2s_3$; the remaining monomials have distinct exponent vectors, so there is no further relation before imposing the moment maps. Substituting (IX.2.70) therefore gives the affine complex Higgs quotient explicitly:

$$XY = \left(z - \frac{2\eta_1+\eta_2}{3}\right)\left(z + \frac{\eta_1-\eta_2}{3}\right)\left(z + \frac{\eta_1+2\eta_2}{3}\right). \tag{IX.2.73}$$

This derivation used the elementary mirror fields, their integral charges and two moment-map equations.

The independent field-theory input is the quantum electric Coulomb ring for abelian SQED. In compatible complex coordinates it reads

$$V_+V_- = \prod_{i=1}^{N_f}(\phi - m_i). \tag{IX.2.74}$$

Here $V_\pm$ are operators of magnetic charge ±1 and ϕ is the complex vector-multiplet scalar. The quantum relation is not derived by the elementary Higgs quotient above. Its operator normalization allows constant rescalings, which must be fixed when comparing algebraic coordinates. We use (IX.2.74) with the same half-projection as in (IX.2.62). For three centered masses, the parameter map has the inverse

$$m_1 = \frac{2\eta_1+\eta_2}{3}, \qquad m_2 = \frac{-\eta_1+\eta_2}{3}, \qquad m_3 = \frac{-\eta_1-2\eta_2}{3}, \qquad \sum_i m_i = 0. \tag{IX.2.75}$$

Consequently (IX.2.73) agrees with the electric relation under $z = \phi$, $X = V_+$, $Y = V_-$. It compares a two-parameter family of holomorphic relations. It establishes neither equality of branch metrics nor equality of the full quantum theories.

For a concrete asymmetric deformation choose

$$(m_1, m_2, m_3) = (-4, 1, 3), \qquad (\eta_1, \eta_2) = (-5, -2). \tag{IX.2.76}$$

All numbers are expressed in a common mass unit. The mirror equations give $(s_1, s_2, s_3) = (z+4, z-1, z-3)$, and hence

$$XY = (z+4)(z-1)(z-3) = z^3 - 13z + 12. \tag{IX.2.77}$$

The pairwise root separations remember both relative deformations. For a monic cubic $z^3 + pz + q$, their squared product is

$$\Delta = \prod_{i<j}(m_i - m_j)^2 = -4p^3 - 27q^2, \qquad \Delta = 25 \cdot 49 \cdot 4 = 4900. \tag{IX.2.78}$$

A change in only one FI sign is physically distinguishable from a common change of orientation. If one instead takes $(\eta_1, \eta_2) = (5, -2)$ while leaving the charge basis fixed, the roots and the polynomial become

$$(m_1, m_2, m_3) = \left(\frac{8}{3}, -\frac{7}{3}, -\frac{1}{3}\right), \qquad P(z) = z^3 - \frac{19}{3}z - \frac{56}{27}, \qquad \Delta = 25 \cdot 9 \cdot 4 = 900. \tag{IX.2.79}$$

These are different deformations, even though they have the same number of parameters and the same branch dimension. The root separations in Figure IX.2.7 display the difference. A simultaneous permutation of all masses would leave the polynomial unchanged; a single relative-sign error does not have that protection.

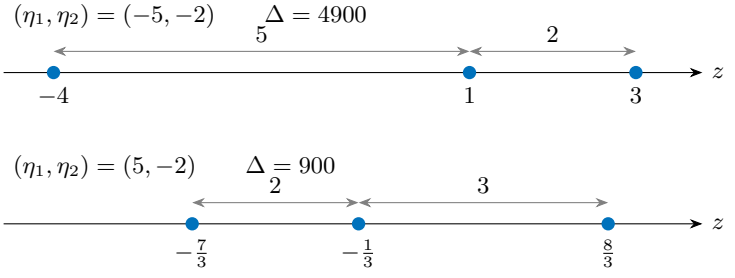


Figure IX.2.7: The roots of the two centered cubics in a common real slice. The original relative FI values give consecutive separations $5, 2$; changing only η_1 gives $2, 3$. The squared product of all three pair separations changes from 4900 to 900.

Several simpler limits clarify the meaning of the result. At zero complex deformation the relation is $XY = z^3$. If two masses coincide, its discriminant vanishes; the polynomial then retains a repeated root. For the two-flavor example the same elementary calculation has $Q = (-1, 1)$, one moment map, and centered masses $\pm\eta/2$:

$$s_2 - s_1 = \eta, \qquad z = \frac{s_1 + s_2}{2}, \qquad XY = s_1 s_2 = z^2 - \frac{\eta^2}{4}. \tag{IX.2.80}$$

Its symmetry under $\eta \mapsto -\eta$ explains why that example cannot by itself determine a relative sign between two different FI parameters. Finally, a single ungauged hypermultiplet has independent coordinates u, v and $z = uv$:

$$X = u, \qquad Y = v, \qquad XY = z, \qquad \mathbb{C}[X, Y, z]/(XY - z) \simeq \mathbb{C}[X, Y]. \tag{IX.2.81}$$

This algebra is consistent with the free mirror. Its metric statement still relies on the infrared and unitarity argument given earlier. Real FI resolutions, exceptional cycles and the metric interpretation of these surfaces are the subject of Chapter 3.

IX.2.10 What the mirror construction establishes

The finite examples exhibit a mechanism, rather than a prescription that guesses a quiver from the number of flavors. We exchanged oriented fivebrane species, restored the axes, conserved the linking of each labeled fivebrane, and specified when a newly created D3 was joined to an existing one. The endpoint rules then produced the gauge fields and all matter representations. Keeping both endpoint flavors in the three-flavor mirror was essential: omitting either one would change the gauge action and the Higgs quotient.

The representation calculation gives a first consistency condition. The two pairs of branch dimensions exchange as required. The parameter calculation adds considerably more information. A common electric mass shift is absorbed into the vector scalar; its remaining differences become independent mirror FI parameters. The mirror masses have one primitive gauge-invariant combination, paired with the electric FI triplet. The explicit orientation keeps track of the sign that a second S transformation leaves behind. Two transformations return the species labels, but act by charge conjugation on the oriented data.

The asymmetric quotient then tests the correspondence where dimensions alone are insensitive. Two independently adjustable relative masses specify three centered roots. The mirror elementary fields reproduce these roots and their product, while the electric quantum ring supplies the independent comparison. The comparison applies on the specified pure branches. Nonzero electric FI or nonzero primitive mirror mass requires a different vacuum analysis, not substitution into the same cubic.

Several physical ingredients remain indispensable. The IIB duality, the local creation law and s-rule, and infrared continuity along the chosen motions are inputs. Neither charge arithmetic nor an algebraic branch relation proves them. Likewise, finite gauge coupling retains metric information that need not be mirrored by a weakly coupled Lagrangian. The free one-flavor infrared theory has a special unitarity argument; it does not justify calling every simple Coulomb branch free.

Chapter 3 takes the branch exchange further, including the meaning of complex deformations and real resolutions. Chapter 4 returns to the same duality through boundary conditions. Circular arrangements, nonabelian rank reconstruction and more general fivebrane charges need additional hypotheses and are outside the construction established here. A useful preparation for those topics is to repeat the three finite paths while retaining each endpoint label, and then to recover the two relative masses from the two mirror moment maps without using branch dimensions as a guide.

Status and sources

The source notes distinguish finite interval calculations from the physical premises of the infrared mirror map.

The principal brane source is Hanany–Witten (HW), `hep-th/9611230v3` (Hanany and Witten 1997). Other sources are Intriligator–Seiberg (IS), `hep-th/9607207v1` (Intriligator and Seiberg 1996); de Boer et al., `hep-th/9612131v1` (Boer et al. 1997); Gaiotto–Witten (GW), `0807.3720v1` (Gaiotto and Witten 2009); and Bullimore–Dimofte–Gaiotto (BDG), `1503.04817v2` (Bullimore et al. 2017). Page anchors below are printed source pages.

§IX.2.2 Oriented IIB operation. [DUAL]: equations (IX.2.1)–(IX.2.9) specify the bosonic S/rotation convention. HW §2, (2.5) and the following paragraph, pp. 3–4, supply the duality and restoring rotation. The chosen active matrix and its tangent-orientation consequences are calculated here. GW §4.3.2, p. 95, supplies the $S^2 = C$ interpretation. The spinor lift is outside this calculation. The route uses nonperturbative IIB S-duality, a coordinate rotation and separate brane creation and infrared-continuation assumptions. Only the rotation is a coordinate/field redefinition; linking conservation is not a proof of the nonperturbative generator.

§IX.2.3–§IX.2.6 Finite paths and spectra. [MATH]: under the sourced linking law, fixed spectator endpoints, adjacent branes and zero exterior D3 charge where required, equations (IX.2.10)–(IX.2.17) are finite conservation identities. [GEO-E]: the individual paths (IX.2.18)–(IX.2.20), (IX.2.25)–(IX.2.28), (IX.2.32)–(IX.2.39) are conditional brane constructions using the endpoint dictionary. HW §5, (5.9)–(5.10), p. 23 supplies the linking law; §5.2, p. 28 supplies the scoped s-rule. HW §5.1, Fig. 9, pp. 24–26; §6.1, Fig. 12, pp. 29–30; and §6.2, Figs. 16–17, pp. 36–38 support the three selected constructions. GW §2.2.2, pp. 12–13 uses an integer-shifted linking convention, $\ell_{\mathrm{GW}} = N_{\mathrm{opposite}}/2 - \ell_{\mathrm{HW}}$; it is not silently substituted here. GW §2.3, pp. 15–17 supports the motion discussion. Zero-deformation alignment and infrared continuity of the specified reconnections remain hypotheses. There is no general rank-reconstruction theorem.

[GEO-E]: the endpoint interpretation and (IX.2.29), (IX.2.40) give the named spectra. The endpoint rules are inherited from IX.1 and HW §3, pp. 5–6; HW §6.2, p. 37 gives the three mirror charge vectors. Figures IX.2.2–IX.2.4 are locally drawn from the finite endpoint paths, with created bridges distinguished from joined segments; they are not copies of source figures. Figure IX.2.5 uses the resulting faithful representations.

[DUAL]: the three examples use the infrared mirror map within the stated finite scope. IS §2, pp. 4–6 and §3.1, pp. 6–8, (3.1)–(3.4), support the abelian mirror interpretation. GW §2.4.1, pp. 20–21 supplies the minimal monopole and free-field argument in (IX.2.21)–(IX.2.22). It uses the monopole dimension and scalar unitarity bound as sourced field-theory inputs, only for the primitive one-flavor example. The finite-coupling metric is not asserted to be flat. Circular configurations require a separate construction.

§IX.2.7 Faithful lattices and dimensions. [MATH]: equations (IX.2.41)–(IX.2.43) derive the integral affine-presentation conversion. Under a regular moment-map level and free effective action, (IX.2.45)–(IX.2.49) give the smooth Higgs dimension. Q5b has no separate physical primary classification here: the generic Coulomb rank rule and its non-lifting are sourced physical premises, not consequences of the matrix rank test. IS §3.2, pp. 8–10, (3.5)–(3.10), supplies the affine abelian presentation. The explicit integral section removes its continuous diagonal kernel without adding a finite quotient. The hypermultiplet representation and free quotient give the Higgs arithmetic; the generic abelian Coulomb rank rule and $\mathcal{N} = 4$ branch interpretation are physical inputs. Singular tangent dimensions and deformed vacuum existence do not follow from that arithmetic.

§IX.2.8 Parameter normalization. [GEO-E]: equations (IX.2.50)–(IX.2.63) state and derive the scoped signed map. HW §3, pp. 11–12 and §6.2, pp. 36–38 supply the position/parameter identification, not the absolute 2π coefficient in the canonical action. That coefficient uses Chapter 1's leading small-slope classical DBI/action matching, $\zeta = \Delta w/(4\pi^2 g_s \alpha')$, specialized to $\tau = i$. The normalization uses the leading action matching derived in Chapter 1. Generic-g_s normalization, quantum exactness and finite-slope exactness are unclaimed. The stated field convention fixes the common half-projection and distinguishes canonical q from algebraic $u = \sqrt{2\pi}q$. IS §3.2 independently supports the parameter counts. Figure IX.2.6 is a local linear-map diagram. Figure IX.2.1 represents the explicit matrix in (IX.2.4).

§IX.2.9 Elementary quotient and quantum input. [MATH]: over the complex polynomial ring of the three oriented hypermultiplets, with zero primitive mirror mass and zero real mirror FI, equations (IX.2.67)–(IX.2.73) derive the mirror invariant ring by the integer charge kernel and moment-map elimination. The root and discriminant examples (IX.2.76)–(IX.2.81) are exact algebraic consequences. Figure IX.2.7 uses these exact roots. This is the zero-real-FI affine complex quotient; a real FI resolution requires separate stability/metric information.

[BPS:1/2|holo]: the equality with (IX.2.74) imports BDG §3.1, (3.6), printed p. 10 (PDF page 12), as its independent quantum electric target. BDG writes factors $\varphi + m_i$; our electric effective-mass sign uses $\phi - m_i$. If the source holomorphic components are taken as full $a_1 + ia_2$, the translation is $\varphi_{\mathrm{BDG}} = 2\phi$, $m_{i,\mathrm{BDG}} = -2m_i$ and $V_\pm = 2^{-N_f/2} v_{\pm,\mathrm{BDG}}$. This is an algebraic normalization, not an independently established symplectic or metric match. The comparison explicitly requires (IX.2.64): zero electric FI and zero primitive mirror mass. Equations (IX.2.65) and (IX.2.66) explain why nonzero values remove the selected loci. These restrictions do not prohibit the general parameter dictionary or Higgs-resolution examples of IX.3. Full quantum duality, partition functions, contact terms and complete branch geometry are outside the calculation. De Boer et al. §2.2, (2.15)–(2.17), pp. 13–15 is a comparison source for circular abelian mirrors, not validation of a circular brane path in this chapter.

References

Boer, J. de et al. (1997). "Mirror symmetry in three-dimensional theories, SL(2,Z) and D-brane moduli spaces". In: *Nucl. Phys. B* 493, pp. 148–176. DOI: 10.1016/S0550-3213(97)00115-6. arXiv: hep-th/9612131.

Bullimore, M., T. Dimofte, and D. Gaiotto (2017). "The Coulomb Branch of 3d $\mathcal{N} = 4$ Theories". In: *Commun. Math. Phys.* 354.2, pp. 671–751. DOI: 10.1007/s00220-017-2903-0. arXiv: 1503.04817 [hep-th].

Gaiotto, D. and E. Witten (2009). "S-Duality of Boundary Conditions In N=4 Super Yang-Mills Theory". In: *Adv. Theor. Math. Phys.* 13.3, pp. 721–896. DOI: 10.4310/ATMP.2009.v13.n3.a5. arXiv: 0807.3720 [hep-th].

Hanany, A. and E. Witten (1997). "Type IIB superstrings, BPS monopoles, and three-dimensional gauge dynamics". In: *Nucl. Phys. B* 492, pp. 152–190. DOI: 10.1016/S0550-3213(97)00157-0. arXiv: hep-th/9611230.

Intriligator, K. A. and N. Seiberg (1996). "Mirror symmetry in three-dimensional gauge theories". In: *Phys. Lett. B* 387, pp. 513–519. DOI: 10.1016/0370-2693(96)01088-X. arXiv: hep-th/9607207.

Chapter IX.3

Higgs, Coulomb and mixed branches

IX.3.1 From movable branes to a space of vacua

A brane drawing can suggest a continuous family of configurations before it tells us what that family means in the gauge theory. A suspended D3 can move while its fivebrane endpoints remain fixed. A flavor D5 can also move in the same transverse plane. The first motion changes a state of one theory; the second changes a parameter in its Lagrangian. A useful picture of the vacuum space must distinguish these operations before counting any coordinates.

There is a second distinction even after the dynamical coordinates have been identified. Charged scalar expectation values are redundant under gauge transformations. Their vacuum equations define a level set, and the space of vacua is a quotient of that level set. Polynomial invariants provide coordinates on an associated affine space, but can forget a compact exceptional cycle. Finally, a complex equation does not specify the metric measured by the kinetic energy of slowly varying vacua. These distinctions become concrete in small theories with eight real supercharges.

We will follow a $U(1)$ gauge field coupled to two or three charge-one hypermultiplets. The Higgs branch can be calculated directly from charged fields. Its two-flavor example gives a resolved A_1 surface, while the three-flavor example, with coincident masses and zero complex FI, gives the minimal nilpotent cone of $\mathfrak{sl}_3$ at zero real FI and $T^*\mathbb{CP}^2$ at positive real FI. Its complex dimension is four; the electric Coulomb branch and mirror Higgs branch in the comparison below are instead A_2 surfaces of complex dimension two. The Coulomb branch has a fourth coordinate supplied by the photon. Its quantum metric contains a circle fiber that shrinks at massless-hyper locations. An asymmetric three-flavor example then compares its complex ring with the Higgs ring of the two-node theory constructed in Chapter 2.

Take-home message of this chapter

A branch is specified by its vacuum equations, gauge quotient and unbroken fields. Real FI parameters select a stable quotient; complex FI parameters deform its holomorphic equations. The compact dual photon completes an abelian Coulomb branch to four real dimensions. Its finite-coupling metric, infinite-coupling metric and affine coordinate ring contain different information. On a mixed stratum, determine the massless slice and stabilizer before subtracting gauge directions.

We use the multiplets and charge-one normalization of Chapter 1 and the mirror frame of Chapter 2. The field-theory language of hyperkähler quotients is recalled through explicit coordinates, so no general classification of such spaces is required. The final nonabelian example is one open stratum of $U(2)$ with three fundamentals. It teaches how partial Higgsing and a residual photon coexist; it will not identify the entire quantum closure of that stratum. Chapter 4 supplies a different application of moment maps, where fields live at a boundary.

IX.3.2 Which positions are fields?

The interval construction provides a direct way to distinguish a vacuum coordinate from a coupling. The NS5, D3 and D5 orientations are those of Chapter 1. With fivebranes held fixed, a finite D3 has normalizable zero modes in the 345 directions. Its position becomes the triplet of vector-multiplet scalars. A D5 position in the same directions is an external mass triplet. In physical mass units,

$$\boldsymbol{\phi} = \frac{\boldsymbol{x}^{345}_{D3}}{2\pi\alpha'}, \qquad \boldsymbol{m}_i = \frac{\boldsymbol{x}^{345}_{D5_i}}{2\pi\alpha'}, \qquad M_i = |\boldsymbol{\phi} - \boldsymbol{m}_i|. \tag{IX.3.1}$$

The mass is a relative separation. Translating both the color brane and all flavor branes changes the origin of the vector scalar, not a mass splitting. Displacing only one D5 changes the theory.

The length of the interval and the relative 789 position of its NS5 ends determine two other external parameters. In the charge-one Maxwell normalization and the leading small-slope classical matching of Chapter 1,

$$\frac{1}{e^2} = \frac{L_6}{2\pi g_s}, \qquad g^2_{3,\mathrm{YM}} = 2e^2, \qquad \boldsymbol{\zeta} = \frac{\boldsymbol{w}_L - \boldsymbol{w}_R}{4\pi^2 g_s \alpha'}. \tag{IX.3.2}$$

The FI coefficient in this equation is conditional on that classical action matching. It is not an exact quantum conversion between brane distances and gauge-theory parameters. A D3 piece between D5s may instead move in 789 and describe hypermultiplet moduli after an allowed splitting. Which object moves and which objects are external matter as much as the coordinate direction.

For n hypermultiplets write their canonical complex scalars as q_i, p_i, with charges $+1, -1$. Choose one complex structure on the triplet space, using the same projection for scalars, masses and FI levels,

$$a_C = \frac{a_1 + ia_2}{2}, \qquad a_R = a_3, \qquad |\boldsymbol{a}|^2 = a_R^2 + 4|a_C|^2. \tag{IX.3.3}$$

The factor four is part of the physical mass norm. For a canonical adjoint chiral field in the superpotential $W = \sqrt{2}\sum_i p_i \Phi q_i$, this choice means $\Phi = \sqrt{2}\phi_C$. It does not make ϕ_C a separately canonically normalized chiral field.

A moment map is the function whose level is constrained by the auxiliary fields of the gauge multiplet. Here its real and complex components are

$$\mu_R = \sum_i (|q_i|^2 - |p_i|^2), \qquad \mu_C = \sum_i q_i p_i, \qquad \boldsymbol{\mu} = (2\Re\mu_C, 2\Im\mu_C, \mu_R). \tag{IX.3.4}$$

Eliminating the auxiliaries gives a sum of nonnegative terms,

$$V = \frac{e^2}{2}(\mu_R - \zeta_R)^2 + 2e^2|\mu_C - \zeta_C|^2 + \sum_i \big[(\phi_R - m_{R,i})^2 + 4|\phi_C - m_{C,i}|^2\big](|q_i|^2 + |p_i|^2). \tag{IX.3.5}$$

A supersymmetric vacuum makes every term vanish. In particular a nonzero hypermultiplet requires its mass triplet to coincide with the vector scalar. The engineering dimensions are

$$[q_i] = [p_i] = \tfrac{1}{2}, \qquad [\phi_R] = [\phi_C] = [m] = [\zeta] = [e^2] = 1, \qquad [V] = 3. \tag{IX.3.6}$$

Both components of the moment map have dimension one, as required by the FI terms.

At zero masses and FI there are two immediate possibilities. On the Higgs locus, nonzero hypers force $\boldsymbol{\phi} = 0$; on the pure Coulomb locus all hypers vanish and the vector scalar remains free. The latter survives as a supersymmetric locus only if

$$q = p = 0 \quad \Longrightarrow \quad V = \frac{e^2}{2}\zeta_R^2 + 2e^2|\zeta_C|^2 = \frac{e^2}{2}|\boldsymbol{\zeta}|^2 = 0. \tag{IX.3.7}$$

At positive finite coupling, changing the sign of a nonzero FI parameter does not evade this obstruction.

For a concrete different regime, take distinct mass triplets, $\zeta_C = 0$ and $\zeta_R > 0$. Each flavor gives an isolated vacuum,

$$\boldsymbol{\phi} = \boldsymbol{m}_i, \qquad q_i = \sqrt{\zeta_R}, \qquad q_{j\neq i} = 0, \qquad p_j = 0. \tag{IX.3.8}$$

The phase of q_i is removed by the gauge action. There are two such vacua for $n = 2$ and three for $n = 3$. Distinct masses prevent two flavors from being simultaneously active. At zero FI, a single active flavor instead obeys

$$qp = 0, \qquad |q|^2 - |p|^2 = 0 \quad \Longrightarrow \quad q = p = 0. \tag{IX.3.9}$$

An extended Higgs branch therefore requires enough coincident masses. These examples explain why one cannot vary arbitrary deformations while continuing to describe the same pure branch.

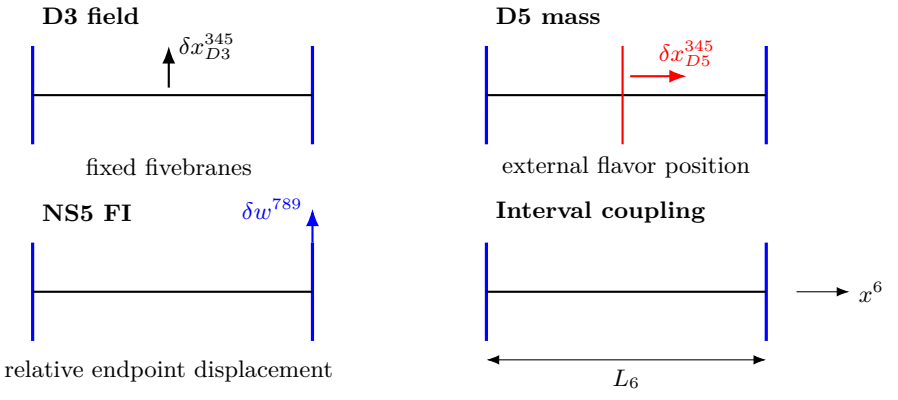


Figure IX.3.1: Field and parameter motions in the fixed electric frame. The finite D3 position is dynamical. The D5 position, NS5 relative displacement and interval length are external parameters. The arrows label changes, not additional brane segments; the diagrams suppress the common 012 directions.

IX.3.3 A quotient before a dimension count

We now hold coincident masses fixed and translate their common value to zero. The Higgs branch is the space of solutions of the three real moment-map equations, with gauge-equivalent solutions identified,

$$\mathcal{H}_\zeta = \{(q,p) \in \mathbb{C}^n \oplus \mathbb{C}^n : \mu_C = \zeta_C,\ \mu_R = \zeta_R\}/U(1), \qquad (q,p) \mapsto (e^{i\lambda}q, e^{-i\lambda}p). \tag{IX.3.10}$$

It is called a hyperkähler quotient because the three moment maps correspond to the three compatible complex structures. We need only its explicit equations, its gauge action and their regularity here.

Suppose $\zeta_C = 0$ and $\zeta_R > 0$. Then q cannot vanish. A nonzero charge-one component forces any stabilizing phase to be the identity, so the compact gauge action is free. To see why the three constraints are independent, let K be the infinitesimal gauge vector and let I_1, I_2, I_3 be the orthogonal quaternionic complex structures on flat hypermultiplet space. The moment-map gradients satisfy, up to fixed nonzero component normalizations,

$$\nabla\mu_a \ \propto\ I_a K, \qquad \langle I_a K, I_b K\rangle = \delta_{ab}|K|^2, \qquad K \neq 0. \tag{IX.3.11}$$

Thus the level set is regular at these points. Removing three real constraints and one gauge orbit gives

$$\dim_{\mathbb{R}} \mathcal{H}_\zeta = 4n - 3 - 1 = 4(n-1), \qquad n = 2:\ 4, \quad n = 3:\ 8. \tag{IX.3.12}$$

This subtraction describes a free, regular locus. At $q = p = 0$ the gauge group stabilizes the point and the derivatives of the quadratic moment maps vanish. It would be incorrect to apply the same subtraction to its linear tangent space.

There is a useful direct description of the positive-FI quotient. First solve the complex equation and divide by the complexified gauge group $\mathbb{C}^*$. On a patch where $q_1 \neq 0$, choose its representative $q_1 = 1$ and define

$$z_a = \frac{q_a}{q_1}, \qquad \pi_a = q_1 p_a \quad (a = 2, \ldots, n), \qquad p_1 = -\sum_{a=2}^{n} z_a \pi_a. \tag{IX.3.13}$$

The z_a are projective coordinates. The remaining variables transform as cotangent coordinates, as can be seen directly from the one-form,

$$\sum_i p_i \, dq_i = \sum_{a=2}^{n} \pi_a \, dz_a \quad \text{on the slice } q_1 = 1. \tag{IX.3.14}$$

On overlaps, the equation $p \cdot q = 0$ removes the derivative of the complex gauge factor. This makes the reduced one-form independent of which nonzero q_i is chosen. The resulting complex manifold is $T^*\mathbb{CP}^{n-1}$.

For two flavors the chart transition can be written without any geometric shorthand. If $z = q_2/q_1$ and $\pi = q_1 p_2$, the chart with $q_2 = 1$ has

$$z' = \frac{1}{z}, \qquad \pi' = -z^2 \pi, \qquad \pi' \, dz' = \pi \, dz. \tag{IX.3.15}$$

The minus sign and the factor z^2 are the cotangent transition on $\mathbb{CP}^1$. For three flavors there are two independent z_a and two π_a, giving four complex coordinates on each chart.

We have still to impose the real equation. Along a complex gauge orbit, write $q \mapsto \sqrt{t}\, q$, $p \mapsto p/\sqrt{t}$ with $t > 0$ and let $A = \|q\|^2 > 0$, $B = \|p\|^2$. The required representative obeys

$$tA - \frac{B}{t} = \zeta_R, \qquad t = \frac{\zeta_R + \sqrt{\zeta_R^2 + 4AB}}{2A} > 0, \qquad \frac{d}{dt}\left(tA - \frac{B}{t}\right) = A + \frac{B}{t^2} > 0. \tag{IX.3.16}$$

Existence and uniqueness follow from the displayed positive root and monotonicity. The remaining phase is precisely the compact quotient. For example $q = (1, 0)$, $p = (0, 2)$ at $\zeta_R = 3$ has $t = 4$ and physical representative $q = (2, 0)$, $p = (0, 1)$.

At negative real FI the analogous stable set has $p \neq 0$. At zero level, a nonzero solution such as $q = (a, 0, \ldots)$, $p = (0, a, 0, \ldots)$ with $a > 0$ is still free and regular; the origin is not. A nonzero complex level forces both q and p to be nonzero. We will now see how complex and real levels leave different traces in invariant coordinates.

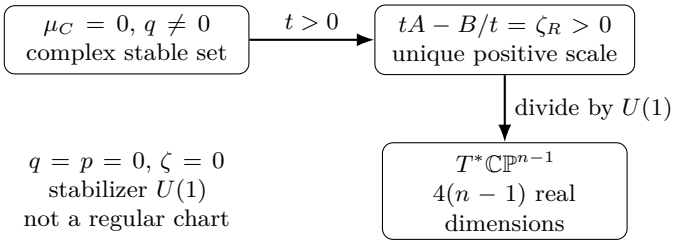


Figure IX.3.2: The stable quotient at $\zeta_C = 0$. Positive real FI selects $q \neq 0$; the positive part of each complex gauge orbit has a unique intersection with $\mu_R = \zeta_R$. The $U(1)$ phase is then identified. At zero FI the origin has a stabilizer and is excluded from the regular count. Negative FI exchanges the roles of q and p.

This is the quotient underlying the Higgs-side dimension counts in Chapter 2. A count is reliable only after the action and its stabilizer have been identified.

IX.3.4 Invariant matrices, resolutions and deformations

Gauge-invariant functions let us describe the quotient without choosing a gauge patch. A neutral monomial in q_i, p_j has equally many factors of each charge. Pairing one positive and one negative factor shows that all such monomials are products of mesons,

$$M_{ij} = q_i p_j, \qquad M = qp^T, \qquad M_{ij}M_{kl} - M_{il}M_{kj} = 0. \tag{IX.3.17}$$

The last equations express every 2×2 minor. They also generate all relations among the mesons: two pairings of the same q and p factors are related by successive exchanges of paired partners, and each exchange is one displayed minor. Thus the matrix has rank at most one, including the zero matrix.

Let $c = \zeta_C$. The complex moment map is the trace, so the affine ring is

$$\mathbb{C}[\mathcal{H}]_{\text{aff}} = \mathbb{C}[M_{ij}]/(\text{all } 2 \times 2 \text{ minors},\ \operatorname{tr} M - c). \tag{IX.3.18}$$

Here "affine" means that the space is reconstructed from its global polynomial functions. Taking invariants commutes with imposing the invariant trace equation: a complex torus decomposes polynomials into weight spaces, and multiplication by a weight-zero polynomial preserves each space. Only the weight-zero part contributes.

The matrix form gives a further useful identity without any elimination,

$$M^2 = q(p^T q)p^T = cM. \tag{IX.3.19}$$

At zero level the nonzero matrices are rank-one nilpotent matrices with square zero. Together with the origin they form the closure of the minimal nilpotent orbit of $\mathfrak{sl}_n$. For $c \neq 0$ the same identity instead makes M/c a rank-one projector. A complex deformation has changed the eigenvalues, not just the size of an exceptional cycle.

For $n = 2$, introduce x, y, z by a definite sign convention,

$$M = \begin{pmatrix} z + c/2 & x \\ -y & c/2 - z \end{pmatrix}, \qquad \det M = xy - z^2 + \frac{c^2}{4} = 0. \tag{IX.3.20}$$

At $c = 0$ the affine equation is $xy = z^2$. Its gradient $(y, x, -2z)$ vanishes only at the origin. For $c \neq 0$ that point does not lie on the surface, so the deformed affine surface is smooth. The level c appears squared because the two eigenvalues of the traceless part are $\pm c/2$.

The positive-real-FI quotient at $c = 0$ is instead $T^*\mathbb{CP}^1$. Its zero section has $p = 0$, $q \neq 0$, and consequently all mesons vanish,

$$T^*\mathbb{CP}^1 \longrightarrow \{xy = z^2\}, \qquad \mathbb{CP}^1 \longmapsto M = 0. \tag{IX.3.21}$$

The affine functions collapse the entire zero section to a point. Changing the real FI level changes the stable quotient and its Kähler geometry while leaving the complex invariant equation unchanged. Figure IX.3.3 separates this resolution from the complex smoothing. A complex ring by itself cannot measure the size of the exceptional $\mathbb{CP}^1$.

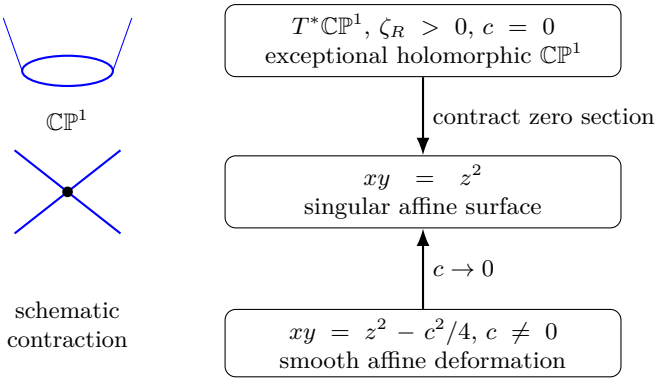


Figure IX.3.3: Three objects associated with two-flavor SQED. The middle is the singular affine surface. The upper object replaces its origin by a holomorphic $\mathbb{CP}^1$ at nonzero real FI. The lower object changes the equation at nonzero complex FI. Arrows label contraction or a family limit, not a diffeomorphism or metric equality.

For $n = 3$, keep all nine mesons, all nine minors and the trace equation. The patch $q_1 = 1$ has the explicit representative

$$q = (1, z_2, z_3)^T, \qquad p = (c - z_2\pi_2 - z_3\pi_3, \pi_2, \pi_3)^T, \qquad M = qp^T. \tag{IX.3.22}$$

There are four freely variable complex coordinates. At $c = 0$ and positive real FI this is a chart of $T^*\mathbb{CP}^2$, with an exceptional $\mathbb{CP}^2$ collapsed by the mesons. It is not the A_2 surface, which has only two complex dimensions. At nonzero c, M is conjugate to $\mathrm{diag}(c, 0, 0)$. Its conjugation stabilizer is $GL(1) \times GL(2)$, giving

$$\dim_{\mathbb{C}} \mathcal{H}_{c\neq 0} = \dim GL(3) - \dim GL(1) - \dim GL(2) = 9 - 1 - 4 = 4. \tag{IX.3.23}$$

Here the stabilizer has been specified for this orbit. It is a separate calculation from a free compact gauge quotient.

A Hilbert series counts homogeneous polynomial functions. Give each q and p degree one and write t for that degree. Before imposing $\mu_C = 0$, a neutral monomial of degree $2k$ consists of a degree-k monomial in n positive-charge variables and another in n negative-charge variables. Thus

$$H_{\mathrm{inv}}(t) = \sum_{k\geq 0} \binom{k+n-1}{n-1}^2 t^{2k}, \qquad H_H(t) = (1-t^2)H_{\mathrm{inv}}(t). \tag{IX.3.24}$$

The factor $1 - t^2$ is justified because multiplication by the nonzero polynomial μ_C is injective in the invariant domain. It subtracts one shifted copy of that ring. Simply multiplying by a factor for every written equation would fail when equations have relations among them.

Writing $x = t^2$, the coefficient after imposing the trace is

$$h^{(2)}_{2k} = (k+1)^2 - k^2 = 2k+1, \qquad h^{(3)}_{2k} = \binom{k+2}{2}^2 - \binom{k+1}{2}^2 = (k+1)^3. \tag{IX.3.25}$$

Summing these polynomial sequences gives

$$H^{(2)}_H = \frac{1+t^2}{(1-t^2)^2}, \qquad H^{(3)}_H = \frac{1+4t^2+t^4}{(1-t^2)^4}. \tag{IX.3.26}$$

For example their coefficients through t^6 are respectively $(1, 3, 5, 7)$ and $(1, 8, 27, 64)$. The poles have orders two and four, agreeing with the complex dimensions already derived. This agreement counts functions of the declared ring; the physical protection of the Higgs description is an additional supersymmetric input. Chapter 2's mirror exchange will compare this Higgs geometry with a Coulomb geometry of another theory, not with an arbitrary same-dimension space.

IX.3.5 The photon as a compact scalar

The vector triplet supplies only three real coordinates. In three spacetime dimensions the photon carries one local degree of freedom, which can be written as a scalar. Its compactness follows from the global gauge group and is essential for the geometry near a massless hypermultiplet.

Use a charge-one connection, so magnetic flux through a surrounding sphere is quantized as

$$\frac{1}{2\pi}\int_{S^2} F = a \in \mathbb{Z}, \qquad \mathcal{L}_{\mathrm{Maxwell}} = \frac{1}{4e^2} F_{\mu\nu}F^{\mu\nu}. \tag{IX.3.27}$$

In Euclidean signature introduce $B = *F$ as an independent field. A Lagrange multiplier θ imposes the Bianchi identity. After an integration by parts the first-order density is

$$\mathcal{L}_1 = \frac{B^2}{2e^2} - \frac{i}{2\pi} d\theta \cdot B. \tag{IX.3.28}$$

The coefficient ensures that a flux-one insertion carries phase $e^{i\theta}$. Hence θ is an angular variable with period 2π. A different period would change which magnetic charges are allowed.

Complete the square before eliminating B,

$$\mathcal{L}_1 = \frac{1}{2e^2}\left(B - \frac{ie^2}{2\pi}d\theta\right)^2 + \frac{e^2}{8\pi^2}(d\theta)^2. \tag{IX.3.29}$$

The Gaussian saddle is complex in Euclidean signature. Omitting the i would give the wrong sign for the scalar kinetic energy. Integrating out B yields

$$\mathcal{L}_\theta = \frac{e^2}{8\pi^2}(d\theta)^2, \qquad \theta \sim \theta + 2\pi, \qquad \psi = \frac{\theta}{2\pi} \sim \psi + 1. \tag{IX.3.30}$$

The period-one variable ψ will simplify the circle connection. If instead a source defines $F = *d\gamma$, its classical variable here is $\gamma = e^2\theta/(2\pi)$ and has period e^2.

Combine the scalar and photon kinetic energies using the convention one-half the metric evaluated on spacetime derivatives. The classical Coulomb metric is

$$ds^2_{\rm cl} = \frac{1}{e^2}d\boldsymbol{\phi}^2 + e^2 d\psi^2 = \frac{1}{e^2}d\boldsymbol{\phi}^2 + \frac{e^2}{4\pi^2}d\theta^2. \tag{IX.3.31}$$

It is locally $\mathbb{R}^3 \times S^1$, with real dimension four. In particular the angular radius, in the normalization where its angle has period 2π, is

$$R_\theta^2 = \frac{e^2}{4\pi^2}. \tag{IX.3.32}$$

The radius is not fixed by dimensional counting. Both the Maxwell coefficient and the compact period enter it.

More generally, at a separated Cartan point of rank r, each surviving abelian photon supplies one angular coordinate. Before Weyl identifications the local count is

$$\dim_{\mathbb{R}} \mathcal{C}_{\rm local} = 3r + r = 4r. \tag{IX.3.33}$$

For the residual $U(1)$ in our later mixed example, this is the origin of four Coulomb directions. It does not determine the global metric or the behavior at coincident color eigenvalues. The quantum correction already changes the global topology for a single gauge node, as we now derive from its harmonic function and period.

IX.3.6 Circle fibers and the Coulomb metric

A charged hypermultiplet becomes massless at $\boldsymbol{\phi} = \boldsymbol{m}_i$. Away from these points it can be integrated out in a derivative expansion. In the charge-one action normalization, the one-hyper correction on the real-scalar axis is $1/(4\pi|\phi_R - m_R|)$. We use this one-loop coefficient as a physical input. Rotations of the physical triplet, with the norm in (IX.3.3), complete it to

$$H(\boldsymbol{\phi}) = \frac{1}{e^2} + \sum_{i=1}^{n}\frac{1}{4\pi r_i}, \qquad r_i = \sqrt{(\phi_R - m_{R,i})^2 + 4|\phi_C - m_{C,i}|^2}. \tag{IX.3.34}$$

The abelian $\mathcal{N}=4$ two-derivative result says that this harmonic function gives the protected Coulomb metric. Its protection and its completion at massless centers are physical inputs beyond the Gaussian dualization; they do not follow from the number of coordinates.

A hyperkähler circle fibration with this function has the Gibbons–Hawking form

$$ds^2 = H\,d\boldsymbol{\phi}^2 + H^{-1}(d\psi+\omega)^2, \qquad d\omega = *_3 dH, \qquad \psi \sim \psi + 1. \tag{IX.3.35}$$

The star uses the oriented flat physical triplet coordinates. This fixes the sign of the connection curvature. Reversing the fiber and base orientation consistently gives an equivalent description.

To construct the connection rather than infer it from a metric name, consider one center with $H = h_0 + c/r$. In spherical coordinates (r,ϑ,φ) around that center,

$$*_3 d(c/r) = -c\sin\vartheta\,d\vartheta\wedge d\varphi, \qquad \omega = c\cos\vartheta\,d\varphi. \tag{IX.3.36}$$

The displayed potential is singular on the polar axes. Regular north and south choices, respectively, are

$$\omega_N = c(\cos\vartheta - 1)d\varphi, \qquad \omega_S = c(\cos\vartheta + 1)d\varphi, \qquad \psi_N = \psi_S + 2c\varphi. \tag{IX.3.37}$$

They give the same $d\psi+\omega$ on their overlap. As φ winds by 2π, the fiber coordinate changes by $4\pi c$. For a primitive center and period-one ψ, its magnitude must be one. Equivalently the first Chern number is

$$c_1 = \frac{1}{2\pi}\int_{S^2} d(2\pi\omega) = -4\pi c = -1, \qquad c = \frac{1}{4\pi}. \tag{IX.3.38}$$

The sourced radial coefficient and the compact period therefore give a primitive circle bundle, rather than a finite cover or quotient. For several centers, sum their local potentials; the constant in H has no curvature.

Near an isolated center the singular term dominates the constant and other centers. Define a radial coordinate and Hopf angle by

$$\rho = 2\sqrt{cr}, \qquad \chi = \frac{\psi}{c}, \qquad \Delta\chi = \frac{1}{c} = 4\pi. \tag{IX.3.39}$$

Substitution into the leading metric gives

$$ds^2 = d\rho^2 + \frac{\rho^2}{4}\left[d\vartheta^2 + \sin^2\vartheta\,d\varphi^2 + (d\chi + \cos\vartheta\,d\varphi)^2\right]. \tag{IX.3.40}$$

The period makes this a smooth origin of $\mathbb{R}^4$. One explicit pair of Cartesian complex coordinates is

$$Z_1 = \rho\cos\frac{\vartheta}{2}e^{i(\chi+\varphi)/2}, \qquad Z_2 = \rho\sin\frac{\vartheta}{2}e^{i(\chi-\varphi)/2}, \qquad ds^2 = |dZ_1|^2 + |dZ_2|^2. \tag{IX.3.41}$$

Thus a primitive shrinking circle is not a singularity merely because a fiber has zero size. If n centers coincide, the coefficient is instead $c = n/(4\pi)$ and $\Delta\chi = 4\pi/n$. The same local calculation gives $\mathbb{R}^4/\mathbb{Z}_n$.

The asymptotic region distinguishes two metric limits. At finite e^2 and large $r = |\boldsymbol{\phi}|$,

$$H = \frac{1}{e^2} + \frac{n}{4\pi r} + O(r^{-2}), \qquad g_{\theta\theta} \longrightarrow \frac{e^2}{4\pi^2}. \tag{IX.3.42}$$

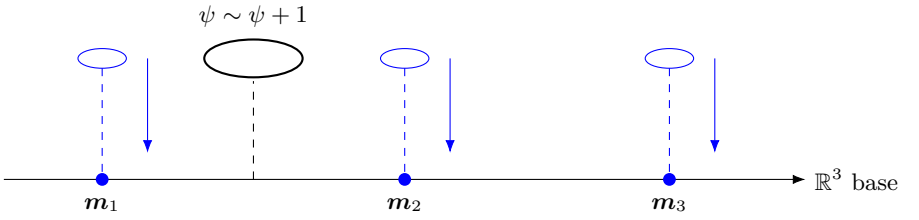
The fiber retains finite radius while the three-dimensional base grows. This is asymptotically locally flat, or ALF, multi-Taub–NUT geometry. At fixed positions and masses the infinite-coupling limit removes the constant,

$$e^2 \longrightarrow \infty : \qquad H \longrightarrow \sum_i \frac{1}{4\pi|\boldsymbol{\phi} - \boldsymbol{m}_i|}. \tag{IX.3.43}$$

The resulting asymptotically locally Euclidean, or ALE, metric has an asymptotic cone $\mathbb{R}^4/\mathbb{Z}_n$. It is a cone everywhere only when the centers also coincide. Separated centers retain dimensionful separations. For example two centers at $\pm\boldsymbol{m}$ satisfy

$$H_\infty(\lambda\boldsymbol{\phi}; \boldsymbol{m}) = \lambda^{-1} H_\infty(\boldsymbol{\phi}; \boldsymbol{m}/\lambda), \qquad \lambda > 0. \tag{IX.3.44}$$

Rescaling coordinates at fixed nonzero mass does not give conical homogeneity. Sending the coupling to infinity also does not decompactify ψ; its period remains one throughout.



finite e^2: ALF $\qquad 1/e^2 \to 0$: ALE

ALE + coincident centers
$H = n/(4\pi r)$, $\Delta\chi = 4\pi/n$, $\mathbb{R}^4/\mathbb{Z}_n$

Figure IX.3.4: A circle fibration over three distinct centers in the physical triplet base. The circles indicate fibers and are schematic, not an embedding of the four-dimensional metric. Each primitive fiber shrinks smoothly at its center. At finite positive e^2 the asymptotic geometry is ALF. Removing $1/e^2$ gives the ALE limit; a global cone requires the additional coincidence of all centers.

In a chosen complex structure, real mass components affect resolution and Kähler data. If complex masses coincide but real masses separate the centers, the affine equation may be singular even though the metric space is smooth. The affine space then contracts compact cycles, just as in the Higgs example. This is why the infrared mirror statement of Chapter 2 cannot be replaced by equality of two finite-coupling metrics.

IX.3.7 Quantum functions and integer magnetic flux

The circle fibration suggests where Coulomb coordinates can degenerate, but a holomorphic ring also needs the quantum multiplication law of monopole operators. A monopole operator specifies a magnetic flux through a small sphere surrounding its insertion. For charge-one $U(1)$ the minimal positive and negative charges are $+1$ and -1; denote their holomorphic operators by V_+ and V_-. Set $\varphi = \phi_C$ and write $m_i = m_{C,i}$ in this section.

At zero electric FI, the protected abelian multiplication law is the physical input

$$\mathbb{C}[\mathcal{C}]_{\mathrm{aff}} = \mathbb{C}[V_+, V_-, \varphi] / \left(V_+ V_- - \prod_{i=1}^{n} (\varphi - m_i) \right). \tag{IX.3.45}$$

Each mass factor is consistent with the degeneration at a massless hyper. Magnetic charge conservation makes the product neutral. These observations explain the form of the relation but do not derive its quantum operator product. In particular a classical Higgs quotient in a proposed mirror cannot by itself establish that input independently.

The equation refers to algebraic coordinates. Starting from a convention with complex coordinate φ_{s}, masses entering as $\varphi_{\mathrm{s}} + m_{\mathrm{s},i}$ and monopoles $v_\pm$, the translation used here is

$$\varphi_{\mathrm{s}} = 2\varphi, \qquad m_{\mathrm{s},i} = -2m_i, \qquad V_\pm = 2^{-n/2} v_\pm. \tag{IX.3.46}$$

It accounts for the half-complex projection and mass sign. Such a rescaling says nothing by itself about canonical kinetic energies or a normalized holomorphic symplectic form.

At zero masses this ring is homogeneous. Let w count the integral topological charge and t count twice the protected dimension. A charge-a bare monopole in SQED has $\Delta(a) = n|a|/2$, while the neutral scalar has dimension one. Thus

$$\deg_t \varphi = 2, \qquad \deg_t V_\pm = n, \qquad J(\varphi) = 0, \qquad J(V_\pm) = \pm 1. \tag{IX.3.47}$$

The dimension formula here is the abelian specialization of the ultraviolet charge assignment derived below; for $n = 2, 3$ it is used in the protected Coulomb counting. In each flux sector, dressing by powers of φ contributes $1/(1 - t^2)$.

Summing positive and negative integer flux separately gives

$$H_C(t, w) = \frac{1}{1 - t^2} \sum_{a \in \mathbb{Z}} t^{n|a|} w^a = \frac{1}{1 - t^2} \left[1 + \frac{w t^n}{1 - w t^n} + \frac{w^{-1} t^n}{1 - w^{-1} t^n} \right]. \tag{IX.3.48}$$

The expression is a formal series in t with Laurent-polynomial coefficients in w. Combining the three terms yields

$$H_C(t, w) = \frac{1 - t^{2n}}{(1 - t^2)(1 - w t^n)(1 - w^{-1} t^n)}. \tag{IX.3.49}$$

The numerator removes the single relation of degree $2n$. This symbolic identity holds for positive integer n within the declared counting rule; the detailed physical examples here remain $n = 2, 3$.

An independent enumeration starts with two auxiliary polynomial variables u, v and the finite-group action

$$(u,v) \mapsto (\epsilon u, \epsilon^{-1} v), \qquad \epsilon = e^{2\pi i/n}, \qquad u^A v^B \text{ invariant iff } A - B \in n\mathbb{Z}. \tag{IX.3.50}$$

If $A \geq B$, factor out $(uv)^B$; the remaining power of u is divisible by n. For $B \geq A$ exchange u, v. This proves that all invariants are generated by u^n, v^n, uv, with their one relation,

$$\mathbb{C}[u,v]^{\mathbb{Z}_n} = \mathbb{C}[X,Y,z]/(XY - z^n), \qquad (X,Y,z) = (u^n, v^n, uv). \tag{IX.3.51}$$

Pairing powers removes any mixed XY factor, leaving a unique polynomial normal form built from z^k, $X^a z^k$ or $Y^a z^k$ with $a > 0$. The enumeration with degree $A + B$ and charge $(A - B)/n$ therefore gives the coefficient rule

$$[t^d w^a] H_C = \begin{cases} 1, & d - n|a| \text{ is a nonnegative even integer,} \\ 0, & \text{otherwise.} \end{cases} \tag{IX.3.52}$$

This is an exact mathematical derivation of the invariant ring and its series. Its identification with the quantum Coulomb ring still uses (IX.3.45).

The first terms display the difference between the two examples. Write $s_j = w^j + w^{-j}$. Then

$$\begin{aligned} H_C^{(2)} &= 1 + (1+s_1)t^2 + (1+s_1+s_2)t^4 + (1+s_1+s_2+s_3)t^6 + O(t^8), \\ H_C^{(3)} &= 1 + t^2 + s_1 t^3 + t^4 + s_1 t^5 + (1+s_2)t^6 + O(t^7). \end{aligned} \tag{IX.3.53}$$

The three-flavor monopoles first appear at degree three, not degree two. At degree twelve, the same rule gives

$$[t^{12}] H_C^{(2)} = \sum_{a=-6}^{6} w^a, \qquad [t^{12}] H_C^{(3)} = 1 + w^2 + w^{-2} + w^4 + w^{-4}. \tag{IX.3.54}$$

Integer-flux counting and a separate enumeration of invariant monomials agree at every charge through degree twelve. That finite comparison is a test of the counting, not a replacement for the symbolic generation argument or a proof of the quantum multiplication law.

Nonzero masses break this grading unless treated as transforming parameters. We will compare the deformed polynomials directly instead of assigning a massless Hilbert series to an inhomogeneous equation. For three flavors the electric Coulomb branch is the A_2 surface, whereas its own Higgs branch had complex dimension four. The correct Higgs partner is the two-node theory of Chapter 2.

IX.3.8 An asymmetric mirror in an integral charge basis

We can now make the three-flavor comparison without guessing a matching polynomial. Chapter 2 gives a mirror with two $U(1)$ nodes and three hypermultiplets. In a fixed

orientation its charge matrix, whose columns are hypermultiplet charges, is

$$Q = \begin{pmatrix} -1 & 1 & 0 \\ 0 & -1 & 1 \end{pmatrix}. \tag{IX.3.55}$$

The first and last hypers are charged at one end of the chain; the middle hyper links both nodes. The signs will determine the FI differences.

An affine three-node presentation has a redundant diagonal action. Removing it once gives the framed matrix above,

$$Q_{\text{aff}} = \begin{pmatrix} -1 & 1 & 0 \\ 0 & -1 & 1 \\ 1 & 0 & -1 \end{pmatrix}, \qquad \begin{aligned} (g_1, g_2, g_3) &\longmapsto (g_1/g_3, g_2/g_3), \\ (h_1, h_2) &\longmapsto (h_1, h_2, 1). \end{aligned} \tag{IX.3.56}$$

The final map is an integral section. The affine FI triplet has sum zero, but the two framed levels are independent. There is no second redundant center to remove. The integral nature of this operation can be checked by completing the charge rows to

$$B = \begin{pmatrix} -1 & 1 & 0 \\ 0 & -1 & 1 \\ 0 & 0 & 1 \end{pmatrix}, \qquad \det B = 1, \qquad \ker_{\mathbb{Z}} Q = \mathbb{Z}(1,1,1). \tag{IX.3.57}$$

A maximal minor also has magnitude one. Thus the action is faithful, and the integer lattice has not acquired a finite quotient. A real change of basis alone would not guarantee this.

For example, every integer vector (x, y, z) with $x + y + z = 0$ can be written as $Q^T(-x, z)^T$. Hence

$$\operatorname{im}_{\mathbb{Z}} Q^T = \{(x, y, z) \in \mathbb{Z}^3 : x + y + z = 0\}, \qquad B_{\text{mass}} = b_1 + b_2 + b_3. \tag{IX.3.58}$$

The b_i are mirror hypermultiplet mass markers. Shifting the two vector scalar origins removes their component in $\operatorname{im} Q^T$; the primitive background mass B_{mass} survives. This establishes the normalization of the mass direction at the level of the integral charge lattice.

The comparison in this section has two essential restrictions: the electric FI triplet is zero and the primitive mirror mass triplet is zero. The first follows from (IX.3.7). To see the second directly, on a dense mirror Higgs patch all three hypers are nonzero, so their effective masses require, component by component,

$$-\phi_1' - b_1 = 0, \qquad \phi_1' - \phi_2' - b_2 = 0, \qquad \phi_2' - b_3 = 0. \tag{IX.3.59}$$

Their sum is $-B_{\text{mass}}$. The first two equations leave a residual $-B_{\text{mass}}$ in the third, so this patch exists only at $B_{\text{mass}} = 0$. These restrictions do not forbid the nonzero-real-FI Higgs quotients studied earlier. They specify this pure Coulomb versus pure Higgs comparison.

At $\tau = i$, conditional on the leading classical displacement/FI normalization in Chapter 1, the triplet map of Chapter 2 is

$$\boldsymbol{\eta}_j = 2\pi \boldsymbol{\zeta}_j' = \boldsymbol{m}_j - \boldsymbol{m}_{j+1}, \qquad \boldsymbol{B}_{\text{mass}} = 2\pi \boldsymbol{\zeta}_{\text{electric}}. \tag{IX.3.60}$$

A common mass shift cancels. We now take zero real components of the masses and mirror FI levels, and centered complex masses $\sum_i m_i = 0$. The electric complex masses and mirror complex FI levels are allowed to be nonzero. In particular the branch restrictions do not set the polynomial deformation to zero.

Canonical mirror fields q_i', p_i' obey $Q(q_i'p_i') = \zeta_C'$. To express this in mass units, introduce algebraic coordinates only,

$$u_i = \sqrt{2\pi}\, q_i', \qquad v_i = \sqrt{2\pi}\, p_i', \qquad s_i = u_i v_i, \qquad Qs = \eta_C. \tag{IX.3.61}$$

Their kinetic terms acquire a factor $1/(2\pi)$. We will identify complex rings in these coordinates, not infer a canonically normalized metric map from the rescaling.

Dropping the complex subscript on η, solve the two moment maps and define a neutral coordinate z by their average,

$$-s_1 + s_2 = \eta_1, \qquad -s_2 + s_3 = \eta_2, \qquad z = \frac{s_1 + s_2 + s_3}{3}. \tag{IX.3.62}$$

The solution is

$$s_1 = z - \frac{2\eta_1 + \eta_2}{3}, \qquad s_2 = z + \frac{\eta_1 - \eta_2}{3}, \qquad s_3 = z + \frac{\eta_1 + 2\eta_2}{3}. \tag{IX.3.63}$$

This step computes the three factors from the physical charge matrix and FI levels. It has not used the electric Coulomb equation.

An invariant monomial in the six fields has exponent difference in $\ker_{\mathbb{Z}} Q$. If that difference is positive, extract powers of $X = u_1u_2u_3$; if negative, extract powers of $Y = v_1v_2v_3$. What remains is a product of the s_i. Consequently

$$\mathbb{C}[u_i, v_i]^{(\mathbb{C}^*)^2} = \mathbb{C}[X, Y, s_1, s_2, s_3]/(XY - s_1s_2s_3). \tag{IX.3.64}$$

After eliminating the moment maps, the ring is

$$XY = \left(z - \frac{2\eta_1 + \eta_2}{3}\right)\left(z + \frac{\eta_1 - \eta_2}{3}\right)\left(z + \frac{\eta_1 + 2\eta_2}{3}\right). \tag{IX.3.65}$$

Since $\eta_1 = m_1 - m_2$, $\eta_2 = m_2 - m_3$ and $\sum m_i = 0$, these are exactly $z - m_1, z - m_2, z - m_3$. Identifying (X, Y, z) with (V_+, V_-, φ) matches the independently supplied electric relation.

Choose the asymmetric masses in a fixed unit,

$$\begin{gathered}(m_1, m_2, m_3) = (-4, 1, 3), \qquad (\eta_1, \eta_2) = (-5, -2), \\ XY = (z + 4)(z - 1)(z - 3) = z^3 - 13z + 12.\end{gathered} \tag{IX.3.66}$$

The discriminant measures the squared root separations,

$$\operatorname{disc} P = \prod_{i<j} (m_i - m_j)^2 = 25 \cdot 49 \cdot 4 = 4900. \tag{IX.3.67}$$

For comparison, changing only η_1 to $+5$ would give $P = z^3 - (19/3)z - 56/27$ and discriminant 900. A legitimate gauge-basis change transforms both Q and η together. A sign change in the FI vector alone does not describe that operation.

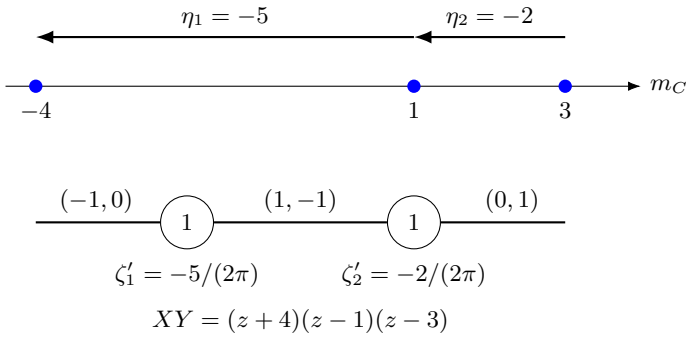


Figure IX.3.5: The asymmetric three-flavor comparison. The marked complex mass components are real numbers in this example; the plotted horizontal coordinate is m_C, not a physical triplet distance. Their ordered differences supply the two mirror complex levels. The charge columns fix the signs. Electric FI and primitive mirror mass are zero throughout.

For two flavors the same elimination with $Q = (-1, 1)$ gives $XY = z^2 - \eta^2/4$, the A_1 deformation. These ring computations support the branch exchange of Chapter 2. They neither prove full infrared duality nor identify the two finite-coupling metrics. The complex-root collision limit also has to be read together with the real mass components before declaring a physical singularity.

IX.3.9 A mixed stratum with an unbroken photon

A nonabelian gauge theory can Higgs only part of its gauge group. Some hypermultiplets then remain massless while a residual vector multiplet moves along Coulomb directions. The reliable local procedure is to solve the mass equations, identify the massless slice, and only then form its gauge quotient.

Consider $U(2)$ with three fundamentals, zero central FI and coincident zero masses. Let Q be a 2×3 matrix and $\widetilde{Q}$ a 3×2 matrix. Choose one real component of the vector triplet to be nonzero and take the following point with $a > 0$, $v \neq 0$,

$$Q = \begin{pmatrix} a & 0 & 0 \\ 0 & 0 & 0 \end{pmatrix}, \qquad \widetilde{Q} = \begin{pmatrix} 0 & 0 \\ a & 0 \\ 0 & 0 \end{pmatrix}, \qquad \phi_R = \begin{pmatrix} 0 & 0 \\ 0 & v \end{pmatrix}, \qquad \phi_C = 0. \tag{IX.3.68}$$

The nonzero fundamental and antifundamental occupy different flavors, so their complex product vanishes. Their equal magnitudes cancel in the real moment map. Direct multiplication gives

$$Q\widetilde{Q} = 0, \qquad QQ^\dagger - \widetilde{Q}^\dagger \widetilde{Q} = 0, \qquad \phi_R Q = 0, \qquad \widetilde{Q}\phi_R = 0. \tag{IX.3.69}$$

The commuting vector scalar also has vanishing commutator potential. This is an actual vacuum, not a dimension-based guess for a branch.

Write an infinitesimal complex gauge generator as $T = (t_{ij})$. A stabilizer must annihilate the hypermultiplet configuration and commute with the vector scalar,

$$TQ = 0, \qquad \widetilde{Q}T = 0, \qquad [T, \phi_R] = 0. \tag{IX.3.70}$$

The first equation forces $t_{11} = t_{21} = 0$, the second forces $t_{11} = t_{12} = 0$, and the remaining diagonal entry commutes with ϕ_R. The compact stabilizer is therefore

$$T = t_{22} \begin{pmatrix} 0 & 0 \\ 0 & 1 \end{pmatrix}, \qquad G_{\text{unbroken}} = \{\text{diag}(1, e^{i\beta})\} \simeq U(1). \tag{IX.3.71}$$

It is the photon of the unoccupied color that survives.

Diagonalizing the separated vector scalar makes its contribution to the hypermultiplet masses transparent. For each of the three flavors,

$$\phi_{R,1} - m_i = 0, \qquad \phi_{R,2} - m_i = v, \qquad M_{W,\text{Coulomb}} = |v|. \tag{IX.3.72}$$

Only the first-color row of Q and column of $\widetilde{Q}$ belong to the massless hypermultiplet slice. The off-diagonal gauge fields are massive as well. The displayed $|v|$ is their Coulomb contribution; the nonzero hypermultiplet expectation values also supply a positive Higgs contribution. The nonzero Coulomb gap is enough to select this slice, which has three hypermultiplets, not the six of the original ultraviolet representation.

On the massless slice write $q = (q_1, q_2, q_3)$ and $p = (p_1, p_2, p_3)$, with background $q = (a, 0, 0)$, $p = (0, a, 0)$. The restricted moment maps and their first variations are

$$\begin{aligned} \mu_C &= \sum_{i=1}^{3} q_i p_i, & \delta\mu_C &= a(\delta p_1 + \delta q_2), \\ \mu_R &= \sum_{i=1}^{3} (|q_i|^2 - |p_i|^2), & \delta\mu_R &= 2a\Re(\delta q_1 - \delta p_2). \end{aligned} \tag{IX.3.73}$$

The real and imaginary parts of the first row and the second row are three independent real linear constraints. The active first-color $U(1)$ has a nonzero orbit vector,

$$\delta q_1 = i\epsilon a, \qquad \delta p_2 = -i\epsilon a, \qquad \dim_{\mathbb{R}} \mathcal{O} = 1. \tag{IX.3.74}$$

Its charge-one nonzero fields make the action free. The residual second-color $U(1)$ acts trivially on this hyper slice and is not subtracted from it. Thus the open patch has

$$\dim_{\mathbb{R}} \mathcal{H}_{\text{slice}} = 12 - 3 - 1 = 8, \qquad \dim_{\mathbb{R}} \mathcal{C}_{\text{residual}} = 3 + 1 = 4. \tag{IX.3.75}$$

The $8 + 4$ count requires zero central FI, rank-one Q, three coincident masses c and a residual eigenvalue $v \neq c$; the displayed point takes $c = 0$. The count is a local stratum count. It is not a claim that the full quantum metric globally factors as a product.

A common mass shift is a useful nonzero example. Put all real masses at $c = 5$, keep $a = 1$, and take $\phi_R = \text{diag}(5, -7)$. Then

$$M = 5\mathbb{1}_3, \qquad \phi_R Q - QM = 0, \qquad \widetilde{Q}\phi_R - M\widetilde{Q} = 0, \qquad \phi_{R,2} - m_i = -12. \tag{IX.3.76}$$

The negative separation is harmless; the Coulomb mass contribution is 12. Moving the occupied scalar to 6 instead leaves a nonzero first-color mass residual and destroys this Higgs vacuum. Coincidence with the flavor mass, rather than the numerical value zero, is the relevant condition.

Two tempting subtractions fail. Subtracting all four generators of $U(2)$ from the already selected massless slice would give $12 - 4 \cdot 4 = -4$. Subtracting only the three broken generators from all six original hypermultiplets would give $24 - 4 \cdot 3 = 12$ purported Higgs directions. The first removes gauge directions that are not acting on that slice; the second retains fields that have been made massive. The moment-map rank and stabilizer must be evaluated on the same physical slice.

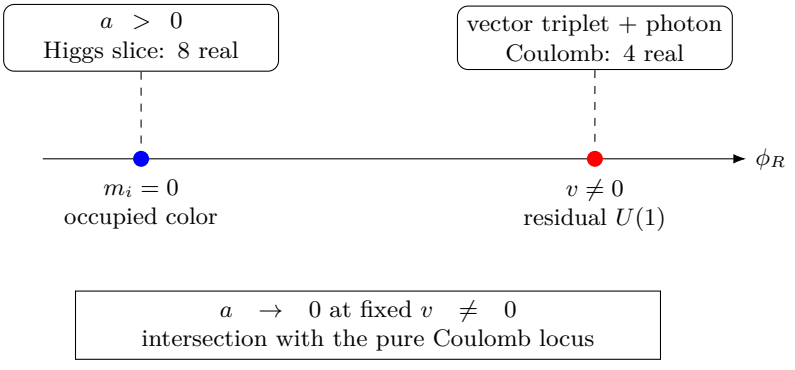


Figure IX.3.6: The separated mixed patch of $U(2)$ with three equal masses. The occupied color sits at the common mass and has a nonzero Higgs coordinate a. The other color is separated and retains a photon. The $a \to 0$ arrow is a local incidence statement; the $v \to 0$ boundary invalidates the separated-color chart. This is not a global branch classification or a metric-product diagram.

As $a \to 0$ at fixed nonzero v, the first-color Higgs factor approaches its origin and its photon is restored. The mixed closure meets a pure Coulomb locus there, with the first color at its massless point and the four second-color Coulomb directions still available. If v also tends to zero, the separated-color description fails. Resolving that joint quantum neighborhood requires more than the quotient above. A nonzero central FI also excludes this chart: its unoccupied-color real moment map is zero and cannot equal a nonzero central level. Neither exclusion asserts the absence of all vacua in that theory. The boundary constructions of Chapter 4 use related moment-map equations, but also need their own boundary conditions and residual symmetry analysis.

IX.3.10 What monopole dimensions diagnose

The mixed example has three flavors and two colors. A monopole-charge diagnostic explains why this theory differs from a balanced $U(2)$ theory with four flavors. Its

starting point is the global gauge group, not only its Lie algebra. For $U(N)$, a cocharacter can be diagonalized as

$$e^{i\lambda} \longmapsto \operatorname{diag}(e^{ia_1\lambda}, \ldots, e^{ia_N\lambda}), \qquad (a_1, \ldots, a_N) \in \mathbb{Z}^N/S_N. \tag{IX.3.77}$$

The permutation quotient is the Weyl group. These integers specify the GNO magnetic flux. A fundamental weight e_i evaluates on the flux as a_i, while a root $e_i - e_j$ evaluates as $a_i - a_j$.

With the ultraviolet $\mathcal{N} = 4$ R-assignment, the hypermultiplet and vector zero-mode contributions give

$$\Delta_{\mathrm{UV}}(a) = \frac{1}{2} \sum_{\text{hyper weights } \rho} |\rho(a)| - \frac{1}{2} \sum_{\text{roots } \alpha} |\alpha(a)| = \frac{N_f}{2} \sum_i |a_i| - \sum_{i<j} |a_i - a_j|. \tag{IX.3.78}$$

Here each hyper contributes the weights of one complex fundamental; the conjugate chiral is already included in the stated hypermultiplet coefficient. Roots occur in opposite pairs, giving the last sum over unordered pairs. Omitting that term would miss the charged vector fields.

The formula is a sourced zero-mode charge assignment. Its consequences for this family can be derived by the triangle inequality. Rearrange it as

$$\Delta_{\mathrm{UV}}(a) = \frac{N_f - 2N + 2}{2} \sum_i |a_i| + \sum_{i<j} \big(|a_i| + |a_j| - |a_i - a_j| \big). \tag{IX.3.79}$$

The final sum is nonnegative. If the first coefficient is positive, nonzero integral flux has $\sum |a_i| \geq 1$. The flux $(1, 0, \ldots, 0)$ saturates the resulting minimum,

$$\Delta_{\mathrm{UV}}(1, 0, \ldots, 0) = \frac{N_f - 2N + 2}{2}. \tag{IX.3.80}$$

Consequently the unitary SQCD thresholds are $N_f \geq 2N$ for minimum charge at least one, called good, and $N_f = 2N - 1$ for minimum charge one-half, called ugly. In a superconformal interpretation a scalar at one-half saturates the free-field bound. That interpretation requires the infrared R-symmetry, not just the ultraviolet charge arithmetic.

For $U(2)$ the smallest flux illustrates all three possibilities,

N_f	4	3	2
$\Delta_{\mathrm{UV}}(1,0)$	1	1/2	0

. (IX.3.81)

At $N_f \leq 2N - 2$, this flux has nonpositive ultraviolet charge. The naive identification of this R-assignment with the superconformal R-symmetry then fails; the name bad does not imply that the quantum field theory does not exist or determine its corrected infrared description.

A flux with unequal signs tests the root contribution directly. For $U(2)$ with four flavors,

$$\Delta_{\mathrm{UV}}(2, -1) = 2(|2| + |-1|) - |2 - (-1)| = 6 - 3 = 3. \tag{IX.3.82}$$

A central flux $(1,1)$ has no root contribution and would not reveal an omission of that term. For SQED the root sum is empty. Its zero-flavor limit is instructive,

$$N_f = 0, \quad U(1): \quad \Delta_{\mathrm{UV}}(a) = 0, \qquad \sum_{a\in\mathbb{Z}} t^{2\Delta_{\mathrm{UV}}(a)} = \sum_{a\in\mathbb{Z}} 1. \tag{IX.3.83}$$

The divergent would-be Hilbert series signals an unsuitable grading. The pure abelian theory still has its photon and dual scalar. One must not use this ultraviolet series to declare its infrared geometry absent.

For the actual two-node mirror, the charge columns of (IX.3.55) instead give

$$\Delta_{\mathrm{UV}}(a,b) = \tfrac{1}{2}\big(|a| + |a-b| + |b|\big), \qquad (a,b) \in \mathbb{Z}^2. \tag{IX.3.84}$$

If one integer is zero, the minimum nonzero value is one; if both are nonzero, $|a|+|b| \geq 2$ already proves the same bound. The asymmetric flux $(2,-1)$ gives three. This tests the whole matter-charge list, including the linking hypermultiplet. It does not furnish a general nonabelian Coulomb-ring construction. The charge lattice, equations and branch hypotheses remain the actual content of each example.

IX.3.11 Reading a branch without losing its conditions

The two-flavor example supplies a compact reconstruction exercise. Start with the canonical potential, select coincident masses, and solve the complex moment map in a patch. The real equation chooses a unique representative in each stable complex orbit. Its quotient is $T^*\mathbb{CP}^1$ at positive real FI, while the mesons obey $xy = z^2$. The exceptional curve is present in the quotient and invisible to these polynomial functions. Turning on complex FI changes that equation instead. Each step answers a different question about the vacuum space.

For three flavors at zero FI and coincident masses, the electric Higgs branch is the minimal nilpotent cone of $\mathfrak{sl}_3$, of complex dimension four; nonzero real FI at zero complex FI resolves it to $T^*\mathbb{CP}^2$. Its Coulomb branch is a surface whose ring contains quantum monopoles. The mirror surface is obtained by quotienting three hypers by the faithful two-node charge matrix. The mass/FI differences and the integral basis are needed to compare the actual deformation family. Electric FI and primitive mirror mass must vanish in that comparison; its nonzero complex mass differences remain meaningful and measurable in the discriminant.

The metric asks for further information. A dual-photon period together with the one-loop coefficient fixes the primitive circle fibration. The finite-coupling constant, its infinite-coupling removal and the collision of centers distinguish ALF, ALE and conical geometry. Canonical masses use the full physical triplet norm throughout. Algebraic rescaling of a ring coordinate does not supply a metric match.

Finally, the $U(2)$ example demonstrates why a mixed branch cannot be read by subtracting a group dimension from the original matter count. Massless directions, moment-map rank and stabilizer must refer to the same vacuum. For coincident real masses c, zero central FI, rank-one Q and $v \neq c$, their explicit computation gives the

open $8+4$ real stratum. At $v=c$ the separated-color chart fails; nonzero central FI excludes this chart without ruling out other vacua. Its joint quantum closure and a classification of all mixed branches lie beyond these calculations. Chapter 4 will apply the same discipline to boundary fields and moment maps, where boundary conditions supply another indispensable part of the problem.

Status and sources

The chapter uses the canonical potential, brane axes, gauge-group and vacuum-branch conventions stated above. The source versions are HW hep-th/9611230v3, IS hep-th/9607207v1, de Boer et al. hep-th/9612131v1, BDG 1503.04817v2, HKT 1308.4416v1 and GW 0807.3720v1. Source locators refer to printed pagination. Model agreement is not physical evidence.

§IX.3.2 Parameters and vacua. Q1 has unassigned physical primary classification: equation (IX.3.1) uses the F1 tension and normalizable finite-D3 modes from IX.1 and HW §3, pp. 5–6, 11–12, §4 p. 13 (Hanany and Witten 1997). The coupling in (IX.3.2) is inherited from the leading DBI action. No local untwisted physical-worldsheet derivation is supplied for these inherited endpoint and tension premises. Here WS means a physical-worldsheet derivation in the untwisted string; worldvolume algebra and polynomial reduction alone do not supply that evidence. Its FI coefficient is a mathematical action comparison conditional on the leading small-slope leading classical action match in Chapter 1; its left-minus-right sign is [GEO-E] from HW p. 12. There is no exact quantum coefficient claim. Equations (IX.3.3)–(IX.3.9) follow from the canonical potential stated above. The common half-complex projection and $\Phi = \sqrt{2}\phi_C$ use the stated field convention. the finite check and the live IX.1/2 interface cover the encoded vacuum and normalization consequences; source protection is separate.

§IX.3.3–§IX.3.4 Higgs quotients. [MATH]: calculations C2–C3 derive (IX.3.10)–(IX.3.26) on the specified regular/free locus, excluding the origin from dimension subtraction. BDG §3.1, (3.1)–(3.3), pp. 8–9 supplies the quotient and meson presentation (Bullimore et al. 2017); its rank-one shorthand means rank at most one in the affine closure. Invariant generation, cotangent charts, real representative and injective trace multiplication are derived here. [BPS:1/2|NRth]: use of the classical Higgs quotient as the protected branch is a nonrenormalization premise, not proved by the Hilbert count. the finite check and the symbolic calculation test the finite identities and regularity. the ALE hyperkähler construction and Hilbert-series methods retain the broader hyperkähler and Hilbert foundations. Figures IX.3.2 and IX.3.3 are original schematics of these equations.

§IX.3.5–§IX.3.6 Compact photon and metric. Q3 and Q6 have distinct supports. Gaussian dualization and the connection, Chern number and Hopf metric in (IX.3.27)–(IX.3.44) are [MATH] consequences of the stated action, period and harmonic function (C4). The physical one-loop harmonic function and its protected abelian two-derivative completion are [BPS:1/2|NRth], sourced from BDG §3.1 (3.7)–(3.8), p. 10 and HKT §2.2 (2.17), p. 8 (Bullimore et al. 2017; Hook et al. 2013). HKT (2.6), (2.8) and footnote 1, p. 5 fix the Maxwell normalization and compact period. Only its real-axis $1/(4\pi|\sigma|)$ coefficient is used. Its printed triplet/connection package is not imported; the physical norm and connection are completed separately here. de Boer et al. §4.2 (4.8)–(4.17), pp. 27–29 supports the circle and toric metric structure, with its stated higher-loop assumption retained (Boer et al. 1997). IS §3.2 (3.6), (3.10), pp. 9–10 separates the quotient metric from the finite-coupling Coulomb metric (Intriligator and Seiberg 1996). the symbolic calculation and the consistency check verify normalization and limits; they are not a loop-integral or nonrenormalization proof. Figure IX.3.4 is an original fibration schematic.

§IX.3.7 Quantum ring and counting. [BPS:1/2|holo]: the OPE in (IX.3.45) is imported from BDG §3.1 (3.6), p. 10, with the explicit conversion (IX.3.46). C5 derives the subsequent symbolic series and orbifold invariant generation [MATH]. The two independent enumerations in the finite check agree in every charge through degree twelve for $n = 2, 3$; finite agreement is not a proof of the OPE or an all-degree numerical certification. The all-degree identity is the

displayed geometric-series algebra. General quantum Coulomb foundations remain quantum Coulomb-ring foundations.

§IX.3.8 Asymmetric mirror. [MATH]: C6 derives the integral basis, saturated kernel, invariant generation and six-field elimination in (IX.3.55)–(IX.3.67). HW §6.2, pp. 36–38 and IS §3.2, pp. 8–10 support the mirror matter/deformation interpretation; de Boer et al. §4.3, pp. 29–30 explains integral transformations versus covers. The absolute map (IX.3.60) remains conditional at $\tau = i$ on the leading classical FI matching of Chapter 1. The algebraic rescaling is not a metric or symplectic normalization match. [DUAL]: physical branch exchange inherits the Chapter 2 route, with nonperturbative IIB S-duality, creation and occupancy A-001 and infrared continuity A-002. The ring match does not independently prove these premises. the finite check and the symbolic calculation cover the symbolic family and asymmetric cubic. I23's repaired scope requires zero electric FI and zero primitive mirror mass, enforced on actual IX.2 fields by the live interface. This does not exclude nonzero-real-FI Higgs examples in §IX.3.3. Figure IX.3.5 uses the unchanged masses and charge matrix of the finite example.

§IX.3.9 Mixed open stratum. [MATH]: C7 derives (IX.3.68)–(IX.3.76), including the actual massless slice, moment-map rank and stabilizer. GW §2.4.2, p. 24 provides the broader mixed-branch interpretation (Gaiotto and Witten 2009). the finite check and the symbolic calculation verify the vacuum equations, residual generator and open dimensions; shifted coincident masses and a negative residual eigenvalue are included. The $8 + 4$ result does not determine the full quantum closure or global product metric. Figure IX.3.6 is a local incidence schematic only.

§IX.3.10 Monopole diagnostic. [BPS:1/2|short]: GW §2.4.1–2.4.2, (2.13)–(2.17), pp. 19–24 supplies the monopole zero-mode charge assignment and good/ugly/bad terminology. Its pp. 18–19 explain the free-photon R-symmetry issue. C8 derives the integral-weight/root specialization and bounds (IX.3.77)–(IX.3.84); the finite check tests the thresholds and asymmetric flux. No arbitrary bad-theory infrared R-symmetry or nonabelian Coulomb-ring algorithm is inferred.

The calculations apply to the finite meson ideals, Coulomb coefficients, mirror elimination, circle geometry and separated mixed slice described above. Figures IX.3.1–IX.3.6 are original local vector diagrams; positional meanings use HW §3 and the explicit equations cited above. No general branch classification, quantum brane/FI normalization theorem or finite-coupling mirror metric equality is claimed.

References

Boer, J. de et al. (1997). "Mirror symmetry in three-dimensional theories, SL(2,Z) and D-brane moduli spaces". In: *Nucl. Phys. B* 493, pp. 148–176. DOI: 10.1016/S0550-3213(97)00115-6. arXiv: hep-th/9612131.

Bullimore, M., T. Dimofte, and D. Gaiotto (2017). "The Coulomb Branch of 3d $\mathcal{N} = 4$ Theories". In: *Commun. Math. Phys.* 354.2, pp. 671–751. DOI: 10.1007/s00220-017-2903-0. arXiv: 1503.04817 [hep-th].

Gaiotto, D. and E. Witten (2009). "S-Duality of Boundary Conditions In N=4 Super Yang-Mills Theory". In: *Adv. Theor. Math. Phys.* 13.3, pp. 721–896. DOI: 10.4310/ATMP.2009.v13.n3.a5. arXiv: 0807.3720 [hep-th].

Hanany, A. and E. Witten (1997). "Type IIB superstrings, BPS monopoles, and three-dimensional gauge dynamics". In: *Nucl. Phys. B* 492, pp. 152–190. DOI: 10.1016/S0550-3213(97)00157-0. arXiv: hep-th/9611230.

Hook, A., S. Kachru, and G. Torroba (2013). "Supersymmetric Defect Models and Mirror Symmetry". In: *JHEP* 11, p. 004. DOI: 10.1007/JHEP11(2013)004. arXiv: 1308.4416 [hep-th].

Intriligator, K. A. and N. Seiberg (1996). "Mirror symmetry in three-dimensional gauge theories". In: *Phys. Lett. B* 387, pp. 513–519. DOI: 10.1016/0370-2693(96)01088-X. arXiv: hep-th/9607207.

Chapter IX.4

Boundary conditions and Nahm poles

IX.4.1 What an endpoint must remember

A single D3-brane ending on a fivebrane has a simple geometric description. It can move along the fivebrane and cannot move away from it. Chapter 1 used this observation to select the fields that survive on a finite D3 interval. Several coincident D3-branes bring in a new ingredient. Their transverse coordinates are matrices, and an endpoint can require those matrices to become noncommuting and singular. A list of allowed constant modes no longer describes the boundary.

We will keep the fourth D3 direction noncompact and study the resulting boundary problem. The bulk theory is four-dimensional $\mathcal{N} = 4$ Yang–Mills theory, with sixteen real Poincaré supercharges. A boundary preserving eight is called half-BPS. It has three-dimensional $\mathcal{N} = 4$ supersymmetry, but the bulk has not been reduced to three dimensions. Nor is this the four-dimensional $\mathcal{N} = 2$ theory on D4-branes that we will construct in Chapter 5.

The first task is to turn the endpoint into a variational problem. The normal derivative and the outward normal have signs, and the nonabelian scalar boundary condition requires a cubic surface interaction. Once these are fixed, a simple pole becomes an equation for three finite matrices. Those matrices tell us how many D3s end together and which boundary symmetry can survive. Finally, IIB S-duality changes the type of fivebrane at the endpoint. For one boundary it produces ordinary Neumann data; for another it produces Neumann data coupled to a new three-dimensional theory. We will follow the difference explicitly at ranks two and three.

Take-home message of this chapter

A nonabelian D5 endpoint can carry a Nahm pole whose residue is an $\mathfrak{su}(2)$ representation. The full triple of residues determines a compact commutant, with more information than its dimension alone. Ordinary Dirichlet data and an irreducible pole are different boundaries: the former acquire a $T[SU(N)]$ boundary theory under S-duality. Its quiver specifies actual representations and moment maps. The global symmetry acting on its local operators still leaves a separate question about which background bundles can be coupled consistently.

We use the brane orientations and gauge normalization of Chapter 1, the hypermultiplet quotient language of Chapter 3, and elementary unitary representation theory. We derive the needed matrix statements below. The two physical identifications that connect them to branes are the D3–D5 pole prescription and IIB S-duality. Neither follows merely from solving a matrix equation.

IX.4.2 From the brane frame to the surface variation

The normal direction must be identified before assigning Neumann or Dirichlet data. Let u^M denote the coordinates commonly used for the D3 boundary problem. Its source frame has

$$\mathrm{D3}:0123, \qquad \mathrm{D5}:012456, \qquad \mathrm{NS5}:012789, \qquad y=u^3\geq 0. \tag{IX.4.1}$$

The coordinates x^M of Chapter 1 are obtained by the passive change

$$(x^0,\dots,x^9)=(u^0,u^1,u^2,u^7,u^8,u^9,u^3,u^4,u^5,u^6). \tag{IX.4.2}$$

Every coordinate sign in this map is positive. Moving the block 789 past 3456 gives twelve transpositions, so the ten-dimensional orientation is preserved. The induced map on the branes and the normal is

$$\begin{gathered}\mathrm{D3}:0126, \quad \mathrm{D5}:012789, \quad \mathrm{NS5}:012345, \quad \det P=(-1)^{12}=+1,\\ s=x^6=u^3\geq 0, \qquad n=-ds=-du^3.\end{gathered} \tag{IX.4.3}$$

This operation changes names of axes. It does not exchange D5 and NS5 charges, transform the IIB coupling, or act on a charge doublet. The S-duality operation later in the chapter is a separate physical step.

Write X_i for the scalar triplet in 789 and Y_i for that in 345, with $i=1,2,3$ in each ordered triplet. In the source frame these are the 456 and 789 triplets, respectively. Our conventions are

$$X_i^\dagger=X_i, \quad Y_i^\dagger=Y_i, \quad A_M^\dagger=A_M, \qquad D_M=\partial_M-i[A_M,\,\cdot\,], \quad \epsilon_{123}=+1. \tag{IX.4.4}$$

The ordered X triplet and the choice $s\geq 0$ fix the sign of the pole below. The anti-Hermitian source fields are $X_i^{\mathrm{GW}}=-iX_i$.

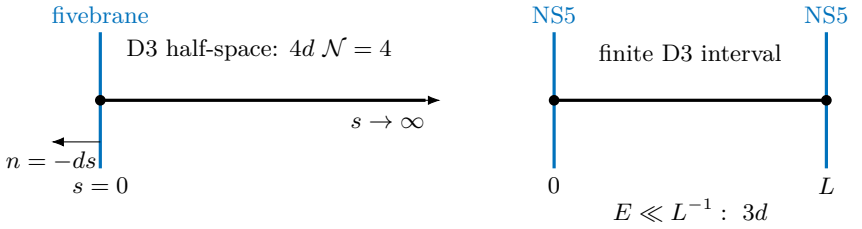


Figure IX.4.1: A D3 half-space and a finite D3 interval are different field-theory problems. Common 012 directions are suppressed. In the left panel the bulk retains four dimensions, and the outward normal at $s=0$ points to decreasing s. In the right panel, energies below $1/L$ select a three-dimensional theory. A vertical fivebrane stroke is a projection, not its complete tangent space.

To obtain the boundary terms, continue the worldvolume action to Euclidean signature, keeping the same real normal coordinate. Set $\theta=0$, and write the six scalars as $\Phi_A=(X_i,Y_i)$. With fundamental matrix trace,

$$S_{\text{bulk}}=\kappa\int_{s\ge0}d^4x\ \operatorname{Tr}\left\{\frac{1}{4}F_{MN}F_{MN}+\frac{1}{2}D_M\Phi_AD_M\Phi_A-\frac{1}{4}[\Phi_A,\Phi_B][\Phi_A,\Phi_B]\right\},$$
$$\kappa=\frac{2}{g^2_{4,\text{YM}}}. \tag{IX.4.5}$$

Repeated A,B are summed over all ordered pairs. A commutator of Hermitian matrices is anti-Hermitian, so the minus sign makes the potential nonnegative. For generators normalized by $\operatorname{Tr}T^aT^b=\delta^{ab}/2$, the gauge term has the usual component coefficient $1/(4g^2_{4,\text{YM}})$.

Varying the gauge kinetic term first exposes the normal momentum. The antisymmetry of F removes a factor of two:

$$\delta S_F=\kappa\int\operatorname{Tr}(F_{MN}D_M\delta A_N)=-\kappa\int\operatorname{Tr}(D_MF_{MN}\delta A_N)+\kappa\int_\partial\operatorname{Tr}(n_MF_{MN}\delta A_N). \tag{IX.4.6}$$

Covariant integration by parts uses cyclicity of the trace. Applying it to the scalar kinetic terms gives

$$\delta S_{\text{kin},\Phi}=-\kappa\int\operatorname{Tr}(D_MD_M\Phi_A\,\delta\Phi_A)+\kappa\int_\partial\operatorname{Tr}(n_MD_M\Phi_A\,\delta\Phi_A). \tag{IX.4.7}$$

The potential has no normal derivatives and contributes no surface term. Scalar dependence on A_M changes the bulk gauge equation but also creates no derivative of δA_M. Thus, for tangential indices $\mu=0,1,2$, the entire bosonic boundary variation is

$$\delta S_{\text{bulk}}\big|_\partial=-\kappa\int_{s=0}d^3x\ \operatorname{Tr}\left(F_{s\mu}\delta A_\mu+D_sX_i\delta X_i+D_sY_i\delta Y_i\right). \tag{IX.4.8}$$

There is no normal gauge momentum multiplying δA_s, because $F_{ss}=0$. Setting $A_s=0$ is a useful local gauge choice, not an additional gauge-invariant boundary equation.

For regular fields with no boundary matter, an NS5 endpoint allows motion in 345 and fixes motion in 789. Its bosonic data are

$$F_{s\mu}\big|_0 = 0, \qquad D_s Y_i\big|_0 = 0, \qquad X_i\big|_0 = 0. \tag{IX.4.9}$$

The free variations of A_μ, Y_i force their normal momenta to vanish; the fixed X_i have $\delta X_i = 0$. For a D5 endpoint the gauge field and Y have Dirichlet data. The elementary abelian choice is

$$A_\mu\big|_0 = a_\mu^{(0)}, \quad \delta A_\mu\big|_0 = 0, \qquad Y_i\big|_0 = 0, \qquad \partial_s X_i\big|_0 = 0. \tag{IX.4.10}$$

Usually we choose $a^{(0)} = 0$. A fixed flat connection implies $F_{\mu\nu} = 0$ locally, but that field-strength equation alone does not specify the fixed connection and its possible holonomies. The nonabelian replacement for the last equation will require a surface action.

These conditions reproduce the motion of one D3. A constant abelian $Y_i = y_i$ obeys the NS5 conditions and translates the endpoint along the NS5; a constant $X_i = x_i$ obeys the D5 conditions and translates it along the D5. On a finite interval the same choices select zero modes. On the half-space they constrain fields that can still vary in the bulk.

Boundary degrees of freedom modify the surface equations. Define their gauge current by variation, including its normalization:

$$\delta S_{\mathcal{B}} = \int_\partial d^3x \ \mathrm{Tr}(j^\mu \delta A_\mu) + \cdots, \qquad -\kappa F_{s\mu} + j_\mu = 0. \tag{IX.4.11}$$

The sign follows directly from the lower boundary normal. In an $\mathcal{N} = 4$ coupling, a boundary moment map also shifts the triplet that was fixed in (IX.4.9). In the bulk normalization we will denote that sourced condition by

$$\boldsymbol{X}(0) + \boldsymbol{\mu}_Z = 0. \tag{IX.4.12}$$

Here $\boldsymbol{\mu}_Z$ is defined in the normalization of this bulk boundary equation. A canonical three-dimensional hypermultiplet has a quadratic moment map, but identifying it numerically with $\boldsymbol{\mu}_Z$ requires a coupling coefficient. We will not need that coefficient: our quiver calculations use zero moment-map levels and holomorphic representations, and never substitute $q\widetilde{q}$ into (IX.4.12). The fermionic boundary conditions completing these bosonic equations are part of the half-BPS boundary construction.

IX.4.3 The cubic boundary action and Nahm's equation

A D5 endpoint allows the X triplet to fluctuate. In a nonabelian theory its interactions can balance a normal gradient. This balance is the origin of Nahm's equation. We first identify its sign from supersymmetry, then derive the same equation by completing the energy square and varying the boundary action.

Take fields independent of the boundary coordinates, set $Y = 0$, and work locally in $A_s = 0$. Define the Hermitian quadratic expression

$$C_i = -\frac{i}{2}\epsilon_{ijk}[X_j, X_k], \qquad (C_1, C_2, C_3) = -i([X_2, X_3], [X_3, X_1], [X_1, X_2]). \quad \text{(IX.4.13)}$$

The reduced gaugino variation inherited from the bulk theory has the form

$$\delta\Psi \;\propto\; \left(\sum_i \Gamma^{si} X_i' - i\sum_{i<j} \Gamma^{ij}[X_i, X_j]\right)\varepsilon. \quad \text{(IX.4.14)}$$

The index i here denotes the ordered 789 directions, not a boundary spacetime index. To see which first-order equation annihilates the chosen spinors, use the Clifford algebra in the four Euclidean directions $(s, 7, 8, 9)$. Its oriented product obeys

$$K = \Gamma^{s789}, \qquad K^2 = 1, \qquad K\varepsilon = -\varepsilon, \qquad \Gamma^{89} = -\Gamma^{s7}K, \quad \text{(IX.4.15)}$$

with cyclic versions of the last identity. For example, $\Gamma^{s7}\Gamma^{s789} = -\Gamma^{89}$. Acting on the chosen spinors, (IX.4.14) therefore becomes

$$\delta\Psi \;\propto\; \sum_i \Gamma^{si}(X_i' + C_i)\varepsilon. \quad \text{(IX.4.16)}$$

A sufficient static half-BPS equation, restored to a covariant gauge, is

$$B_i := D_s X_i - \frac{i}{2}\epsilon_{ijk}[X_j, X_k] = 0. \quad \text{(IX.4.17)}$$

This reduced Clifford computation fixes the nonlinear sign in the chosen frame. The statement that the full boundary preserves eight of the sixteen bulk supercharges also uses the bulk reality conditions and the complete supersymmetric boundary construction. In anti-Hermitian source variables the same equation reads

$$D_s X_i^{\mathrm{GW}} + \frac{1}{2}\epsilon_{ijk}[X_j^{\mathrm{GW}}, X_k^{\mathrm{GW}}] = 0, \qquad X_i^{\mathrm{GW}} = -iX_i. \quad \text{(IX.4.18)}$$

A sign copied from this form without converting the matrices would give the wrong Hermitian pole.

The cubic whose gradient is C_i is real for Hermitian fields:

$$W(X) = -i\,\mathrm{Tr}\, X_1[X_2, X_3] = -\frac{i}{3}\epsilon_{ijk}\,\mathrm{Tr}\, X_i X_j X_k. \quad \text{(IX.4.19)}$$

This is a scalar functional per unit boundary volume. To differentiate it with respect to all three matrices, move the varied matrix to the left inside the trace. For instance, $\mathrm{Tr}\, X_1[\delta X_2, X_3] = \mathrm{Tr}[X_3, X_1]\delta X_2$. The result is

$$\delta W = \sum_i \mathrm{Tr}(C_i \delta X_i), \qquad \frac{dW}{ds} = \sum_i \mathrm{Tr}(C_i D_s X_i). \quad \text{(IX.4.20)}$$

The second identity is gauge covariant because W is gauge invariant. It supplies precisely the cross term in the square.

Regulate the lower boundary by $s = \epsilon$ and hold the upper endpoint at L. The energy in this static sector is

$$\frac{E_{\text{bulk}}}{\kappa} = \int_{\epsilon}^{L} ds \ \mathrm{Tr} \left\{ \frac{1}{2} \sum_{i} (D_s X_i)^2 - \frac{1}{2} \sum_{i<j} [X_i, X_j]^2 \right\}. \tag{IX.4.21}$$

Each unordered commutator occurs once here, whereas the potential in (IX.4.5) sums ordered pairs. Since $\sum_i C_i^2 = -\sum_{i<j} [X_i, X_j]^2$, expanding the positive square gives

$$\frac{E_{\text{bulk}}}{\kappa} = \frac{1}{2} \int_{\epsilon}^{L} ds \ \mathrm{Tr} \sum_{i} B_i^2 - W(X(L)) + W(X(\epsilon)). \tag{IX.4.22}$$

At the lower boundary, the surface interaction is consequently

$$S_{\partial,X} = -\kappa \int_{s=\epsilon} d^3x \, W(X). \tag{IX.4.23}$$

Its variation combines with the lower normal momentum to give

$$(\delta S_{\text{bulk}} + \delta S_{\partial,X})\big|_{\epsilon} = -\kappa \int d^3x \ \mathrm{Tr} \sum_{i} (D_s X_i + C_i) \delta X_i. \tag{IX.4.24}$$

Free X variations thus impose exactly (IX.4.17). For commuting fields, $W = C_i = 0$ and the condition reduces to the ordinary normal derivative in (IX.4.10). For noncommuting fields, omitting the cubic would impose a different condition.

There is a useful elementary sign check. Set $X_i = f(s) J_i$, where $[J_i, J_j] = i\epsilon_{ijk} J_k$. Then $C_i = f^2 J_i$, and the entire matrix equation reduces to

$$f' + f^2 = 0, \qquad f(s) = \frac{1}{s + c} \quad \text{or} \quad f = 0. \tag{IX.4.25}$$

The positive residue solution decreases into the bulk. Reversing either the outward normal without changing the surface action, or the nonlinear term without changing Hermiticity, would destroy this agreement. Singular data require a regulated variational problem; the square establishes its leading boundary structure, not all possible subleading counterterms.

IX.4.4 Noncommuting poles at small rank

A scale-invariant endpoint has no preferred length along the half-line. Since a scalar has mass dimension one, the candidate singularity is a simple pole. Assume a regular asymptotic expansion after this leading term, so that differentiating the remainder introduces no term of order s^{-2}. Insert it into the already oriented equation:

$$X_i(s) = \frac{J_i}{s} + O(s^0), \qquad -J_i - \frac{i}{2} \epsilon_{ijk} [J_j, J_k] = 0. \tag{IX.4.26}$$

Contracting the second equation with $\epsilon_{\ell m i}$ recovers the individual commutators,

$$[J_\ell, J_m] = i\epsilon_{\ell m i} J_i, \qquad J_i^\dagger = J_i. \tag{IX.4.27}$$

Thus the residue is a unitary finite-dimensional representation of $\mathfrak{su}(2)$. This conclusion concerns the leading pole; choosing all subleading boundary data is an additional problem.

For two D3s the smallest noncommuting choice is spin one-half. All three matrices are needed:

$$J_1 = \frac{1}{2}\begin{pmatrix} 0 & 1 \\ 1 & 0 \end{pmatrix}, \quad J_2 = \frac{1}{2}\begin{pmatrix} 0 & -i \\ i & 0 \end{pmatrix}, \quad J_3 = \frac{1}{2}\begin{pmatrix} 1 & 0 \\ 0 & -1 \end{pmatrix}. \tag{IX.4.28}$$

For example, direct multiplication gives $[J_1, J_2] = \frac{i}{2}\,\mathrm{diag}(1,-1) = iJ_3$. The other two cyclic commutators follow by the same multiplication, and

$$\sum_i J_i^2 = \frac{3}{4}\mathbf{1}_2, \qquad \mathrm{Tr}\sum_i J_i^2 = \frac{3}{2}. \tag{IX.4.29}$$

Neither the matrices nor their pole can be simultaneously diagonalized. Treating the diagonal entries of three unrelated matrices as three ordinary D3 positions would lose the commutator that supports the solution.

At rank three, spin one gives a different irreducible endpoint:

$$\begin{gathered} J_1 = \frac{1}{\sqrt{2}}\begin{pmatrix} 0 & 1 & 0 \\ 1 & 0 & 1 \\ 0 & 1 & 0 \end{pmatrix}, \qquad J_2 = \frac{1}{\sqrt{2}}\begin{pmatrix} 0 & -i & 0 \\ i & 0 & -i \\ 0 & i & 0 \end{pmatrix}, \\ J_3 = \begin{pmatrix} 1 & 0 & 0 \\ 0 & 0 & 0 \\ 0 & 0 & -1 \end{pmatrix}, \qquad \sum_i J_i^2 = 2\mathbf{1}_3. \end{gathered} \tag{IX.4.30}$$

One can construct these matrices without guessing their entries. In an orthonormal basis $|j,m\rangle$, diagonalize J_3 and use $J_\pm = J_1 \pm iJ_2$. The algebra and Hermiticity require

$$\begin{aligned} &J_3|j,m\rangle = m|j,m\rangle, \\ &J_+|j,m\rangle = \sqrt{(j-m)(j+m+1)}\,|j,m+1\rangle, \qquad J_- = J_+^\dagger. \end{aligned} \tag{IX.4.31}$$

Setting $j = 1/2$ or 1 reproduces the two displayed triples. The highest and lowest weights force $2j$ to be a nonnegative integer, and the irreducible dimension is $d = 2j+1$.

The normalization of a nonzero pole is fixed, not a free amplitude. If we multiply a valid residue by a real number a, its Nahm residual is

$$B_i\left[\frac{aJ}{s}\right] = \frac{a(a-1)J_i}{s^2}. \tag{IX.4.32}$$

Only $a = 1$ gives the nonzero pole; $a = 0$ removes it. A deformation that changes just one component fails even more visibly:

$$(X_1, X_2, X_3) = \frac{1}{s}(J_1, J_2, 2J_3) \quad \Longrightarrow \quad (B_1, B_2, B_3) = \frac{1}{s^2}(J_1, J_2, -J_3). \tag{IX.4.33}$$

Both examples distinguish an actual solution from three matrices with the right size and mass dimension. A commuting nonzero residue also fails: without the quadratic commutator, its $-J_i/s^2$ derivative has nothing to cancel it.

A shifted profile illustrates a different distinction. For $c > 0$,

$$X_i(s) = \frac{J_i}{s+c}, \qquad B_i = 0, \qquad \lim_{s\to 0} sX_i(s) = 0. \tag{IX.4.34}$$

It is a regular solution with zero pole residue at the chosen boundary. Taking $c \to 0^+$ creates the pole. The gauge-invariant size that we may plot is

$$R_X(s) := \sqrt{\frac{1}{d}\operatorname{Tr}\sum_i X_i^2} = \frac{\sqrt{j(j+1)}}{s+c}. \tag{IX.4.35}$$

This norm is not a set of simultaneous eigenvalue positions or an exact spacetime funnel radius.

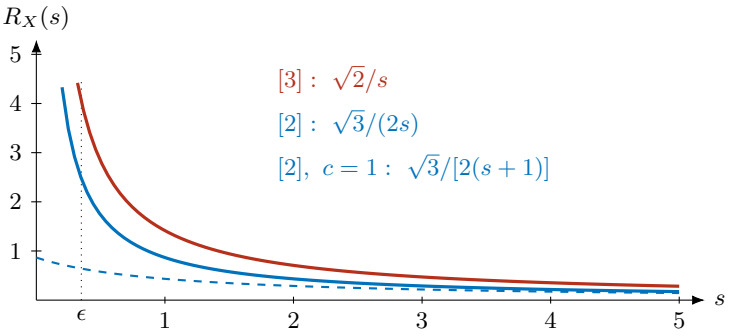


Figure IX.4.2: An invariant norm for the rank-two and rank-three irreducible solutions. The solid curves have a boundary pole; the dashed rank-two curve has $c = 1$ and remains finite. The vertical dotted line is a regulator at $s = \epsilon$. All axes use the scalar and length units of (IX.4.35); the drawing represents the matrix norm, not a classical brane embedding.

The regulated energy provides another quantitative check. Put $\mathcal{C} = \operatorname{Tr}\sum_i J_i^2$. On the pole the derivative and potential terms in (IX.4.21) are equal. Consequently,

$$\frac{E_{\text{bulk}}}{\kappa} = \mathcal{C}\int_\epsilon^L \frac{ds}{s^4} = \frac{\mathcal{C}}{3}(\epsilon^{-3} - L^{-3}), \qquad W(X(s)) = \frac{\mathcal{C}}{3s^3}. \tag{IX.4.36}$$

The lower surface term $-\kappa W(X(\epsilon))$ cancels the leading ϵ^{-3} divergence. For the rank-two and rank-three poles the coefficients $\mathcal{C}/3$ are $1/2$ and 2. This calculation explains why the same cubic appears in the singular problem; it does not specify a complete renormalization prescription for arbitrary fluctuations.

What turns this solution into a D3 endpoint is a brane-to-field identification. Consider a D5 defect with D3s on both sides, then send the transverse eigenvalues of the

D3s on one side to infinity. In the complex Nahm description the remaining matrix is regular nilpotent: the defect changes it by rank one, and the surviving rank is $N-1$. The decaying real solution is an irreducible shifted pole. Removing the other D3s sends the shift to zero. In our notation this is

$$\frac{J_i^{(N)}}{s+c} \xrightarrow{c\to 0^+} \frac{J_i^{(N)}}{s}, \qquad N \text{ D3s ending on one D5.} \tag{IX.4.37}$$

The rank-one defect relation and the physical removal limit supply the brane interpretation. Matrix agreement by itself establishes only that the resulting pole solves the boundary equation.

IX.4.5 Partitions and the symmetry of the full residue

A pole can be reducible: different groups of D3s can carry different irreducible blocks. To find the symmetry left at the boundary, we must commute with all three residues. We first explain why partitions enter, then solve the commutant in examples where dimensions alone would hide the answer.

Hermiticity supplies a short complete-reducibility argument. If a subspace V is invariant under every J_i, its orthogonal complement is invariant as well. For $v \in V$ and $w \in V^\perp$,

$$\langle v, J_i w\rangle = \langle J_i v, w\rangle = 0. \tag{IX.4.38}$$

We can therefore split off irreducible subspaces until the finite vector space is exhausted. Within each subspace the raising and lowering operators in (IX.4.31) fix one representation of dimension d. Collecting equivalent copies gives

$$\mathbb{C}^N = \bigoplus_{d\geq 1} V_d \otimes \mathbb{C}^{m_d}, \qquad J_i = \bigoplus_d J_i^{(d)} \otimes \mathbf{1}_{m_d}, \qquad N = \sum_d d\, m_d. \tag{IX.4.39}$$

The nonzero multiplicities m_d specify a partition of N. This is a classification of finite Hermitian residue representations up to unitary equivalence. It is not a classification of all half-BPS boundaries, which can include additional gauge choices and boundary matter.

The symmetry equation is $UJ_i = J_iU$ for every i. A block mapping two inequivalent irreducible representations must vanish; a block mapping two equivalent ones is a scalar on V_d. Thus the unitary transformation can act freely only on the multiplicity spaces:

$$Z_{U(N)}(\rho) = \prod_d U(m_d), \qquad \dim_{\mathbb{R}} Z_{U(N)}(\rho) = \sum_d m_d^2. \tag{IX.4.40}$$

For $SU(N)$ there is one further condition. The transformation $\mathbf{1}_d \otimes u_d$ repeats every eigenvalue of u_d exactly d times, so its determinant is $(\det u_d)^d$. Hence

$$Z_{SU(N)}(\rho) = \left\{ (u_d) \in \prod_d U(m_d) : \prod_d (\det u_d)^d = 1 \right\}, \quad \dim_{\mathbb{R}} Z_{SU(N)}(\rho) = \sum_d m_d^2 - 1. \tag{IX.4.41}$$

The dimension follows by differentiating the determinant constraint at the identity. The group itself can have disconnected or finite parts that this differentiation cannot detect.

It is instructive to solve the rank-two system without using the general formula. If T commutes with the J_3 in (IX.4.28), its off-diagonal entries vanish. Commuting with J_1 then equates the diagonal entries:

$$[T, J_3] = 0 \implies T = \begin{pmatrix} a & 0 \\ 0 & d \end{pmatrix}, \qquad [T, J_1] = 0 \implies a = d. \tag{IX.4.42}$$

The complex commutant is scalar, and its unitary part is $U(1)$. For $SU(2)$ the determinant condition leaves only $\{\mathbf{1}, -\mathbf{1}\}$. More generally, the principal, meaning irreducible, embedding has

$$Z_{U(N)}(\rho_{\text{prin}}) = U(1), \qquad Z_{SU(N)}(\rho_{\text{prin}}) = \mathbb{Z}_N, \qquad \dim Z_{SU(N)}(\rho_{\text{prin}}) = 0. \tag{IX.4.43}$$

Zero Lie-algebra dimension therefore does not mean a trivial group. At the opposite extreme, the trivial representation has $J_i = 0$ on all of $\mathbb{C}^N$; every unitary matrix commutes with it, giving $U(N)$, or $SU(N)$ after imposing unit determinant.

A first reducible example is the partition $[2, 1]$. It gives an actual three-by-three triple by adjoining a zero block to each spin-half matrix:

$$J_i^{[2,1]} = \begin{pmatrix} J_i^{(2)} & 0 \\ 0 & 0 \end{pmatrix}, \qquad T = \begin{pmatrix} A & v \\ w & b \end{pmatrix}. \tag{IX.4.44}$$

The equations $[T, J_i] = 0$ require $[A, J_i^{(2)}] = 0$ and $J_i^{(2)} v = w J_i^{(2)} = 0$. Since $J_3^{(2)}$ is invertible, $v = w = 0$; the preceding rank-two calculation gives $A = a\mathbf{1}_2$. Therefore

$$Z_{U(3)}([2,1]) = \{\text{diag}(e^{i\alpha}\mathbf{1}_2, e^{i\beta})\}, \qquad Z_{SU(3)}([2,1]) : \; e^{2i\alpha+i\beta} = 1. \tag{IX.4.45}$$

The dimensions are two and one. The singlet block is a D3 with zero residue; it is not a smaller copy of the nonzero pole.

Repeated blocks behave differently. For $[2, 2]$, order the basis by the two repeated copies of the spin-half representation. View every four-by-four commuting matrix as a two-by-two array of two-by-two blocks. Each block must be a scalar multiple of $\mathbf{1}_2$, including the off-diagonal ones. The multiplicity space can therefore rotate:

$$\begin{aligned} J_i^{[2,2]} &= \mathbf{1}_2 \otimes J_i^{(2)}, \qquad Z_{U(4)}([2,2]) = U(2), \\ Z_{SU(4)}([2,2]) &= \{u \in U(2) : (\det u)^2 = 1\}. \end{aligned} \tag{IX.4.46}$$

The latter group has two components, labeled by $\det u = \pm 1$, and its identity component is $SU(2)$. In contrast, $[3, 1]$ has two inequivalent irreducible blocks and a $U(1) \times U(1)$ commutant in $U(4)$. The finite calculations agree with the general rule:

ρ	$[2]$	$[3]$	$[2,1]$	$[2,2]$	$[3,1]$
$\dim Z_{U(N)}$	1	1	2	4	2
$\dim Z_{SU(N)}$	0	0	1	3	1
$\text{Tr} \sum_i J_i^2$	3/2	6	3/2	3	6

. (IX.4.47)

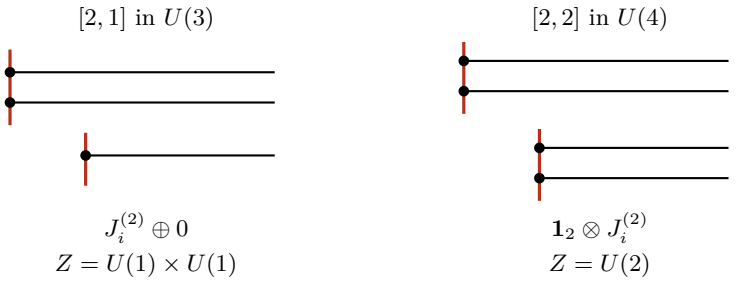


Figure IX.4.3: Endpoint groupings for $[2,1]$ and $[2,2]$, with common 012 suppressed. The drawings distinguish D5s before their allowed coincidence limit; offsets of D3 strands only separate labels. One group of two ending D3s contributes a spin-half block. Two equivalent blocks have a multiplicity space admitting $U(2)$ rotations, while an inequivalent singlet gives a separate $U(1)$. The group formulas refer to the coincident residue data.

There is a common confusion when switching to complex coordinates. The raising operator J_+ alone has a larger complex centralizer. Already for spin one-half,

$$J_+ = \begin{pmatrix} 0 & 1 \\ 0 & 0 \end{pmatrix}, \qquad [T, J_+] = 0 \iff T = \begin{pmatrix} a & b \\ 0 & a \end{pmatrix}. \tag{IX.4.48}$$

In $\mathfrak{sl}_2(\mathbb{C})$ this leaves the one-dimensional space spanned by J_+, whereas commuting with the full triple in $\mathfrak{su}(2)$ leaves no continuous generator. The former is relevant to a complex nilpotent orbit; the latter is the compact symmetry of the pole. For a principal $N \times N$ nilpotent matrix, its complex $\mathfrak{sl}_N$ centralizer similarly has dimension $N-1$, not zero.

The distinction extends to reducible residues. Let λ be the partition of N and let λ'_k count its blocks of size at least k. For the nilpotent matrix $e = J_+$, a block of size a is the module $\mathbb{C}[t]/(t^a)$, with t acting as e. An intertwiner from a block of size a to one of size b is determined by the image of 1, which must be killed by t^a. There are $\min(a,b)$ independent choices. Thus

$$\dim_{\mathbb{C}} Z_{\mathfrak{gl}_N}(e) = \sum_{r,s} \min(\lambda_r, \lambda_s) = \sum_k (\lambda'_k)^2, \qquad \dim_{\mathbb{C}} \mathcal{O}_\lambda = N^2 - \sum_k (\lambda'_k)^2. \tag{IX.4.49}$$

The second equality counts each pair of blocks once for every shared height k. Passing to $\mathfrak{sl}_N$ subtracts one from both the ambient algebra and the centralizer, leaving the orbit dimension unchanged. For $[2,2]$, the nilpotent centralizer has complex dimension eight and the orbit has dimension eight, whereas the compact full-triple commutant is $U(2)$ of real dimension four. These count different transformations. Neither number determines which S-dual boundary theory must appear.

Finally, a commutant describes transformations preserving the residue. Whether those transformations are boundary global symmetries or are partly gauged depends on the rest of the boundary condition. A choice of bulk global group can also change finite quotients. The formulas above specify the actual $U(N)$ and $SU(N)$ matrix groups and do not infer a line-operator spectrum from their Lie-algebra dimensions.

IX.4.6 Boundary S-duality and the rank-two theory

The pole distinguishes two ways to end two D3s. If both end on one D5, the residue is the irreducible spin-half triple. If one ends on each of two D5s, the residue is $[1, 1]$, hence zero. Bringing the D5s together in the second arrangement gives ordinary Dirichlet data with the full boundary group, not the principal pole.

IIB S-duality exchanges the fivebrane charges and sends $\tau \mapsto -1/\tau$. Its boundary dictionary for the interacting $\mathfrak{su}(2)$ sector is

$$\begin{aligned} \text{principal D5 pole} &\overset{S}{\longleftrightarrow} \text{unadorned Neumann}, \\ \text{ordinary Dirichlet} &\overset{S}{\longleftrightarrow} \text{Neumann coupled to } T[SU(2)]. \end{aligned} \tag{IX.4.50}$$

These are physical duality statements. The dual description exchanges the roles of the two transverse triplets. If both brane systems are to be written in the fixed axes of Chapter 1, the proper restoring rotation of Chapter 2 must also be included. It is separate from the passive source-to-book permutation (IX.4.2). Our endpoint drawings show only s and suppress these transverse directions. The center of the D3 $U(2)$ theory requires its own abelian boundary data, so the interacting-sector notation does not remove that center by declaration.

To understand why the second line needs a boundary theory, separate the two D5 endpoints along the half-line. The number of D3s increases by one at each endpoint. After converting D5s to NS5s, a finite rank-one interval precedes the rank-two half-space. At energies below its inverse length, that finite interval contributes a three-dimensional $U(1)$ vector multiplet. The common-NS5 coupling to the rank-two side contributes a bifundamental, which becomes two fundamentals when that side is regarded as a background flavor group. Thus

$$T[SU(2)]: \quad U(1) \text{ with } (q_a, \widetilde{q}^a), \quad a = 1, 2, \qquad Q_g(q_a) = +1, \quad Q_g(\widetilde{q}^a) = -1. \tag{IX.4.51}$$

The theory is the infrared limit of this ultraviolet description. The direct endpoint construction changes the fivebrane species without reordering them. Additional motions used to display a standalone self-mirror brane configuration are a different argument, requiring brane creation and infrared continuity. They are not steps in the direct boundary transformation used here.

Specifying just the dimension of the hypermultiplets would miss their charges. Let e be the $U(1)$ gauge Cartan weight and f_1, f_2 the weights of the flavor cover. Regard q as a 1×2 matrix and $\widetilde{q}$ as a 2×1 matrix, transforming by

$$q \mapsto gqh^{-1}, \qquad \widetilde{q} \mapsto h\widetilde{q}g^{-1}, \qquad g \in U(1), \quad h \in U(2). \tag{IX.4.52}$$

The full complex weight multiset of this single hypermultiplet representation is

$$\{e - f_1,\ e - f_2,\ -e + f_1,\ -e + f_2\}. \tag{IX.4.53}$$

Every entry has multiplicity one. The two positive gauge charges label two different flavor components; replacing one with a duplicate of the other changes the representation

even though its dimension stays four. The cover weights describe elementary charged fields, not yet the faithful symmetry on gauge-invariant operators.

We can see the Higgs geometry with no boundary-coupling coefficient. In one complex structure take the adjoint chiral scalar φ of the $U(1)$ vector multiplet and the holomorphic superpotential

$$W_{3d} = \varphi(q_1\widetilde{q}^1 + q_2\widetilde{q}^2), \qquad \mu_{\mathbb{C}} = q_1\widetilde{q}^1 + q_2\widetilde{q}^2 = 0. \tag{IX.4.54}$$

The nonzero overall superpotential coefficient has been absorbed in this holomorphic presentation; this is not a normalization of $\boldsymbol{\mu}_Z$ in (IX.4.12). On the Higgs branch $\varphi = 0$ away from the origin, and the gauge-invariant generators can be chosen as

$$x = q_1\widetilde{q}^2, \qquad y = -q_2\widetilde{q}^1, \qquad z = q_1\widetilde{q}^1 = -q_2\widetilde{q}^2. \tag{IX.4.55}$$

Their product has the required sign:

$$xy = -(q_1\widetilde{q}^1)(q_2\widetilde{q}^2) = z^2, \qquad \mathbb{C}[\mathcal{M}_H] = \mathbb{C}[x,y,z]/(xy - z^2). \tag{IX.4.56}$$

To see that these generate the invariant ring, every charge-neutral monomial pairs a q with a $\widetilde{q}$. The four pairings form a rank-at-most-one two-by-two matrix; its trace vanishes by (IX.4.54). Eliminating that trace leaves precisely the three entries and their determinant relation in (IX.4.56). This is the A_1 surface. The origin is singular, so a smooth quotient count should be performed away from it.

For example, choose $q = (v, 0)$ and $\widetilde{q} = (0, v)^t$ with $v \neq 0$. Both complex and real zero-level moment maps vanish, and the charge-one action has no continuous stabilizer. The dimension count there is

$$\dim_{\mathbb{R}} \mathcal{M}_H = 8 - 3 - 1 = 4, \qquad \dim_{\mathbb{H}} \mathcal{M}_H = 2 - 1 = 1. \tag{IX.4.57}$$

The three subtractions impose the real moment-map triplet, and the last one divides by $U(1)$. This calculation is local on the regular stratum; it does not make the apex smooth.

Chapter 3 supplies a distinct protected quantum statement for the Coulomb branch of charge-one $U(1)$ theory with two massless hypers, with FI parameters zero:

$$v_+v_- = \varphi^2, \qquad \mathbb{C}[\mathcal{M}_C] = \mathbb{C}[v_+, v_-, \varphi]/(v_+v_- - \varphi^2). \tag{IX.4.58}$$

The monopole product is not obtained by the elementary-field Higgs elimination above. Once that quantum relation is supplied, the two complex surfaces agree. This comparison exhibits a protected part of the self-mirror theory; equality of the polynomial alone would not establish its full infrared duality or its global background couplings.

The two flavor Lie algebras are conventionally called $\mathfrak{su}(2)_H^{\mathrm{fl}}$ and $\mathfrak{su}(2)_C^{\mathrm{fl}}$. The first acts on the hypers; the second is the infrared enhancement of the topological symmetry. They must be distinguished from the $SU(2)_H^R \times SU(2)_C^R$ R-symmetry that rotates supercharges and complex structures. The global form of the flavor symmetries will be our last rank-two calculation.

IX.4.7 Quiver matter and nilpotent moment maps

The direct endpoint construction extends without changing its mechanism. End one D3 at a time on N D5s, then apply S. The finite cumulative ranks are $1, 2, \ldots, N-1$; the last rank-N segment is a half-space. Figure IX.4.4 shows the direct construction for $N = 3$.

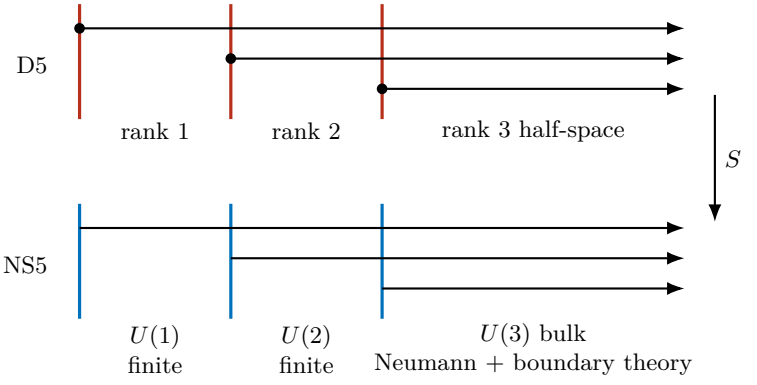


Figure IX.4.4: The direct boundary S operation for ordinary Dirichlet data. Top: one D3 ends on each D5, so the cumulative ranks are $1, 2$, then 3 in the half-space. Bottom: S converts the D5s to NS5s in the same order; finite ranks $1, 2$ become boundary gauge factors, and rank 3 remains a four-dimensional bulk field. In the standalone quiver the terminal node is a flavor square; coupling it to the bulk gauges that flavor symmetry with the boundary value of the bulk connection. No fivebrane crossing is drawn or used.

Treating the last boundary connection as an external flavor field gives

$$G = \prod_{i=1}^{N-1} U(i), \qquad (1) - (2) - \cdots - (N-1) - [N]. \tag{IX.4.59}$$

In this display circles, written as parentheses, are gauge nodes and brackets denote a flavor node. Each link carries one hypermultiplet in the indicated bifundamental representation. The terminal flavor symmetry is coupled to the bulk in the boundary problem; it remains external in the standalone three-dimensional theory $T[SU(N)]$.

Choose vector spaces $V_i = \mathbb{C}^i$ and $F = V_N = \mathbb{C}^N$. In a complex structure, the two chiral fields on link i are

$$A_i \in \mathrm{Hom}(V_{i+1}, V_i), \quad B_i \in \mathrm{Hom}(V_i, V_{i+1}), \quad A_i \mapsto g_i A_i g_{i+1}^{-1}, \quad B_i \mapsto g_{i+1} B_i g_i^{-1}. \tag{IX.4.60}$$

At $i = N-1$, g_N is a flavor transformation. These are actual $i \times (i+1)$ and $(i+1) \times i$ matrices. A hypermultiplet in a complex representation of dimension d has quaternionic dimension d and contains $2d$ complex scalar components in this description.

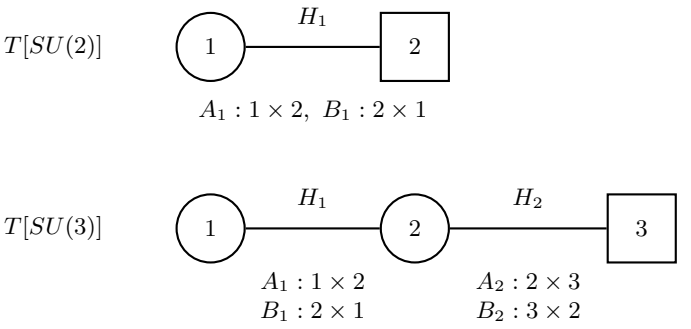


Figure IX.4.5: The standalone $T[SU(2)]$ and $T[SU(3)]$ quivers. Circular nodes are $U(1)$ and $U(2)$ gauge factors, while the squares are flavor spaces. Each drawn link denotes one hypermultiplet, containing the two opposite chiral representations. For $T[SU(3)]$ the 1×2 and 2×3 matrices contribute quaternionic dimensions two and six. The terminal square is coupled to a four-dimensional connection only when the quiver is used as a boundary theory.

For $T[SU(3)]$, let e be the $U(1)$ weight, u_1, u_2 the $U(2)$ weights, and f_1, f_2, f_3 the flavor-cover weights. The complete matter content, with the attachment of each weight retained, is

link	weights, each with multiplicity one	complex components
$H_1 : (1)$–(2)	$\pm(e - u_1),\ \pm(e - u_2)$	4
$H_2 : (2)$–$[3]$	$\pm(u_b - f_a), \quad b = 1, 2,\ a = 1, 2, 3$	12

. (IX.4.61)

One independent way to recover each entry is to apply the diagonal Cartan generators to a matrix unit. If E_{ba} is an elementary rectangular matrix, then

$$H_L E_{ba} - E_{ba} H_R = (h_{L,b} - h_{R,a}) E_{ba}. \tag{IX.4.62}$$

The reverse matrix has the negative weight. This also explains why moving a weight from the first link to the second changes the theory: the left and right Cartan generators are attached to different spaces. Reordering the matrix-unit basis or consistently conjugating an entire hyper changes only its presentation.

No common gauge center is ineffective in this framed quiver. A central transformation $g_i = e^{i\alpha_i} \mathbf{1}_i$ acts on an interior A_i by $e^{i(\alpha_i - \alpha_{i+1})}$. At the terminal link, with the flavor transformation held fixed to the identity, it acts by $e^{i\alpha_{N-1}}$. Acting trivially on every field requires

$$e^{i\alpha_{N-1}} = 1, \qquad e^{i(\alpha_i - \alpha_{i+1})} = 1 \quad (1 \le i < N - 1), \qquad g_i = \mathbf{1}_i \text{ for every } i. \tag{IX.4.63}$$

Removing another diagonal $U(1)$ would change both this representation and the quotient dimension. The diagonal flavor center, by contrast, can be compensated by gauge transformations when studying local invariants. The cover notation in the weight table does not settle all global background questions for general N.

The representation dimensions now give a quantitative check of the quiver. Sum the quaternionic dimensions of all links, including the terminal fundamentals:

$$n_H = \sum_{i=1}^{N-2} i(i+1) + N(N-1) = \sum_{i=1}^{N-1} i(i+1) = \frac{N(N^2-1)}{3}. \tag{IX.4.64}$$

The real dimension and rank of the gauge group are

$$\dim_{\mathbb{R}} G = \sum_{i=1}^{N-1} i^2 = \frac{N(N-1)(2N-1)}{6}, \qquad \operatorname{rank} G = \sum_{i=1}^{N-1} i = \frac{N(N-1)}{2}. \tag{IX.4.65}$$

At a regular Higgs point where the gauge action is free and the moment map has full rank, imposing three real equations and dividing by one gauge orbit per generator removes four real dimensions. The generic Coulomb dimension is the gauge rank. Thus

$$\dim_{\mathbb{H}} \mathcal{M}_H = n_H - \dim G = \frac{N(N-1)}{2} = \dim_{\mathbb{H}} \mathcal{M}_C. \tag{IX.4.66}$$

The neighboring ranks also give each $U(i)$ node $2i$ effective fundamentals: $(i-1)+(i+1)$ in the interior, and $(N-2)+N$ at the last node. The balance condition is consistent with this infrared construction, but neither balance nor dimension equality proves a duality. At small rank the arithmetic is

N	n_H	$\dim G$	$\dim_{\mathbb{H}} \mathcal{M}_H = \dim_{\mathbb{H}} \mathcal{M}_C$
2	2	1	1
3	8	5	3
4	20	14	6

. (IX.4.67)

The $N = 4$ row is a count in the same quiver family; we will work through the matrices only for $N = 2, 3$.

At zero FI level the complex gauge moment maps are

$$A_1 B_1 = 0, \qquad A_i B_i - B_{i-1} A_{i-1} = 0 \quad (2 \le i \le N-1). \tag{IX.4.68}$$

Each equation is an endomorphism of V_i, so its two terms have exactly the same size. The flavor endomorphism is

$$M = B_{N-1} A_{N-1} \in \operatorname{End}(F), \qquad \operatorname{Tr} M = \operatorname{Tr}(A_1 B_1) = 0. \tag{IX.4.69}$$

Trace cyclicity and the intervening moment maps give the equality. Multiplying M by itself and moving one moment-map equation through at a time gives

$$\begin{aligned} M^2 &= B_{N-1} B_{N-2} A_{N-2} A_{N-1} \quad (N \ge 3), \\ M^a &= B_{N-1} \cdots B_{N-a} \, A_{N-a} \cdots A_{N-1} \quad (1 \le a \le N-1), \\ \operatorname{rank} M^a &\le N - a, \qquad M^N = 0. \end{aligned} \tag{IX.4.70}$$

At $N = 2$ the first line is replaced by $M^2 = B_1(A_1 B_1)A_1 = 0$; there is no link with index zero. The final vanishing uses $A_1 B_1 = 0$. Hence the flavor moment map is nilpotent, and the progressively smaller intermediate vector spaces bound the ranks of its powers.

For $N = 3$ every multiplication can be displayed. Choose

$$A_1 = \begin{pmatrix} 0 & 1 \end{pmatrix}, \quad B_1 = \begin{pmatrix} 1 \\ 0 \end{pmatrix}, \quad A_2 = \begin{pmatrix} 0 & 1 & 0 \\ 0 & 0 & 1 \end{pmatrix}, \quad B_2 = \begin{pmatrix} 1 & 0 \\ 0 & 1 \\ 0 & 0 \end{pmatrix}. \tag{IX.4.71}$$

These are a representative of the complex equations, not a claim that this particular representative also solves the real moment-map equations. Their products are

$$A_1 B_1 = 0, \qquad A_2 B_2 = B_1 A_1 = \begin{pmatrix} 0 & 1 \\ 0 & 0 \end{pmatrix}, \qquad M = B_2 A_2 = \begin{pmatrix} 0 & 1 & 0 \\ 0 & 0 & 1 \\ 0 & 0 & 0 \end{pmatrix}. \tag{IX.4.72}$$

The last matrix has ranks $2, 1, 0$ for M, M^2, M^3 and is regular nilpotent. Its orbit supplies another dimension calculation. A matrix commuting with one regular Jordan block is a polynomial in that block: its action on a cyclic vector determines its action on the entire Jordan chain. In $\mathfrak{sl}_N$ the constant polynomial is removed, leaving

$$\dim_{\mathbb{C}} Z_{\mathfrak{sl}_N}(M) = N - 1, \qquad \dim_{\mathbb{C}} \mathcal{O}_{\mathrm{reg}} = (N^2 - 1) - (N - 1) = N(N - 1). \tag{IX.4.73}$$

For $N = 3$ this is six complex dimensions, or three quaternionic dimensions, agreeing with (IX.4.66). The full zero-level affine Higgs branch is identified with the nilpotent cone, including its lower-rank strata. This further result uses the quotient construction. Our rectangular derivation shows why nilpotence is necessary and realizes the regular orbit explicitly; it does not turn a generic smooth count into a proof about every singular point.

In using this quiver at a boundary, keep its three-dimensional gauge factors distinct from the terminal four-dimensional gauge field. A fully global $U(N)$ S operation also needs the abelian background couplings: its center is not a spectator that can always be dropped. We have specified the interacting $T[SU(N)]$ sector and its matter. The rank-two example next gives a concrete reason to treat the global background question separately.

IX.4.8 Faithful flavor symmetry and one anomaly probe

The $T[SU(2)]$ fields transform as doublets of a flavor cover, but the symmetry acting faithfully on gauge-invariant local operators is smaller. Apply the central element $-\mathbf{1} \in SU(2)_H^{\mathrm{fl}}$. It multiplies both q and $\widetilde{q}$ by -1, and the $U(1)$ gauge transformation $g = -1$ cancels it:

$$(g, h) = (-1, -\mathbf{1}_2): \quad g q h^{-1} = q, \qquad h \widetilde{q} g^{-1} = \widetilde{q}. \tag{IX.4.74}$$

Thus the faithful Higgs flavor group on local operators is $SO(3)_H^{\mathrm{fl}}$. The Coulomb flavor algebra is an infrared enhancement of the topological $\mathfrak{u}(1)$. In the standalone theory the magnetic charge is integral,

$$m = \frac{1}{2\pi} \int_{S^2} f \in \mathbb{Z}, \qquad Q_C(v_+) = 1, \quad Q_C(v_-) = -1, \quad Q_C(\varphi) = 0, \tag{IX.4.75}$$

where $f = da$ is the $U(1)$ gauge field strength. With the sourced enhancement and this normalization of its Cartan, the operators carry integer spin. The faithful flavor group for standalone local operators is consequently

$$G_{\text{local}}^{\text{fl}} = SO(3)_H^{\text{fl}} \times SO(3)_C^{\text{fl}}. \tag{IX.4.76}$$

This is a statement about flavor symmetries, not about the R-symmetry of the supersymmetry algebra.

A background $SO(3)_H$ bundle need not lift to $SU(2)_H$. Its obstruction is the second Stiefel–Whitney class w_2^H. To couple the charged fields, the gauge and flavor transition functions combine in

$$\frac{U(1)_g \times SU(2)_H^{\text{fl}}}{\mathbb{Z}_2} = U(2). \tag{IX.4.77}$$

On a two-sphere consider a $U(2)$ bundle represented by the cocharacter $\operatorname{diag}(1,0)$. Its central and traceless parts are

$$\begin{pmatrix} 1 & 0 \\ 0 & 0 \end{pmatrix} = \frac{1}{2}\mathbf{1}_2 + \begin{pmatrix} 1/2 & 0 \\ 0 & -1/2 \end{pmatrix}, \qquad \frac{1}{2\pi}\int_{S^2} f = \frac{1}{2}, \qquad \int_{S^2} w_2^H = 1 \pmod 2. \tag{IX.4.78}$$

The half gauge flux is allowed in this combined bundle even though it was absent in (IX.4.75). It carries a half-integral topological charge. If the $SO(3)_H$ background is made dynamical, these sectors require half-integer representations of the Coulomb flavor algebra, changing the relevant global form there to its $SU(2)$ cover. Faithful local symmetry in the absence of backgrounds therefore does not imply independent anomaly-free gauging of both $SO(3)$ factors.

The same obstruction is visible in a four-dimensional extension of the three-dimensional background coupling. If $\mathcal{F}$ is the combined $U(2)$ curvature and B a Cartan background for the Coulomb flavor symmetry, then $\operatorname{Tr}\mathcal{F} = 2f$ and

$$\frac{i}{2\pi}\int_{X_3} B \wedge f = \frac{i}{4\pi}\int_{X_3} B \wedge \operatorname{Tr}\mathcal{F} \quad \rightsquigarrow \quad \frac{i}{4\pi}\int_{Y_4} dB \wedge \operatorname{Tr}\mathcal{F}, \qquad \partial Y_4 = X_3. \tag{IX.4.79}$$

Here X_3 is the boundary theory's spacetime; the extension Y_4 is used to diagnose its background dependence and is not identified with the physical D3 half-space. Changing extensions produces a closed four-manifold Z_4. The flux congruences in the global background construction are

$$\frac{1}{2}dB = \pi w_2^C \pmod{2\pi}, \qquad \frac{1}{2}\operatorname{Tr}\mathcal{F} = \pi w_2^H \pmod{2\pi}. \tag{IX.4.80}$$

Substituting them into the difference of the extension terms gives the mixed phase

$$\mathcal{A}(Z_4; w_2^H, w_2^C) = \exp\left(i\pi \int_{Z_4} w_2^H \smile w_2^C\right). \tag{IX.4.81}$$

The nonabelian background interpretation and its anomaly formula are physical source results. We can evaluate a probe completely without assuming any classification for arbitrary N.

Take $Z_4 = S^2 \times S^2$ with product orientation. Let a, b be the mod-two degree-two classes pulled back from the first and second spheres. Their cup products satisfy

$$a^2 = b^2 = 0, \qquad \int_{S^2 \times S^2} a \smile b = 1. \tag{IX.4.82}$$

Choose $w_2^H = a$ and $w_2^C = b$. For example, each can be obtained by pulling back the nontrivial $SO(3)$ bundle on the corresponding sphere. Then

$$\mathcal{A}(S^2 \times S^2; a, b) = e^{i\pi} = -1. \tag{IX.4.83}$$

If either bundle lifts to $SU(2)$, its w_2 vanishes and this mixed phase is $+1$. The probe detects the stated rank-two mixed coefficient. It does not determine all genuine line operators, all choices of bulk global form, or the anomaly data of $T[SU(N)]$ for general N. The boundary S operation must be supplied with compatible global data when those questions are asked.

IX.4.9 What the boundary construction establishes

The surface variation tells us which boundary values can fluctuate. For the D5 triplet the cubic interaction changes ordinary Neumann data into Nahm's equation. Its simple pole reduces the leading boundary problem to a unitary representation of $\mathfrak{su}(2)$, and the multiplicity spaces of that representation determine the compact commutant. The rank-two example already distinguishes three different objects: a zero residue with a full commutant, a principal pole with only a finite $SU(2)$ commutant, and a boundary theory with charged hypermultiplets. None can replace another merely because the total number of D3s agrees.

The direct S operation explains why a boundary can acquire its own gauge dynamics. Finite segments contribute three-dimensional gauge factors while a semi-infinite segment continues to carry the four-dimensional bulk. The ranks alone are insufficient: the rectangular fields, their Cartan weights, and their attachments fix the moment maps. Their nilpotent flavor composite gives a calculable bridge between the quiver and the complex geometry. Chapter 3 supplies the protected abelian Coulomb relation used in the rank-two comparison; it does not supply a general nonabelian metric from that relation.

Several questions remain beyond this construction. A general singular boundary condition needs allowed subleading fields and a complete supersymmetric variational prescription. More general partitions can be combined with boundary gauge groups and interacting matter, and the space of Nahm solutions has geometry beyond the explicit poles studied here. Likewise, the rank-two background calculation shows why global form matters without determining the full S-duality action on genuine lines for every gauge group. These extensions require additional data, not more examples of the same finite commutator equation.

The atlas in Chapter 8 will retain the residue, commutant and boundary quiver as distinct data. Chapter 5 instead changes the suspended brane to a D4. Its four-dimensional $\mathcal{N} = 2$ fields belong to a different bulk theory from the $\mathcal{N} = 4$ D3 problem studied here.

Status and sources

Evidence and assumptions. WS means a controlled physical-worldsheet derivation in the untwisted string. Worldvolume variation and finite matrix algebra do not supply WS evidence. MATH refers only to a statement with the mathematical domain, hypotheses and proof basis specified here. The protected Coulomb relation uses Chapter 3 at zero mass and FI.

We abbreviate Gaiotto–Witten, arXiv:0804.2902v2, Gaiotto and Witten 2009b as GW–BC, and arXiv:0807.3720v1, Gaiotto and Witten 2009a as GW–S. Page numbers below are printed page numbers in these exact versions; their PDF viewer pages are one larger. The rank-two background source is the published version of Gang and Yonekura 2018, JHEP 07 (2018) 145, Appendix B.2, pp. 49–50, not an unspecified arXiv edition.

Frame and classical boundary variation. [MATH]: §IX.4.2, (IX.4.1)–(IX.4.4), is the explicit passive orientation-preserving permutation. Source anchors are GW–BC §2.3, p. 16 for the name change and §2.5.1, Fig. 1, pp. 27–28 for the axes. The triplet names here follow the source after its §2.3 interchange of its earlier X, Y names. The chosen brane axes give the outward conormal $n = -ds$. No IIB charge or spinor transformation is inferred from the coordinate permutation.

[MATH]: (IX.4.6)–(IX.4.8) derive the surface momenta for the specified classical action. The action and physical half-BPS endpoint assignments have unassigned physical primary status here; they remain source premises rather than consequences of this tag. The physical action and regular half-BPS boundary conditions are GW–BC §2, (2.1)–(2.4), p. 5, and §2.1, (2.9), (2.13)–(2.18), pp. 8–10. The trace coefficient uses convention entry 3 and Chapter 1. Fermionic boundary conditions, quantum boundary terms, oblique boundaries and nonzero theta are not derived by the bosonic integration by parts.

(IX.4.11) is a classical variational identity with j defined there. The half-BPS moment-map shift (IX.4.12) is the sourced boundary-coupling prescription of GW–BC §2.3.2–2.3.4, pp. 19–21, (2.30)–(2.34). Only its bulk-normalized μ_Z is used. The numerical conversion from canonically normalized boundary hypers is uncomputed and does not enter a worked example.

Nahm equation and the pole. [MATH]: §IX.4.3, (IX.4.13)–(IX.4.25), proves the reduced Clifford identity, cubic gradient, square and lower-boundary sign within the stated Hermitian classical ansatz. The physical supersymmetry and Nahm premises are GW–BC §2.4, (2.37)–(2.41), pp. 23–24, with the pole in §2.4.1, (2.42)–(2.43), p. 25. The reduced Clifford calculation is not a standalone ten-dimensional reality or supercharge-count proof.

[MATH]: §IX.4.4, (IX.4.26)–(IX.4.36), and (IX.4.38)–(IX.4.39), derive the residue algebra, explicit spin-half/spin-one solutions, failed rescalings and anisotropic deformation, regular shifted solution, and finite Hermitian decomposition. Classification is confined to residue representations, not all boundaries. The leading energy cancellation does not establish an analytic fluctuation prescription.

[GEO-E]: the D3–D5 interpretation in (IX.4.37) is a physical dictionary input from GW–BC §3.4.3, Fig. 6 and (3.44)–(3.45), pp. 52–53. Its rank-one defect/removal

argument is distinct from the finite matrix verification. The endpoint drawings retain that evidence level.

Centralizers. [MATH]: §IX.4.5, (IX.4.40)–(IX.4.48), together with (IX.4.49), gives the Schur-lemma, Jordan-module and explicit matrix computations. The full-triple commutant is distinguished from the nilpotent centralizer. GW–BC p. 25 after (2.43) supplies its boundary-symmetry interpretation. The weighted $SU(N)$ determinant, finite principal centralizer and disconnected $[2, 2]$ example prevent a Lie-algebra count from being used as a global-group classification. Gauging a subgroup of this commutant is extra boundary data.

Boundary duality and quiver matter. [DUAL]: (IX.4.50) and the rank-jump mechanism in §IX.4.6–§IX.4.7 use GW–S §3.2.1, Figs. 13–14, pp. 39–41, and §3.3.1, Fig. 22, p. 51. The direct exchange uses nonperturbative IIB S-duality. The Fig. 23 rearrangement in the same source is not an unrecorded step: it would need the creation and continuity assumptions as separate links. The common-NS5 matter dictionary is reused from Chapter 1 at its sourced geometric scope. Matching rings or dimensions does not prove S-duality. The center/background warning is GW–S §4.4, pp. 96–98, in particular the abelian BF coupling (4.5), p. 96.

[MATH]: the representation calculations in (IX.4.52)–(IX.4.53) and (IX.4.59)–(IX.4.73) give the conditional algebraic consequences of the sourced quiver and moment-map prescription: the attached representations, their complete weight multisets, faithful gauge centers, dimensions, moment-map consequences and explicit regular nilpotent representative. The quiver premise is GW–S §3.3.1, Figs. 22 and 24, pp. 51–52, with (3.4)–(3.6), pp. 52–53. The complete nilpotent-cone identification is sourced there; the local free-action count does not prove its singular strata. The $N = 4$ table row claims dimensions only, not a new worked global theory.

[MATH]: (IX.4.55)–(IX.4.57) are the zero-level Higgs invariant-ring calculation and regular-stratum count. The separate Coulomb relation (IX.4.58) uses Chapter 3's protected abelian result at zero mass/FI, ultimately Bullimore et al. 2017, arXiv:1503.04817v2, §3.1, (3.6), pp. 9–10. Quantum protection is a physical premise; no elementary-field derivation of the monopole OPE or metric equality is claimed. GW–S §2.4.1, pp. 21–22 supplies the rank-two theory.

Rank-two global backgrounds. (IX.4.74)–(IX.4.76) combine a center-compensation calculation with the sourced infrared flavor enhancement and integer monopole lattice. The exact global-form premise is published Gang–Yonekura Appendix B.2, p. 49 preceding (B.5), with the enhancement reviewed in Appendix B.1. It concerns standalone gauge-invariant local operators and distinguishes both flavor factors from R-symmetry. The source's global statement, rather than its Lie-algebra shorthand, is used here.

[ANOM]: (IX.4.77)–(IX.4.83) use the same published Appendix B.2, (B.5)–(B.12), pp. 49–50. The odd $U(2)$ lift, half flux and one $S^2 \times S^2$ cup product are computed explicitly. The mixed anomaly formula and background-gauging interpretation are sourced premises. Neither this single probe nor the exact quiver weights classify all-N global anomalies or genuine line operators.

Figures and scope. All five figures are original local vector drawings. Figure IX.4.1 uses the stated coordinate frame; Fig. IX.4.2 plots (IX.4.35); Fig. IX.4.3 combines

the sourced endpoint dictionary with the derived block commutants. Figure IX.4.4 is a rank-three specialization of GW–S Fig. 22, not Fig. 23. Figure IX.4.5 uses its Fig. 24 representations. Equation (IX.4.67) gives the finite count for the fixed quiver data. The sourced anomaly phase and its single cohomology calculation have distinct roles. The direct exchange remains conditional on nonperturbative IIB S-duality. General Nahm geometry and boundary theories lie outside the examples here. No magnetic-quiver program, general boundary category, all-N line-operator classification, or canonical-hyper/bulk moment-map coefficient is added.

References

Bullimore, M., T. Dimofte, and D. Gaiotto (2017). "The Coulomb Branch of 3d $\mathcal{N} = 4$ Theories". In: *Commun. Math. Phys.* 354.2, pp. 671–751. DOI: 10.1007/s00220-017-2903-0. arXiv: 1503.04817 [hep-th].

Gaiotto, D. and E. Witten (2009a). "S-Duality of Boundary Conditions In N=4 Super Yang-Mills Theory". In: *Adv. Theor. Math. Phys.* 13.3, pp. 721–896. DOI: 10.4310/ATMP.2009.v13.n3.a5. arXiv: 0807.3720 [hep-th].

Gaiotto, D. and E. Witten (2009b). "Supersymmetric Boundary Conditions in N=4 Super Yang-Mills Theory". In: *J. Statist. Phys.* 135, pp. 789–855. DOI: 10.1007/s10955-009-9687-3. arXiv: 0804.2902 [hep-th].

Gang, D. and K. Yonekura (2018). "Symmetry enhancement and closing of knots in 3d/3d correspondence". In: *JHEP* 07, p. 145. DOI: 10.1007/JHEP07(2018)145. arXiv: 1803.04009 [hep-th].

Chapter IX.5

D4–NS5 constructions and the M-theory lift

IX.5.1 From an interval to a quantum curve

A finite brane interval turns a higher-dimensional gauge field into a lower-dimensional one. In Chapter 1 this mechanism produced a three-dimensional theory. A D4-brane suspended between two parallel NS5-branes instead has four common spacetime directions. Its massless fields form a four-dimensional $\mathcal{N} = 2$ gauge theory, and moving the color branes in their common transverse plane changes its Coulomb vacuum. The interval length initially appears to be an ordinary constant fixing the gauge coupling. Once the color branes pull on the fivebranes, that length depends logarithmically on the transverse position. Gauge-theory running has become a visible shape.

The next step changes what counts as the basic geometric object. In M theory, a D4-brane wraps the extra circle and an NS5-brane does not. The two join into one M5-brane whose internal surface has thin tubes in the IIA limit. The positions and joins of those tubes determine a complex curve. A membrane ending on the curve measures a period of a differential, so the same construction can determine central charges and the loci where charged particles become massless. The curve matters because it carries these periods, not merely because it has an appealing polynomial equation.

We will carry the pure $SU(2)$ theory through this construction and then extend the curve calculation to pure $SU(3)$. Volume I, Chapter 5 supplies the field-theory language of Coulomb branches, central charges and Seiberg–Witten periods. Here we derive their brane realization using the protected M-theory continuation stated below. Along the way we must distinguish four objects: the Coulomb-branch base, the auxiliary curve over each vacuum, its integral cycles, and the charges of physical particles. Their distinctions are already visible at rank one. The quartic obtained from the M5 and a familiar cubic presentation have a degree-two map between them; their primitive cycle lattices are not the same period normalization.

The physical use of the smooth M5 description rests on protected holomorphic continuation. The large-circle regime in which the geometry is directly useful differs

from the small-length field-theory limit. We use the curve and its normalized periods across these regimes; this does not identify arbitrary nonprotected metrics. The interval, its asymptotic boundary conditions and the membrane prescription will therefore be stated before they enter the calculation.

IX.5.2 The interval spectrum and full hypermultiplets

Let $X^0, \ldots, X^9$ be physical IIA coordinates, and suspend N D4-branes on an interval of length L_6 in X^6. The two NS5-branes are parallel. An inside-interval D6-brane supplies flavor degrees of freedom. The coordinate table fixes which motions become scalars in four dimensions.

	0	1	2	3	4	5	6	7	8	9
NS5	×	×	×	×	×	×				
D4	×	×	×	×			interval			
D6	×	×	×	×				×	×	×

(IX.5.1)

Here X^3 belongs to spacetime. The internal rotations of the three-dimensional construction must consequently be reconsidered: rotations of 45 provide the classical $U(1)_R$ direction and the spin cover of rotations of 789 provides $SU(2)_R$. The compatible branes preserve eight real supercharges. In the asymptotically free quantum theory the continuous $U(1)_R$ can be anomalous; the rotation identifies its classical action, not an exact continuous symmetry at fixed strong scale. This supersymmetric endpoint and open-string spectrum is the physical starting prescription.

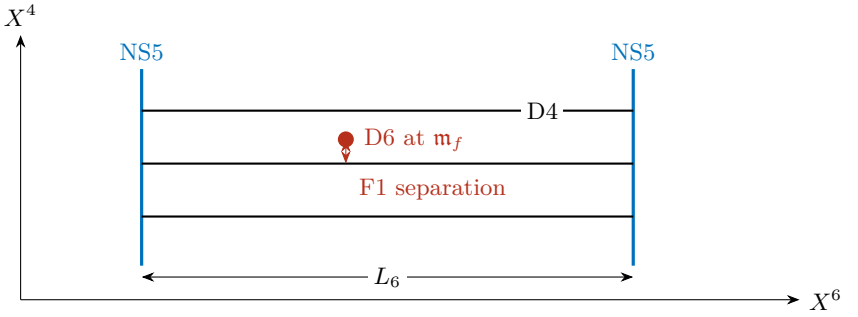


Figure IX.5.1: The finite D4 interval, projected onto X^6 and one direction of the 45 plane. Three separated color branes illustrate Coulomb motion. The red point is the projection of a D6-brane extending in 789; its separation from a color brane measures an F1 mass. The drawing suppresses X^5, so a generic separation is complex.

The five transverse D4 scalars are $X^{4,5,7,8,9}$. At an NS5 endpoint, $X^{4,5}$ are tangent and obey Neumann conditions, while $X^{7,8,9}$ are normal and obey Dirichlet conditions.

For a massless interval mode write

$$-\partial_6^2 f = 0, \qquad f(X^6) = c_0 + c_1 X^6. \tag{IX.5.2}$$

Neumann conditions at both ends set $c_1 = 0$ and leave c_0. Dirichlet conditions at $0, L_6$ set first $c_0 = 0$ and then $c_1 = 0$. With one condition of each type both coefficients also vanish. Thus

$$\dim\ker(-\partial_6^2)_{NN} = 1, \qquad \dim\ker(-\partial_6^2)_{DD,ND,DN} = 0. \tag{IX.5.3}$$

The surviving complex scalar is $X^4 + iX^5$. Together with A_μ, $\mu = 0, 1, 2, 3$, and the surviving fermions, it forms an $\mathcal{N} = 2$ vector multiplet. The gauge endpoint prescription removes an independent A_6 zero mode: these endpoints do not support a gauge-invariant open Wilson-line modulus. That statement requires the gauge boundary prescription in addition to the scalar equation. There is no adjoint hypermultiplet from 789.

For comparison, rotate the right fivebrane to 012389. A scalar must now be tangent to both fivebranes to have two Neumann endpoints. Among the D4 transverse directions there is no such common direction:

$$\{4, 5\} \cap \{8, 9\} = \varnothing. \tag{IX.5.4}$$

The adjoint scalar disappears. This is the orientation relevant to the four-supercharge construction in Chapter 6, rather than another vacuum of the parallel-fivebrane theory.

A D4–D6 string has common Neumann directions 0123, mixed directions 6789, and common Dirichlet directions 45. The NS-sector vacuum energy in string units is therefore

$$a_{\mathrm{NS}} = -\frac{1}{2} + \frac{n_{ND}}{8} = 0, \qquad n_{ND} = 4. \tag{IX.5.5}$$

The four-ND GSO spectrum and the two string orientations combine into a full hypermultiplet. To count it correctly, let $V_c = \mathbb{C}^N$ and $V_f = \mathbb{C}^{N_f}$ be color and flavor spaces. Its two complex scalar matrices transform as

$$Q \in \mathrm{Hom}(V_f, V_c), \qquad \widetilde{Q} \in \mathrm{Hom}(V_c, V_f), \qquad Q \mapsto g_c Q g_f^{-1}. \tag{IX.5.6}$$

Choose diagonal generators $H_c = \mathrm{diag}(h_i)$ and $H_f = \mathrm{diag}(k_a)$. Acting on the rectangular matrix unit E_{ia} makes every weight explicit:

$$H_c E_{ia} - E_{ia} H_f = (h_i - k_a) E_{ia}, \qquad w(Q_{ia}) = e_i - f_a, \quad w(\widetilde{Q}_{ai}) = -e_i + f_a. \tag{IX.5.7}$$

Here e_i and f_a are unit vectors in the color and flavor Cartan coordinate spaces. For $N = 3, N_f = 2$ the six Q weights are

$$\{e_1 - f_1, e_1 - f_2, e_2 - f_1, e_2 - f_2, e_3 - f_1, e_3 - f_2\}; \qquad \widetilde{Q} \text{ has their negatives.} \tag{IX.5.8}$$

There are twelve complex scalar components, or twenty-four real ones. These are two full hypermultiplets in the color fundamental, not twelve flavors. More generally there are $2NN_f$ complex components. The weight matrix W, with these weights as rows, satisfies for $N, N_f > 0$

$$W^T W = 2 \begin{pmatrix} N_f I_N & -\mathbf{1}_{N \times N_f} \\ -\mathbf{1}_{N_f \times N} & N I_{N_f} \end{pmatrix}, \qquad \mathrm{rank}\, W = N + N_f - 1. \tag{IX.5.9}$$

The common color-plus-flavor diagonal acts trivially, whereas the color identity alone gives charges $+1, -1$. Thus an abstract flavored $U(N)$ SQCD center is charged. We will obtain the dynamical $\mathfrak{su}(N)$ algebra from a finite-norm boundary condition, not from a free-center claim.

Finally define a physical complex position $V = X^4 + iX^5$ and its mass coordinate v. The F1 tension fixes the classical separation masses:

$$v = \frac{V}{2\pi\alpha'}, \quad \mathfrak{m}_a = \frac{V_{D6,a}}{2\pi\alpha'}, \qquad M_{ij} = |v_i - v_j|, \quad M_{ia} = |v_i - \mathfrak{m}_a|. \tag{IX.5.10}$$

The D6 kinetic norm includes its noncompact 789 volume, so its gauge field supplies a flavor symmetry rather than another finite-norm four-dimensional gauge field. An unattached D6 outside the interval need not supply such a hypermultiplet. The mass markers in (IX.5.10) are classical stretched-string masses; they do not by themselves determine residues of a quantum flavored differential.

IX.5.3 Coupling normalization and the field-theory limit

The length of the interval is a coupling only after a kinetic convention has been fixed. Use fundamental generators satisfying $\mathrm{Tr}_f(T_a T_b) = \delta_{ab}/2$ and the component coupling defined by

$$S_{\mathrm{YM}} = -\frac{1}{2g_4^2}\int d^4x\ \mathrm{Tr}_f\, F_{\mu\nu}F^{\mu\nu} = -\frac{1}{4g_4^2}\int d^4x\, F^a_{\mu\nu}F^{a\mu\nu}. \tag{IX.5.11}$$

The D4 Dirac–Born–Infeld action has tension

$$T_4 = \frac{1}{(2\pi)^4 g_s \alpha'^{5/2}}, \qquad \ell_s = \sqrt{\alpha'}. \tag{IX.5.12}$$

Its quadratic expansion can be seen in one magnetic block. For $F_{12} = f$, the square root of the determinant is

$$\sqrt{1 + (2\pi\alpha' f)^2} = 1 + \frac{(2\pi\alpha')^2 f^2}{2} + O(f^4), \qquad F_{\mu\nu}F^{\mu\nu} = 2f^2. \tag{IX.5.13}$$

Integrating the constant interval mode therefore gives

$$S_{F^2} = -\frac{T_4(2\pi\alpha')^2 L_6}{4}\int d^4x\ \mathrm{Tr}_f\, F^2, \qquad \frac{1}{g_4^2} = \frac{L_6}{8\pi^2 g_s \ell_s}. \tag{IX.5.14}$$

Equivalently the five-dimensional coupling is $g_5^2 = 8\pi^2 g_s \ell_s$ and $g_4^2 = g_5^2/L_6$. The factor of two in the trace action is essential: using $-\mathrm{Tr}\, F^2/(4g^2)$ would name a different coupling.

M theory identifies a D0-brane with one unit of circle momentum. In the same asymptotic IIA length frame its mass gives

$$M_{D0} = \frac{1}{g_s \ell_s} = \frac{1}{R_{10}}, \qquad R_{10} = g_s \ell_s, \qquad S_{D0} = \frac{L_6}{R_{10}} = \frac{8\pi^2}{g_4^2}. \tag{IX.5.15}$$

The Euclidean D0 worldline crossing the interval thus reproduces the four-dimensional instanton action. All lengths in these equations use one frame; a common change to M-theory length units leaves the ratio L_6/R_{10} invariant.

Distinguish the physical coordinate X^{10} from its angular coordinate ϑ_{10}. Introduce the complex cylinder coordinate s and its single-valued exponential t by

$$X^{10} \sim X^{10} + 2\pi R_{10}, \qquad \vartheta_{10} = X^{10}/R_{10}, \qquad s = \frac{X^6 + iX^{10}}{R_{10}}, \quad t = e^{-s}. \tag{IX.5.16}$$

Take all separations as right minus left. The orientation $\theta_{\mathrm{YM}} = -\Delta X^{10}/R_{10}$ then fixes the complex coupling:

$$\tau_{\mathrm{UV}} = \frac{\theta_{\mathrm{YM}}}{2\pi} + \frac{4\pi i}{g_4^2} = \frac{i\Delta s}{2\pi}, \qquad q = e^{2\pi i \tau_{\mathrm{UV}}} = e^{-\Delta s}. \tag{IX.5.17}$$

A shift of the right endpoint by one physical circle period changes θ_{YM} by -2π and leaves q unchanged. This determines the absolute factors independently of notation for the logarithmic bending.

At a finite matching scale, the interval approximation asks for

$$E,\ |v_i|,\ |\mathfrak{m}_a| \ll L_6^{-1},\ \ell_s^{-1},\ R_{10}^{-1}. \tag{IX.5.18}$$

For an asymptotically free theory let $b_0 > 0$ denote its one-loop coefficient, defined by $\beta(g) = -b_0 g^3/(16\pi^2)$. Choose $\mu_{\mathrm{UV}} = L_6^{-1}$ as a matching convention. A fixed physical strong scale requires

$$\Lambda_{\mathrm{RG}} = \frac{1}{L_6} \exp\left[-\frac{8\pi^2}{b_0 g_4^2}\right] = \frac{1}{L_6} \exp\left[-\frac{L_6}{b_0 R_{10}}\right]. \tag{IX.5.19}$$

Holding $L_6/R_{10} = c$ while sending L_6 to zero instead sends $\Lambda_{\mathrm{RG}} = e^{-c/b_0}/L_6$ to infinity. A fixed bare dimensionless coupling is therefore not the required fixed-scale limit.

One explicit trajectory uses a positive parameter r tending to infinity:

$$L_6 = \frac{e^{-r}}{\Lambda_{\mathrm{RG}}}, \qquad R_{10} = \frac{L_6}{b_0 r}, \qquad g_4^2 = \frac{8\pi^2}{b_0 r}. \tag{IX.5.20}$$

With fixed small g_s, choose $\ell_s = R_{10}/g_s$. All three inverse lengths in (IX.5.18) diverge, while direct substitution into (IX.5.19) returns the chosen Λ_{RG}. Alternatively, specifying R_{10} first gives

$$L_6 = b_0 R_{10}\, \mathcal{W}\!\left(\frac{1}{b_0 R_{10} \Lambda_{\mathrm{RG}}}\right), \qquad \mathcal{W}(z) e^{\mathcal{W}(z)} = z. \tag{IX.5.21}$$

The positive Lambert function supplies the same trajectory. Neither formula is a prescription for $b_0 = 0$. Also, the finite normalization relating Λ_{RG} to the curve scale Λ introduced below depends on a matching scheme. Logarithmic running does not fix that constant. This construction exhibits the hierarchy needed for the field-theory limit; using a smooth M5 surface to extract its protected data still requires the continuation described in Section IX.5.6.

IX.5.4 Logarithmic bending and the matter coefficient

A D4 endpoint is a localized source on the 45 plane of an NS5-brane. Far from the endpoint, its transverse displacement solves the planar Laplace equation. The logarithm is forced by the flux through a large circle, since

$$\nabla^2 \log|V| = 2\pi\delta^{(2)}(V), \qquad \oint_{|V|=r} \partial_r \log|V|\, r\, d\theta = 2\pi. \tag{IX.5.22}$$

The imaginary part is fixed by the M-circle winding. A unit endpoint changes X^{10} by one physical period when encircled. Thus a holomorphic logarithm in s, whose imaginary change is 2π, has unit coefficient. With the orientation of (IX.5.16), endpoints from the left and right contribute with opposite signs:

$$s(V) = s_0 + \sum_{i\in L} \log\frac{V - A_i}{V_0} - \sum_{j\in R} \log\frac{V - B_j}{V_0}. \tag{IX.5.23}$$

Here V_0 is a reference length, and A_i, B_j are physical endpoint positions. Changing V_0 shifts a constant coupling, not the running. The same formula in the mass coordinate v absorbs $2\pi\alpha'$ into the reference scale.

For the running calculation it is convenient to realize flavors by semi-infinite D4-branes. Put N_L to the left of the first NS5 and N_R to the right of the second, with N finite color branes between them. This is a chart for counting signed endpoint asymptotics. Actual D6 flavors have the same matter coefficient but a different global M-theory ambient space. The two large-$|v|$ slopes are

$$s_L \sim (N_L - N)\log(v/v_0) + c_L, \qquad s_R \sim (N - N_R)\log(v/v_0) + c_R. \tag{IX.5.24}$$

Consequently the right-minus-left separation obeys

$$\Delta s \sim (2N - N_L - N_R)\log(v/v_0) + \Delta c, \qquad \frac{d}{d\log\mu}\frac{8\pi^2}{g_4^2} = 2N - N_f, \tag{IX.5.25}$$

where $N_f = N_L + N_R$ and μ is proportional to $|v|$ in the weak region. Only the separation controls the gauge coupling. Neither fivebrane must individually be flat in a conformal example.

For the independent matter calculation, define the quadratic index by $\mathrm{Tr}_{\mathcal{R}}(T_a T_b) = T(\mathcal{R})\delta_{ab}$. To see its normalization, choose $H = \mathrm{diag}(1/2, -1/2, 0, \ldots, 0)$. Then

$$\mathrm{Tr}_f\, H^2 = \frac{1}{2}, \qquad \mathrm{Tr}_{\mathrm{ad}}(\mathrm{ad}\, H)^2 = \sum_{i,j}(h_i - h_j)^2 = N. \tag{IX.5.26}$$

The second identity uses $\sum h_i = 0$ and $\sum h_i^2 = 1/2$. An $\mathcal{N} = 2$ vector is an $\mathcal{N} = 1$ vector plus an adjoint chiral; each full hyper supplies a fundamental and an antifundamental chiral. Their one-loop indices therefore give

$$b_0 = 3T(\mathrm{ad}) - T(\mathrm{ad}) - N_f\left[T(\mathbf{N}) + T(\overline{\mathbf{N}})\right] = 3N - N - N_f = 2N - N_f. \tag{IX.5.27}$$

Each extra full hyper lowers b_0 by one. This is an absolute coefficient, not just a proportionality between the two descriptions.

For an asymmetric example take $N = 3, N_L = 1, N_R = 2$. The left and right fivebranes bend with coefficients -2 and 1, so

$$\Delta s \sim 3\log(v/v_0) + \Delta c, \qquad b_0 = 9 - 3 - 3 = 3. \tag{IX.5.28}$$

By contrast $N = 2, N_L = 1, N_R = 3$ gives two coefficients equal to -1:

$$s_L \sim -\log(v/v_0) + c_L, \qquad s_R \sim -\log(v/v_0) + c_R, \qquad b_0 = 0. \tag{IX.5.29}$$

The common bending cancels from the separation. Figure IX.5.2 draws both examples in the asymptotic radial coordinate. The comparison table also includes the two pure theories studied later.

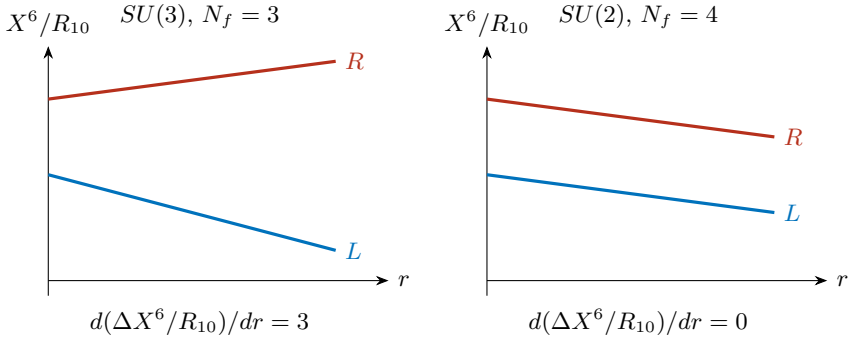


Figure IX.5.2: Large-distance fivebrane profiles against $r = \log(|v|/|v_0|)$. The vertical coordinate is X^6/R_{10} and the intercepts are chosen only to separate the curves. In the asymmetric $SU(3)$ example the separation grows with slope three. In the conformal $SU(2)$ example both profiles bend with slope -1, while their separation is constant. The panels depict asymptotic laws, not endpoint cores.

Theory	left slope	right slope	b_0
pure $SU(2)$	-2	2	4
pure $SU(3)$	-3	3	6
$SU(3)$, $(N_L, N_R) = (1, 2)$	-2	1	3
$SU(2)$, $(N_L, N_R) = (1, 3)$	-1	-1	0

Table IX.5.1: Signed endpoint slopes and the absolute matter coefficient. A full hyper contributes one unit to N_f irrespective of the number of its color components.

For $N_f > 2N$, the coefficient changes sign and the ordinary asymptotically free ultraviolet interpretation fails. The endpoint count remains meaningful, but it cannot supply that interpretation by itself. For $N_f = 2N$, the finite coupling is extra information rather than a scale generated by the positive-b_0 trajectory above.

IX.5.5 Normalizability selects the dynamical algebra

The Chan–Paton algebra of k color branes is initially $\mathfrak{u}(k)$. Which of its apparent scalar motions survive as four-dimensional fields depends on their kinetic norm. The fivebranes are noncompact. Moving an endpoint changes their profile out to infinity, and an infinite kinetic coefficient makes the corresponding motion a fixed asymptotic parameter rather than a dynamical field.

Expand a logarithmic profile for endpoints a_i in the mass plane and allow them to vary slowly with spacetime. The relevant velocity field is

$$\sum_i \frac{\dot a_i}{v-a_i} = \frac{\sum_i \dot a_i}{v} + \frac{\sum_i a_i \dot a_i}{v^2} + O(v^{-3}). \tag{IX.5.30}$$

Constant scale conversions do not affect convergence of the norm. The planar measure $d^2v = r\,dr\,d\theta$ distinguishes the two leading tails:

$$\int_{r_0}^{r_{max}} r\,dr \left|\frac{c}{r}\right|^2 = |c|^2 \log\frac{r_{max}}{r_0} \longrightarrow \infty \quad (c \neq 0), \tag{IX.5.31}$$

$$\int_{r_0}^{\infty} r\,dr \left|\frac{d}{r^2}\right|^2 = \frac{|d|^2}{2r_0^2}. \tag{IX.5.32}$$

These are asymptotic integrals, not a calculation of the full metric near an endpoint. They already show why a trace motion is problematic. For two positions $a, -a$, the common and relative velocities give

$$\frac{1}{v-a} + \frac{1}{v+a} = \frac{2}{v} + O(v^{-3}), \qquad \frac{1}{v-a} - \frac{1}{v+a} = \frac{2a}{v^2} + O(v^{-4}). \tag{IX.5.33}$$

The common displacement has the divergent trace tail; the relative displacement cancels it and is integrable at infinity.

For a finite chain, let $A_\alpha = \sum_i a_i^{(\alpha)}$ be the trace position of interval α, and let $d_\alpha = \dot A_\alpha$. Fixed exterior data mean $d_0 = d_{n+1} = 0$. The logarithmically divergent part of the kinetic form is proportional to

$$\log r_{max} \sum_{\alpha=0}^{n} |d_{\alpha+1} - d_\alpha|^2. \tag{IX.5.34}$$

Finite norm sets every difference to zero. With the two exterior values fixed, all d_α vanish. For three intervals the constraints are particularly transparent:

$$\begin{pmatrix} -1 & 0 & 0 \\ 1 & -1 & 0 \\ 0 & 1 & -1 \\ 0 & 0 & 1 \end{pmatrix} \begin{pmatrix} d_1 \\ d_2 \\ d_3 \end{pmatrix} = 0 \quad \Longrightarrow \quad d_1 = d_2 = d_3 = 0. \tag{IX.5.35}$$

Supersymmetry removes the trace vector multiplets together with these scalar motions. The dynamical algebras are consequently

$$\bigoplus_{\alpha=1}^{n} \mathfrak{u}(k_\alpha) \quad \longrightarrow \quad \bigoplus_{\alpha=1}^{n} \mathfrak{su}(k_\alpha) \qquad \text{at fixed exterior asymptotics.} \tag{IX.5.36}$$

This operation does not assert that a flavored $U(k)$ center was free. Its charged matter was explicit in (IX.5.7).

Close an unflavored equal-rank chain into a circle and the exterior condition disappears. For three intervals one instead has

$$\begin{pmatrix} 1 & -1 & 0 \\ 0 & 1 & -1 \\ -1 & 0 & 1 \end{pmatrix} \begin{pmatrix} d_1 \\ d_2 \\ d_3 \end{pmatrix} = 0, \qquad (d_1, d_2, d_3) = d(1,1,1). \tag{IX.5.37}$$

One common $U(1)$ remains. Bifundamental matter between the circular nodes is neutral under this common diagonal. This provides a concrete counterexample to deleting every trace in every brane construction. The kernel is the physical information; invertible row operations on the displayed constraints cannot change it.

In the M5 description the gauge fields arise by reducing the self-dual tensor along square-integrable harmonic one-forms on the internal surface Σ. A puncture mode with nonzero small-loop period behaves as dv/v and has the divergent norm in (IX.5.31). Allowed forms extend over the compactification. For a connected chain with all $k_\alpha > 0$, joining $n+1$ compactified fivebrane components by $\sum_\alpha k_\alpha$ tubes gives

$$2 - 2g = 2(n+1) - 2\sum_\alpha k_\alpha, \qquad g = \sum_\alpha (k_\alpha - 1). \tag{IX.5.38}$$

The self-duality condition leaves g independent photons, matching the Cartan rank of (IX.5.36). This normalizability argument fixes dynamical algebras and abelian rank. It does not choose the full global gauge group or the allowed genuine line operators.

IX.5.6 The M5 surface and its two sheets

In M theory an NS5 is an M5 transverse to the extra circle, while a D4 is an M5 wrapping it. Their join can be described by one smooth worldvolume

$$\mathbb{R}^{3,1} \times \Sigma, \qquad \Sigma \subset \mathbb{C}_v \times \mathbb{C}_t^* \quad \text{for the pure theory.} \tag{IX.5.39}$$

The surface Σ is internal to the M5. It is neither four-dimensional spacetime nor the Coulomb-branch base. Varying the Coulomb moduli changes which surface occurs over the chosen vacuum.

Figure IX.5.3 separates two useful descriptions. Thin tubes recover the IIA color intervals. A resolved M-circle gives a smooth geometric description. The field-theory trajectory of (IX.5.20) and this geometric regime are different limits. The physical prescription transports protected holomorphic curve and period data between them. A calculation of the shape alone would not prove equality of nonprotected observables.

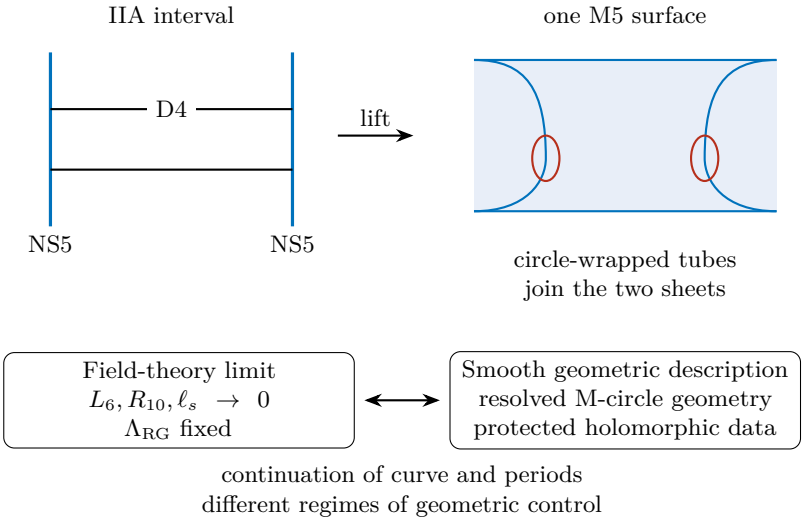


Figure IX.5.3: The IIA D4/NS5 join and its M5 description. The upper-right panel is a schematic tube-and-sheet drawing, not a metric embedding or a plot of the Coulomb base. The lower panels distinguish the field-theory limit at fixed strong scale from smooth geometric control. Their common use here is the protected curve and its periods.

Two asymptotic NS5-branes mean that a generic v has two values of t. The curve is therefore quadratic in t. With no semi-infinite flavors, its leading and constant coefficients have no finite zeros. The N color tubes appear in a degree-N middle coefficient. After choosing the origins of v, s, write the monic polynomial

$$P_N(v) = v^N - \sum_{k=2}^{N} u_k v^{N-k}, \qquad [v] = 1, \quad [u_k] = k. \tag{IX.5.40}$$

The absent v^{N-1} term expresses the fixed trace. Restoring a mass-one scale Λ and choosing its finite normalization gives

$$\Lambda^N(t^2+1) - 2P_N(v)t = 0. \tag{IX.5.41}$$

Every term has mass dimension N; t remains dimensionless. Completing the square makes the double cover explicit. Define

$$y = \Lambda^N t - P_N(v), \qquad [y] = N. \tag{IX.5.42}$$

Multiplying (IX.5.41) by Λ^N and substituting this definition gives

$$(\Lambda^N t - P_N)^2 = P_N^2 - \Lambda^{2N}, \qquad y^2 = P_N(v)^2 - \Lambda^{2N}. \tag{IX.5.43}$$

Thus the two sheets and their product are

$$t_\pm = \frac{P_N \pm \sqrt{P_N^2 - \Lambda^{2N}}}{\Lambda^N}, \qquad t_+ t_- = 1. \tag{IX.5.44}$$

Their branch points solve $P_N = \pm\Lambda^N$. There are $2N$ distinct points on a smooth generic fiber. The Riemann–Hurwitz formula for a degree-two cover of the compact v sphere gives

$$2 - 2g = 2(2) - 2N, \qquad g = N - 1. \tag{IX.5.45}$$

This recovers the normalizable Cartan rank without adding a trace photon.

At large v, expand the square root on the branch with $y \sim P_N$:

$$t_+ \sim \frac{2v^N}{\Lambda^N}, \qquad t_- \sim \frac{\Lambda^N}{2v^N}, \qquad \log\frac{t_+}{t_-} \sim 2N\log\frac{v}{\Lambda} + \log 4. \tag{IX.5.46}$$

Since $s = -\log t$, the large-t sheet is the left asymptotic fivebrane. Its separation from the small-t sheet reproduces $b_0 = 2N$. The constant $\log 4$ changes finite scale matching, not the beta coefficient. For pure $SU(2)$, $P_2 = v^2 - u$ gives four branch points and one handle; for pure $SU(3)$, $P_3 = v^3 - u_2 v - u_3$ gives six and two handles.

The pure ambient product in (IX.5.39) must not be extended globally to actual D6 flavors. A D6 lifts to a Kaluza–Klein monopole. The complex surface for several D6s can be written, in appropriate algebraic coordinates, as

$$z_1 z_2 = \prod_{a=1}^{N_f} (v - \mathfrak{m}_a). \tag{IX.5.47}$$

This is the multi-Taub–NUT ambient description; its algebraic coordinates are not globally the pure t. We retain the flavored spectrum and running examples, but use pure $SU(3)$ as the controlled extension of the full curve calculation.

IX.5.7 Membrane masses and the normalized differential

An equation for Σ does not yet give a particle mass. For this we need a differential and a cycle. A supersymmetric membrane may end on the M5 with boundary $\gamma \subset \Sigma$. The BPS prescription relates its area to a period of a calibration form in the transverse geometry. Existence and stability of such a membrane are physical conditions; an arbitrary integral cycle does not automatically represent a stable particle.

Use physical complex coordinates $V = X^4 + iX^5$ and $S = X^6 + iX^{10} = R_{10}s$. With the appropriate complex structure and a fixed common phase, the calibrated membrane mass reduces by Stokes' theorem to

$$M_\gamma = T_{M2}\left|\int_D dV \wedge dS\right| = T_{M2}\left|\oint_\gamma V\, dS\right|, \qquad \partial D = \gamma. \tag{IX.5.48}$$

The equality with mass applies to a BPS membrane saturating the area bound. It is not an evaluation of an arbitrary non-BPS minimal surface. In the IIA length frame the membrane tension is

$$T_{M2} = \frac{1}{4\pi^2 R_{10}\alpha'}, \qquad T_{M2}(2\pi\alpha')R_{10} = \frac{1}{2\pi}. \tag{IX.5.49}$$

Substitute $V = 2\pi\alpha' v$ and $ds = -d\log t$ into (IX.5.48). The result fixes an absolute period mass:

$$M_\gamma = \frac{1}{2\pi}\left|\oint_\gamma v\, d\log t\right|. \tag{IX.5.50}$$

Keep the four-dimensional convention $M_{\rm BPS} = \sqrt{2}|Z|$. Choosing the common central-charge phase so that a weak electric period is positive gives the differential

$$\lambda_M = \frac{v\, d\log t}{2\sqrt{2}\pi i}, \qquad Z_\gamma = \oint_\gamma \lambda_M, \qquad M_\gamma = \sqrt{2}|Z_\gamma|. \tag{IX.5.51}$$

The coefficient has been derived from tension, units and the BPS mass convention. It is not determined by the polynomial alone.

Differentiate the quadratic equation along a fixed curve. Since $\Lambda^N t - P_N = y$, the result is

$$(\Lambda^N t - P_N)\frac{dt}{t} = P_N'(v)\, dv, \qquad \lambda_M = \frac{vP_N'(v)}{2\sqrt{2}\pi i\, y}\, dv. \tag{IX.5.52}$$

Its dimension is one: $[vP_N'/y] = 0$ and $[dv] = 1$. To fix the physical meaning of an electric cycle, go to a weak region where the zeros v_i of P_N are well separated. On the large-t sheet $y \sim P_N$, so a small positive cycle α_i around the associated tube has

$$\lambda_M \sim \frac{v}{2\sqrt{2}\pi i}\, d\log P_N, \qquad \oint_{\alpha_i}\lambda_M \sim \frac{v_i}{\sqrt{2}}. \tag{IX.5.53}$$

A W-boson joining the ith and jth tubes carries their difference. The mass is then

$$\gamma_W = \alpha_i - \alpha_j, \qquad \sqrt{2}\left|\oint_{\gamma_W}\lambda_M\right| \sim |v_i - v_j| = M_{F1}. \tag{IX.5.54}$$

This reproduces the physical F1 separation in (IX.5.10). For two tubes the compact electric cycles satisfy $\alpha_2 = -\alpha_1$; the W wraps $2\alpha_1$, not one primitive electric cycle. In the classical scalar convention $v_i = \sqrt{2}\phi_i$ and $\phi = \mathrm{diag}(a/2, -a/2)$, this becomes

$$v_{1,2} = \pm\frac{a}{\sqrt{2}}, \qquad u \sim \frac{a^2}{2}, \qquad M_W \sim \sqrt{2}|a|. \tag{IX.5.55}$$

The distinction between a primitive tube period and the electric W period is already present before quantum corrections.

For $P_2 = v^2 - u$, set $c_M = (2\sqrt{2}\pi i)^{-1}$. A useful derivative identity follows directly from $y^2 = (v^2-u)^2 - \Lambda^4$:

$$\lambda_M = c_M\frac{2v^2}{y}\, dv, \qquad \partial_u\lambda_M = c_M\left(\frac{dv}{y} - d\frac{v}{y}\right). \tag{IX.5.56}$$

On a closed transported cycle the exact term integrates to zero, so period derivatives are periods of the holomorphic form dv/y. Near either infinity $vP_2'/y = \pm 2 + O(v^{-2})$, with no v^{-1} term. The differential has no residue there, although it has a second-order pole in the inverse coordinate. This is appropriate to the pure theory; it supplies no prescription for flavored residues.

IX.5.8 Two elliptic curves and a degree-two map

Set $N = 2$ and denote the quartic by Q_u. Its four branch points are visible without solving any period integral:

$$Q_u: \quad y^2 = (v^2 - u)^2 - \Lambda^4, \qquad v = \pm\sqrt{u - \Lambda^2},\ \pm\sqrt{u + \Lambda^2}. \tag{IX.5.57}$$

They are distinct for $\Lambda \neq 0$ and $u \neq \pm\Lambda^2$, giving a smooth compact genus-one curve. The polynomial discriminant is the product of squared branch-point differences. Factor into the two quadratics $v^2 - u \pm \Lambda^2$. Each contributes a discriminant $4(u \mp \Lambda^2)$, and their squared resultant is $16\Lambda^8$. Hence

$$\Delta_Q = 256\Lambda^8(u^2 - \Lambda^4). \tag{IX.5.58}$$

The finite collision values are $u = \pm\Lambda^2$.

The Seiberg–Witten cubic target used in Volume I, Chapter 5 is

$$C_u: \quad y_c^2 = (x^2 - \Lambda^4)(x - u), \qquad \lambda_C = \frac{\sqrt{2}}{2\pi}\frac{x - u}{y_c}\,dx. \tag{IX.5.59}$$

Here $[x] = 2$ and $[y_c] = 3$, whereas $[v] = 1$ and $[y] = 2$ on Q_u. The same letter for these two horizontal coordinates would hide a physical dimension difference. The cubic roots $-\Lambda^2, \Lambda^2, u$ give

$$\Delta_C = (2\Lambda^2)^2(u - \Lambda^2)^2(u + \Lambda^2)^2 = 4\Lambda^4(u^2 - \Lambda^4)^2. \tag{IX.5.60}$$

The reduced collision locus agrees with that of Q_u, but the multiplicities do not. Determining the relation requires more than the locations of singular fibers.

For a smooth compact genus-one curve the modular invariant j records its complex structure. It is unchanged by a birational coordinate change. For a monic cubic $Y^2 = X^3 + a_2X^2 + a_4X + a_6$, one may compute it from the polynomial discriminant Δ as

$$j = 256\frac{(a_2^2 - 3a_4)^3}{\Delta}. \tag{IX.5.61}$$

To apply this to Q_u, first construct a genuinely birational cubic for that quartic. Define

$$X = 2(y + v^2 - u), \qquad Y = 2vX, \qquad Y^2 = X^3 + 4uX^2 + 4\Lambda^4X. \tag{IX.5.62}$$

For example, inserting $y = X/2 - v^2 + u$ in the quartic gives $X(v^2 - u) = X^2/4 + \Lambda^4$, which yields the displayed cubic. On the dense open set $X \neq 0$, the inverse is rational:

$$v = \frac{Y}{2X}, \qquad y = \frac{X}{2} - v^2 + u. \tag{IX.5.63}$$

Using $a_2 = 4u, a_4 = 4\Lambda^4$ for this cubic and $a_2 = -u, a_4 = -\Lambda^4$ for C_u gives

$$j_Q = \frac{64(4u^2 - 3\Lambda^4)^3}{\Lambda^8(u^2 - \Lambda^4)}, \tag{IX.5.64}$$

$$j_C = \frac{64(u^2+3\Lambda^4)^3}{\Lambda^4(u^2-\Lambda^4)^2}. \tag{IX.5.65}$$

At the smooth fiber $(u,\Lambda)=(2,1)$ the values are

$$j_Q = \frac{140608}{3}, \qquad j_C = \frac{21952}{9}. \tag{IX.5.66}$$

Thus the two families at the same parameters are generically not birational. Near $u=\Lambda^2$, even the orders of their j poles differ. The cubic in (IX.5.62), rather than (IX.5.59), is the birational cubic of Q_u.

There is nevertheless an explicit useful map to C_u:

$$\phi\colon Q_u \longrightarrow C_u, \qquad (x,y_c) = (u-v^2,\, ivy). \tag{IX.5.67}$$

Indeed $x-u=-v^2$ and $x^2-\Lambda^4=y^2$, so both sides of the cubic equation become $-v^2y^2$. A generic image point has the two preimages (v,y) and $(-v,-y)$. The involution exchanging them is free on a smooth compact fiber: at $v=0$ the nonzero opposite y values are exchanged, and the two infinity points distinguished by $y/v^2=\pm1$ are also exchanged. After choosing origins, this unramified degree-two map of genus-one curves is a *two-isogeny*. It identifies pairs of points rather than changing coordinates invertibly.

The map also determines the relation between physical differentials. On a fixed fiber, $dx=-2v\,dv$, and substitution gives

$$\phi^*\lambda_C = \frac{\sqrt{2}}{2\pi}\frac{(-v^2)(-2v\,dv)}{ivy} = \frac{\sqrt{2}v^2}{\pi iy}\,dv = 2\lambda_M. \tag{IX.5.68}$$

Both the degree of the curve map and this differential factor must enter a period comparison. Neither can be removed by declaring that the singular loci coincide.

IX.5.9 Cycles, contour integrals and a numerical vacuum

Work first in the real chamber $u>\Lambda^2>0$, and define $a_-=\sqrt{u-\Lambda^2}$, $a_+=\sqrt{u+\Lambda^2}$. On Q_u choose a primitive cycle α_M surrounding the positive cut $[a_-,a_+]$. A second primitive cycle β_M goes between $-a_-$ and a_- and returns on the other sheet. A small displacement of paths at their common branch point gives their single intersection. Orient the cycles so that the electric period is positive real and the magnetic one positive imaginary. Define

$$A_M = \oint_{\alpha_M}\lambda_M, \qquad B_M = \oint_{\beta_M}\lambda_M, \qquad \alpha_M\cdot\beta_M = 1. \tag{IX.5.69}$$

Cycle symbols and period symbols are distinct: α_M,β_M are topological paths, while A_M,B_M are their complex integrals.

On the cubic, choose α_C around $[-\Lambda^2,\Lambda^2]$ and β_C around $[\Lambda^2,u]$, with the corresponding positive orientations. Their periods are

$$a = \oint_{\alpha_C}\lambda_C, \qquad a_D = \oint_{\beta_C}\lambda_C. \tag{IX.5.70}$$

Under $x = u - v^2$, the positive quartic cut runs once over the cubic electric cut. On the inner path, v moves from $-a_-$ to 0 to a_-, while x moves from Λ^2 to u and back to Λ^2. The factor iv in y_c changes the sheet at the turn. This already traces the cubic magnetic cycle; returning on the second quartic sheet repeats it. Thus

$$\phi_*\alpha_M = \alpha_C, \qquad \phi_*\beta_M = 2\beta_C. \tag{IX.5.71}$$

Combining this cycle map with (IX.5.68), rather than identifying coordinate equations alone, gives

$$a = 2A_M, \qquad a_D = B_M. \tag{IX.5.72}$$

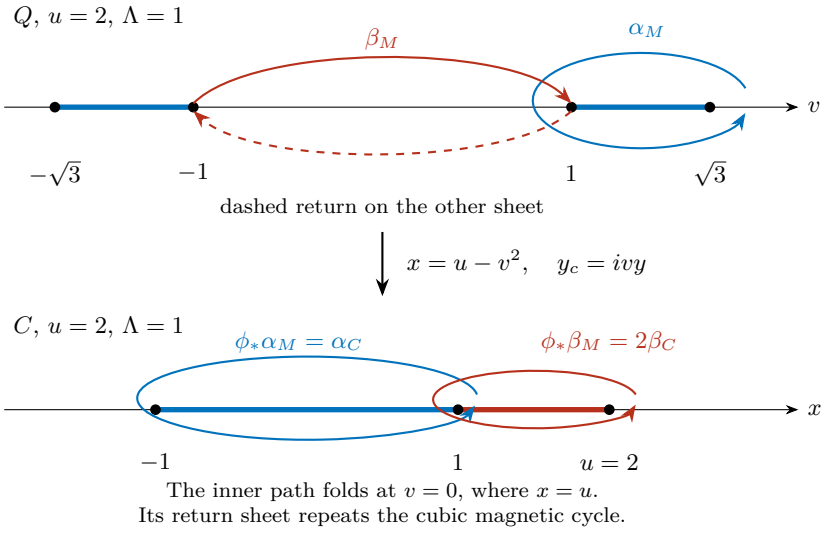


Figure IX.5.4: The cycles of the quartic and their cubic images at $(u, \Lambda) = (2, 1)$. Blue denotes the electric cut/cycle and red the magnetic path. A dashed segment returns on the second quartic sheet. The inner path folds at $v = 0$ and the full quartic magnetic cycle covers the cubic one twice. Path offsets are schematic; orientations are fixed by the positive periods in the text.

The periods can be evaluated directly from those paths. Across a cut, the sign of y changes, so the outgoing and returning contributions add. Using the symmetry of the inner path gives

$$A_M = \frac{\sqrt{2}}{\pi} \int_{a_-}^{a_+} \frac{v^2\, dv}{\sqrt{(a_+^2 - v^2)(v^2 - a_-^2)}}, \tag{IX.5.73}$$

$$B_M = \frac{2i\sqrt{2}}{\pi} \int_{0}^{a_-} \frac{v^2\, dv}{\sqrt{(a_-^2 - v^2)(a_+^2 - v^2)}}. \tag{IX.5.74}$$

These square-root endpoint singularities are integrable. For the first integral, put $v^2 = u + \Lambda^2 \cos\theta$ and reverse the limits. For the second put $v = a_- \sin\theta$. The smooth integrals become

$$A_M = \frac{1}{\sqrt{2}\pi} \int_0^\pi \sqrt{u + \Lambda^2 \cos\theta}\, d\theta, \tag{IX.5.75}$$

$$B_M = \frac{2i\sqrt{2}(u - \Lambda^2)}{\pi} \int_0^{\pi/2} \frac{\sin^2\theta\, d\theta}{\sqrt{u + \Lambda^2 - (u - \Lambda^2)\sin^2\theta}}. \tag{IX.5.76}$$

Independently, the two cubic cuts give

$$a = \frac{\sqrt{2}}{\pi} \int_{-\Lambda^2}^{\Lambda^2} \sqrt{\frac{u - x}{\Lambda^4 - x^2}}\, dx, \tag{IX.5.77}$$

$$a_D = \frac{i\sqrt{2}}{\pi} \int_{\Lambda^2}^{u} \sqrt{\frac{u - x}{x^2 - \Lambda^4}}\, dx. \tag{IX.5.78}$$

The substitution $x = \Lambda^2 \cos\theta$ in the electric integral, followed by $\theta \mapsto \pi - \theta$, immediately gives $a = 2A_M$. The magnetic relation also follows from the folded path or direct substitution. The integrals thus give numerical values without using the period relation as a definition of the quartic answer.

Choose units in which $\Lambda = 1$ and the smooth vacuum $u = 2$. Evaluating the integrals gives the following worked example:

$$A_M \simeq 0.9833426507751652, \qquad B_M \simeq i\,0.4734344365355368, \tag{IX.5.79}$$

$$a \simeq 1.96668530155033, \qquad a_D \simeq i\,0.4734344365355368. \tag{IX.5.80}$$

These are periods, not branch-point positions. For example the branch points are $\pm 1, \pm\sqrt{3}$, while the electric W central charge is $2A_M \simeq 1.9666853$. The distinction is the quantum correction to the classical relation between an eigenvalue and a physical period.

Define the two period ratios using derivatives on the Coulomb base:

$$\tau_M = \frac{\partial_u B_M}{\partial_u A_M}, \qquad \tau_{\mathrm{SW}} = \frac{\partial_u a_D}{\partial_u a}, \qquad \tau_M = 2\tau_{\mathrm{SW}}. \tag{IX.5.81}$$

At this vacuum they are

$$\tau_M \simeq i\,1.709168886557487, \qquad \tau_{\mathrm{SW}} \simeq i\,0.8545844432787435. \tag{IX.5.82}$$

Both have positive imaginary part. The first uses a primitive quartic electric cycle; the second uses the electric normalization in which the W has unit n_e and mass $\sqrt{2}|a|$. They are not two competing values for one identically normalized Cartan coupling. A genus-one complex structure uses a primitive cycle basis, so the factor of two also explains why its j invariant changes under this isogeny. The smooth cut integrals above give these numerical values in the real chamber. The exact map and cycle argument establish the structural relation on smooth continued fibers.

IX.5.10 Weak coupling and a vanishing monopole period

The electric integral makes the semiclassical limit explicit. For $u \gg \Lambda^2$, introduce $\epsilon = \Lambda^2/u$ and set $x = \Lambda^2 \cos\theta$ in (IX.5.77). Then

$$\frac{a}{\sqrt{2u}} = \frac{1}{\pi}\int_0^{\pi} (1 - \epsilon\cos\theta)^{1/2}\, d\theta. \tag{IX.5.83}$$

Odd powers of $\cos\theta$ average to zero. The first even averages are

$$\langle \cos^2\theta \rangle = \frac{1}{2}, \qquad \langle \cos^4\theta \rangle = \frac{3}{8}, \qquad \langle f \rangle = \frac{1}{\pi}\int_0^{\pi} f\, d\theta. \tag{IX.5.84}$$

The square-root coefficients $-1/8$ and $-5/128$ therefore yield

$$a = \sqrt{2u}\left[1 - \frac{\Lambda^4}{16u^2} - \frac{15\Lambda^8}{1024u^4} + O\!\left(\frac{\Lambda^{12}}{u^6}\right)\right]. \tag{IX.5.85}$$

In particular $\sqrt{2}\,2A_M \sim 2\sqrt{u}$, matching the stretched W between $v = \pm\sqrt{u}$. Assigning the W to just α_M would miss this mass by a factor of two.

The magnetic integral develops a logarithm from its lower endpoint. To isolate it, in the range $\Lambda^2 \ll x \ll u$ replace its integrand by $\sqrt{u}/x$. The logarithmic part is

$$a_D = \frac{i\sqrt{2u}}{\pi}\log\frac{u}{\Lambda^2} + \text{a finite multiple of } \sqrt{u} + \cdots. \tag{IX.5.86}$$

The finite multiple contributes an additive constant to the period ratio. A logarithmic derivative of that ratio removes this constant as $u/\Lambda^2 \to \infty$:

$$\frac{d\tau_{\mathrm{SW}}}{d\log\sqrt{u}} \longrightarrow \frac{2i}{\pi} = \frac{ib_0}{2\pi}, \qquad b_0 = 4. \tag{IX.5.87}$$

This is the component-normalized pure $SU(2)$ beta coefficient, obtained now from periods. Increasing u by a factor of ten increases $\operatorname{Im}\tau_{\mathrm{SW}}$ asymptotically by $\log(10)/\pi$. A finite scale convention changes the constant, not this slope.

At the other end of the real chamber, put $\delta = u - \Lambda^2 > 0$. The inner branch points approach each other as $\pm\sqrt{\delta}$ and the cycle β_M shrinks. Substitute $x = \Lambda^2 + \delta z$ in the cubic magnetic integral to obtain

$$a_D = \frac{i\sqrt{2}\delta}{\pi}\int_0^1 \frac{\sqrt{(1-z)/z}}{\sqrt{2\Lambda^2 + \delta z}}\, dz. \tag{IX.5.88}$$

The elementary integral is $\int_0^1 \sqrt{(1-z)/z}\, dz = \pi/2$, as follows from $z = \sin^2\theta$. Thus

$$a_D = \frac{i\delta}{2\Lambda} + O(\delta^2/\Lambda^3), \qquad M_m = \sqrt{2}|a_D| \sim \frac{|\delta|}{\sqrt{2}\Lambda}. \tag{IX.5.89}$$

The electric integral is finite at the same point. At $u = \Lambda^2$ its factor $(\Lambda^2 - x)$ cancels under the square root, giving

$$a(\Lambda^2) = \frac{\sqrt{2}}{\pi} \int_{-\Lambda^2}^{\Lambda^2} \frac{dx}{\sqrt{\Lambda^2 + x}} = \frac{4\Lambda}{\pi}. \tag{IX.5.90}$$

The monopole becomes massless while the W period stays nonzero. This is a statement about a normalized vanishing period, stronger than merely locating a zero of a discriminant.

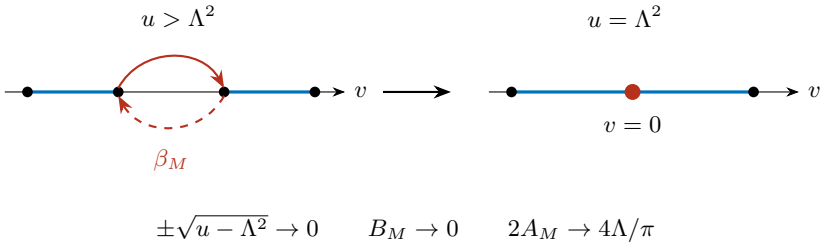


Figure IX.5.5: The monopole degeneration of the pure $SU(2)$ quartic. The inner branch points collide and the magnetic cycle shrinks; the electric period stays finite. Cuts are drawn schematically on the real v axis. The limiting double point is a singular fiber, so the smooth genus-one description applies on its punctured neighborhood.

There is also a distinct classical limit. At $\Lambda = 0$,

$$y^2 = (v^2 - u)^2, \qquad \Delta_Q \equiv 0. \tag{IX.5.91}$$

The right-hand polynomial is now a perfect square. It is not a third isolated quantum singularity, and the smooth-elliptic isogeny discussion cannot be extended through this limit without resolving its degeneration.

IX.5.11 The particle lattice and based monodromies

The primitive integral cycles of a smooth genus-one curve form a rank-two lattice. In electric/magnetic order, let a cycle be $e_M\alpha_M + m_M\beta_M$. Its period is a central charge when the appropriate BPS state exists. Comparing it with the field-theory normalization gives

$$Z = e_M A_M + m_M B_M = n_e a + n_m a_D, \qquad \begin{pmatrix} e_M \\ m_M \end{pmatrix} = D \begin{pmatrix} n_e \\ n_m \end{pmatrix}, \quad D = \begin{pmatrix} 2 & 0 \\ 0 & 1 \end{pmatrix}. \tag{IX.5.92}$$

This makes the Cartan meaning of the factor two explicit. The W has unit n_e in the field-theory convention but even primitive electric charge $e_M = 2$. The monopole has unit magnetic charge. Their span is an index-two sublattice of primitive M5 homology:

$$\Gamma_{\text{part}} = 2\mathbb{Z}\,\alpha_M \oplus \mathbb{Z}\,\beta_M, \qquad [H_1(Q_u, \mathbb{Z}) : \Gamma_{\text{part}}] = |\det D| = 2. \tag{IX.5.93}$$

For $J = \left(\begin{smallmatrix} 0 & 1 \\ -1 & 0 \end{smallmatrix}\right)$, the primitive intersection pairing pulls back to

$$D^T J D = 2J, \qquad \langle W, m \rangle = 2. \tag{IX.5.94}$$

This does not assert that every vector in Γ_{part} is a stable particle in every chamber. Nor does it identify every primitive cycle with a particle. A choice of genuine Wilson and 't Hooft lines, and hence of global gauge form, requires additional information beyond the displayed particle sublattice.

Monodromy compares cycles after continuing the vacuum around a singular point. Fix a base point in $u > \Lambda^2$ and based loops whose composition is stated below. At $u = \Lambda^2$ the vanishing quartic cycle is $\gamma_m = \beta_M$. In the standard continued cubic basis, the other finite singularity has vanishing cycle $\beta_C - \alpha_C$. Its smallest multiple in the image of (IX.5.71) is $2(\beta_C - \alpha_C)$, so the primitive quartic lift is

$$\gamma_m = \beta_M, \qquad \gamma_d = \beta_M - 2\alpha_M, \qquad \phi_* \gamma_d = 2(\beta_C - \alpha_C). \tag{IX.5.95}$$

The cubic vanishing-cycle label includes a choice of continuation from the base point. It is not inferred from a real drawing of the two singular fibers alone.

For completeness, derive the corresponding local Picard–Lefschetz transformation. Let the vanishing cycle be $\gamma = m\beta_M + e\alpha_M$. With the loop orientation used here, a transported cycle changes by minus its intersection with γ times γ. Since $\beta_M \cdot \gamma = -e$ and $\alpha_M \cdot \gamma = m$, the period column obeys

$$\begin{pmatrix} B_M \\ A_M \end{pmatrix} \longmapsto \begin{pmatrix} B_M + e(mB_M + eA_M) \\ A_M - m(mB_M + eA_M) \end{pmatrix}. \tag{IX.5.96}$$

The matrix is consequently

$$K(m,e) = \begin{pmatrix} 1 + me & e^2 \\ -m^2 & 1 - me \end{pmatrix}, \qquad \det K = 1. \tag{IX.5.97}$$

For the two selected vanishing cycles this gives

$$K_m = \begin{pmatrix} 1 & 0 \\ -1 & 1 \end{pmatrix}, \qquad K_d = \begin{pmatrix} -1 & 4 \\ -1 & 3 \end{pmatrix}. \tag{IX.5.98}$$

The field-theory period column has a different electric normalization. Introduce S, acting on magnetic/electric period order, by

$$\begin{pmatrix} a_D \\ a \end{pmatrix} = S \begin{pmatrix} B_M \\ A_M \end{pmatrix}, \qquad S = \begin{pmatrix} 1 & 0 \\ 0 & 2 \end{pmatrix}, \qquad M_i = S K_i S^{-1}. \tag{IX.5.99}$$

It follows that the cubic target matrices are

$$M_m = \begin{pmatrix} 1 & 0 \\ -2 & 1 \end{pmatrix}, \qquad M_d = \begin{pmatrix} -1 & 2 \\ -2 & 3 \end{pmatrix}. \tag{IX.5.100}$$

Choose the based-loop product represented on period columns by $M_m M_d$. The rightmost matrix acts first. Direct multiplication yields

$$K_m K_d = \begin{pmatrix} -1 & 4 \\ 0 & -1 \end{pmatrix}, \qquad M_m M_d = M_\infty = \begin{pmatrix} -1 & 2 \\ 0 & -1 \end{pmatrix}. \tag{IX.5.101}$$

This agrees with the weak-coupling continuation. As $u \mapsto e^{2\pi i}u$, the square root changes sign and the logarithm in (IX.5.86) gains $2\pi i$, so $a \mapsto -a$ and $a_D \mapsto -a_D + 2a$.

The primitive local monodromy has one unit of transvection, while the cubic matrix has two in this normalization. The orders of the finite discriminant zeros and j poles record that family distinction. Multiplying a discriminant by a constant cannot alter these orders. For example

$$\frac{\Delta_Q}{\Delta_C} = \frac{64\Lambda^4}{u^2 - \Lambda^4} \tag{IX.5.102}$$

is not constant on the base. None of this counts two independent monopole hypermultiplets at a cubic singularity. The physical interpretation uses the differential and the charge lattice together.

Finally distinguish active analytic continuation from a change of coordinates used to represent a fixed charge. Write $\Pi = (a_D, a)^T$ and $\boldsymbol{q} = (n_m, n_e)^T$, so the central charge is the dot pairing $Z = \boldsymbol{q}^T\Pi$. Under a period-basis change the same functional is represented by the contragredient charge:

$$\Pi' = M\Pi, \qquad \boldsymbol{q}' = M^{-T}\boldsymbol{q}, \qquad \boldsymbol{q}'^T\Pi' = \boldsymbol{q}^T\Pi. \tag{IX.5.103}$$

For $M = M_m$, $\Pi = (3, 5)^T$ and $\boldsymbol{q} = (1, 2)^T$, one finds

$$\Pi' = (3, -1)^T, \qquad \boldsymbol{q}' = (5, 2)^T, \qquad Z = 3 + 10 = 15 - 2 = 13. \tag{IX.5.104}$$

Applying M to both columns would give $Z = 3$, which is a different operation. Active period monodromy with fixed numerical charge also changes the central charge in general. The correct dual action in (IX.5.103) is compatible with all the cubic monodromies above; the isogeny does not invalidate it.

IX.5.12 Pure SU(3): trace coordinates, a node and a cusp

The rank-one calculation generalizes without introducing flavors. For three finite color branes the monic trace-free polynomial and its quadratic lift are

$$P_3 = v^3 - u_2 v - u_3, \qquad \Lambda^3(t^2 + 1) - 2P_3 t = 0. \tag{IX.5.105}$$

Completing the square gives a degree-six polynomial in v:

$$y^2 = (v^3 - u_2 v - u_3)^2 - \Lambda^6, \qquad \lambda_M = \frac{v(3v^2 - u_2)}{2\sqrt{2}\pi i y}\, dv. \tag{IX.5.106}$$

There are two Coulomb coordinates and, for simple branch points, genus two. For example $u_2 = u_3 = 0$, $\Lambda = 1$ gives $y^2 = v^6 - 1$. Its derivative $6v^5$ has no root in common with $v^6 - 1$, so this particular fiber is smooth.

The coefficient coordinates must be converted before being identified with traces of the adjoint scalar. Let its semiclassical eigenvalues be ϕ_i with $\sum_i \phi_i = 0$, and set

$v_i = \sqrt{2}\phi_i$. Expanding the characteristic polynomial gives

$$\prod_{i=1}^{3}(v - v_i) = v^3 + \left(\sum_{i<j} v_i v_j\right) v - v_1 v_2 v_3. \tag{IX.5.107}$$

The trace-free condition implies $\sum_{i<j} v_i v_j = -\frac{1}{2}\sum_i v_i^2$ and $\sum_i v_i^3 = 3v_1 v_2 v_3$. Matching coefficients therefore yields

$$u_2 = \frac{1}{2}\sum_i v_i^2 = \operatorname{Tr}\phi^2, \qquad u_3 = \frac{1}{3}\sum_i v_i^3 = \frac{2\sqrt{2}}{3}\operatorname{Tr}\phi^3. \tag{IX.5.108}$$

For the explicit traceless triple $(b, c, -b-c)$ this becomes

$$u_2 = 2(b^2 + bc + c^2), \qquad u_3 = -2\sqrt{2}\, bc(b + c). \tag{IX.5.109}$$

In particular u_3 is not the unconverted trace $\operatorname{Tr}\phi^3$. These are the polynomial-coordinate conventions used here; no claim about every possible quantum operator scheme is needed for this match.

The discriminant is most efficiently derived by factoring the sextic into two cubics,

$$f_\pm(v) = v^3 - u_2 v - u_3 \pm \Lambda^3, \qquad y^2 = f_+ f_-. \tag{IX.5.110}$$

For a cubic $v^3 + pv + q$, the discriminant is $-4p^3 - 27q^2$. The two factors thus have

$$\operatorname{disc} f_\pm = 4u_2^3 - 27(u_3 \mp \Lambda^3)^2. \tag{IX.5.111}$$

A resultant measures whether two polynomials share a root. Since $f_+ - f_- = 2\Lambda^3$, evaluating one at the three roots of the other gives a constant at each root. Its square is

$$\operatorname{Res}(f_+, f_-)^2 = (2\Lambda^3)^6 = 64\Lambda^{18}. \tag{IX.5.112}$$

The discriminant of a product multiplies both individual discriminants and this squared resultant. Therefore

$$\begin{aligned}\Delta_3 = 64\Lambda^{18}\big[4u_2^3 - 27(u_3 + \Lambda^3)^2\big] \\ \times \big[4u_2^3 - 27(u_3 - \Lambda^3)^2\big].\end{aligned} \tag{IX.5.113}$$

This separates the two ways in which a pair of branch points can collide. At nonzero Λ, a root cannot belong simultaneously to f_+ and f_-, because their difference is nonzero.

Take $\Lambda = 1, u_2 = 3, u_3 = -3$. The two factors are

$$P_3 - 1 = v^3 - 3v + 2 = (v-1)^2(v+2), \qquad P_3 + 1 = v^3 - 3v + 4. \tag{IX.5.114}$$

The second factor is nonzero at $v = 1$. To determine the local type, set $v = 1 + z$. The curve becomes

$$y^2 = 6z^2 + 2z^3 + 9z^4 + 6z^5 + z^6. \tag{IX.5.115}$$

The quadratic tangent cone factors as $(y - \sqrt{6}z)(y + \sqrt{6}z) = 0$. Its two distinct tangent directions identify an ordinary node. One handle pinches and the normalized curve has genus one.

Now take $u_2 = 0, u_3 = 1$, still with $\Lambda = 1$. Instead one obtains

$$y^2 = v^3(v^3 - 2) = -2v^3 + v^6. \tag{IX.5.116}$$

The leading local equation is a cusp, not two distinct nodal tangents. The repeated-root factor of the sextic and its derivative is v^2, whereas at the ordinary node it was $v - 1$. Thus a vanishing discriminant does not always describe one isolated ordinary monopole node. Extracting the interacting physics of the cusp requires further period, scaling and light-state information. The present extension determines the rank-two curve, trace conversion and local degenerations; it does not supply a full rank-two period matrix or an interacting Argyres–Douglas analysis.

IX.5.13 Exercises on curves, charges and periods

The following three exercises use the pure theory and the orientation conventions of this chapter. Work with the supplied physical curve and differential; the exercises test their consequences. They do not derive the continuation from the interval theory or the existence of a BPS membrane for an arbitrary cycle. See `benchmark/tasks.json` and `benchmark/PROTOCOL.md` for the public structured-answer format.

1. Recognizing the elliptic curve. Set $\Lambda = 1$ and use separately the smooth vacua $u = 2$ and $u = 3$. Calculate the polynomial discriminants of Q_u and C_u. Construct the birational cubic of Q_u and obtain its j invariant. Compare with the invariant of C_u at the same vacuum. Explain why a shared degeneration locus is insufficient for birational equivalence.

Submit the coefficients of the map $x(v)$ and of $h(v)$ in $y_c = iyh(v)$, in ascending powers of v. Substitute them into the cubic equation and reduce using the quartic equation. Determine the number of preimages of a generic point and the action of the deck involution. The chosen phase is the one in (IX.5.67). Retain $u^2 \neq \Lambda^4$ and $\Lambda \neq 0$ when interpreting this as an isogeny of elliptic curves. At the excluded fibers the polynomial identity can still hold although the smooth-curve conclusion fails.

2. Transporting the particle charges. Use electric/magnetic order for D and magnetic/electric order for S. Starting with the two vanishing cycles in (IX.5.95), derive their Picard–Lefschetz matrices, translate them using S, and multiply in the stated based-loop order. Compute the index of the particle sublattice and its intersection form. For $\Pi = (3, 5)^T$ and $q = (1, 2)^T$, transport the period by the monopole matrix and find the coordinates representing the same central-charge functional. Submit both columns and the central charge. Test why using M for both columns fails. This calculation does not choose a genuine line lattice or establish stability of every particle charge.

3. Following the branch points and the differential. At $(u, \Lambda) = (2, 1)$ list the two positive squared branch positions. Derive the differential pullback, then combine it with the cycle pushforward to obtain the electric, magnetic and coupling ratios. Evaluate A_M and B_M/i from the smooth quartic integrals; compute the cubic integrals

separately as a comparison. Derive the first two nonconstant coefficients of $a/\sqrt{2u}$ in powers of $\epsilon = \Lambda^2/u$, and the coefficient of $i\delta$ in a_D near $u = 1 + \delta$. Determine the mass dimension of a period by scaling v, u, Λ together. Finally identify what fails when $\Lambda = 0$ or $u = \Lambda^2$. Numerical integration is restricted to the real chamber $u > \Lambda^2 > 0$; it is not a global continuation prescription.

IX.5.14 What the construction determines

The interval and M5 descriptions answer different parts of one physical question. The interval spectrum identifies the vector and hypermultiplet representations. Its DBI action fixes the coupling, and the fivebrane logarithm reproduces the matter coefficient. Fixed asymptotic data then select the finite-norm gauge algebra. Under the protected M-theory continuation, the same rank appears as the genus of an internal surface, and calibrated membrane periods assign central charges to the selected particle cycles.

Take-home message of this chapter

Under the protected M-theory continuation, recover the four-dimensional Coulomb data by specifying the curve, the normalized differential and the physical cycle/charge convention together. For pure $SU(2)$, the quartic and the SW cubic obey $\phi^*\lambda_C = 2\lambda_M$, $(a_D, a) = (B_M, 2A_M)$ and $\tau_M = 2\tau_{\mathrm{SW}}$. Their generic complex structures differ, while their physically normalized periods match through a degree-two map. The W and monopole span an index-two particle lattice. Primitive homology alone selects neither every stable particle nor every genuine line.

The pure $SU(3)$ example shows how to reuse the polynomial construction and how to distinguish a node from a cusp. Flavored curves require their own residue normalization in the Taub–NUT ambient geometry. Global line choices, complete stability chambers and nonprotected M5 metric data require additional physical information. Chapter 6 changes the fivebrane orientation and the surviving supersymmetry; the unrotated interval and the physical circle conventions established here are its starting configuration.

Status and sources

WS means a controlled physical-worldsheet derivation in the untwisted string. Worldvolume algebra, a supplied DBI action and an imported open-string spectrum do not by themselves supply that payload. The spectrum and DBI origins below therefore retain unclassified physical premises (null primary status in the companion inventory), with explicit worldsheet-derivation debt. Conditional mathematical calculations and source-backed physical statements are recorded separately.

The finite-interval spectrum and running, the pure $SU(2)$ M5 curve and the worked $SU(3)$ extension use the scopes stated below.

The principal texts are Witten (1997), inspected as hep-th/9703166v1, Elitzur et al. (1997), inspected as hep-th/9702014v2, and Seiberg and Witten (1994), inspected as hep-th/9407087v1. All page locators below are printed article pages, excluding the cover. The bibliography uses the shared canonical entries; the source-version qualification here is deliberate, including the SW v1 differential and cycle convention. The physical premises and mathematical consequences are identified in the notes below.

1. Spectrum, Section IX.5.2. The brane spectrum is a sourced physical premise. The endpoint-to-field dictionary is [GEO-E]. Equations (IX.5.1)–(IX.5.10) establish the axis-dependent scalar kernels, full oriented Chan–Paton representation and classical F1 mass markers. Witten §2, pp. 2–3, and §3.1, pp. 21–22; EGK §2, (2.1)–(2.3), p. 2. EGK (2.4) is the rotated $\mathcal{N} = 1$ configuration and is used only as a contrast. The eight-supercharge/GSO spectrum and the A_6 boundary prescription are sourced physical inputs, not a new IIA gamma/RR-sign derivation. The classical versus anomalous quantum $U(1)_R$ distinction follows SW §2.2, pp. 5–6. Chapter IX.1 supplies the interval ODE and DBI calculation inputs. The tensor-product Cartan characters give the complete weight multisets.

2. Coupling and limit, Section IX.5.3. The coefficient reduction is conditional on the supplied DBI action and the stated decoupling limit [DEC]. Equations (IX.5.11)– (IX.5.21) use brane-action and trace normalization, including the component action, and translate Witten (2.7)–(2.14), pp. 6–8, and §3.2, pp. 22–23. Witten suppresses absolute coupling constants; the displayed factors are locally fixed by DBI, D0 action and physical angle periodicity. The interval/circle fixed-scale hierarchy is explicit for $b_0 > 0$; full quantum-gravity decoupling is not proved, and no numerical equality between Λ_{RG} and Λ is admitted. The distinction follows from the two stated normalizations.

3. Running, Section IX.5.4. [GEO-E]. Equations (IX.5.22)– (IX.5.29) and Table IX.5.1 compare matter indices with endpoint asymptotics. Source anchors are Witten (2.1)–(2.8), pp. 4–6, (2.14)–(2.15), p. 8, and the matter interpretation around (3.1), pp. 21–22. The local positive-AF b_0 is minus Witten's signed coefficient. The unit circle vortex fixes the absolute endpoint logarithm; the source's initially unspecified coefficient in (2.2) is not silently set to one. The $N_f \geq 2N$ interpretive boundary follows §2.4, pp. 15–18. The endpoint calculation gives the absolute coefficients $4, 6, 3, 0$ and their full-hyper responses. Only the coefficient/asymptotic comparison is asserted, not a full metric.

4. Normalizability, Section IX.5.5. [GEO-E]. Equations (IX.5.30)– (IX.5.38) make Witten's (2.4)–(2.6), p. 5, §2.2, pp. 6–7, and the square-integrable tensor reduction after (2.16), pp. 10–11, explicit. The circular unflavored equal-rank counterexample is §4.1, pp. 36–37. Fixed noncompact exterior data are essential; the result is a dynamical-algebra statement rather than a universal free-center or FI rule. The tail and kernel analysis uses the fixed exterior data. Constraint-equivalent row systems have the same physics. The group and FI statements apply to the finite chain with the stated boundary conditions.

5. M5 construction, Section IX.5.6. [DUAL], conditional on the nonperturbative M-theory lift. Equations (IX.5.39)–(IX.5.46) derive the two-sheeted pure curve after the physical M5 prescription has been supplied. Witten §2.3–2.4, pp. 8–15, especially (2.17)–(2.23). Protected low-energy continuation is the physical premise. the symbolic calculation and the consistency check test elimination and genus, not M theory itself. Equation (IX.5.47) uses Witten §3.2–3.3, pp. 22–28, (3.2)–(3.5) and (3.7)–(3.14). It prevents confusing actual D6 flavors with a globally flat pure t chart. There is no independent string-access route claimed here.

6. Absolute differential, Section IX.5.7. The calibrated membrane argument uses [BPS:1/2|holo] and the stated action and trace normalization. Equations (IX.5.48)–(IX.5.56) derive the coefficient using membrane tension, physical coordinate conversion, Stokes' theorem and $M = \sqrt{2}|Z|$. Witten's "BPS States" paragraph, §2.3 p. 13, supplies M2 boundaries and area minimization; it does *not* print the

absolute $1/(2\pi)$ factor or λ_M used here. Those are local deductions conditional on the calibrated BPS membrane prescription. SW §2.2 p. 6 and §6, (6.19)–(6.23), pp. 37–39, anchor the field-theory normalization. The F1 match gives the differential identity. Existence of a BPS surface for an arbitrary class requires a separate argument.

7. Isogeny, Section IX.5.8. [MATH]. Equations (IX.5.57)–(IX.5.68) give the exact discriminants, genuinely birational cubic, rational inverse, unequal j invariants and degree-two quotient with its differential pullback. The starting curves are Witten (2.19)–(2.21) and SW (6.6), p. 35, with SW differential (6.19), p. 37. The map and same-parameter comparison are derived locally, not attributed as a quoted equivalence theorem to either source. the symbolic calculation supplies exact invariant and substitution evidence. Smooth-fiber statements exclude $u = \pm\Lambda^2$ and $\Lambda = 0$; exceptional equality of individual j values would not establish equality of the two families.

8. Periods, Sections IX.5.9 and IX.5.10. [BPS:1/2|holo]. Equations (IX.5.69)– (IX.5.82) use oriented cut integrals and the exact cycle map; (IX.5.83)–(IX.5.91) derive the physical limits. SW (6.14), p. 36, (6.19)–(6.23), pp. 37–39, and (6.24)–(6.28), pp. 39–40, fix the cubic target and limits. The quartic and cubic cut integrals displayed in Section IX.5.9 reproduce the printed values at $(u, \Lambda) = (2, 1)$ in the smooth real chamber $u > \Lambda^2 > 0$. Their numerical agreement tests the normalization at that vacuum; the exact map and cycle pushforward supply the structural period relation on smooth fibers.

9. Lattice and monodromy, Section IX.5.11. [BPS:1/2|holo]. Equations (IX.5.92)– (IX.5.104) distinguish the index-two particle embedding, primitive intersection, Cartan period normalization and contragredient charge coordinates. SW (6.1)–(6.3), p. 34, supplies the based-cycle/monodromy target; the dyon lift uses that sourced continuation. the symbolic calculation and the consistency check test the translated matrices and pairing. No independent global branch-braid computation or complete BPS chamber classification is asserted. The genuine-line/global-form restriction is U-004; the abstract unimodular lattice and this particle sublattice are not silently identified.

10. Pure SU(3), Section IX.5.12. [MATH]; [DUAL], using the same nonperturbative M-theory lift. Equations (IX.5.105)–(IX.5.116) derive the rank-two curve, Newton conversion, resultant factorization and local node/cusp types from Witten's pure rank-N construction, (2.19)–(2.21), pp. 14–15. The node tangent expansion and smooth $v^6 - 1$ example illustrate the local singularity calculations. This is curve/discriminant/local-singularity coverage, not a rank-two period matrix, full light spectrum or interacting AD-dynamics result.

11. Calculation and figure coverage. The exact cycle map and displayed cut integrals support the stated period comparison under the specified curve and cycle conventions. Finite algebraic and numerical examples do not replace those physical premises or establish a universal result. The figures illustrate the sourced axes, calculated asymptotic slopes, M5 tube interpretation, exact cycle map and calculated degeneration. Figure offsets and the M5 tube drawing are schematic and make no metric claim.

12. Comparison with Volume I, Chapter 5. The exact j counterexample and the nonconstant discriminant ratio locate two inherited algebraic errors: the sentence following `eq:V05-su2curve` calls the same-parameter quartic birational to the cubic, and the text following `eq:V05-singpts` calls the double discriminant order a convention artifact. The inherited cubic monodromies and central-charge formula remain valid. In particular its explicit fixed-charge rule M^{-T} is correct, as (IX.5.103)–(IX.5.104) demonstrate. Loop-order wording and the particle/global-line comparison must be delimited separately from those two algebraic errors. The chapter's positive teaching comparison is in Sections IX.5.8, IX.5.9 and IX.5.11.

No GEO-X grade is assigned to the M5/SW dictionary. The nodal IIB Calabi–Yau threefold construction is separate from this internal Riemann surface. The complete gauge-theory interpretation remains conditional on the nonperturbative M-theory lift and protected continuation. Deferrals concern full flavored residues, global line choices, BPS stability chambers, rank-two periods and nonprotected geometry. They are not supplied by the numerical examples.

References

Elitzur, S., A. Giveon, and D. Kutasov (1997). "Branes and N=1 duality in string theory". In: *Phys. Lett. B* 400, pp. 269–274. DOI: 10.1016/S0370-2693(97)00375-4. arXiv: hep-th/9702014.

Seiberg, N. and E. Witten (1994). "Electric-magnetic duality, monopole condensation, and confinement in N=2 supersymmetric Yang-Mills theory". In: *Nucl. Phys. B* 426. [Erratum: Nucl.Phys.B 430, 485–486 (1994)], pp. 19–52. DOI: 10.1016/0550-3213(94)90124-4. arXiv: hep-th/9407087.

Witten, E. (1997). "Solutions of four-dimensional field theories via M-theory". In: *Nucl. Phys. B* 500, pp. 3–42. DOI: 10.1016/S0550-3213(97)00416-1. arXiv: hep-th/9703166.

Chapter IX.6

Rotated branes and Seiberg duality

A four-dimensional gauge theory can change when a boundary of its brane construction changes. In Chapter 5, D4-branes suspended between parallel fivebranes supported an adjoint scalar: their endpoints could move together in a common transverse plane. Rotating one fivebrane removes that common motion. The same operation reduces eight real supercharges to four and opens a route to four-dimensional $\mathcal{N} = 1$ gauge theories.

The new ingredient is more than a reduced spectrum. Moving the rotated system through a sequence of creation and reconnection processes produces a second color stack, together with mesons and a meson–quark coupling. We will follow three color D4-branes and five flavor D6-branes all the way through this motion. The final two color branes emerge from actual attachments. A separate field-theory calculation then compares the global anomalies of $SU(3)$ SQCD and its $SU(2)$ magnetic description.

Finally, the M-theory lift replaces a pure-gauge brane configuration by a single holomorphic surface. Fixing its two ends selects a finite set of interiors. We will derive that set, its winding and its relative membrane charge, and examine why the same geometry does not provide a controlled calculation of the ordinary-SYM nonprotected spectrum.

IX.6.1 The rotation and its four supercharges

Let the D4-branes fill $x^{0,1,2,3}$ and an interval $0 \leq x^6 \leq L$. Coordinates x^4, x^5, x^7, x^8, x^9 are transverse to their worldvolume. We use the following ordered axes; a prime

distinguishes the rotated fivebrane from the original one:

object	worldvolume axes	endpoint tangent directions
NS5	012345	45
D4	01236	interval in 6
D6	0123789	789
NS5′	012389	89

(IX.6.1)

The last column records directions in which a D4 endpoint can move. The D6-branes will supply flavors. Their presence is compatible with the supersymmetry left by the two fivebranes.

To count supercharges, a sign convention must accompany the axes. Use upper-index gamma matrices, ordered products with no extra factorial, and mostly-plus signature:

$$\{\Gamma^\mu, \Gamma^\nu\} = 2\eta^{\mu\nu}, \qquad \eta = \mathrm{diag}(-,+,\ldots,+), \qquad \chi = \Gamma^0\Gamma^1\cdots\Gamma^9. \tag{IX.6.2}$$

The two IIA supersymmetry parameters have opposite chirality. Our native orientation and parameter conventions are

$$\chi\epsilon_L = \epsilon_L, \qquad \chi\epsilon_R = -\epsilon_R, \qquad A\epsilon_{L,R} = A'\epsilon_{L,R} = \epsilon_{L,R}, \qquad \epsilon_L = D\epsilon_R = -B\epsilon_R, \tag{IX.6.3}$$

where the four brane matrices are

$$A = \Gamma^{012345}, \quad A' = \Gamma^{012389}, \quad D = \Gamma^{01236}, \quad B = \Gamma^{0123789}. \tag{IX.6.4}$$

This is a compatible convention for the stated IIA system. Its relative D6 sign is part of the spinor declaration; it does not define a negative D6 linking charge. All branes in the motion below carry the positive charges specified by the endpoint convention.

The Clifford algebra gives a short way to solve the constraints:

$$\begin{gathered} A^2 = (A')^2 = B^2 = \chi^2 = 1, \quad D^2 = -1, \quad B = DA\chi, \\ [A, A'] = [A, D] = [A', D] = 0. \end{gathered} \tag{IX.6.5}$$

Choose ϵ_R as the independent parameter. The D4 equation determines ϵ_L from it, so counting both independently would double the answer. Before rotation, the negative-chiral, NS-invariant space is the image of P_8. At the orthogonal endpoint it is the image of P_4:

$$P_8 = \frac{(1-\chi)(1+A)}{4}, \qquad P_4 = \frac{(1-\chi)(1+A)(1+A')}{8}. \tag{IX.6.6}$$

Each factor is a commuting involution projector. All nonidentity blades in the expansion have zero trace, including the mixed products. Therefore

$$P_8^2 = P_8, \quad P_4^2 = P_4, \qquad \mathrm{tr}\, P_8 = 8, \quad \mathrm{tr}\, P_4 = 4, \qquad BP_8 = -DP_8. \tag{IX.6.7}$$

The last equality shows why the declared D6 equation removes no further parameters. Reversing only that equation would instead require both $D\epsilon_R = B\epsilon_R$ and $D\epsilon_R = -B\epsilon_R$; since D is invertible, no nonzero parameter would survive.

These are real supercharge counts. For an explicit realization, let σ_i be Pauli matrices and form ten Euclidean matrices

$$g_{2j} = \sigma_3^{\otimes j} \otimes \sigma_1 \otimes 1^{\otimes(4-j)}, \qquad g_{2j+1} = \sigma_3^{\otimes j} \otimes \sigma_2 \otimes 1^{\otimes(4-j)}, \quad j = 0, \dots, 4. \tag{IX.6.8}$$

Set $\Gamma^0 = ig_0$ and $\Gamma^a = g_a$ for $a > 0$. If K denotes complex conjugation, the antilinear Majorana structure obeys

$$J = \Gamma^{013579} K, \qquad J^2 = 1, \qquad J\Gamma^\mu = \Gamma^\mu J, \qquad J P_a = P_a J. \tag{IX.6.9}$$

Thus each complex projector image has a real form of the same dimension. The counts in (IX.6.7) mean eight and four real parameters, or $\mathcal{N} = 2$ and $\mathcal{N} = 1$ in four dimensions.

There is also a continuous rotation preserving those four parameters. Rotate both transverse planes by the same oriented angle:

$$u_\theta = \cos\theta\, e_4 + \sin\theta\, e_8, \qquad v_\theta = \cos\theta\, e_5 + \sin\theta\, e_9, \qquad A_\theta = \Gamma^{0123}\Gamma(u_\theta)\Gamma(v_\theta). \tag{IX.6.10}$$

At $\theta = 0$ this is A, and at $\theta = \pi/2$ it is A'. With $K_1 = \Gamma^{48}$ and $K_2 = \Gamma^{59}$, direct multiplication yields

$$AA' = K_1 K_2, \qquad (K_1 + K_2) P_4 = 0, \qquad (A_\theta - 1) P_4 = 0. \tag{IX.6.11}$$

For example, angles $(\pi/4, \pi/4)$ in the two planes retain four real parameters, whereas $(\pi/4, 0)$ retain none. At zero angle the space enhances to eight. Rotating a single real direction is consequently not the supersymmetric interpolation depicted in Figure IX.6.1.

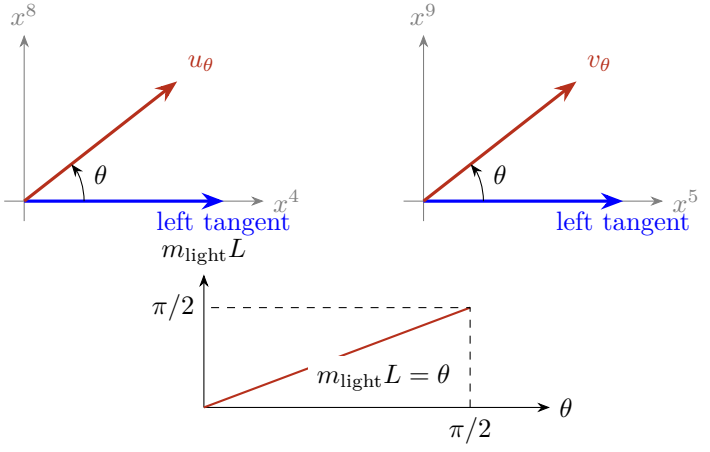


Figure IX.6.1: The balanced endpoint rotation, drawn in its two transverse planes. The left boundary has tangents e_4, e_5; the right boundary has u_θ, v_θ. The lower panel shows the light scalar branch of the rigid interval problem. At the orthogonal endpoint its gap is of interval Kaluza–Klein size.

IX.6.2 Which interval modes disappear?

The supersymmetry count determines the allowed multiplets, but it does not by itself determine which scalar motions exist. Treat the fivebranes as rigid boundaries, and let P_T be the orthogonal projector onto their allowed transverse tangent plane. A scalar displacement $X(x^6)$ obeys

$$(1 - P_T)X = 0, \qquad P_T \partial_6 X = 0 \quad \text{at each endpoint.} \tag{IX.6.12}$$

The first condition fixes the normal displacement; the second permits free tangential motion. These are a linear boundary model, not a microscopic solution of the fivebrane worldvolume dynamics.

The zero-frequency equation is particularly transparent:

$$-\partial_6^2 X = 0, \qquad X = a + x^6 b, \qquad a, b \in \mathbb{R}^5_{45789}. \tag{IX.6.13}$$

For parallel NS endpoints, the normal conditions at 0 and L remove both normal a and normal b, while the tangential derivative conditions remove tangential b. The two remaining constants are X^4, X^5. For an NS–NS$'$ interval, a constant allowed in 45 at one end must also lie in 89 at the other; no nonzero displacement does so. Equivalently,

$$\ker_{\text{scalar}}(\text{NS}, \text{NS}) = \mathbb{R}^2_{45}, \qquad \ker_{\text{scalar}}(\text{NS}, \text{NS}') = 0, \qquad \ker_{\text{scalar}}(\text{D6}, \text{NS}') = \mathbb{R}^2_{89}. \tag{IX.6.14}$$

The last equality will supply the magnetic meson motion. In contrast, a D6–NS interval has no common scalar tangent. The gauge field A_μ, $\mu = 0, 1, 2, 3$, has Neumann conditions at both ends and retains its constant mode. As in Chapter 5, the interval gauge prescription supplies no independent gauge-invariant A_6 Wilson-line scalar. The rotated color segment therefore retains an $\mathcal{N} = 1$ vector and loses the adjoint chiral of the $\mathcal{N} = 2$ vector multiplet.

At finite angle we can follow the mode that becomes light near the parallel configuration. For either $(4, 8)$ or $(5, 9)$, write its two components as X_u, X_v. At $x^6 = 0$, X_u is Neumann and X_v Dirichlet. For $k \neq 0$ the bulk equation gives

$$X_u = a\cos(kx^6), \qquad X_v = b\sin(kx^6), \qquad -\partial_6^2 X = k^2 X. \tag{IX.6.15}$$

At the other end, normal displacement and tangential derivative vanish along the rotated axes. Dividing the derivative equation by k gives

$$\begin{pmatrix} -\sin\theta\cos(kL) & \cos\theta\sin(kL) \\ -\cos\theta\sin(kL) & \sin\theta\cos(kL) \end{pmatrix} \begin{pmatrix} a \\ b \end{pmatrix} = 0. \tag{IX.6.16}$$

A nonzero amplitude requires

$$\det \mathcal{B} = \cos^2\theta \sin^2(kL) - \sin^2\theta \cos^2(kL) = \sin^2(kL) - \sin^2\theta = 0. \tag{IX.6.17}$$

Consequently the positive frequencies come from the two shifted towers

$$kL = j\pi \pm \theta, \qquad m_{\text{light}} = \frac{|\theta|}{L} \quad (|\theta| \leq \pi/2). \tag{IX.6.18}$$

For $\theta = \pi/10$, the light frequency is $\pi/(10L)$ and the next positive frequency is $9\pi/(10L)$. There is then a useful hierarchy inside this boundary model. At $\theta = \pi/2$ the two towers meet at a lowest gap $\pi/(2L)$: the would-be adjoint has reached the interval Kaluza–Klein scale. At exactly $k = 0$, division by k was inadmissible; the affine calculation (IX.6.13) supplies the zero modes instead.

A holomorphic adjoint mass in a four-dimensional action is a different quantity. If Φ has kinetic coefficient Z_Φ and superpotential mass m_Φ, its quadratic physical mass is

$$K_\Phi = Z_\Phi \operatorname{Tr} \Phi^\dagger \Phi, \qquad W_\Phi = \frac{m_\Phi}{2} \operatorname{Tr} \Phi^2, \qquad m_{\text{physical}} = \frac{|m_\Phi|}{Z_\Phi}. \tag{IX.6.19}$$

An interval frequency does not fix the phase of m_Φ or the wavefunction coefficient. Nor does it fix a holomorphic cutoff convention. For comparison, a regulated endpoint-superpotential model with its own zero-mode truncation gives a mass parameter

$$\mu(\theta) = \mu_0 \frac{\sin^2 \theta}{1 + \cos^2 \theta} = \frac{\mu_0}{2} \theta^2 + O(\theta^4). \tag{IX.6.20}$$

Here μ_0 supplies the mass scale; its regulator and field normalization are essential. The quadratic small-angle behavior of this parameter and the linear frequency in (IX.6.18) concern different specified models. Neither is a universal canonical mass–angle equality. In particular, $m = \tan \theta$ lacks a mass scale, and an infinite physical interval frequency at a right angle contradicts the eigenproblem above.

IX.6.3 Eliminating the adjoint

What interaction is left when an adjoint chiral is heavy? This question can be answered directly in four-dimensional fields, without fixing a mass from a brane angle. Let Q^i be a color fundamental and $\widetilde{Q}_j$ a color antifundamental, with $i, j = 1, \ldots, N_f$. Define the color matrix $X = \sum_i Q^i \widetilde{Q}_i$ and the flavor matrix $\mathcal{M}^i{}_j = \widetilde{Q}_j Q^i$. In a reference holomorphic normalization take

$$W = \frac{m_\Phi}{2} \operatorname{Tr}_c \Phi^2 + y \operatorname{Tr}_c(\Phi X), \qquad m_\Phi \neq 0. \tag{IX.6.21}$$

The engineering dimensions are

$$[\Phi] = [Q] = [\widetilde{Q}] = 1, \quad [X] = [\mathcal{M}] = 2, \quad [m_\Phi] = 1, \quad [y] = 0, \quad [W] = 3. \tag{IX.6.22}$$

For an unrestricted $U(N_c)$ adjoint, cyclic differentiation inside the trace gives the full matrix equation

$$\delta W = \operatorname{Tr}_c[(m_\Phi \Phi + yX)\delta\Phi], \qquad \Phi_* = -\frac{y}{m_\Phi} X. \tag{IX.6.23}$$

Substitution has two terms with different coefficients; keeping both is what fixes the sign and the factor of two:

$$W^U_{\text{eff}} = \frac{y^2}{2m_\Phi} \operatorname{Tr}_c X^2 - \frac{y^2}{m_\Phi} \operatorname{Tr}_c X^2 = -\frac{y^2}{2m_\Phi} \operatorname{Tr}_c X^2. \tag{IX.6.24}$$

The quartic coefficient has dimension -1. The trace here is the trace of the matrix square, not the square of a trace.

For an $SU(N_c)$ adjoint the allowed variations are traceless. Decompose X into its trace and traceless parts:

$$X_0 = X - \frac{\mathrm{Tr}_c\, X}{N_c} 1_{N_c}, \qquad \mathrm{Tr}_c\, X_0 = 0, \qquad \mathrm{Tr}_c\, X_0^2 = \mathrm{Tr}_c\, X^2 - \frac{(\mathrm{Tr}_c\, X)^2}{N_c}. \quad \text{(IX.6.25)}$$

Only X_0 couples to the traceless variation, so the solution and effective superpotential become

$$\Phi_*^{SU} = -\frac{y}{m_\Phi} X_0, \qquad W_{\mathrm{eff}}^{SU} = -\frac{y^2}{2m_\Phi}\left[\mathrm{Tr}_c\, X^2 - \frac{(\mathrm{Tr}_c\, X)^2}{N_c}\right]. \quad \text{(IX.6.26)}$$

This difference is visible in a small matrix example with nonzero trace. Choose $N_c = 2$ and

$$X = \begin{pmatrix} 2 & 3 \\ 5 & 7 \end{pmatrix}, \qquad \mathrm{Tr}\, X = 9, \quad \mathrm{Tr}\, X^2 = 83, \quad \mathrm{Tr}\, X_0^2 = \frac{85}{2}. \quad \text{(IX.6.27)}$$

It follows that

$$W_{\mathrm{eff}}^{U} = -\frac{83y^2}{2m_\Phi}, \qquad W_{\mathrm{eff}}^{SU} = -\frac{85y^2}{4m_\Phi}, \qquad W_{\mathrm{eff}}^{U} - W_{\mathrm{eff}}^{SU} = -\frac{81y^2}{4m_\Phi}. \quad \text{(IX.6.28)}$$

A traceless example would have hidden precisely the term that distinguishes the two theories. If the original quadratic term were written as $\mu\,\mathrm{Tr}\,\Phi^2$, our mass would be $m_\Phi = 2\mu$. Choosing $y = \sqrt{2}$ gives coefficient $-1/m_\Phi$ in (IX.6.24); this is a field normalization choice.

The elimination is a tree-level Wilsonian F-term calculation below the adjoint mass. It does not determine the induced Kähler potential. Its flavor consequences also matter. The contraction that identifies i on Q^i with i on $\widetilde{Q}_i$ gives

$$\mathrm{Tr}_c\, X^2 = \mathrm{Tr}_f\, \mathcal{M}^2, \qquad \mathcal{M} \longmapsto U_L \mathcal{M} U_R^{-1}. \quad \text{(IX.6.29)}$$

The trace square is invariant under the diagonal identification $U_L = U_R$, but not under independent left and right flavor rotations. Thus finite adjoint mass leaves a quartic deformation with reduced chiral flavor symmetry. The full-flavor anomaly calculation below concerns undeformed SQCD, with this quartic absent.

At the undeformed interacting $SU(3)$, $N_f = 5$ SQCD fixed point, the chiral quarks have $R = 2/5$; their quartic chiral primary obeys $\Delta = 3R/2$, unlike its canonical UV dimension of four:

$$R(\mathcal{M}) = \frac{4}{5}, \qquad R(\mathcal{M}^2) = \frac{8}{5}, \qquad \Delta(\mathcal{M}^2) = \frac{3}{2} R(\mathcal{M}^2) = \frac{12}{5} < 3. \quad \text{(IX.6.30)}$$

It is a relevant superpotential deformation there. Taking $m_\Phi \to \infty$ at fixed y removes the displayed quartic, but keeping the desired $\mathcal{N} = 1$ strong scale fixed is an additional field-theory limit, not an automatic consequence of drawing a right angle.

IX.6.4 A complete electric-to-magnetic brane move

We now keep the endpoint rotation orthogonal and follow a concrete brane motion. Write N for NS5, P for NS5′, and D_i for the ith D6-brane. The label D_4 below means the fourth D6; the connecting segments are all D4-branes. Begin with three color segments from N to P and five D6s between them. In units used only to draw their ordering, take

$$x^6(N) = 0, \quad x^6(D_i) = i \ (i = 1, \dots, 5), \quad x^6(P) = 7, \qquad x^7(N) = x^7(P) = 0. \tag{IX.6.31}$$

The flavor masses vanish: their displacements in the complex mass plane are zero. Separating the D6s along x^6 resolves successive crossing events and does not introduce a holomorphic quark mass.

To follow conserved charges we must count actual endpoints. For either species of NS fivebrane, define its linking number by a half-count of D6s plus an oriented count of attached D4s. For a D6, exchange the two species in the half-count:

$$\ell_{NS} = \frac{n_{D6,R} - n_{D6,L}}{2} + n_{4,L} - n_{4,R}, \qquad \ell_{D6} = \frac{n_{NS,R} - n_{NS,L}}{2} + n_{4,L} - n_{4,R}. \tag{IX.6.32}$$

Here L, R mean left and right in x^6, and the NS count includes both N and P. A D4 passing through a D6 without ending on it contributes no endpoint. These definitions are independent of the gamma signs used in the supercharge calculation.

Initially N has five D6s to its right and three right endpoints; P has five D6s to its left and three left endpoints. Each D6 sees one NS on either side and has no attached endpoint. The individual values are

$$\ell_N = \frac{5}{2} - 3 = -\frac{1}{2}, \qquad \ell_P = -\frac{5}{2} + 3 = \frac{1}{2}, \qquad \ell_{D_i} = 0. \tag{IX.6.33}$$

Conserving the sum of these numbers would be too weak. Each brane must retain its own value throughout the motion.

First move N to the right across D_1, then D_2, and so on. Suppose k D4s are created at a single crossing. They extend left from N and right from the crossed D6. The changes in the two linking numbers are

$$\Delta\ell_N = -1 + k, \qquad \Delta\ell_{D_i} = 1 - k. \tag{IX.6.34}$$

Both vanish only for $k = 1$. The physical crossing process supplies such a segment; conservation determines its occupancy in this move. After j crossings, place N between D_j and D_{j+1}, or between D_5 and P for $j = 5$. The direct expression

$$\ell_N = \frac{5 - 2j}{2} + j - 3 = -\frac{1}{2} \tag{IX.6.35}$$

shows that all five intermediate positions retain the electric value. For the flavor branes, the same individual calculation reads

$$\ell_{D_i}^{(j)} = \begin{cases} 1 - 1 = 0, & i \le j, \\ (1-1)/2 = 0, & i > j. \end{cases} \tag{IX.6.36}$$

In the first case both NS branes are to the right and the created segment has a right endpoint. In the second case the NS branes still straddle the D6. After the fifth crossing there are three N–P edges and five D_i–N edges.

Next choose an asymmetric reconnection, so that the attachments remain distinguishable. Join the original three color edges to the created edges from D_2, D_4, D_5. At N, each reconnection removes one left and one right endpoint. The replacement edges run directly from those D6s to P:

$$(D_i, N) + (N, P) \longrightarrow (D_i, P), \qquad i = 2, 4, 5, \qquad \Delta\ell_N = -1 + 1 = 0. \tag{IX.6.37}$$

The remaining D_1–N and D_3–N edges terminate on D6s, which extend in x^7. There is now no color edge connecting N to P. Consequently N can be displaced to $x^7 = 2$ while P stays at zero. In the low-energy brane description this is the Higgs/FI detour. It uses the massless-flavor branch and the permitted local occupancy. It is not a motion available without qualification for arbitrary massive flavors.

With the fivebranes separated in x^7, move N to $x^6 = 8$, to the right of P. They do not collide. Their mutual passage changes no D6 half-count; the two D_i–N attachments simply follow N. Finally return N to $x^7 = 0$. Split each of the two remaining segments where it meets P:

$$(D_i, N) \longrightarrow (D_i, P) + (P, N), \qquad i = 1, 3, \qquad \Delta\ell_P = 1 - 1 = 0. \tag{IX.6.38}$$

The result has five flavor segments ending on P and two color segments between P and N. Figure IX.6.2 displays the geometry of these operations; Table IX.6.1 retains every crossing.

State	N–P	D_i–N indices	D_i–P indices	Δx^7
Electric	3	$\varnothing$	$\varnothing$	0
Cross D_1	3	$\{1\}$	$\varnothing$	0
Cross D_2	3	$\{1, 2\}$	$\varnothing$	0
Cross D_3	3	$\{1, 2, 3\}$	$\varnothing$	0
Cross D_4	3	$\{1, 2, 3, 4\}$	$\varnothing$	0
Cross D_5	3	$\{1, 2, 3, 4, 5\}$	$\varnothing$	0
Reconnect and detach	0	$\{1, 3\}$	$\{2, 4, 5\}$	2
Pass P in x^6	0	$\{1, 3\}$	$\{2, 4, 5\}$	2
Return and split	2	$\varnothing$	$\{1, 2, 3, 4, 5\}$	0

Table IX.6.1: The nine endpoint states for three electric colors and five flavors. Every row has individual linking vector $(\ell_N, \ell_P, \ell_{D_1}, \ldots, \ell_{D_5}) = (-1/2, 1/2, 0, \ldots, 0)$. The index sets specify individual D6 attachments, each of multiplicity one. Reconnection and detachment are grouped into one row, as are the final two splits. $\Delta x^7 = x^7(N) - x^7(P)$ is a diagram coordinate.

It is useful to recompute the final numbers directly. At N all five D6s and the two color endpoints lie on its left. At P there are five left flavor endpoints and two right color endpoints:

$$\ell_N = -\frac{5}{2} + 2 = -\frac{1}{2}, \qquad \ell_P = -\frac{5}{2} + 5 - 2 = \frac{1}{2}, \qquad \ell_{D_i} = \frac{2}{2} - 1 = 0. \tag{IX.6.39}$$

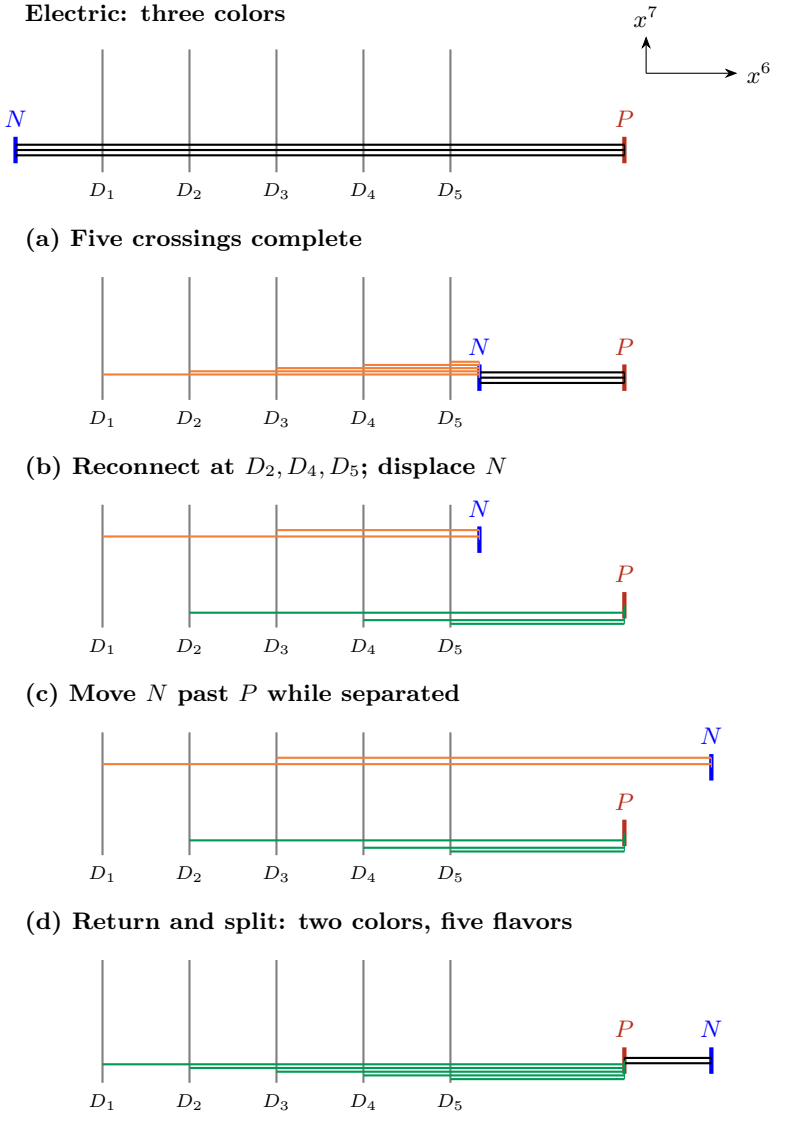


Figure IX.6.2: Five stages of the actual endpoint motion. Orange marks created D_i–N attachments, green marks D_i–P flavor attachments, and black marks color segments. Each drawn line is an attachment; small transverse offsets separate coincident D4s for visibility. D6s extend vertically in x^7, so the D_1–N and D_3–N endpoints can follow the displaced N. The three reconnections use D_2, D_4, D_5. Returning from the bypass creates the two displayed P–N segments by splitting, and leaves all five D_i–P flavor attachments. The diagram specifies incidence and ordering, not a metric solution for brane shapes.

The magnetic rank is the number of P–N edges in this final graph:

$$N_{\text{magnetic}} = \#(P\text{–}N) = 2. \tag{IX.6.40}$$

For general ranks, imposing the same final pattern of flavor attachments and equating ℓ_N gives the familiar relation

$$\frac{N_f}{2} - N_c = -\frac{N_f}{2} + \widetilde{N}_c, \qquad \widetilde{N}_c = N_f - N_c. \tag{IX.6.41}$$

This last equation summarizes the result; it did not supply the nine-state construction. In fact, omitting the final splits can conserve all linking numbers while leaving no P–N stack at all. Before those splits, but after returning to $x^7 = 0$, the alternative attachment graph has

$$\#(P\text{–}N) = 0, \quad \#(D\text{–}P) = 3, \quad \#(D\text{–}N) = 2, \qquad \ell_P = -\frac{5}{2} + 3 = \frac{1}{2}. \tag{IX.6.42}$$

Its N and D6 charges also retain their original values. Conservation must therefore be used together with the physical reconnection and final attachment prescription.

IX.6.5 Magnetic matter and the charged center

An edge count becomes a gauge-theory description only after identifying its light fields. D4–D6 strings share 0123 and have four mixed Neumann–Dirichlet directions, 6789. Their supersymmetric open-string spectrum supplies both orientations of a vectorlike flavor. Thus the initial three-color stack has

$$Q^i \in \mathbf{3}, \quad \widetilde{Q}_i \in \overline{\mathbf{3}}, \qquad i = 1, \ldots, 5, \qquad 5 \cdot 3 + 5 \cdot 3 = 30 \tag{IX.6.43}$$

chiral components. Five flavors mean five pairs, not five isolated fundamental chirals. The latter would have a different gauge anomaly.

At the final stack there are likewise five pairs $q_i, \widetilde{q}^j$ of two-color quarks. There are also five D6–NS$'$ segments. Equation (IX.6.14) permits one complex 89 motion on each such segment. At coincident massless flavor data, the flavor Chan–Paton space supplies the full matrix of meson species:

$$M = \sum_{i,j=1}^{5} M^i{}_j E_{ij}, \qquad E_{ij}E_{kl} = \delta_{jk}E_{il}, \qquad \dim_{\mathbb{C}} \operatorname{End}(\mathbb{C}^5) = 25. \tag{IX.6.44}$$

For example $E_{12}E_{23} = E_{13}$ whereas $E_{12}E_{34} = 0$; the five diagonal motions alone are not the whole matrix. The separated D6 positions used to display the move are a regulator of its ordering. The 25-field low-energy interpretation refers to coincident massless flavor data, not a claim that every off-diagonal string is visibly massless in every separated drawing.

Use matrices q of size 2×5, $\widetilde{q}$ of size 5×2, and M of size 5×5. The magnetic superpotential is

$$W_m = h \operatorname{Tr}_f(M\widetilde{q}q) = h \sum_{i,j=1}^{5} \sum_{a=1}^{2} M^i{}_j \widetilde{q}^j{}_a q^a{}_i. \tag{IX.6.45}$$

This is the holomorphic meson–quark structure of the brane construction. It does not fix a canonically normalized disk amplitude. Its index contractions can be read from Figure IX.6.3. Under color G and independent flavor transformations in the SQCD comparison,

$$q \mapsto G q U_L^{-1}, \qquad \widetilde{q} \mapsto U_R \widetilde{q} G^{-1}, \qquad M \mapsto U_L M U_R^{-1}. \tag{IX.6.46}$$

Then $M\widetilde{q}q \mapsto U_L(M\widetilde{q}q)U_L^{-1}$, and its trace is invariant. This also determines the opposite flavor representations of electric and magnetic quarks used below. The independent left and right flavor groups are the field-theory comparison symmetry; the visible D6 rotation of the brane picture alone exhibits the diagonal action.

For dimension-one magnetic fields, h is dimensionless. The electric meson operator has engineering dimension two, so the operator map must contain a scale:

$$[M] = [q] = [\widetilde{q}] = 1, \quad [h] = 0, \qquad \mathcal{M} = \mu_{\text{match}} M, \quad [\mu_{\text{match}}] = 1. \tag{IX.6.47}$$

As a worked deformation, add an electric mass for the fifth flavor. Its magnetic image and the corresponding meson F equation are

$$\delta W_m = m_5 \mu_{\text{match}} M^5{}_5, \qquad h \sum_{a=1}^{2} \widetilde{q}^5{}_a q^a{}_5 + m_5 \mu_{\text{match}} = 0. \tag{IX.6.48}$$

The linear meson term therefore requires a magnetic quark expectation value when $m_5 \neq 0$. This illustrates the relation between an electric mass and magnetic Higgsing without choosing an absolute value for μ_{match} or h.

There is an essential distinction between this brane gauge system and the standard SQCD comparison. Its initial Chan–Paton algebra is $\mathfrak{u}(3)$, and its final one is $\mathfrak{u}(2)$. The identity matrix acts nontrivially on the quarks:

$$Q \mapsto e^{i\alpha} Q, \qquad \widetilde{Q} \mapsto e^{-i\alpha} \widetilde{Q}, \qquad D_\mu Q \supset -i A_\mu^{\text{center}} Q. \tag{IX.6.49}$$

This central $U(1)$ couples to matter and is not a free Maxwell factor that can simply be discarded. In particular, the x^7 FI bypass used above has no counterpart as an FI term of a pure $SU(N)$ gauge group.

The next section makes a precise, separate comparison: undeformed $SU(3)$ SQCD with five flavors, global background baryon number, and its $SU(2)$ magnetic candidate with 25 singlets. The color ranks, matter pattern and cubic match the corresponding brane outputs. Equating full U theories, weakly gauging the baryon symmetry, or choosing their global quotients requires additional data. The finite-chain M5 trace mode in Chapter 5 presents yet another issue: fixed noncompact asymptotics can exclude a nonnormalizable collective mode. That boundary condition does not erase the charged central photon of the flavored configuration.

IX.6.6 Anomalies of the undeformed SQCD comparison

Anomaly matching is a sensitive way to compare proposed infrared descriptions. It is especially useful here because the ranks are unequal: mesons contribute nonzero fermion

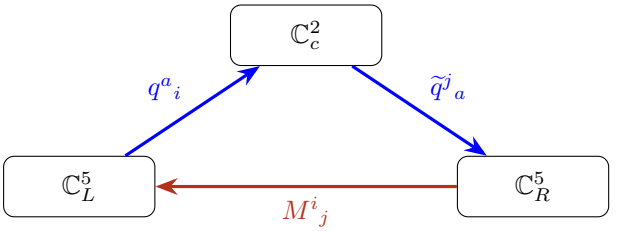


Figure IX.6.3: The magnetic index contraction. Arrows denote matrix maps between a two-dimensional color space and two five-dimensional flavor spaces; the closed composition has trace $\mathrm{Tr}(M\widetilde{q}q)$. The brane construction supplies five magnetic flavor pairs and 25 mesons. Its dynamical central $U(1)$ is kept distinct from the background baryon symmetry of the separate SU comparison.

R charge, and their omission changes several coefficients. We use left-handed fermions throughout. Denote the flavor groups by $SU(5)_L$ and $SU(5)_R$, reserve R charge for $U(1)_R$, and normalize the flavor indices as

$$T(\mathbf{5}) = T(\overline{\mathbf{5}}) = \frac{1}{2}, \qquad A(\mathbf{5}) = 1, \qquad A(\overline{\mathbf{5}}) = -1. \tag{IX.6.50}$$

Quadratic indices do not distinguish conjugate representations; cubic indices do. The complete fermion content is shown in Table IX.6.2. For a chiral multiplet its fermion charge is $r = R_{\text{scalar}} - 1$, while a gaugino has $r = 1$.

Fermion	Color dimension	$SU(5)_L$	$SU(5)_R$	B	r
Q	3	$\mathbf{5}$	$\mathbf{1}$	1	$-3/5$
$\widetilde{Q}$	3	$\mathbf{1}$	$\overline{\mathbf{5}}$	-1	$-3/5$
λ_e	8	$\mathbf{1}$	$\mathbf{1}$	0	1
q	2	$\overline{\mathbf{5}}$	$\mathbf{1}$	$3/2$	$-2/5$
$\widetilde{q}$	2	$\mathbf{1}$	$\mathbf{5}$	$-3/2$	$-2/5$
M	1	$\mathbf{5}$	$\overline{\mathbf{5}}$	0	$-1/5$
λ_m	3	$\mathbf{1}$	$\mathbf{1}$	0	1

Table IX.6.2: Representation and charge data for the undeformed $SU(3)$ and $SU(2)$ theories. The meson has $5 \cdot 5 = 25$ components. Color dimensions multiply the flavor indices; the gaugino rows already include their adjoint multiplicities. Baryon number is a global symmetry in this table.

The nonanomalous color–color–R condition fixes the quark fermion charges. The two orientations each contribute $N_f T(\square) r$, giving

$$3 + 5r_Q = 0, \qquad 2 + 5r_q = 0, \qquad r_Q = -\frac{3}{5}, \quad r_q = -\frac{2}{5}. \tag{IX.6.51}$$

The electric composite then fixes $R(M) = 2R(Q) = 4/5$, and the cubic has

$$R(M) + R(q) + R(\widetilde{q}) = \frac{4}{5} + \frac{3}{5} + \frac{3}{5} = 2. \tag{IX.6.52}$$

The baryon normalization follows independently. Set $B(Q) = 1$, so an $SU(3)$ baryon has charge three. Its magnetic partner uses two quarks:

$$B(Q^3) = 3 = B(q^2) = 2B(q), \qquad B(q) = \frac{3}{2}, \qquad \binom{5}{3} = \binom{5}{2} = 10. \tag{IX.6.53}$$

Antisymmetric flavor tensors of ranks three and two are paired by the five-index epsilon tensor, with the conjugate magnetic flavor representation supplying the correct transformation. The rational magnetic baryon charge is thus required by the operator map; it is not a unit central charge copied from a brane endpoint. The ten magnetic Weyl doublets also give an even number of $SU(2)$ doublets, so there is no mod-two gauge anomaly for this matter content.

To calculate a flavor cubic anomaly, multiply its cubic index by the spectator multiplicities. The left and right coefficients are

$$\mathcal{A}^e_{L^3} = 3, \quad \mathcal{A}^m_{L^3} = -2 + 5 = 3, \qquad \mathcal{A}^e_{R_f^3} = -3, \quad \mathcal{A}^m_{R_f^3} = 2 - 5 = -3. \tag{IX.6.54}$$

Here R_f labels the right flavor group rather than the R symmetry. The meson's spectator flavor index contributes the five in the magnetic sums. Assigning q the electric flavor representation would reverse the -2 and spoil the equality.

Mixed flavor–baryon coefficients use the quadratic index:

$$\mathcal{A}^e_{L^2B} = 3\frac{1}{2} = \frac{3}{2}, \qquad \mathcal{A}^m_{L^2B} = 2\frac{1}{2}\frac{3}{2} = \frac{3}{2}, \qquad \mathcal{A}^e_{R_f^2B} = \mathcal{A}^m_{R_f^2B} = -\frac{3}{2}. \tag{IX.6.55}$$

For flavor–R coefficients the meson is indispensable:

$$\mathcal{A}^e_{L^2R} = 3\frac{1}{2}\left(-\frac{3}{5}\right) = -\frac{9}{10}, \qquad \mathcal{A}^m_{L^2R} = 2\frac{1}{2}\left(-\frac{2}{5}\right) + 5\frac{1}{2}\left(-\frac{1}{5}\right) = -\frac{9}{10}. \tag{IX.6.56}$$

The right flavor coefficient is the same, since conjugation changes no quadratic index. These computations already distinguish rank, flavor conjugation, baryon normalization and the singlet matrix.

The gravitational–R anomaly counts every fermion component, including the gaugi-nos:

$$\operatorname{Tr} R_e = 8 + 30\left(-\frac{3}{5}\right) = -10, \qquad \operatorname{Tr} R_m = 3 + 20\left(-\frac{2}{5}\right) + 25\left(-\frac{1}{5}\right) = -10. \tag{IX.6.57}$$

Likewise the cubic R anomaly is

$$\operatorname{Tr} R_e^3 = 8 - 30\left(\frac{3}{5}\right)^3 = \frac{38}{25}, \qquad \operatorname{Tr} R_m^3 = 3 - 20\left(\frac{2}{5}\right)^3 - 25\left(\frac{1}{5}\right)^3 = \frac{38}{25}. \tag{IX.6.58}$$

Finally, the baryon-squared–R coefficient is

$$\operatorname{Tr} B^2 R_e = 30\left(-\frac{3}{5}\right) = -18, \qquad \operatorname{Tr} B^2 R_m = 20\left(\frac{3}{2}\right)^2\left(-\frac{2}{5}\right) = -18. \tag{IX.6.59}$$

The vectorlike pairs cancel the odd baryon traces:

$$\operatorname{Tr} B = \operatorname{Tr} B^3 = \operatorname{Tr} B R^2 = 0 \qquad \text{in both descriptions.} \tag{IX.6.60}$$

Together these equations give twelve tensor components: nine nonzero and three zero. Conjugation relates the three left/right pairs, leaving six nonredundant nonzero structures. Anomalies with a single nonabelian flavor generator vanish by its tracelessness. This is a comparison of local continuous-symmetry coefficients, not a classification of flavor-group quotients, line operators or all discrete background anomalies.

The agreement is necessary for the proposed infrared equivalence, but it is not a derivation of that equivalence. In the brane argument, physical creation and local occupancy are one input. Continuity of the intended infrared theory along a path that traverses strong coupling is a second input. Neither the linking numbers nor the anomaly sums eliminate that second assumption. This is also why the undeformed comparison must not be silently applied to the adjoint-induced quartic, whose flavor symmetry and infrared behavior differ.

IX.6.7 The pure-gauge lift and its two fixed ends

To see what survives beyond a picture of separate branes, return to the pure-gauge system with n suspended D4s and no flavor D6s. The M-theory lift joins them and their fivebrane endpoints into a connected holomorphic M5 surface. Its worldvolume is four-dimensional spacetime times a complex curve Σ. The question is now a boundary-value problem: which holomorphic interiors have the same prescribed behavior at both infinities?

First put the geometry in a single frame. The common pure-MQCD source frame uses $\mathrm{NS}' = 012378$ and $w_W = X^7_W + iX^8_W$, whereas our rotated plane is 89. A proper cyclic permutation gives

$$\begin{pmatrix} X^7_B \\ X^8_B \\ X^9_B \end{pmatrix} = \begin{pmatrix} 0 & 0 & 1 \\ 1 & 0 & 0 \\ 0 & 1 & 0 \end{pmatrix} \begin{pmatrix} X^7_W \\ X^8_W \\ X^9_W \end{pmatrix}, \qquad \det P = +1. \tag{IX.6.61}$$

It sends the oriented 78 plane to 89 and preserves the oriented D6 789 volume element if that brane is included in a frame comparison. The spectator X^9_W becomes X^7_B. No reflection or complex conjugation is required:

$$v = X^4 + iX^5 = v_W, \qquad w = X^8_B + iX^9_B = w_W. \tag{IX.6.62}$$

Here v and w are geometric lengths. They are not the normalized mass coordinate used for a Seiberg–Witten curve in Chapter 5.

Let R be the physical M-theory circle radius in the same length frame, and distinguish its angle ϑ_{10} from its physical coordinate:

$$\vartheta_{10} \sim \vartheta_{10} + 2\pi, \qquad X^{10} = R\vartheta_{10} \sim X^{10} + 2\pi R, \qquad s = \frac{X^6 + iX^{10}}{R}, \quad t = e^{-s}. \tag{IX.6.63}$$

Thus t is dimensionless and nonzero at every interior point. Its modulus measures X^6. Since $X^{10} = R\vartheta_{10}$ with $R > 0$, this rescaling preserves orientation. An extra radius in the phase spoils normalization and periodicity; $e^{-i\vartheta_{10}}$ reverses winding.

We use the two-ended holomorphic class appropriate to the pure rotated construction. Compactify its two ends to points p_∞, p_0. The coordinate v has one simple pole at p_∞, no other poles, and vanishes at the opposite end. A meromorphic function with a single simple pole has degree one as a map to the Riemann sphere. A degree-one map is an isomorphism, so

$$\overline{\Sigma} \simeq \mathbb{P}^1, \qquad g(\overline{\Sigma}) = 0, \qquad z = v, \quad p_0 = \{z = 0\}, \quad p_\infty = \{z = \infty\}. \tag{IX.6.64}$$

The second transverse coordinate has a single simple pole at p_0 and vanishes at p_∞. A rational function with exactly these properties is fixed up to a nonzero complex coefficient:

$$v = z, \qquad w = \frac{\zeta}{z}, \qquad \Sigma = \mathbb{P}^1 \setminus \{0, \infty\} \simeq \mathbb{C}^*. \tag{IX.6.65}$$

The complex parameter $\zeta = vw$ measures an interior holomorphic invariant. It has dimension length squared. It is not the real FI level that displaced the earlier fivebrane, nor a triplet of moment-map levels.

The n suspended D4s determine the degree of the circle projection. In the chosen ordering t has a zero of order n at 0, a pole of order n at infinity, and no interior zeros or poles. Thus

$$\mathrm{div}(v) = [0] - [\infty], \quad \mathrm{div}(w) = [\infty] - [0], \quad \mathrm{div}(t) = n[0] - n[\infty]. \tag{IX.6.66}$$

Two rational functions with the same divisor differ by a nonzero constant. It follows that

$$t = Az^n, \qquad vw = \zeta, \qquad tw^n = A\zeta^n, \qquad A \neq 0. \tag{IX.6.67}$$

The familiar choice $A = 1$ uses a coordinate and scale convention. With length-valued v, w retained, $[A] = \mathrm{length}^{-n}$; it is preferable to keep A explicit until the asymptotic problem is fixed.

At the first end prescribe the coefficient of v^n in t; at the second prescribe the coefficient of w^{-n}. These are two conditions on one surface:

$$\lim_{v\to\infty} \frac{t}{v^n} = A, \quad w \to 0; \qquad \lim_{w\to\infty} tw^n = B, \quad v \to 0, \qquad A, B \neq 0. \tag{IX.6.68}$$

Here $[B] = \mathrm{length}^n$. Substitution of the functions already determined by their divisors into the second condition gives

$$A\zeta^n = B. \tag{IX.6.69}$$

The vacuum polynomial has therefore been derived from the boundary conditions. Fixing only A would leave ζ free and would define a different problem. Rescaling t

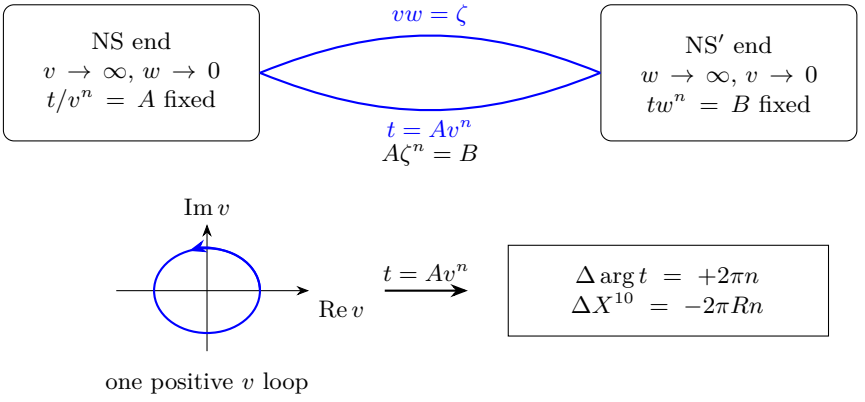


Figure IX.6.4: The two ends of the holomorphic M5 curve and the two asymptotic coefficients held fixed. The drawing represents the punctured curve and its maps, not an isometric surface in real three-space. A positive loop of v produces positive winding of $\arg t$ and negative winding of the physical circle coordinate. Numerical labels use the length unit ℓ_0 of the worked example. Its two interior products vw have the same end data.

changes both A and B; it shifts the chosen X^6 and circle origins and is not another vacuum at fixed data.

Why are there n distinct interiors? The polynomial $p(\zeta) = A\zeta^n - B$ has degree n and derivative

$$p'(\zeta) = nA\zeta^{n-1}, \qquad \gcd(p, p') = 1 \quad \text{when } AB \neq 0. \tag{IX.6.70}$$

The derivative can vanish at a root only if $\zeta = 0$, which would require $B = 0$. Hence every root is simple. Multiplication by $e^{2\pi i/n}$ preserves both asymptotic coefficients and permutes the interiors:

$$\zeta_k = \left(\frac{B}{A}\right)^{1/n} e^{2\pi ik/n}, \qquad k = 0, \ldots, n-1. \tag{IX.6.71}$$

The choice of one initial nth root only labels this set. The discrete chiral action relates different vacua; it does not identify their interior products as a gauge redundancy.

For a small-rank example, choose a length unit ℓ_0 and set $A = 2\ell_0^{-n}$ and $B = 2^{n+1}\ell_0^n$. Equation (IX.6.69) gives

n	ζ/ℓ_0^2
1	2
2	$2,\ -2$
3	$2,\ -1+i\sqrt{3},\ -1-i\sqrt{3}$
4	$2,\ -2,\ 2i,\ -2i$

(IX.6.72)

For $n = 2, 3, 4$ these are the pure-MQCD holomorphic vacua in the specified class. The $n = 1$ line is only algebra: $SU(1)$ has no interacting pure-SYM sector. Sending B to zero coalesces all roots at $\zeta = 0$ and destroys the assumed smooth two-ended embedding. One cannot keep the same vacuum interpretation at that degenerate boundary.

IX.6.8 Winding and relative membrane charge

The curve contains more information than its number of interiors. It also tells us how a loop on the fivebrane winds the ambient M-theory circle. On the positively oriented loop $z = re^{i\varphi}$, $0 \le \varphi \le 2\pi$, logarithmic differentiation gives

$$\frac{dt}{t} = n\frac{dz}{z}, \qquad \frac{1}{2\pi i}\oint \frac{dt}{t} = n. \tag{IX.6.73}$$

This integral measures the phase of t, not directly the positively oriented physical circle. From (IX.6.63),

$$\arg t = -\vartheta_{10} \pmod{2\pi}, \qquad \Delta\vartheta_{10} = -2\pi n, \qquad \Delta X^{10} = -2\pi R n. \tag{IX.6.74}$$

For $n = 3$, one positive turn in the v plane winds the physical circle three times in the negative direction, with displacement $-6\pi R$. Reversing t to t^{-1} would reverse that sign but would also exchange its prescribed zero and pole; it is not a harmless change at fixed ends.

A different contour detects the interior rather than the circle degree:

$$w\,dv = \zeta\frac{dz}{z}, \qquad \frac{1}{2\pi i}\oint w\,dv = \zeta. \tag{IX.6.75}$$

For the $n = 2$ example the two values are $+2\ell_0^2$ and $-2\ell_0^2$ although their logarithmic winding integrals are identical. The residue is a holomorphic invariant of the embedding; by itself it does not supply a normalized four-dimensional gluino condensate or superpotential.

Both ends and the full divisor matter. For instance, multiplying t by $(z - a)/\ell_0$, with $a \neq 0$ a fixed length, leaves its winding on a sufficiently small circle about zero unchanged. But it introduces an interior zero and changes the order at infinity:

$$\operatorname{div}\left(t\frac{z-a}{\ell_0}\right) = n[0] + [a] - (n+1)[\infty]. \tag{IX.6.76}$$

It no longer defines the same map into the ambient $\mathbb{C}^*$ coordinate. A small contour at one end alone cannot establish the full boundary problem.

The ambient transverse space has the topology $Y \simeq \mathbb{R}^5 \times S^1$, while $\Sigma \simeq \mathbb{C}^*$ has one noncontractible loop. A membrane string can be represented by a path in Y whose boundary lies on Σ. Paths differing by a deformation through the fivebrane belong to the same relative class. The relevant part of the long exact sequence is

$$\begin{aligned} H_1(\Sigma;\mathbb{Z}) \xrightarrow{\iota_*} H_1(Y;\mathbb{Z}) &\longrightarrow H_1(Y,\Sigma;\mathbb{Z}) \\ &\longrightarrow H_0(\Sigma;\mathbb{Z}) \longrightarrow H_0(Y;\mathbb{Z}). \end{aligned} \tag{IX.6.77}$$

Both spaces are connected, so the final map is an isomorphism. The two first homology groups are each $\mathbb{Z}$, and (IX.6.74) identifies the inclusion map:

$$\iota_* : \mathbb{Z} \longrightarrow \mathbb{Z}, \qquad m \longmapsto -nm. \tag{IX.6.78}$$

Exactness then yields

$$H_1(Y, \Sigma; \mathbb{Z}) = \mathbb{Z}/n\mathbb{Z} = \mathbb{Z}_n. \tag{IX.6.79}$$

The orientation sign does not change the quotient. For $n = 3$, classes $0, 1, 2$ add modulo three; three unit relative paths can be absorbed into a loop on the fivebrane. For $n = 2$ and 4 the groups are $\mathbb{Z}_2$ and $\mathbb{Z}_4$, while for the algebraic $n = 1$ case the quotient is trivial. These statements determine relative topological charge. They do not determine the tension of its lightest representative, its excitation spectrum, or the dynamics of confinement in ordinary SYM.

IX.6.9 A rational degeneration of the parent curve

The genus-zero surface also has a useful holomorphic connection to the $\mathcal{N} = 2$ construction of Chapter 5. Use a dimensionless normalization of the parent curve in this section, with its nonzero scale absorbed into the coordinates. This is a fresh local normalization, not the length assignment of (IX.6.62). Write

$$t^2 + P_n(v)t + 1 = 0. \tag{IX.6.80}$$

Generically this is a two-sheeted curve over v. At special coefficients it admits a rational parametrization. To find them rather than assume them, introduce $\lambda \in \mathbb{C}^*$ and a nonzero constant c:

$$v = \lambda + \frac{c}{\lambda}, \qquad t = -\lambda^n. \tag{IX.6.81}$$

The involution $\lambda \mapsto c/\lambda$ leaves v fixed. Symmetric combinations of its two preimages should therefore be polynomials in v. Define

$$S_n = \lambda^n + c^n\lambda^{-n}, \qquad S_0 = 2, \quad S_1 = v. \tag{IX.6.82}$$

Multiplication by $v = \lambda + c/\lambda$ gives the recurrence

$$vS_{n-1} = S_n + cS_{n-2}, \qquad P_0 = 2, \quad P_1 = v, \quad P_n = vP_{n-1} - cP_{n-2}. \tag{IX.6.83}$$

Thus $P_n(v) = S_n$ on the parametrization. The first nontrivial polynomials are obtained without solving for λ:

$$P_2 = v^2 - 2c, \qquad P_3 = v^3 - 3cv, \qquad P_4 = v^4 - 4cv^2 + 2c^2. \tag{IX.6.84}$$

Substitution into the parent equation now gives a constant residual:

$$t^2 + P_n(v)t + 1 = \lambda^{2n} - (\lambda^n + c^n\lambda^{-n})\lambda^n + 1 = 1 - c^n. \tag{IX.6.85}$$

The fixed constant term of the parent curve therefore requires

$$c^n = 1. \tag{IX.6.86}$$

This condition is not an arbitrary root count added after parametrizing the curve: it enforces its second asymptotic coefficient.

For example, with $n = 2$ and $c = 1$, the parent equation becomes $t^2+(v^2-2)t+1 = 0$. Setting $v = \lambda + \lambda^{-1}$ and $t = -\lambda^2$ gives zero identically. With the same parametrization but $c = 2$, the residual is $1 - 4 = -3$, so it is not the fixed parent curve. For $n = 3$ the allowed c values are the cube roots of unity, and for $n = 4$ they are $1, -1, i, -i$. These are dimensionless degeneration parameters; they have not been identified with the length-squared ζ of the previous section.

To rotate the rational curve holomorphically, add $w = \zeta/\lambda$ in these dimensionless coordinates. For $\zeta \neq 0$ the change of variables

$$v' = v - \frac{c}{\zeta} w = \lambda, \qquad t' = -t = \lambda^n, \qquad v'w = \zeta \tag{IX.6.87}$$

has the form of the rotated pure curve with $A = 1$. It gives a controlled algebraic bridge from a rational degeneration of the parent to the holomorphic rotated surface.

The word holomorphic is essential here. For $a = c/\zeta$, the old flat metric in the two transverse complex coordinates becomes

$$\begin{aligned} |dv|^2 + |dw|^2 &= |dv' + a\, dw|^2 + |dw|^2 \\ &= |dv'|^2 + (1 + |a|^2)|dw|^2 + 2\,\mathrm{Re}(\overline{dv'} a\, dw). \end{aligned} \tag{IX.6.88}$$

This is not the flat metric $|dv'|^2 + |dw|^2$ in general. The shear is not a unitary spatial rotation, and does not provide a canonical mass–angle relation or an equality of nonprotected spectra. Its use is to relate complex equations with their chosen ends.

IX.6.10 The extra circle scale in MQCD

The holomorphic curve makes a sharp statement about vacua at fixed ends. Can its semiclassical geometry also calculate the ordinary-SYM spectrum? A scale comparison shows the difficulty. An ordinary four-dimensional pure gauge theory has an infrared scale Λ. To obtain its nonprotected spectrum from a larger construction, extra excitations would need masses parametrically above Λ in a regime where the calculation remains controlled.

In the curve $t = Av^n$, a single turn of the t circle permutes the n preimages of t. If f_j denotes a mode on sheet j, with the index understood modulo n, the identification takes the form

$$f_j(\vartheta + 2\pi) = f_{j+1}(\vartheta), \qquad f_j(\vartheta + 2\pi n) = f_j(\vartheta). \tag{IX.6.89}$$

The sign of the sheet permutation depends on the orientation assigned to the circle; its order is n in either orientation. The effective radius is therefore nR and its momentum scale is

$$m_k \sim \frac{|k|}{nR}, \qquad m_{\mathrm{KK}} = \frac{\kappa}{nR}, \qquad \kappa = O(1). \tag{IX.6.90}$$

The existence and interpretation of light fivebrane modes use the semiclassical MQCD description. The covering argument explains the factor of n; it is not a full fluctuation-spectrum calculation. Figure IX.6.5 displays the sheet identification.

Restore a common physical length frame and let $Z = |\zeta_{\text{curve}}|$ have dimension length squared. The semiclassical string and domain-wall tension estimates, with order-one coefficients absorbed into their matching constants, scale as

$$T \sim \frac{Z^{1/2}}{n\ell_p^3}, \qquad T_D \sim \frac{RZ}{\ell_p^6}, \tag{IX.6.91}$$

where ℓ_p is the eleven-dimensional Planck length. Their dimensions are mass squared and mass cubed, respectively. To attempt matching to ordinary-SYM scales, write the proportionality equations as

$$\frac{Z^{1/2}}{n\ell_p^3} = \alpha\Lambda^2, \qquad \frac{RZ}{\ell_p^6} = \beta n\Lambda^3, \qquad \alpha, \beta > 0 \text{ of order one.} \tag{IX.6.92}$$

The first equation fixes Z and the second then fixes R:

$$Z = \alpha^2 n^2 \ell_p^6 \Lambda^4, \qquad R = \frac{\beta}{\alpha^2 n\Lambda}. \tag{IX.6.93}$$

The unwanted circle modes consequently obey

$$\frac{m_{\text{KK}}}{\Lambda} = \frac{\kappa}{nR\Lambda} = \frac{\kappa\alpha^2}{\beta} = O(1). \tag{IX.6.94}$$

There is no parameter in these equations that separates the extra modes from the gauge-theory scale while keeping the matching constants bounded and nonzero. In particular, large n does not help: R shrinks as $1/n$ and the effective product nR stays fixed.

As a scaling illustration, taking $\alpha = \beta = \kappa = 1$ gives

n	2	3	4
$R\Lambda$	1/2	1/3	1/4
$nR\Lambda$	1	1	1
m_{KK}/Λ	1	1	1

(IX.6.95)

The numerical ones are illustrative choices of unknown coefficients, not predictions for particle masses. If the wrapping factor were incorrectly omitted, the same matching would appear to give $(R\Lambda)^{-1} = n$ and a false large-rank separation.

Semiclassical fivebrane control asks for geometric scales large in Planck units, whereas an ordinary weak-IIA gauge-theory limit lies in a different regime. The obstruction just derived is conditional on the stated semiclassical mode and tension estimates; it is not a theorem excluding every possible string realization of SYM. It does prevent using those estimates as a controlled calculation of the ordinary-SYM nonprotected spectrum.

The surviving conclusion is substantial but specific. The two fixed asymptotic coefficients determine the holomorphic curve and its distinct interiors; its divisor determines winding and the relative charge group. Their physical interpretation uses the supersymmetric M-theory lift and protected continuation. Those statements do not require identifying the entire semiclassical spectrum with that of ordinary SYM. Likewise, the electric-to-magnetic brane motion organizes ranks, mesons and couplings, while its infrared-continuity assumption remains separate from endpoint conservation. Keeping these distinctions permits both constructions to be used without asking them to determine observables outside their controlled scope.

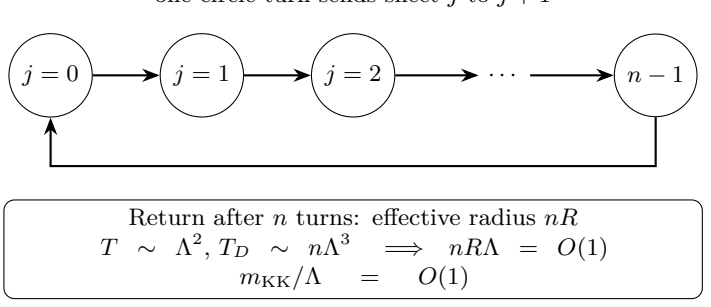


Figure IX.6.5: The circle acts cyclically on the sheets of $t = Av^n$. A mode returns to the same sheet after n turns, producing the scale $1/(nR)$. Matching the two stated tension scalings leaves this scale of order Λ. No normalized string tension or glueball mass is plotted.

IX.6.11 Exercises

Rotation and elimination. For the rigid boundary problem, construct the right tangent projector at $\theta = 0, \pi/4, \pi/2$ and solve the affine zero-mode equations before using the nonzero-frequency determinant. Give the light gap in units of π/L and compare μ/μ_0 in the regulated model. For $X = \left(\begin{smallmatrix} 2 & 3 \\ 5 & 7 \end{smallmatrix}\right)$, $m_\Phi = 2$ and $y = 3$, submit the quadratic and Yukawa coefficients of W, the stationary adjoint and the substituted superpotential for both $U(2)$ and $SU(2)$. Explain why neither calculation fixes a universal canonical mass from an angle. The finite nonzero quartic must remain visible in the answer.

Attachments and the separate anomaly comparison. Reconstruct every attachment in the nine states of Table IX.6.1, using the reconnection choice D_2, D_4, D_5. Compute each brane's linking number from those attachments. Read the final flavors from the D_i–P segments and construct all matrix units E_{ij} of the meson space. Then use Table IX.6.2 to calculate both twelve-component anomaly vectors for the undeformed SU comparison. Repeat the magnetic sum after removing the meson row. Identify an attachment change that conserves linking but violates the specified path. State separately the creation and infrared-continuity premises.

Fixed ends and oriented winding. In units of ℓ_0, take $A = 2$, $B = 2^{n+1}$ and $n = 2, 3, 4$. Starting from the prescribed poles, determine v, w, t, their full divisors, the polynomial for ζ and its complete root set. Derive the winding of t and of the physical circle, and the relative charge group. Repeat for $n = 1$ as an algebraic example, for $B = 0$ as a degenerate boundary, and with reversed physical-circle orientation at $n = 3$. Keep $m_{\mathrm{KK}} = \kappa/(nR)$ and derive its ratio to Λ under the stated tension matching. Explain which step would fail if an interior zero of t were inserted.

The accompanying exercise instructions specify finite rational matrices, labeled graphs and algebraic-number coordinates for submitting these answers. They distinguish a wrong calculation from a missing answer or an expression outside the declared interface.

Status and sources

WS means a physical-worldsheet derivation in the untwisted string. No WS derivation is supplied here. The physical spectrum and meson identifications remain sourced premises with an unassigned physical primary classification in the companion inventory. MATH below refers to the stated boundary, matrix, meromorphic or topological problem and its displayed argument. It does not classify the physical identification of that problem. The conditional duality statements and the separate anomaly comparison retain the scopes specified below.

1. Native IIA supersymmetry and endpoint spectrum. Sections IX.6.1–IX.6.2 implement The brane axes and physical four-supercharge system are Elitzur et al. (1997), hep-th/9702014v2, §2, (2.1)–(2.4), printed p. 2, and the spectrum discussion on p. 3 (source anchors E1–E2). The declared mostly-plus equations (IX.6.3) are a native calculation, not a literal transport of EGK's RR/gamma signs. EGK prints plus D4 and D6 relations but does not supply the correlated signature/orientation dictionary needed for that identification. The native relative minus neither corrects the paper nor assigns an anti-D6 charge. Exact Clifford/reality and rigid endpoint identities are MATH; the physical brane spectrum uses the sourced four-ND string input, with physical primary classification left unassigned until a complete construction payload is supplied. The finite-angle calculation is the stated scalar boundary model, not an interacting fermionic boundary spectrum.

2. Mass and quartic normalization. Section IX.6.3, Q2b, is exact tree holomorphic elimination for $m_\Phi \neq 0$ with the written kinetic reference. The regulated comparison (IX.6.20) is Barbon (1997), hep-th/9703051v2, §3, (3.1)–(3.6), printed pp. 4–5, particularly (3.6). It retains that model's regulator, zero-mode truncation and field normalization; no universal canonical angle–mass map is claimed. Its §4, pp. 7–8 also discusses the baryon-gauging and infrared-continuity issues. The stated field normalization fixes the mass, Yukawa, trace subtraction and meson scale.

3. Endpoint motion and magnetic matter. Sections IX.6.4–IX.6.5, Q3/Q4, use EGK §3, steps (a)–(d), printed pp. 4–5, and (3.1), p. 5; item 4 on p. 6 supplies the deformation comparison (E3–E5). The complete nine-state endpoint sequence conserves each declared linking number and ends with rank two, five flavor pairs and 25 mesons. The linking formula uses the stated IIA endpoint convention; it is not attributed as a printed equation in EGK. The physical flavor and meson dictionary remains source-only with unassigned physical primary classification. The matrix count and cubic contraction do not calculate a canonical disk Yukawa. Equation (IX.6.48) retains an unspecified matching scale.

4. Creation, continuity and the gauge-group boundary. The infrared comparison is DUAL and uses two physical assumptions: A-001-HW-CREATION, pinned to EGK §3 pp. 4–5 and §4 pp. 6–7 for creation/reconnection and occupancy; and A-002-HW-CONT, pinned to §3 p. 4 and §5 item 1, p. 8 for the infrared-continuity assumption. Endpoint conservation does not prove either physical premise. The charged-center action is an elementary representation calculation. The brane U systems and the undeformed SU comparison remain distinct; weak gauging, global quotients and nonnormalizable trace modes have not been identified with deleting a free central photon. The IX.5 finite-chain boundary qualification is reused only for the stated finite chain.

5. Anomaly comparison. Section IX.6.6, Q6, has status ANOM. It compares the standard undeformed SQCD descriptions of Seiberg (1995), with representation and charge conventions from Volume I, Chapter 3. That field-theory comparison is not evidence that the brane construction exists. Twelve continuous-symmetry tensor components are calculated, with six nonredundant nonzero structures after conjugation and three zero traces. The finite quartic breaks the full chiral flavor symmetry and is relevant at the undeformed $(3, 5)$ fixed point. No equality of full anomaly polynomials for all quotient backgrounds is claimed.

6. Frame, asymptotics and holomorphic vacua. Section IX.6.7 covers Q8, Q9a, Q9b and Q9c. It uses Witten (1997), hep-th/9706109v2, §2.1 pp. 3–4 for the 78 source plane and trace-mode qualification; §2.2, (2.2)–(2.4), pp. 5–6 for the circle and curve; and the fixed-infinity discussion pp. 6–7, including (2.6), p. 7 (W1–W3). Algebraic curve and root statements are MATH under their meromorphic hypotheses. Their protected MQCD interpretation is DUAL conditional on the nonperturbative M-theory lift at §2.2 pp. 5–7. Supporting supersymmetry is four of 32 bulk real supercharges. Both nonzero asymptotic coefficients are fixed. The $n = 1$ example is algebra only. The complex curve parameter `zeta_curve` is not an FI level.

7. Winding and relative charge. Section IX.6.8, Q10, uses Witten §3.1, (3.4)–(3.7), printed pp. 12–13 (W5). The physical-circle sign follows $t = e^{-s}$ and is also printed explicitly in §6, *(6.3), printed p. 35*: $x^{10} = -n \operatorname{Im} \log \lambda$ in angular units. Equation (6.2) is not that coordinate locator. The divisor, contour and relative-homology calculations establish topology, not a tension.

8. Rational degeneration. Section IX.6.9, Q11, uses Witten §2.3, (2.10)–(2.11) and the rational parametrization, printed p. 9 (W4). The recurrence and residual $1 - c^n$ are explicit algebra. The coordinate shear is holomorphic and nonunitary; it is not a metric or mass identification. The normalized parent curve is specified afresh and does not import the distinct period/charge conventions of IX.5.

9. The nonprotected boundary. Section IX.6.10, Q12, uses Witten §4, (4.16), p. 29, footnote 17 and p. 30 for the effective nR scale; §5, (5.1)–(5.3), pp. 30–31 and discussion through pp. 32–33 for the semiclassical comparison (W6–W7). The conditional scaling calculation retains bounded order-one constants. No ordinary-SYM glueball spectrum, normalized string tension or complete domain-wall solution is obtained. Those extensions remain confinement and MQCD strings, with a planned discussion of confinement and MQCD strings. General Seiberg duality and the comparison of its separate construction routes remain the field-theory derivation of Seiberg duality/XVI.3; brane endpoint and projector foundations and global gauge groups and line operators retain the wider brane/global-form work.

The flavored U/SU comparison, rotated-brane examples and MQCD calculations for $n = 1, 2, 3, 4$ use the endpoint, normalization and supersymmetry conditions stated above. The M-theory interpretation concerns protected data.

References

Barbon, J. L. F. (1997). "Rotated branes and N=1 duality". In: *Phys. Lett. B* 402, pp. 59–63. DOI: 10.1016/S0370-2693(97)00451-6. arXiv: hep-th/9703051.

Elitzur, S., A. Giveon, and D. Kutasov (1997). "Branes and N=1 duality in string theory". In: *Phys. Lett. B* 400, pp. 269–274. DOI: 10.1016/S0370-2693(97)00375-4. arXiv: hep-th/9702014.

Seiberg, N. (1995). "Electric - magnetic duality in supersymmetric nonAbelian gauge theories". In: *Nucl. Phys. B* 435, pp. 129–146. DOI: 10.1016/0550-3213(94)00023-8. arXiv: hep-th/9411149.

Witten, E. (1997). "Branes and the dynamics of QCD". In: *Nucl. Phys. B* 507, pp. 658–690. DOI: 10.1016/S0550-3213(97)00648-2. arXiv: hep-th/9706109.

Chapter IX.7

Three-dimensional dualities from branes

IX.7.1 What survives a compactification?

A circle can disappear from the low-energy spectrum while leaving an interaction behind. This is the central difficulty in reducing the four-dimensional brane duality of Chapter 6. A field with nonzero momentum around a small circle becomes heavy, but a Euclidean brane can wrap the circle. Its contribution to the superpotential depends on the circumference and can change which low-energy theories are dual. Keeping only the gauge group and its light quarks misses this interaction.

We begin with the rotated D4–NS5 construction and compactify one of its spacetime directions. T-duality turns the wrapped D4s into suspended D3s and turns the gauge holonomy into their positions on a dual circle. Euclidean D1-branes stretch between neighboring D3s. Besides the intervals visible on a line, the circle permits an additional interval joining the last D3 back to the first. That last process is the origin of the Kaluza–Klein monopole term. We will compute its action and explain why its fermion zero modes, rather than charge neutrality alone, determine its contribution.

The desired strictly three-dimensional duality follows from a further operation. Two heavy flavors are removed in a chosen real-mass background. On the magnetic side this background separates two individual D3s from the central stack. Each separated brane carries an abelian theory with one flavor. Replacing those two theories by their interacting singlet descriptions, and only then eliminating the heavy fields, leaves two monopole singlets coupled to the central magnetic theory. We will follow the nonselfdual example with two electric colors and five light flavors, so that the magnetic rank, the monopole charges and the separated sectors can all be distinguished.

Giving masses of the same sign produces a different endpoint. The massive fermions induce Chern–Simons terms, and part of the flavor-brane charge recombines with a fivebrane. Counting the created and reconnected D3 segments then gives the Giveon–Kutasov magnetic rank. The sign of the magnetic level needs a separate fermion calculation; it cannot be read from an unsigned count of segments. Finally we put the

suspension direction itself on a circle. This is a different geometry, with a different radius and a different fivebrane orientation. Its torus degeneration data will provide the bridge to Volume VIII.

IX.7.2 A spacetime circle and its T-dual interval

The starting point has four real supercharges. Let X^μ denote physical length coordinates, and let the D4 suspension interval have length L_6. The two fivebranes of Chapter 6 are NS and NS$'$, with worldvolumes

IIA object	worldvolume directions
NS	012345
NS$'$	012389
D4	01236
D6	0123789

(IX.7.1)

The coordinate X^3 is a spacetime direction of the D4 theory; X^6 is an interval. Compactify only X^3 and perform T-duality along it. The radius and string coupling transform as

$$X^3 \sim X^3 + 2\pi R_3, \qquad \widetilde{R}_3 = \frac{\alpha'}{R_3}, \qquad g_s^B = \frac{g_s^A \sqrt{\alpha'}}{R_3}. \tag{IX.7.2}$$

A wrapped Neumann direction becomes a transverse Dirichlet direction. Thus the D4 loses 3, the D6 loses 3, and the longitudinally dualized NS fivebranes retain their type. The resulting IIB rows are

$$\text{D3} = 0126, \quad \text{D5} = 012789, \quad \text{NS} = 012345, \quad \text{NS}' = 012389. \tag{IX.7.3}$$

The three-dimensional fields propagate in 012. The color branes remain suspended in 6, while their positions in $\widetilde{X}^3$ now measure the Wilson line around the original spacetime circle.

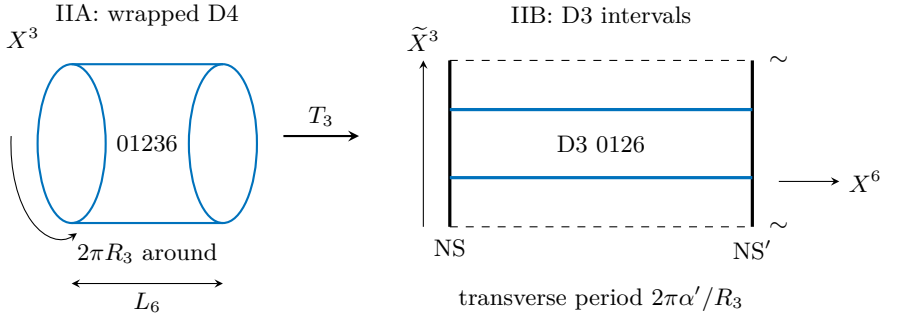


Figure IX.7.1: Compactification of the spacetime direction X^3. T-duality removes the wrapped direction from each D4, leaving a D3 interval in X^6. The right panel is a cylinder in $\widetilde{X}^3$ and X^6; its upper and lower edges are identified. The dual circle is transverse to the D3s. Neither panel makes X^6 a circle.

To fix the coupling, take the fundamental-trace Yang–Mills action to have coefficient $1/(2g^2)$ in front of $\mathrm{Tr}\, F_{\mu\nu}F^{\mu\nu}$. The D4 tension and the quadratic DBI coefficient give

$$T_{D4} = \frac{1}{(2\pi)^4 g_s^A \alpha'^{5/2}}, \qquad \frac{L_6 T_{D4}(2\pi\alpha')^2}{4} = \frac{L_6}{16\pi^2 g_s^A \sqrt{\alpha'}} = \frac{1}{2g_4^2}. \tag{IX.7.4}$$

Integrating the four-dimensional action over the circle, or expanding the D3 action and integrating over the interval, gives the same result:

$$g_4^2 = \frac{8\pi^2 g_s^A \sqrt{\alpha'}}{L_6}, \qquad \frac{1}{g_3^2} = \frac{2\pi R_3}{g_4^2}, \qquad g_3^2 = \frac{4\pi g_s^B}{L_6}. \tag{IX.7.5}$$

Here g_4^2 is dimensionless, whereas g_3^2 has mass dimension one. For a constant diagonal gauge holonomy the T-dual map and its large-gauge period are

$$\sigma_i = A_{3,i} = \frac{\widetilde{X}_i^3}{2\pi\alpha'}, \qquad \Delta\widetilde{X}^3 = \frac{2\pi\alpha'}{R_3} \quad \Longrightarrow \quad \Delta\sigma = \frac{1}{R_3}. \tag{IX.7.6}$$

The dual circumference is a length; the eigenvalue period is a mass. For example, if the period in scalar units is $P = 12m_0$ for a reference mass m_0, then $R_3 = (12m_0)^{-1}$ and the dual circumference is $24\pi\alpha' m_0$. The distinction will fix the instanton exponent.

The low-energy interval theory is useful in a window

$$E \ll \min\{R_3^{-1}, L_6^{-1}, \alpha'^{-1/2}\}. \tag{IX.7.7}$$

When we compare infrared descriptions, the energy must also be below the scales at which those descriptions approach their common infrared limit. Equation (IX.7.7) alone is a dimensional-reduction condition, not a proof of that infrared equivalence.

There is a gauge-group choice before taking this limit. We use a vectorlike $U(N_c)$ parent obtained by weakly gauging baryon number, with global form

$$U(N_c) = \frac{SU(N_c) \times U(1)_B}{\mathbb{Z}_{N_c}}. \tag{IX.7.8}$$

The four-dimensional abelian factor is treated as an effective weakly gauged theory below its ultraviolet cutoff. This changes the boundary and gauging problem. Chapter 5's removal of a nonnormalizable trace mode on a finite noncompact brane configuration therefore remains valid in its own setting. Compactification does not restore that mode by decree; the abelian gauge field here was included in the parent theory from the start.

IX.7.3 D1 instantons and the affine monopole

A separated stack has abelian gauge fields and real eigenvalues σ_i. Dualizing each abelian photon introduces an angular scalar γ_i of period 2π. In an open Weyl alcove choose

$$\sigma_1 > \cdots > \sigma_{N_c}, \qquad \sigma_1 - \sigma_{N_c} < \frac{1}{R_3}, \qquad Z_i = \frac{4\pi\sigma_i}{g_3^2} + i\gamma_i. \tag{IX.7.9}$$

The following exponential coordinates describe the semiclassical ends of the Coulomb branch:

$$Y_i = e^{Z_i - Z_{i+1}}, \qquad X_+ = e^{Z_1}, \qquad X_- = e^{-Z_{N_c}}, \qquad \prod_{i=1}^{N_c-1} Y_i = X_+ X_-. \tag{IX.7.10}$$

They specify holomorphic normalizations, not a canonical Kähler metric. The elementary monopole joining neighboring eigenvalues is a Euclidean D1 sheet spanning their separation and the suspension interval. Using the physical D1 tension gives

$$\begin{aligned} S_i &= \frac{L_6 \Delta \widetilde{X}_i^3}{2\pi\alpha' g_s^B} = \frac{L_6}{g_s^B}(\sigma_i - \sigma_{i+1}) \\ &= \frac{4\pi}{g_3^2}(\sigma_i - \sigma_{i+1}). \end{aligned} \tag{IX.7.11}$$

Its boundary coupling to the dual photon supplies the phase. In the orientation of (IX.7.9), the combined weight is

$$e^{-S_i - i(\gamma_i - \gamma_{i+1})} = Y_i^{-1}. \tag{IX.7.12}$$

This fixes the possible holomorphic monomial. To obtain a superpotential amplitude, one must also saturate the fermion zero modes. The instanton calculation supplies two universal gaugino zero modes. An uninserted term is generated when no additional unlifted matter zero modes remain. A fundamental flavor pair with threshold t strictly between the two eigenvalues adds two matter zero modes. For N_f thresholds t_f the selection rule in this chamber is

$$n_{\mathrm{matter},i} = 2 \sum_{f=1}^{N_f} \mathbf{1}_{\sigma_{i+1} < t_f < \sigma_i}, \qquad n_{\mathrm{matter},i} = 0 \implies W_i \propto Y_i^{-1}. \tag{IX.7.13}$$

The implication uses the nonzero instanton measure in this supersymmetric configuration. Symmetry alone would permit a coefficient to vanish and cannot supply this premise. A threshold on an eigenvalue is a wall with additional light fields; the strict inequalities exclude it.

The circle adds a remaining arc from the last eigenvalue to the first through the identified boundary. The associated affine, or KK, monopole has

$$\Delta\sigma_0 = \frac{1}{R_3} - (\sigma_1 - \sigma_{N_c}), \qquad S_0 = \frac{4\pi}{g_3^2 R_3} - \frac{4\pi}{g_3^2}(\sigma_1 - \sigma_{N_c}). \tag{IX.7.14}$$

When the matter thresholds lie on the ordinary arcs, the affine sheet has only its universal modes. Its dual-photon phase closes the chain of ordinary constituents and gives

$$W_0 \propto \eta X_+ X_-, \qquad \eta \propto e^{-4\pi/(R_3 g_3^2) + i\theta_4} = e^{-8\pi^2/g_4^2 + i\theta_4}. \tag{IX.7.15}$$

Indeed, summing all constituent areas yields exactly the four-dimensional instanton action:

$$\sum_{i=1}^{N_c-1} S_i + S_0 = \frac{4\pi}{g_3^2 R_3} = \frac{8\pi^2}{g_4^2}. \tag{IX.7.16}$$

For a concrete zero-mode calculation take three eigenvalues and five equal flavor thresholds, expressed in units of m_0:

$$(\sigma_1, \sigma_2, \sigma_3) = (5, 2, -3)m_0, \qquad R_3^{-1} = 12m_0, \qquad t_f = 0. \tag{IX.7.17}$$

The ordinary gaps are $3m_0, 5m_0$, and the affine gap is $4m_0$. The five thresholds all lie between $2m_0$ and $-3m_0$, so

$$(n_{\text{matter},1}, n_{\text{matter},2}, n_{\text{matter},0}) = (0, 10, 0), \qquad W \supset c_1 Y_1^{-1} + c_0 \eta Y_1 Y_2. \tag{IX.7.18}$$

Moving the thresholds to $4m_0$ changes the counts to $(10, 0, 0)$ and moves the unscreened ordinary term from Y_1^{-1} to Y_2^{-1}. The sum of the areas is unchanged. This is a local semiclassical configuration, not a claim that these eigenvalues solve the five-flavor vacuum equations.

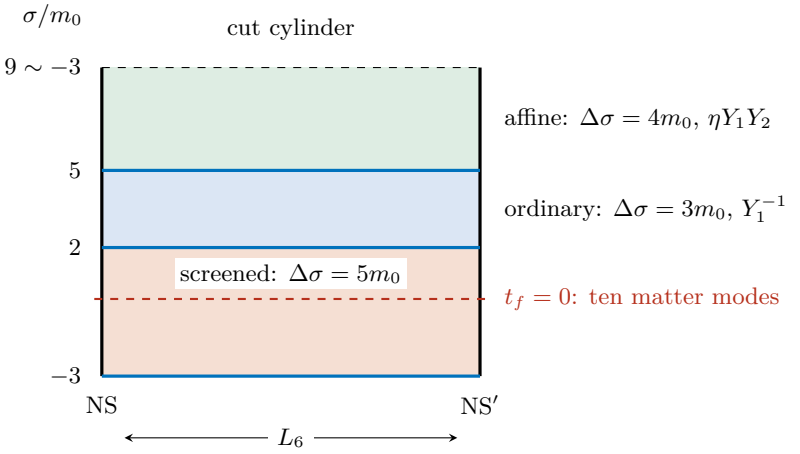


Figure IX.7.2: The three constituent arcs in the example $\sigma/m_0 = (5, 2, -3)$ with period 12. The cut is taken at -3 and 9, which are identified. The flavor threshold at zero screens the gap of length 5; the ordinary gap of length 3 and affine gap of length 4 have no extra matter zero modes. Each colored strip represents a D1 sheet extending over the same suspension length L_6.

The exponential in (IX.7.15) is dimensionless, whereas a three-dimensional superpotential has mass dimension two. Let Λ_{match} be a matching scale, and let $\widehat{\mathcal{O}}_a$ denote a chosen dimensionless holomorphic coordinate. Restoring a dimensionful operator of dimension d_a means

$$\mathcal{O}_a = \Lambda_{\text{match}}^{d_a} \widehat{\mathcal{O}}_a, \qquad W_a = c_a \Lambda_{\text{match}}^{2-d_a} \mathcal{O}_a, \qquad [W_a] = 2. \tag{IX.7.19}$$

Thus a physical coefficient multiplying a dimensionful monopole product carries the complementary power of the matching scale. Its exponential dependence is fixed by the D1 area; neither that calculation nor the notation η fixes a canonical operator normalization.

A useful contrast is pure $SU(3)$, where both ordinary terms are present. After absorbing nonzero holomorphic coefficients into the coordinates,

$$W = Y_1^{-1} + Y_2^{-1} + \eta Y_1 Y_2. \tag{IX.7.20}$$

The equations in logarithmic coordinates require all three monomials to be equal. Setting their common value to z gives

$$Y_1^{-1} = Y_2^{-1} = \eta Y_1 Y_2 = z, \qquad z^3 = \eta. \tag{IX.7.21}$$

At nonzero η there are three solutions in this chart. Deleting the affine term leaves no finite stationary point. Pure $U(3)$ additionally has a common shift $Z_i \mapsto Z_i + c$ which leaves every difference and X_+X_- fixed. The abelian branch therefore survives. More generally, monopole coordinates are not globally independent elementary fields, so differentiating $\eta X_+ X_-$ as if it were a two-field elementary model does not determine the full $U(N)$ vacuum space. At $N_c = 1$ there is no nonabelian affine constituent of this kind; its abelian dual description will enter by a separate argument below.

IX.7.4 Seven flavors and a separated magnetic vacuum

To reach five-flavor $U(2)$ SQCD, begin at finite radius with seven flavors. The four-dimensional parent duality, weakly baryon-gauged before reduction, gives an electric $U(2)$ description and a magnetic $U(5)$ description. Both retain their finite-circle monopole interactions. More generally the parent and desired magnetic ranks are

$$N_f^{\text{parent}} = N_f + 2, \qquad N_c^{\text{parent,mag}} = N_f + 2 - N_c, \qquad N_c^{\text{final,mag}} = N_f - N_c. \tag{IX.7.22}$$

The loss of two magnetic colors will be realized by separation, not by discarding color branes. Let a, b label the two heavy flavors and $M > 0$ their mass scale. A real mass is a background vector-multiplet scalar, which enters a fermion's signed mass together with the gauge scalar:

$$m_{\text{eff}}(Q_i) = \sigma + m_{Q_i}, \qquad m_{\text{eff}}(\widetilde{Q}^i) = -\sigma + m_{\widetilde{Q}^i}. \tag{IX.7.23}$$

It is not a holomorphic mass in the superpotential. In the original flavor labels choose the heavy real masses

	Q_a	Q_b	$\widetilde{Q}^a$	$\widetilde{Q}^b$
m	M	$-M$	M	$-M$
dual background	$-M$	M	$-M$	M

(IX.7.24)

The opposite dual backgrounds follow from the flavor representation of the magnetic quarks. The light magnetic vacuum selected by the mass flow is

$$\sigma_m = \operatorname{diag}(M, 0, 0, 0, -M), \qquad U(5) \longrightarrow U(1)_1 \times U(3) \times U(1)_2. \tag{IX.7.25}$$

This is a choice of vacuum in the dual flow. Algebra in this vacuum does not establish that all other possible vacua are absent.

At a remote color, solving (IX.7.23) gives the following full heavy-flavor signed spectrum. The five light-flavor backgrounds are zero and can be added separately.

σ_m	$m(q_a)$	$m(q_b)$	$m(\widetilde{q}^a)$	$m(\widetilde{q}^b)$	massless pair
M	0	$2M$	$-2M$	0	$q_a, \widetilde{q}^b$
0	$-M$	M	$-M$	M	none of a, b
$-M$	$-2M$	0	0	$2M$	$q_b, \widetilde{q}^a$

(IX.7.26)

At each central color there are five massless light pairs. At $+M$ the light-flavor masses are $+M, -M$, and at $-M$ they are $-M, +M$, so these flavors do not add remote massless matter. Each remote $U(1)$ has precisely one vectorlike flavor, but its two fields have different original labels.

Define the meson $\mathcal{M}_{ij} = Q_i \widetilde{Q}^j$ and choose dual indices so that its coupling is $\mathcal{M}_{ij} q_i \widetilde{q}^j$. Its real background mass is the sum of the two electric masses:

$$m(\mathcal{M}_{ij}) = m_{Q_i} + m_{\widetilde{Q}^j}, \qquad m(\mathcal{M})|_{a,b} = \begin{pmatrix} 2M & 0 \\ 0 & -2M \end{pmatrix}. \tag{IX.7.27}$$

The massless remote flips are consequently $\mathcal{M}_{ab}$ and $\mathcal{M}_{ba}$, in addition to the central 5×5 meson block. The count of massless mesonic fields before remote elimination is

$$5^2 + 1 + 1 = 27. \tag{IX.7.28}$$

The two extra fields will be eliminated with the remote sectors; the final Aharony pair has 25 mesons and two different singlets of monopole origin.

A geometric drawing using two complete displaced D5s is most transparent after interchanging the heavy antiflavors. Write $\widetilde{\widetilde{Q}}^a = \widetilde{Q}^b$ and $\widetilde{\widetilde{Q}}^b = \widetilde{Q}^a$, with the same relabeling for dual fields and mesons. Then

$$(m_{Q_a}, m_{Q_b}; m_{\underset{\sim}{\widetilde{Q}}^a}, m_{\underset{\sim}{\widetilde{Q}}^b}) = (M, -M; -M, M), \qquad \widehat{\mathcal{M}}_{aa} = \mathcal{M}_{ab}, \quad \widehat{\mathcal{M}}_{bb} = \mathcal{M}_{ba}. \tag{IX.7.29}$$

The remote massless pairs now have matching labels. Nothing about their physical masses has changed. In units of M, the mass vectors and magnetic scalar values in this chart are

$$\begin{aligned} &m_Q/M = (0,0,0,0,0,1,-1), \quad m_{\underset{\sim}{\widetilde{Q}}}/M = (0,0,0,0,0,-1,1), \\ &\sigma_m/M = (1,0,0,0,-1), \qquad\qquad m_q = -m_Q, \quad m_{\underset{\sim}{\widetilde{q}}} = -m_{\underset{\sim}{\widetilde{Q}}}. \end{aligned} \tag{IX.7.30}$$

For $M = 11m_0$, a remote $+M$ row has q masses $(11, 11, 11, 11, 11, 0, 22)m_0$ and antiquark masses $(-11, -11, -11, -11, -11, 0, -22)m_0$. The central rows keep exactly five flavors. This displays the $1 + 3 + 1$ splitting without suppressing the heavy-flavor labels that caused it.

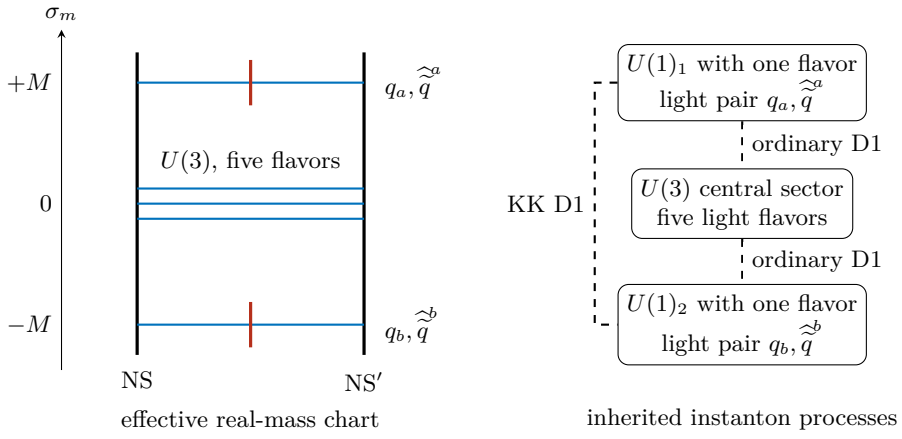


Figure IX.7.3: The magnetic vacuum in scalar coordinates after the antiflavor permutation. Each displaced flavor D5 carries one color D3, giving two remote $U(1)$ theories with one flavor each, while three colors and five flavors remain centrally. The dashed links denote ordinary and affine D1 processes between the blocks. The vertical label is σ_m, whose sign is opposite to the electric physical-position chart.

This last sign matters when comparing with Chapter 1. There a positive D5 position was a geometric mass marker. The effective electric background in (IX.7.23) has the opposite sign. With X_3 and X_5 denoting color and flavor positions on the dual transverse circle,

$$\sigma_e = \frac{X_3}{2\pi\alpha'}, \quad m_Q = -\frac{X_5}{2\pi\alpha'}, \qquad \sigma_m = -\frac{X_3}{2\pi\alpha'}, \quad m_q = +\frac{X_5}{2\pi\alpha'}. \tag{IX.7.31}$$

The magnetic scalar chart is charge conjugated with its gauge field and dual photon. Both descriptions then reproduce the stretched-string mass:

$$|\sigma_e + m_Q| = |\sigma_m + m_q| = \frac{|X_3 - X_5|}{2\pi\alpha'}. \tag{IX.7.32}$$

The label $+M$ on Figure IX.7.3 is therefore a scalar eigenvalue label, not an unlabeled positive spatial displacement.

IX.7.5 Remote theories and surviving singlets

Separating the three color blocks does not erase the D1 processes between them. Denote the central $U(3)$ monopole operators by v_+, v_-, with the sign giving their topological charge. For each remote $U(1)_i$ let p_i, n_i denote its positive and negative monopoles. The two adjacent interactions and the interaction across the remaining circle arc take the form

$$W_{\text{inter}} = v_+ n_1 + v_- p_2 + \mu p_1 n_2. \tag{IX.7.33}$$

The coefficients of the first two terms have been absorbed in holomorphic field normalizations. The renormalized coefficient μ is kept nonzero. Its origin is the remote KK interaction, so removing it before eliminating the remote fields changes the problem.

The abelian theory with one flavor has an infrared description by three chirals, conventionally called the XYZ model. Here the three fields are the meson $N_i = q_i\widetilde{q}^i$ and the monopoles p_i, n_i, with

$$W_{\mathrm{XYZ},i} = N_i p_i n_i. \tag{IX.7.34}$$

The selected brane realization uses an NS/D exchange in each remote sector, the nonperturbative IIB mirror operation discussed in Chapter 2. The three-dimensional theory here has four real supercharges; it is not the free twisted hypermultiplet example of the eight-supercharge theory. The one-flavor abelian duality supplies the effective XYZ description, including its interaction. A separate field-theory derivation supports that description but does not remove the NS/D exchange from this brane construction.

The light electric mesons in (IX.7.27) act as flips of the two remote mesons. Set $M_1 = \widehat{\mathcal{M}}_{aa}$ and $M_2 = \widehat{\mathcal{M}}_{bb}$. Suppressing the central flavor sums only after writing their contraction, the full effective superpotential is

$$\begin{aligned} W = {} & \sum_{i,j=1}^{5} \mathcal{M}_{ij} q_i \widetilde{q}^j + M_1 N_1 + N_1 p_1 n_1 + M_2 N_2 + N_2 p_2 n_2 \\ & + v_+ n_1 + v_- p_2 + \mu p_1 n_2. \end{aligned} \tag{IX.7.35}$$

Every rescaling used here is nonsingular at the matching point. Restoring canonical dimensions requires the matching coefficients described in (IX.7.19); this notation does not determine their Kähler normalizations.

Eliminate the six elementary fields $M_1, N_1, M_2, N_2, p_1, n_2$, holding the central monopole operators as coefficients. The first four equations are

$$\frac{\partial W}{\partial M_i} = N_i = 0, \qquad \frac{\partial W}{\partial N_1} = M_1 + p_1 n_1 = 0, \qquad \frac{\partial W}{\partial N_2} = M_2 + p_2 n_2 = 0. \tag{IX.7.36}$$

The remaining two then reduce to

$$\frac{\partial W}{\partial p_1} = N_1 n_1 + \mu n_2 = 0, \qquad \frac{\partial W}{\partial n_2} = N_2 p_2 + \mu p_1 = 0. \tag{IX.7.37}$$

For $\mu \neq 0$ they set $n_2 = p_1 = 0$ and hence $M_1 = M_2 = 0$. The complete solution in these heavy variables is

$$N_1 = N_2 = M_1 = M_2 = p_1 = n_2 = 0, \qquad n_1, p_2 \text{ remain.} \tag{IX.7.38}$$

Order the heavy fields as $M_1, N_1, M_2, N_2, p_1, n_2$. Their quadratic matrix on this locus makes the nonzero-coupling requirement explicit:

$$H = \begin{pmatrix} 0 & 1 & 0 & 0 & 0 & 0 \\ 1 & 0 & 0 & 0 & n_1 & 0 \\ 0 & 0 & 0 & 1 & 0 & 0 \\ 0 & 0 & 1 & 0 & 0 & p_2 \\ 0 & n_1 & 0 & 0 & 0 & \mu \\ 0 & 0 & 0 & p_2 & \mu & 0 \end{pmatrix}, \qquad \det H = -\mu^2. \tag{IX.7.39}$$

This is holomorphic nonsingularity, not a computed canonical physical mass. At $\mu = 0$, the family

$$N_1 = N_2 = 0, \quad p_1 = u, \quad n_2 = w, \quad M_1 = -un_1, \quad M_2 = -p_2 w \tag{IX.7.40}$$

solves the heavy equations for arbitrary u, w. These fields cannot be discarded in that order of limits.

Identifying the two surviving singlets with the electric monopoles gives the Aharony superpotential and ranks:

$$\begin{aligned} &U(2)_0 \text{ with five flavors} \quad \longleftrightarrow \quad U(3)_0 \text{ with five dual flavors,} \\ &V_- = n_1, \quad V_+ = p_2, \qquad W_m = \sum_{i,j=1}^{5} \mathcal{M}_{ij} q_i \widetilde{q}^j + V_- v_+ + V_+ v_-. \end{aligned} \tag{IX.7.41}$$

The meson map is $\mathcal{M}_{ij} \leftrightarrow Q_i \widetilde{Q}^j$ up to the chosen nonzero matching normalization. The two elementary V fields instead encode electric monopole operators. They were supplied by the remote sectors rather than by an extra flavor pair in the final theory.

The order of operations has physical content. First establish the finite-circle pair including its monopole terms. Turn on the two real backgrounds, select (IX.7.25), retain the interactions (IX.7.33), use the two abelian dual descriptions, and eliminate the six fields at nonzero μ. Only then take the low-energy decoupling limit in which the electric KK term disappears and axial symmetry is restored. For instance an electric kinematic window can be displayed with a dimensionless ϵ and fixed reference mass m_0:

$$R_3 = \frac{\epsilon^2}{m_0}, \qquad M = \frac{m_0}{\epsilon}, \qquad \frac{M}{R_3^{-1}} = \epsilon \longrightarrow 0, \qquad \eta_e \propto e^{-4\pi m_0/(g_3^2 \epsilon^2)} \longrightarrow 0. \tag{IX.7.42}$$

At fixed low energy, $E \ll M \ll R_3^{-1}$ is possible. This demonstrates an electric scale window. The magnetic elimination also requires energies below the physical remote masses, whose canonical matching is additional dynamical information. The holomorphic determinant above does not compute that matching. Setting both microscopic KK couplings to zero at the outset would omit the mechanism that produced (IX.7.41).

IX.7.6 Monopole charges and the singlet equations

The opposite signs in (IX.7.41) are measurable global charges. To compute them, define a monopole insertion by its diagonal magnetic flux $m = (m_1, \ldots, m_N)$ on a small surrounding two-sphere. For the group $U(N)$ the m_i are integers, modulo permutations. A fundamental weight e_i evaluates to m_i and an antifundamental weight $-e_i$ to $-m_i$. If a chiral multiplet Φ has axial charge A_Φ and trial R charge r_Φ, the fermion zero-mode charge formula is

$$\begin{aligned} A(T_m) &= -\frac{1}{2} \sum_{\Phi,\rho} A_\Phi |\rho(m)|, \\ R(T_m) &= \frac{1}{2} \sum_{\Phi,\rho} (1 - r_\Phi) |\rho(m)| - \sum_{\alpha > 0} |\alpha(m)|, \qquad J(T_m) = \sum_i m_i. \end{aligned} \tag{IX.7.43}$$

The last sum subtracts the vector-multiplet contribution over positive roots $\alpha = e_i - e_j$, $i < j$. Axial charges count matter modes; R charges also see the roots. This explains why a rank change modifies the R charge even when the number of flavors is unchanged.

For the electric flux $(1, 0)$, each of five flavors supplies the four evaluations $(1, 0, -1, 0)$. The positive root evaluates to 1, giving

$$\sum_{\Phi,\rho} |\rho(m)| = 5(1 + 0 + 1 + 0) = 10, \qquad \sum_{\alpha>0} |\alpha(m)| = 1. \tag{IX.7.44}$$

With $A_Q = A_{\widetilde{Q}} = 1$ and $r_Q = r_{\widetilde{Q}} = r$, the electric monopole charges are

$$(R, A, J)_{V_+} = \left[\frac{1}{2}(1 - r)10 - 1, -\frac{1}{2}10, 1\right] = (4 - 5r, -5, 1). \tag{IX.7.45}$$

Reversing the flux leaves the absolute-value sums unchanged, giving $J(V_-) = -1$ with the same R and axial charges.

The meson coupling requires $r(q) = 1 - r$ and $A(q) = -1$. For the opposite magnetic flux $(-1, 0, 0)$, each dual flavor has evaluations $(-1, 0, 0, 1, 0, 0)$. Its three positive roots evaluate to $(-1, -1, 0)$. Consequently

$$\sum_{\Phi,\rho} |\rho(m)| = 10, \qquad \sum_{\alpha>0} |\alpha(m)| = 2, \tag{IX.7.46}$$

and

$$(R, A, J)_{v_-} = \left[\frac{1}{2}r\,10 - 2, +\frac{1}{2}10, -1\right] = (5r - 2, 5, -1). \tag{IX.7.47}$$

Again flux reversal changes only J. Each cross coupling therefore has

$$(R, A, J)_{V_+ v_-} = (R, A, J)_{V_- v_+} = (2, 0, 0). \tag{IX.7.48}$$

For general $N_f > N_c$ the same sums read

$$\begin{aligned} R(V_\pm) &= N_f(1 - r) - N_c + 1, \qquad A(V_\pm) = -N_f, \\ R(v_\pm) &= N_f r - (N_f - N_c) + 1, \quad A(v_\pm) = N_f. \end{aligned} \tag{IX.7.49}$$

Here r is a mixing parameter for a trial R symmetry. We have not selected the exact superconformal R symmetry by an extremization. More basically, neutrality of the monomials would also hold if either coefficient were zero. It confirms their charges but cannot replace the instanton and remote-sector arguments for their presence.

The elementary singlet equations supply a sharper consequence. Give the two couplings arbitrary nonzero constants c_-, c_+ and vary only the elementary V_-, V_+ fields:

$$\partial_{V_-} W = c_- v_+ = 0, \qquad \partial_{V_+} W = c_+ v_- = 0. \tag{IX.7.50}$$

In the polynomial algebra used to describe this constraint, the ideal is

$$I = \langle c_- v_+, c_+ v_- \rangle = \langle v_+, v_- \rangle, \qquad \mathbb{C}[v_+, v_-]/I \simeq \mathbb{C}. \tag{IX.7.51}$$

Deleting $V_- v_+$ changes the constraint to

$$I_{c_-=0} = \langle v_- \rangle, \qquad \mathbb{C}[v_+, v_-]/I_{c_-=0} \simeq \mathbb{C}[v_+]. \tag{IX.7.52}$$

The point $(v_+, v_-) = (3, 0)$ is excluded by (IX.7.50) but allowed by the second ideal. Nonzero rescalings leave the ideal unchanged; deletion changes it. This elementary computation is a statement about the singlet constraints on gauge-sector operators. It is not the full quantum moduli space. In particular, $v_\pm$ are composite monopole operators, so varying them as independent elementary fields to infer $V_\pm = 0$ would discard gauge dynamics. Electric monopole branches can still be encoded by the singlets. The confining case $N_f = N_c$ has a different description and cannot be obtained by treating the generic formula as a $U(0)$ gauge theory with the same superpotential.

IX.7.7 Signed masses, Chern–Simons terms and BF couplings

A massive fermion in three dimensions distinguishes positive from negative real mass. The parity-odd part of its determinant induces a gauge Chern–Simons term. Fix the spacetime orientation $dX^0 dX^1 dX^2$ and use a common spin-regulator prescription on both sides of a proposed duality. For dynamical or background abelian connections A_a, write the action with a symmetric matrix K as

$$S_K = \frac{1}{4\pi} \int K_{ab} A_a \wedge dA_b, \qquad K_{ab} = K_{ba}. \tag{IX.7.53}$$

For $a \neq b$, integration by parts equates the two off-diagonal terms, so the mixed, or BF, term has coefficient

$$S_{ab} = \frac{K_{ab}}{2\pi} \int A_a \wedge dA_b. \tag{IX.7.54}$$

This factor of two must be fixed before comparing a matrix entry with a printed BF coefficient.

One charged complex two-component fermion of signed mass m and charge vector q contributes, in the declared prescription,

$$\Delta K_{ab} = \frac{1}{2} \operatorname{sgn}(m) q_a q_b. \tag{IX.7.55}$$

The integer counterterm at the massless point is part of the regulator choice. For a charge-one abelian factor the parity-anomaly quantization condition reads

$$k + \frac{1}{2} \sum_{\text{chirals}} q^2 \in \mathbb{Z}. \tag{IX.7.56}$$

A vectorlike pair permits integer k; a single charge-one chiral shifts the allowed bare value by a half-integer. A superpotential mass pairing two chirals is not the same deformation as two real masses with equal sign.

Now retain both the central gauge connection a and an axial background A_A. The charges of a vectorlike pair are $(1,1)$ and $(-1,1)$. Including N colors and writing the two mass signs as $s_Q, s_{\widetilde{Q}}$, the two outer products give

$$\begin{aligned}\Delta K_{(a,A)} &= \frac{N}{2}\left[s_Q\begin{pmatrix}1\\1\end{pmatrix}(1\ \ 1)+s_{\widetilde{Q}}\begin{pmatrix}-1\\1\end{pmatrix}(-1\ \ 1)\right]\\ &= \frac{N}{2}\begin{pmatrix}s_Q+s_{\widetilde{Q}} & s_Q-s_{\widetilde{Q}}\\ s_Q-s_{\widetilde{Q}} & s_Q+s_{\widetilde{Q}}\end{pmatrix}.\end{aligned} \tag{IX.7.57}$$

The difference between axial and vector mass deformations is now explicit:

$(s_Q, s_{\widetilde{Q}})$	$\Delta K_{(a,A)}$	Δk_{SU}
$(+,+)$	$\mathrm{diag}(N,N)$	1
$(-,-)$	$-\mathrm{diag}(N,N)$	-1
$(+,-)$	$\begin{pmatrix}0 & N\\ N & 0\end{pmatrix}$	0
$(-,+)$	$\begin{pmatrix}0 & -N\\ -N & 0\end{pmatrix}$	0

(IX.7.58)

For $N=2$, opposite masses give $K_{aA}=2$ even though the gauge level shift is zero. Thus absence of gauge CS does not imply absence of a threshold interaction. The supersymmetric BF completion also ties a background scalar to an FI source. In the two-flavor Aharony deformation, the two displaced pairs have opposite BF shifts and cancel; in the original flavor chart their opposite same-sign gauge shifts cancel instead, with the background generators relabeled along with the fields.

To generate nonzero gauge level, start with an Aharony pair with $F = N_f + |k|$ flavors and give $|k|$ pairs an axial real mass of sign s. The dual quarks have opposite axial charges. On the corresponding branch, the electric and magnetic fermion masses have signs s and $-s$. Summing their Cartan charge outer products gives

$$\Delta K_e = s|k| I_{N_c}, \qquad \Delta K_m = -s|k| I_{F-N_c}, \qquad (k_e, k_m) = (s|k|, -s|k|). \tag{IX.7.59}$$

For $N_c = 2, N_f = 3, |k| = 2$, two positive electric pairs and two negative magnetic pairs produce

s	k_e	k_m	$K_{e,aa}$	$K_{m,aa}$
1	2	-2	4	-6
-1	-2	2	-4	6

(IX.7.60)

The center levels follow by evaluating the Cartan form on the all-ones vector, not by assigning a single color's level to the whole center. The monopole singlets of the parent have axial charge $-F$ and acquire real masses in this flow. They are removed at its low-energy endpoint. At nonzero gauge level, a bare monopole also carries induced electric charge and generally requires dressing; the Aharony elementary-singlet couplings are not retained unchanged.

These are supersymmetric bare levels of the effective theory after the specified matter fields are removed. Integrating out a vector-multiplet gaugino is an additional

operation. To see its distinct effect, sum the roots of a complex adjoint fermion of mass sign s_λ:

$$\Delta K_{\rm adj} = \frac{s_\lambda}{2}\sum_{i\neq j}(e_i-e_j)(e_i-e_j)^T = s_\lambda\big(NI_N - \mathbf{u}\mathbf{u}^T\big), \quad \mathbf{u}=(1,\dots,1)^T. \quad \text{(IX.7.61)}$$

On traceless vectors this shifts the nonabelian level by $s_\lambda N$; on the central vector it vanishes. At $N=3$ the matrix is

$$\Delta K_{\rm adj} = s_\lambda \begin{pmatrix} 2 & -1 & -1 \\ -1 & 2 & -1 \\ -1 & -1 & 2 \end{pmatrix}, \qquad \Delta K_{\rm adj}\mathbf{u} = 0. \qquad \text{(IX.7.62)}$$

Calling the resulting bosonic theory a single-trace $U(N)_{k+s_\lambda N}$ would wrongly shift its center as well. The brane rank formula below uses the supersymmetric k in (IX.7.59). The selected gauge and axial matrices do not establish a complete equality of flavor, R or gravitational contact terms.

IX.7.8 The resolved fivebrane move and the GK rank

The rank must be obtained from an actual brane move. In IIB combine $|k|$ D5 constituents with NS$'$. For positive k this is the source $(1,k)$ fivebrane in NS/D charge order. In the D/NS order used here its charge is $(k,1)$, and the tangent directions are

$$012[3,7]_\theta 89, \qquad [3,7]_\theta = \cos\theta\,\partial_3 + \sin\theta\,\partial_7, \qquad \tan\theta = g_s^B k \qquad \text{(IX.7.63)}$$

at zero IIB axion. This is a one-plane rotation with fixed $8,9$ tangents. With the other NS fivebrane and the suspended D3s it preserves four real supercharges. The sign-reversed configuration reverses the D5 charge and geometric angle together.

Resolve the bound state back into NS$'$ and its D5 constituents. For the example $(N_c,N_f,k)=(2,3,2)$ there are five resolved D5 labels:

$$F_0,F_1,F_2,C_0,C_1, \qquad F = N_f + |k| = 5. \qquad \text{(IX.7.64)}$$

The F_i will remain flavor branes. The C_i will recombine with NS$'$ at the end. Initially all five lie between NS and NS$'$, and there are two color D3s from NS to NS$'$.

For each resolved fivebrane b, use the linking number of Chapter 1, where "opposite" means the other fivebrane species:

$$\ell_b = \frac{1}{2}(n_{{\rm opp},R} - n_{{\rm opp},L}) + n_{3,L} - n_{3,R}. \qquad \text{(IX.7.65)}$$

The initial NS has all F D5s to the right and N_c D3 endpoints to the right. Thus

$$\ell_{\rm NS} = \frac{F}{2} - N_c, \qquad \ell_{\rm NS'} = -\frac{F}{2} + N_c, \qquad \ell_{F_i} = \ell_{C_i} = 0. \qquad \text{(IX.7.66)}$$

For the five-label example these values are $1/2, -1/2$ and five zeros. Each D5 initially has an NS on either side and no D3 endpoint, explaining its zero individually.

Move NS across all five D5s and create one D5–NS D3 at every crossing. After j crossings the half-count on NS is $F/2 - j$, and it has j new left endpoints as well as N_c right endpoints:

$$\ell_{\rm NS}^{(j)} = \left(\frac{F}{2} - j\right) + j - N_c = \frac{F}{2} - N_c. \tag{IX.7.67}$$

A crossed D5 has both NS branes to the right and one D3 endpoint to the right, hence $\ell_{D5} = 1 - 1 = 0$. The creation rule and linking conservation are separate ingredients: the former specifies an allowed physical process, while the latter constrains its endpoints.

Reconnect N_c created segments with the original color intervals. Each such reconnection replaces D5–NS and NS–NS$'$ by D5–NS$'$. It removes one left and one right endpoint from NS, conserving its linking number. There remain $F - N_c$ segments ending on NS from the left. Exchange the NS order by a transverse displacement and split each passing D5–NS segment at NS$'$. The result contains

$$F \text{ D5–NS}' \text{ flavor segments}, \qquad F - N_c \text{ NS}'\text{–NS color segments}. \tag{IX.7.68}$$

The final half-count on NS is $-F/2$, and its color endpoints lie to the left, so its linking number is again

$$\ell_{\rm NS}^{\rm final} = -\frac{F}{2} + (F - N_c) = \frac{F}{2} - N_c. \tag{IX.7.69}$$

On NS$'$, the F flavor endpoints contribute from the left and $F - N_c$ color endpoints from the right. Its value is $-F/2 + F - (F - N_c) = -F/2 + N_c$. Every D5 still has one right endpoint. The endpoint calculation therefore conserves all individual linking numbers, not merely their sum.

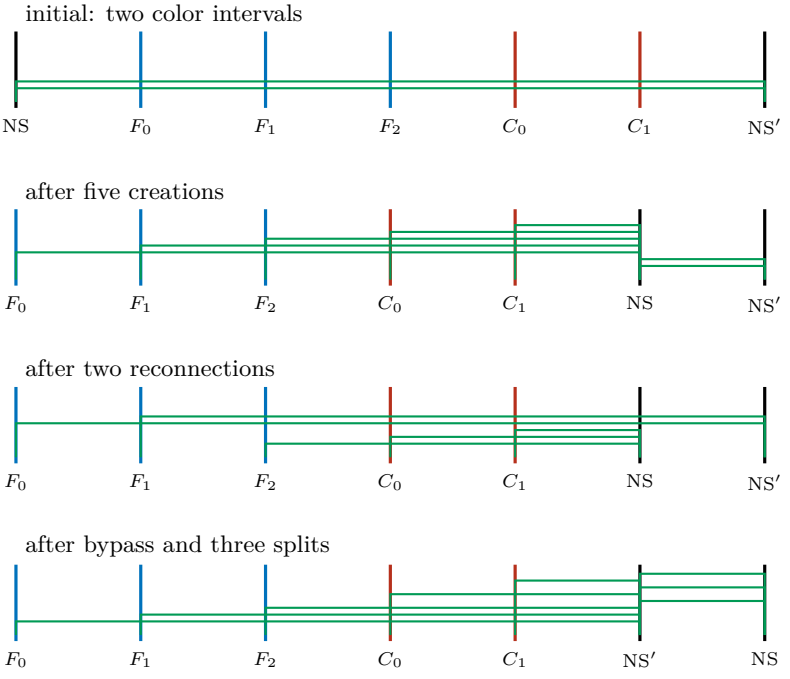


Figure IX.7.4: Resolved endpoint graphs for two colors and five D5 labels. Multiple D3s are drawn as separated tracks solely for legibility. Crossing creates five segments, reconnection uses two, and splitting at NS′ leaves three color intervals. The two red C constituents subsequently recombine with NS′, leaving the three blue flavor labels. The projected horizontal coordinate orders branes along X^6.

After recombination the two C constituents no longer count as external flavors. The final color count is unchanged. This yields

$$\widetilde{N}_c = N_f + |k| - N_c = 3 + 2 - 2 = 3. \tag{IX.7.70}$$

There are five positive creations, two reconnections and three splits. For $k = -2$ there are again five slots and three magnetic colors. Treating k as a signed number of D5 constituents would incorrectly give a negative creation capacity. The capacity condition for this supersymmetric configuration is

$$N_c \leq N_f + |k|. \tag{IX.7.71}$$

For $(N_c, N_f, |k|) = (3, 0, 2)$ it fails. Equality leaves no magnetic color segment and requires separate analysis of the infrared theory.

Combining the segment count with the independently obtained signed levels of (IX.7.59) gives the GK pair in a common spacetime orientation:

$$U(N_c)_k \longleftrightarrow U(N_f + |k| - N_c)_{-k}, \qquad W_m = \sum_{i,j=1}^{N_f} \mathcal{M}_{ij} q_i \widetilde{q}^j. \tag{IX.7.72}$$

The original brane presentation labels both descriptions by a positive k. The signed mass flow fixes how those labels are translated into the same orientation used in (IX.7.72); the minus sign is not obtained by quoting the positive labels as if they already contained it. The passage through the brane move uses infrared continuity in the chosen supersymmetric chamber. Segment conservation alone cannot prove that dynamical premise. Setting $k = 0$ in the displayed matter content also does not restore Aharony duality: the monopole sectors and their singlet couplings must be restored by the earlier finite-circle construction.

IX.7.9 The central level and the primitive magnetic flux

The symbol $U(N)_k$ includes a global-form convention. Separate the matrix connection locally into a traceless part and a central part,

$$A = A_{\mathrm{su}} + aI_N, \qquad \operatorname{Tr} A_{\mathrm{su}} = 0, \tag{IX.7.73}$$

so a fundamental has unit charge under a. To determine its level, first expand the quadratic part of the single-trace CS form:

$$\operatorname{Tr}(A \wedge dA) = \operatorname{Tr}(A_{\mathrm{su}} \wedge dA_{\mathrm{su}}) + Na \wedge da. \tag{IX.7.74}$$

The two mixed bilinear terms vanish by tracelessness. In the cubic part, terms with two central one-forms vanish because $a \wedge a = 0$. Terms linear in a contain $\operatorname{Tr}(A_{\mathrm{su}} \wedge A_{\mathrm{su}})$, which vanishes because the trace of a commutator is zero. For the connection-form notation $\omega_3(A) = \operatorname{Tr}(A \wedge dA + \frac{2}{3} A \wedge A \wedge A)$, this establishes

$$\omega_3(A) = \omega_3(A_{\mathrm{su}}) + Na \wedge da, \qquad k_a = Nk. \tag{IX.7.75}$$

The conventional factors of i when using Hermitian matrix connections do not change this trace multiplicity. For the electric $U(2)_2$ theory, the central coefficient is four; for magnetic $U(3)_{-2}$ it is minus six, as in the direct fermion calculation.

The group map $(g, z) \mapsto zg$ from $SU(N) \times U(1)$ to $U(N)$ has kernel

$$\ker(g, z \mapsto zg) = \left\{ \left(e^{2\pi i j/N} I_N, e^{-2\pi i j/N} \right) : j \in \mathbb{Z}_N \right\}. \tag{IX.7.76}$$

Therefore the notation for the single-trace theory is

$$U(N)_k = \left[SU(N)_k \times U(1)_{Nk} \right] / \mathbb{Z}_N. \tag{IX.7.77}$$

This denotes the correlated quotient and levels, not independent gauge bundles for a freely factorized product. In particular, the locally defined a need not carry an integer flux by itself.

Let $m_i \in \mathbb{Z}$ be the diagonal cocharacter of a $U(N)$ monopole. Writing the flux in traceless and central pieces gives

$$m_i = \left(m_i - \frac{\sum_j m_j}{N} \right) + \frac{\sum_j m_j}{N}, \qquad J = \frac{1}{2\pi} \int_{S^2} \operatorname{Tr} F = \sum_i m_i. \tag{IX.7.78}$$

The central flux and the coupling to a topological background B are

$$\frac{1}{2\pi}\int_{S^2} da = \frac{J}{N}, \qquad S_B = \frac{1}{2\pi}\int B \wedge d\,\mathrm{Tr}\, A = \frac{N}{2\pi}\int B \wedge da. \tag{IX.7.79}$$

Thus a primitive topological charge of one is compatible with a central flux $1/N$. The factor N in the background coupling is necessary.

For $U(3)$ the primitive diagonal flux provides a concrete example:

$$\mathrm{diag}(1,0,0) = \mathrm{diag}(2/3,-1/3,-1/3) + \tfrac{1}{3}I_3, \qquad J = 1. \tag{IX.7.80}$$

The lifted transition functions separately close only up to center elements,

$$e^{2\pi i\,\mathrm{diag}(2/3,-1/3,-1/3)} = e^{-2\pi i/3}I_3, \qquad e^{2\pi i/3}I_3, \tag{IX.7.81}$$

whose product is the identity in $U(3)$. By contrast the pure central unit flux is $\mathrm{diag}(1,1,1)$ and has $J = 3$. Replacing the quotient by $SU(3)\times U(1)$ with independent integer central flux would lose the primitive monopoles used in the Aharony charge calculation. Other global forms and the classification of genuine line operators require their own choices; they do not follow from the local Lie algebra alone.

IX.7.10 The suspension circle and its supercharges

We now change the geometry rather than continue the small-R_3 flow. The D3 suspension direction X^6 becomes a circle. There are two ordered intervals between two fivebranes on that circle:

$$X^6 \sim X^6 + 2\pi R_6, \qquad \mathrm{D3} = 0126. \tag{IX.7.82}$$

The first fivebrane is NS along 012345. The second has book charge $(k,1)$, or source charge $(1,k)$ in NS/D order. Its tangent geometry is now an equal rotation in three planes,

$$012[3,7]_\theta[4,8]_\theta[5,9]_\theta, \qquad \theta = \arg\tau - \arg(k+\tau), \qquad \tau = \chi + i/g_s^B. \tag{IX.7.83}$$

At $\chi = 0$, finite positive g_s^B and nonzero finite integer k, take the continuous branch $\tan\theta = kg_s^B$. In this regime the equal-angle construction preserves exactly six real supercharges, as stated in Aharony, Bergman, et al. (2008, §3.1). At $k = 0$ the second fivebrane is parallel to the first NS5, and the configuration instead preserves eight. The unrestricted angle formula also has special loci. For example, $k = 2$ and $\tau = -1 + i$ give $\theta = \pi/2$ and eight real supercharges in Aharony, Bergman, et al. (2008, §3.5). That locus has finite bulk coupling and does not give a weakly coupled decoupled three-dimensional $\mathcal{N} = 4$ Yang–Mills–Chern–Simons description. These counts are physical source inputs, not consequences of the charge vector or the lattice index. The distinction from the GK brane is visible in its internal tangents:

geometry	internal fivebrane tangents	real supercharges
GK interval	$[3,7]_\theta, 8, 9$	4
circular equal-angle, $\chi = 0,\ k \neq 0$	$[3,7]_\theta, [4,8]_\theta, [5,9]_\theta$	6

(IX.7.84)

Negative k reverses the D5 charge and all three angles together. A charge phase reversal at fixed tangent planes would be a different configuration. The ordered intervals NS$\to$ $(k,1)$ and $(k,1)$ $\to$NS carry the levels

$$(k_1, k_2) = (k, -k). \tag{IX.7.85}$$

This geometric starting point is the one needed for the theories developed in Volume VIII; here we derive only its circle and torus data.

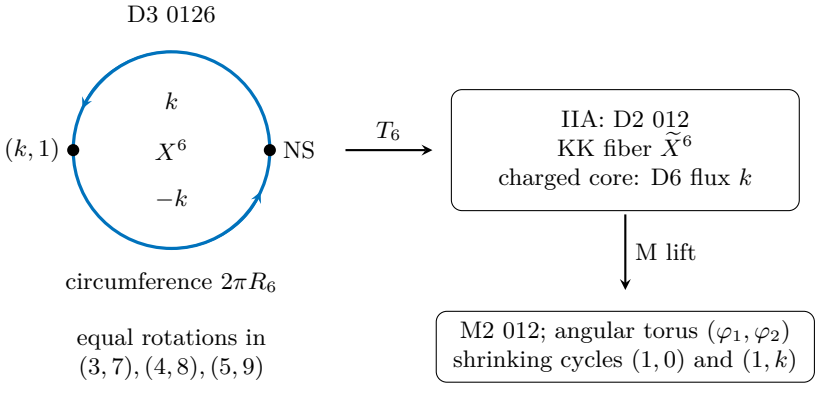


Figure IX.7.5: The compact suspension circle X^6 and its IIA and M-theory images. The two oriented arcs have levels k and $-k$. T-duality along the wrapped D3 direction gives D2s; the fivebranes give KK geometry and dissolved D6 flux. In M theory the two degeneration cycles lie in the torus with angular basis $(\widetilde{X}^6, X^{10})$. This circle is distinct from the spacetime compactification of Figure IX.7.1.

T-duality along 6 removes a wrapped direction of the D3. The radius and coupling relations are therefore

$$\mathrm{D3}_{0126} \xrightarrow{T_6} \mathrm{D2}_{012}, \qquad \widetilde{R}_6 = \frac{\alpha'}{R_6}, \qquad g_s^A = \frac{g_s^B \sqrt{\alpha'}}{R_6}. \tag{IX.7.86}$$

The NS fivebrane is transverse to 6, so it maps to a KK monopole with fiber $\widetilde{X}^6$. The charged fivebrane supplies KK geometry with k units of D6 charge carried by flux. Those units are not an instruction to add k isolated D6-branes at arbitrary positions. Upon lifting to M theory, the D2 becomes an M2 and D6 charge becomes X^{10} KK charge. The asymptotic physical radii in these IIA string-frame length units obey

$$R_{10} = g_s^A \sqrt{\alpha'} = \frac{g_s^B \alpha'}{R_6}, \qquad \varphi_1 = \frac{\widetilde{X}^6}{\widetilde{R}_6}, \quad \varphi_2 = \frac{X^{10}}{R_{10}}, \quad \varphi_i \sim \varphi_i + 2\pi. \tag{IX.7.87}$$

For $R_6 = \sqrt{\alpha'}$ and $g_s^B = 1$, both asymptotic torus radii equal $\sqrt{\alpha'}$. Their equality in this example does not identify the two angular directions or their degeneration cycles. The conversion to M-theory metric units discussed in Chapter 5 is a further Weyl rescaling; it does not change the integral angular periods.

The geometric T-dual description uses an isometry, or the corresponding zero-mode supergravity description. A localized NS5 transverse to the circle does not by itself meet the naive Buscher isometry hypothesis. Consequently these charge, flux and period relations are controlled geometric information in the stated regime. They are not an exact localized transverse T-dual background with winding corrections already removed. The M-theory lift supplies another physical duality step, beyond the local exchange of Neumann and Dirichlet directions.

IX.7.11 Primitive cycles and the finite quotient

The integral torus cycles can be computed without assuming an action on four complex coordinates. In the ordered angular basis (φ_1, φ_2) of (IX.7.87), a book fivebrane charge $(p, q) = (D, NS)$ supplies a shrinking vector (q, p). The two fivebranes in the circular geometry therefore give

$$v_1 = \begin{pmatrix} 1 \\ 0 \end{pmatrix}, \qquad v_2 = \begin{pmatrix} 1 \\ k \end{pmatrix}, \qquad L = (v_1 \; v_2) = \begin{pmatrix} 1 & 1 \\ 0 & k \end{pmatrix}. \tag{IX.7.88}$$

The circle identification is also visible in the singular terms of the toric hyperkähler harmonic matrix. Let h_i denote the scalar harmonic pole associated with the ith degeneration core. Its singular matrix contribution has the form

$$U_{\text{sing}} = h_1 v_1 v_1^T + h_2 v_2 v_2^T = h_1 \begin{pmatrix} 1 & 0 \\ 0 & 0 \end{pmatrix} + h_2 \begin{pmatrix} 1 & k \\ k & k^2 \end{pmatrix}. \tag{IX.7.89}$$

Each vector is primitive because its first component is one. The individual core thus has unit KK charge in its own shrinking-circle direction, even when the pair spans a sublattice of nonunit index.

Subtracting the first column from the second and, for negative k, reversing the second generator yields the integer normal form

$$\begin{pmatrix} 1 & 1 \\ 0 & k \end{pmatrix} \begin{pmatrix} 1 & -1 \\ 0 & 1 \end{pmatrix} = \begin{pmatrix} 1 & 0 \\ 0 & k \end{pmatrix} \sim \operatorname{diag}(1, |k|). \tag{IX.7.90}$$

The matrices used here are unimodular, so they preserve the integral lattice. For $k \neq 0$ the quotient is

$$\mathbb{Z}^2 / L\mathbb{Z}^2 \simeq \mathbb{Z}_{|k|}, \qquad [\mathbb{Z}^2 : L\mathbb{Z}^2] = |k|. \tag{IX.7.91}$$

At $k = 1$ the lattice is the whole torus lattice. At $k = 2$ the second coordinate is constrained to be even modulo the first generator, leaving two cosets. At $k = -2$ the same two cosets remain, with reversed orientation. At $k = 0$ the vectors coincide and the rank falls to one; this is not a finite quotient of order zero.

The angular periods provide a second calculation. Let the base coordinates transform by $B = L^T$, where the same matrix acts separately on each of the three base components. Angles transform contragrediently so that the base-angle pairing is preserved:

$$x' = Bx, \qquad \varphi' = B^{-T}\varphi, \qquad B = \begin{pmatrix} 1 & 0 \\ 1 & k \end{pmatrix}, \quad B^{-T} = \begin{pmatrix} 1 & -1/k \\ 0 & 1/k \end{pmatrix}. \tag{IX.7.92}$$

The two original 2π shifts then give

$$\Delta\varphi' = 2\pi(1,0), \qquad \Delta\varphi' = 2\pi(-1/k, 1/k). \tag{IX.7.93}$$

Modulo the ordinary integral periods, the second shift has order $|k|$. For $k = 2$ applying it twice gives $2\pi(-1,1)$, an ordinary period, while one application is not an ordinary period. The finite examples, including their ordered gauge levels, are

k	(k_1, k_2)	normal form	quotient	period generator/2π
1	$(1,-1)$	$(1,1)$	$\{0\}$	$(-1,1)$
2	$(2,-2)$	$(1,2)$	$\mathbb{Z}_2$	$(-\frac{1}{2},\frac{1}{2})$
-2	$(-2,2)$	$(1,2)$	$\mathbb{Z}_2$	$(\frac{1}{2},-\frac{1}{2})$

These results use angular rather than physical-length coordinates. No factor of R_{10} belongs inside the integer matrix L.

The index determines a finite group in the period lattice. It does not determine its representation on local complex coordinates or on spinors. For example the two order-two actions

$$(z_1,z_2,z_3,z_4) \mapsto (-z_1,-z_2,-z_3,-z_4), \qquad (z_1,z_2,z_3,z_4) \mapsto (-z_1,-z_2,z_3,z_4) \tag{IX.7.94}$$

have the same group order, but their fixed loci have complex dimensions zero and two. Determining the particular $\mathbb{C}^4$ quotient action requires the local geometric coordinates in addition to (IX.7.91). The full ABJM Lagrangian, moduli-space analysis and infrared supersymmetry enhancement belong to Volume VIII. General fivebrane webs and their higher-dimensional dynamics belong to Volume VII-B.

IX.7.12 What the construction determines

The interval remains the organizing physical object, but its additional data change with the question. A compact spacetime direction supplies a dual transverse circle and an affine D1 process. A real-mass deformation selects remote abelian sectors and retains their interactions until their heavy fields can be eliminated. A same-sign mass deformation instead generates CS terms and recombines fivebrane charges. Finally a compact suspension direction supplies two gauge intervals and a torus lattice after T-duality and the M-theory lift.

Take-home message of this chapter

To obtain Aharony duality, retain the finite-circle monopole physics, choose the matching mass-flow vacuum, and eliminate both remote sectors at nonzero KK coupling. To obtain GK duality, count actual created and reconnected D3s and determine the signed levels from massive fermions. For either theory, the $U(N)$ quotient fixes which monopoles are allowed. The circular bridge to Volume VIII uses X^6, equal-angle fivebranes and primitive torus cycles; its index alone supplies neither the complex quotient action nor a supersymmetry enhancement.

The protected holomorphic interactions, charge sums and lattice relations are the quantities derived here once their physical construction is specified. The passage

through strong brane motion, the instanton measure, the abelian duality and the usable remote mass window remain dynamical premises. Neither conserved linking numbers nor polynomial F-equations prove all of them. Complete background contact terms, canonical remote Kähler masses, a global quantum chiral ring and an exact localized T-dual metric would require further calculations.

IX.7.13 Three calculations to carry out

The three constructions can be tested by changing a physical ingredient whose effect is visible in an equation. Keep the reference units fixed throughout each calculation. The exercises below ask for the intermediate objects as well as the final ranks, since a correct rank can conceal an incorrect attachment or an omitted interaction.

The finite-circle mass flow. Start with the spacetime X^3 circle and the IIA rows of (IX.7.1). Determine the wrapped-direction exchange. For $\sigma/m_0 = (5, 2, -3)$, five thresholds at zero and period $12m_0$, calculate the three gaps, matter zero-mode counts and holomorphic monomials. Express each action in units of $4\pi m_0/g_3^2$ and check that their sum is the full instanton action. The zero-mode selection rule and nonzero instanton measure are physical inputs to this step.

Next use the seven-flavor masses of (IX.7.30) in units of M and the chosen magnetic eigenvalues $(1, 0, 0, 0, -1)M$. Write every signed quark and antiquark mass, identify their zero entries, and locate all 27 massless mesons before elimination. In the remote superpotential (IX.7.35), set $\mu = 2$ in holomorphic units and hold v_+, v_- as coefficients. Solve the six heavy equations, compute the Hessian determinant, and differentiate the light superpotential with respect to each surviving elementary singlet. Delete $n_1 v_+$ and then $p_2 v_-$ separately. In each case determine which of v_+, v_- is still in the singlet ideal. Explain why the $\mu = 0$, $N_f = N_c$ and $N_c = 1$ limits require different descriptions. The selected remote mirror step continues to require the NS/D exchange.

The signed GK pair. For $(N_c, N_f, k) = (2, 3, 2)$ and $(2, 3, -2)$, draw all nine resolved stages: the initial graph, five successive crossings, reconnection, bypass and final splitting. Keep the labels F_0, F_1, F_2, C_0, C_1 on their branes. Compute every individual linking number from the actual endpoints. Count the final color intervals and identify the two constituents that recombine with NS$'$. Check the negative-k example without assigning a negative number of created segments.

For each sign, sum the fermion charge outer products in the ordered basis of gauge Cartans followed by the axial background. Use two heavy pairs with electric mass sign $\operatorname{sgn}(k)$ and magnetic mass sign $-\operatorname{sgn}(k)$; the dual axial charge is minus one. Compute also the BF matrix of one electric pair with opposite masses. Project each GK matrix onto the central gauge direction, and split the magnetic flux $(1, 0, 0)$ into its central and traceless pieces. Explain why its central flux is $1/3$ while its topological charge is one. The quoted levels remain supersymmetric bare levels. At $k = 0$, identify the missing Aharony monopole sectors instead of applying the GK matter card unchanged.

The suspension-circle lattice. Begin anew with the compact X^6 direction and D3 row 0126. For $k = 1, 2, -2$, translate source NS/D charges to book D/NS charges and then to the two primitive torus cycles. Obtain the Smith form by integer column operations. Starting from $B = L^T$, derive the angle matrix by preserving the base-angle pairing and list both period columns. Check that the residual period has order $|k|$ and that $k = 0$ loses rank. Retain the exact six-real-supercharge statement only for the sourced $\chi = 0$, finite $g_s^B > 0$, $k \neq 0$ geometry; the parallel $k = 0$ case has eight. Leave the complex-coordinate action, moduli space and infrared enhancement unspecified: none is determined by the finite lattice index.

See `benchmark/tasks.json` and `benchmark/PROTOCOL.md` for the public structured-answer format. The three exercises use exact rational entries, finite labeled graphs and polynomial coefficient lists. Equivalent rational fractions, rearranged polynomial terms and reordered undirected edge lists describe the same answers. These calculations test consequences of the physical premises used above.

Status and sources

The calculations use the stated fundamental trace, brane tensions and linking charges. The remote and Chern–Simons comparisons use the conditional duality routes described below.

physical-worldsheet derivation in the untwisted stringThe local T3 dictionary is source-supported here. Its physical primary classification is left unassigned because this chapter contains no local untwisted-worldsheet derivation. Algebraic consequences have separate mathematical records with stated domains. The same distinction applies to the sourced six-supercharge count and to the physical identification of shrinking cycles.

IX.7.2, finite spacetime reduction. The T3 premise is sourced. Equations (IX.7.1)–(IX.7.8). Amariti et al. (2015), arXiv:1501.06571v2, §2.2 pp. 5–7, Tables 2/3 and (2.4)–(2.5), supplies the finite-circle brane map. Aharony, Razamat, et al. (2013), arXiv:1305.3924v2, §2.1 pp. 11–12, footnote 4 and (2.4), fixes the trace/action normalization; §4.2 pp. 38–41 supplies weak baryon gauging and the abelian qualification. The DBI and radius algebra are local deductions. the finite check, the symbolic calculation and the consistency check test the wrapped directions and scales. Figure IX.7.1 is a local schematic drawing of these rows.

IX.7.3, ordinary and affine terms. The half-BPS holomorphic instanton prescription is sourced. Equations (IX.7.9)–(IX.7.21). ARSW v2 §2.2 pp. 13–15, (2.5)–(2.11), supplies the zero-mode selection and finite-circle instanton premises; Braneology v2 §2.2, (2.4)–(2.5), Fig. 1, supplies the Euclidean D1 realization. The monomial convention is translated by $\Sigma_{\mathrm{source},i} = -Z_i$; the D1 tension calculation restores dimensionful coefficients rather than equating suppressed source constants to the book convention. the finite check and the symbolic calculation test gaps, action and stationary equations. Figure IX.7.2 uses the actual $(5, 2, -3)$, period-12 example. ARSW §4.1–4.2 and Aharony (1997), hep-th/9703215v1, §3 pp. 5–7, qualify the residual $U(1)$ branch and the $N_c > 1$ restriction. No path-integral determinant is calculated.

IX.7.4, selected mass-flow vacuum. [MATH]; the derivation, equations (IX.7.22)– (IX.7.32). Braneology v2 §2.1 pp. 4–5, (2.1)–(2.3), and §3.2 pp. 10–11, Fig. 4, supply the mass flow and separated vacuum. The off-diagonal flips, signed mass table and antiflavor permutation are explicit deductions; the finite check, the symbolic calculation verify both charts and the physical separation mass. Chapter 1's flavor-position marker and the conjugate magnetic scalar chart are related by the field and charge translation stated above. Figure IX.7.3 uses the $1 + 3 + 1$ vacuum and labels its vertical coordinate explicitly. Vacuum uniqueness is not claimed.

IX.7.5, remote mirror and elimination. The protected-interaction and conditional-duality premises are sourced. Equations (IX.7.33)–(IX.7.42). Braneology v2 §3.2 (3.1)–(3.2), p. 11, supplies the inherited interactions and remote brane-mirror replacement; ARSW v2 §4.4 pp. 43–44, (4.4)–(4.5), is separate field-theory support for the one-flavor XYZ object. This route requires nonperturbative IIB S-duality for the selected NS/D route, together with A-001 creation, A-002 continuity and P T3. The exchange is anchored also by Hanany and Witten (1997), hep-th/9611230v3 §2 (2.5); Chapter 2 supplies the frame distinction. The six-field solution and Hessian are the symbolic calculation. They require nonzero renormalized μ and an appropriate physical low-energy mass window; canonical Kähler masses are not computed. Aharony v1 (3.1)–(3.3) and ARSW v2 (4.3) identify the resulting infrared pair. These routes share premises and receive no independence upgrade.

IX.7.6, charges and operator constraints. [MATH]; the derivation and equations (IX.7.43)–(IX.7.52). Aharony v1 §3 (3.1)–(3.3) and ARSW v2 §4.1 (4.3) supply the operator dictionary and cross pairing. the finite check, the symbolic calculation give the weight/root sums. the

finite check test the changed singlet ideal when either coupling is deleted, with a nonzero point on the newly allowed slice. the finite check bind the actual exported charges and symbolic coupling support; they are integration contracts, not extra independent physics results. The trial R algebra does not determine the exact superconformal R charge; the singlet ideal is not the complete quantum moduli space.

IX.7.7, signed CS and BF thresholds. The fermion threshold and duality premises are sourced. Equations (IX.7.53)–(IX.7.62). ARSW v2 §2.1 p. 12 after (2.4) fixes the half-Dirac shift. Braneology v2 §4.1 p. 12 explicitly gives the opposite signed magnetic level; this is the translation source, not a claim that the original GK positive labels already print $-k$. the finite check22p/m, the symbolic calculation and the consistency check test Cartan/axial outer products, BF normalization and signed examples. The adjoint root sum is kept separate from the quoted supersymmetric bare k. No full background contact-term identity is inferred.

IX.7.8, resolved GK move. The geometric creation and continuity premises are sourced. Equations (IX.7.63)–(IX.7.72). Giveon and Kutasov (2009), arXiv:0808.0360v1, §2 pp. 2–4, (2.4), and §3 pp. 4–7, Fig. 3 and (3.1)–(3.2), supply the positive-label geometry, capacity and move. The resolved linking convention is the one stated in Chapter 1, with the parent rotated construction in Elitzur et al. (1997), hep-th/9702014v2 §3 pp. 3–5. The route uses brane creation and infrared-continuation assumptions. The endpoint calculation conserves individual linking numbers and counts final color edges. The negative example has $|k|$ constituents and correlated parity reversal. Figure IX.7.4 is generated from the delivered endpoint graphs. Continuity and the supersymmetric capacity bound remain physical premises; the arithmetic does not prove them.

IX.7.9, global form. [MATH]; the derivation and equations (IX.7.73)– (IX.7.81). ARSW v2 §4.1 pp. 35–38, (4.1)–(4.3), anchors the $U(N)$ quotient and minimal monopoles. The central coefficient is derived by expanding the trace, while the cocharacter calculation explains its fractional central flux. the finite check, the symbolic calculation and the consistency check support the $U(3)$ example. The compact level conventions apply to this example. Alternative global forms and genuine lines require separate data.

IX.7.10–11, bounded circular interface. The six-supercharge count and duality inputs are sourced. The lattice calculation is conditional [MATH]. Equations (IX.7.82)–(IX.7.94). Aharony, Bergman, et al. (2008), arXiv:0806.1218v4, §3.1 pp. 15–18, (3.1) and Fig. 4, supplies the equal-angle six-real-Q statement for $\chi = 0$, $k \neq 0$ and ordered levels. Its §3.5 p. 21, (3.2), and Appendix B p. 35, (B.13)–(B.14), identify an orthogonal eight-Q locus at $k = 2$, $\tau = -1 + i$ and explain the bulk decoupling limit. It is source-only supersymmetry evidence; no new native projector or Majorana derivation is asserted. Its §3.2 p. 19 supplies T6, KK/flux and M-lift; Appendix B pp. 32–35, (B.7)–(B.12), supplies the primitive torus and period map. the finite check, the symbolic calculation and the consistency check test the finite lattice and orientation examples. The local table is generated from the validated evidence and live interface calculation. Figure IX.7.5 is schematic geometry, not a localized Buscher solution. The Volume VIII route uses nonperturbative IIB S-duality, perturbative T-duality along the interval circle and the nonperturbative M-theory lift. Neither the lattice index nor this chapter establishes the $\mathbb{C}^4$ action, ABJM moduli or enhancement; those arguments remain in Volume VIII.

Finite evidence and remaining work. The examples are Aharony $(2, 5)$, Giveon–Kutasov $(2, 3, \pm 2)$ and the circular interface at $k = 1, 2, -2$. No D1 determinant, canonical remote mass matching, full quantum chiral ring, complete contact matching, native six-Q projector or exact localized transverse-duality background was calculated.

References

Aharony, O. (1997). "IR duality in d = 3 N=2 supersymmetric USp(2N(c)) and U(N(c)) gauge theories". In: *Phys. Lett. B* 404, pp. 71–76. DOI: 10.1016/S0370-2693(97)00530-3. arXiv: hep-th/9703215.

Aharony, O., O. Bergman, et al. (2008). "N=6 superconformal Chern-Simons-matter theories, M2-branes and their gravity duals". In: *JHEP* 10, p. 091. DOI: 10.1088/1126-6708/2008/10/091. arXiv: 0806.1218 [hep-th].

Aharony, O., S. S. Razamat, et al. (2013). "3d dualities from 4d dualities". In: *JHEP* 07, p. 149. DOI: 10.1007/JHEP07(2013)149. arXiv: 1305.3924 [hep-th].

Amariti, A. et al. (2015). "The braneology of 3D dualities". In: *J. Phys. A* 48.26, p. 265401. DOI: 10.1088/1751-8113/48/26/265401. arXiv: 1501.06571 [hep-th].

Elitzur, S., A. Giveon, and D. Kutasov (1997). "Branes and N=1 duality in string theory". In: *Phys. Lett. B* 400, pp. 269–274. DOI: 10.1016/S0370-2693(97)00375-4. arXiv: hep-th/9702014.

Giveon, A. and D. Kutasov (2009). "Seiberg Duality in Chern-Simons Theory". In: *Nucl. Phys. B* 812, pp. 1–11. DOI: 10.1016/j.nuclphysb.2008.09.045. arXiv: 0808.0360 [hep-th].

Hanany, A. and E. Witten (1997). "Type IIB superstrings, BPS monopoles, and three-dimensional gauge dynamics". In: *Nucl. Phys. B* 492, pp. 152–190. DOI: 10.1016/S0550-3213(97)00157-0. arXiv: hep-th/9611230.

Chapter IX.8

Atlas of Hanany–Witten constructions

IX.8.1 Choosing a construction

A brane picture becomes useful when we know what to ask of it. An interval can reveal a gauge group and its matter, a motion of fivebranes can suggest a second infrared description, and an M5 curve can encode protected low-energy information. These are different uses of a construction. A successful count of suspended branes does not by itself determine a moduli space metric, just as a curve equation does not by itself specify the allowed line operators of a gauge theory.

This chapter collects the worked constructions of Chapters 1–7 into a finite atlas. Its purpose is to help us choose a route and carry the appropriate qualifications to the answer. We will reconstruct several rows rather than repeat every brane motion. The examples are small enough that the relation between a diagram, a representation, and an algebraic answer remains visible. The atlas covers three-dimensional theories with eight or four real supercharges, four-dimensional theories with eight or four, half-BPS boundaries, and two suspension-circle interfaces whose geometry preserves six real supercharges at $\chi = 0$ and finite positive string coupling.

There are five kinds of entry. A *setup* specifies a construction and the quantities extracted from it. A *dual pair* relates two descriptions under the physical assumptions of the corresponding chapter. A *branch* entry selects a protected algebra rather than a new theory. A *boundary* entry describes a condition on a four-dimensional half-space, possibly with an intrinsic three-dimensional theory. An *interface* here supplies the limited geometric information needed to connect descriptions; it is not a completed construction of every theory one might associate with that geometry.

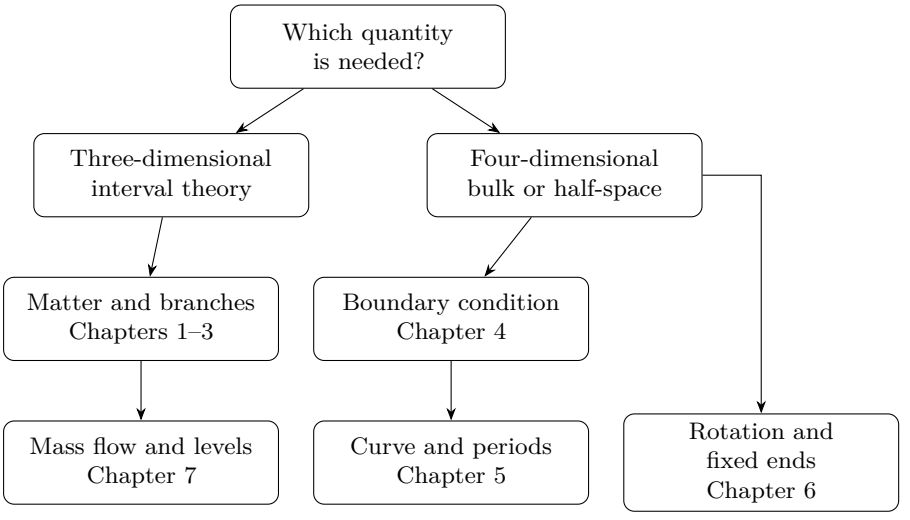


Figure IX.8.1: Routes through the worked constructions. The arrows organize a reader's choices, not a sequence of dualities. Choose a quantity before choosing a brane manipulation.

For example, start with three-dimensional $U(1)$ gauge theory with three hypermultiplets. Its setup entry answers the matter question. Its mirror entry gives a two-node abelian quiver. Its branch entry gives a complex surface at one specified mass deformation. These are three views of the same example, not three independent constructions of a duality. Conversely, the two-node framed $U(1) \times U(2)$ interval below is a genuinely different matter configuration. It must not be substituted for the abelian mirror merely because both diagrams have two circles.

The same care applies across dimensions. The pure $SU(2)$ M5 curve and the rank-two fixed-end MQCD curve answer different questions and preserve different supersymmetry. The rotated $U(3)$ brane construction and the $SU(3)$ anomaly comparison share useful rank arithmetic, but do not share a gauge-group global form. The two circles used in Chapter 7 also have different physical roles. Figure IX.8.1 therefore gives a selection procedure, not a universal path through all rows.

The short row labels in the tables allow us to refer to a particular example without repeating its description. There are exactly twenty-two entries: eight setups, seven dual pairs, two branch views, three boundary views, and two interfaces. No completeness claim is made beyond this finite selection. In particular, arbitrary quivers, general Nahm partitions, flavored M5 curves, and M2-probe dynamics are not supplied by interpolating between these rows.

IX.8.2 Eight supercharges on an interval

The interval construction of Chapter 1 translates D3 segments into gauge factors and D5 intersections into hypermultiplets. In the standard IIB frame, the D3 occupies 0126,

the NS5 occupies 012345, and the D5 occupies 012789. The finite x^6 direction leaves a three-dimensional field theory on 012. The compatible supersymmetry conditions leave eight real supercharges. We first use this dictionary to distinguish a matter count from a branch dimension.

IX.8.2.1 Setups and their mirror views

For a single $U(1)$ node with N_f charge-one hypermultiplets, the unconstrained hypermultiplet space has quaternionic dimension N_f. On a locus where the gauge action is free, imposing the three moment maps and dividing by $U(1)$ removes four real dimensions. Thus

$$\dim_{\mathbb{H}} \mathcal{H} = N_f - 1, \qquad \dim_{\mathbb{H}} \mathcal{C} = \operatorname{rank} U(1) = 1. \tag{IX.8.1}$$

The second equality counts the Coulomb-branch quaternionic dimension, not its metric. For $N_f = 1$ the Higgs branch is a point, whereas the mirror is a free hypermultiplet. A free hypermultiplet has a Higgs branch of quaternionic dimension one and no gauge Coulomb branch. This is the first instance of the branch exchange in Chapter 2.

Table IX.8.1: Electric interval setups. All are three-dimensional with eight real supercharges; dimensions are quaternionic.

Row	Gauge group	N_f	$\dim_{\mathbb{H}} \mathcal{H}$	$\dim_{\mathbb{H}} \mathcal{C}$
S1	U(1)	1	0	1
S2	U(1)	2	1	1
S3	U(1)	3	2	1

Table IX.8.2: Mirror-pair views of S1–S3. The ordered pair is $(\dim_{\mathbb{H}} \mathcal{H}, \dim_{\mathbb{H}} \mathcal{C})$; an empty flavor vector means no gauge node.

Row	N_f	Mirror	Framing	Electric	Mirror
M1	1	1 free hyper	()	$(0,1)$	$(1,0)$
M2	2	$U(1)$	(2)	$(1,1)$	$(1,1)$
M3	3	$U(1) \times U(1)$	$(1,1)$	$(2,1)$	$(1,2)$

For three flavors the mirror has two $U(1)$ nodes, one hypermultiplet between them, and one fundamental at each end. The three charge columns can be oriented as

$$Q = \begin{pmatrix} -1 & 1 & 0 \\ 0 & -1 & 1 \end{pmatrix}, \qquad Q \begin{pmatrix} 1 \\ 1 \\ 1 \end{pmatrix} = 0. \tag{IX.8.2}$$

All three representations have quaternionic dimension one. There are two gauge generators, and the charge matrix has full row rank. At a regular quotient point the mirror dimensions are therefore

$$\dim_{\mathbb{H}} \mathcal{H}_{\mathrm{mir}} = 3 - 2 = 1, \qquad \dim_{\mathbb{H}} \mathcal{C}_{\mathrm{mir}} = 1 + 1 = 2. \tag{IX.8.3}$$

The ordered pair $(1,2)$ reverses the electric pair $(2,1)$. For two flavors the same reasoning gives one gauge node and two hypers, with pair $(1,1)$. The dimension exchange is a necessary consistency test of mirror symmetry. It does not derive the nonperturbative IIB transformation or the infrared continuation of the brane path. Those physical inputs are explained in Chapter 2 and remain inputs here.

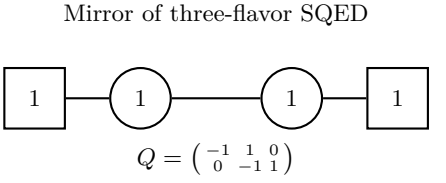


Figure IX.8.2: Two different two-node quivers. The upper graph is the mirror of three-flavor $U(1)$ SQED. The lower graph is the intrinsic $T[SU(3)]$ boundary theory. Ranks and framing, not the number of drawn circles, determine their representation dimensions.

IX.8.2.2 Reconstructing the asymmetric surface

To obtain more than a dimension, select one complex structure and the pure-branch comparison of Chapter 3. The electric FI triplet and the primitive mirror mass triplet both vanish. The real-mass components and mirror real FI levels obey $m_{R,i} = \zeta'_{R,j} = 0$; their complex components can remain nonzero. Use algebraic mirror coordinates $(q_i, \widetilde{q}_i)$, $i = 1,2,3$, related to canonical fields by

$$(q_i, \widetilde{q}_i) = \sqrt{2\pi}\,(q_i^{\mathrm{can}}, \widetilde{q}_i^{\mathrm{can}}), \qquad \eta_j = 2\pi\zeta'_{C,j}. \tag{IX.8.4}$$

Their charges are opposite within each pair. This rescaling fixes the algebraic units, not a canonically normalized metric. At $\tau = i$, the identification $\eta_j = m_j - m_{j+1}$ retains the leading classical displacement/FI matching of Chapters 1–3. Put $t_i = q_i\widetilde{q}_i$. The complex moment maps for (IX.8.2) then become

$$-t_1 + t_2 = \eta_1, \qquad -t_2 + t_3 = \eta_2. \tag{IX.8.5}$$

The asymmetric example fixes complex masses $m = (-4,1,3)$. Their sum vanishes, so the neutral coordinate can be chosen as

$$z = \frac{t_1 + t_2 + t_3}{3}, \qquad (\eta_1, \eta_2) = (m_1 - m_2, m_2 - m_3) = (-5,-2). \tag{IX.8.6}$$

Solving the two moment maps together with this definition gives, without any remaining shift ambiguity,

$$(t_1, t_2, t_3) = (z + 4, z - 1, z - 3). \tag{IX.8.7}$$

The null vector of Q makes the products $U = q_1 q_2 q_3$ and $W = \widetilde{q}_1 \widetilde{q}_2 \widetilde{q}_3$ gauge invariant. Multiplying the three equations in (IX.8.7) gives

$$UW = t_1 t_2 t_3 = (z + 4)(z - 1)(z - 3) = z^3 - 13z + 12. \tag{IX.8.8}$$

Under the mirror identification, U and W correspond to the electric monopole coordinates V_+ and V_-. The protected Coulomb relation of Chapter 3 is consequently the full equation $V_+V_- = z^3 - 13z + 12$. Its left side matters. Replacing the product by a sum would allow us to eliminate one monopole coordinate linearly, producing a different coordinate ring even though the complex dimension would remain two.

The three roots are distinct. Their squared separations give the polynomial discriminant directly,

$$\Delta = (-4 - 1)^2(-4 - 3)^2(1 - 3)^2 = 25 \cdot 49 \cdot 4 = 4900. \tag{IX.8.9}$$

For the surface $F = UW - P(z) = 0$, a singular point must satisfy

$$\partial_U F = W = 0, \qquad \partial_W F = U = 0, \qquad \partial_z F = -P'(z) = 0, \qquad P(z) = 0. \tag{IX.8.10}$$

Thus distinct roots exclude affine singularities in this example. This is a complex mass deformation of the affine surface; it is not the construction of a resolved hyperkähler metric. The massless two-flavor entry instead has $P(z) = z^2$ and a singular point at the origin.

Table IX.8.3: Affine branch views. B2 is massless; B3 has complex masses $(-4, 1, 3)$. No resolved metric is supplied.

Row	Affine equation	$\dim_{\mathbb{C}}$	Resolved metric
B2	$V_+V_- = z^2$	2	Not determined here
B3	$V_+V_- = z^3 - 13z + 12$	2	Not determined here

Equations that differ only by moving terms across the equals sign, by expanding a product, or by an overall nonzero complex constant define the same principal ideal in $\mathbb{C}[V_+, V_-, z]$. Multiplication by z does not: it adds a component. Squaring the equation also changes the coordinate ring by introducing nilpotents. The atlas therefore retains the algebra of the branch, not merely the polynomial's list of roots. The relation is one protected sector of the mirror dictionary, and does not turn the three overlapping SQED views into independent routes.

IX.8.2.3 A framed interval is not a dimension subtraction

The separate framed example of Chapter 1 has ranks $(1, 2)$, one fundamental hypermultiplet at each node, and one bifundamental between them. Its actual suspended

multiplicities give $U(1) \times U(2)$, not two abelian factors. The representation dimensions are

$$n_H = 1 \cdot 1 + 2 \cdot 1 + 1 \cdot 2 = 5, \qquad \dim_{\mathbb{R}} G = 1^2 + 2^2 = 5. \tag{IX.8.11}$$

These are dimensions before imposing moment maps. Their equality alone does not show that the Higgs branch is a point. A quotient dimension formula also needs control of stabilizers and the relevant stratum. Unlike the regular loci used above, no such extra conclusion is included in this entry.

Table IX.8.4: The two-node framed interval. The two dimensions count matter and gauge parameters before taking a quotient.

Row	Gauge group	Framing	n_H	$\dim_{\mathbb{R}} G$
F12	U(1) × U(2)	$(1, 1)$	5	5

The ordered fivebranes are N_0, F_0, N_1, F_1, N_2, with the N labels denoting NS5 branes and F labels denoting D5 branes. One D3 spans the first NS5 interval and two span the second. In Chapter 1's linking convention the individual linking values are

$$(\ell_{N_0}, \ell_{F_0}, \ell_{N_1}, \ell_{F_1}, \ell_{N_2}) = \left(0, \frac{1}{2}, -1, -\frac{1}{2}, 1\right). \tag{IX.8.12}$$

This vector remembers the ordered endpoints that the rank pair alone forgets. The bifundamental prescription at the intervening NS5 is the physical boundary input of the interval construction, not a perturbative open-string calculation performed in this atlas.

IX.8.3 Half-BPS boundaries and T theories

For a half-BPS boundary of four-dimensional $\mathcal{N} = 4$ Yang–Mills, there are two dimensions to keep distinct. The ambient theory occupies a four-dimensional half-space. The boundary locus is three-dimensional and preserves eight real supercharges. A three-dimensional theory placed there is not an additional four-dimensional bulk theory. This is why the boundary entries carry ambient dimension four even when their matter is described by a three-dimensional quiver.

IX.8.3.1 The rank-two pole

Let $s = x^6 > 0$ measure distance from the boundary. In the Hermitian convention of Chapter 4 the three scalars along 789 obey

$$\frac{dX_i}{ds} = \frac{i}{2}\epsilon_{ijk}[X_j, X_k], \qquad X_i = \frac{J_i}{s}, \qquad [J_i, J_j] = i\epsilon_{ijk}J_k. \tag{IX.8.13}$$

Indeed, substituting the pole gives $-J_i/s^2$ on each side. For the irreducible rank-two residue $J_i = \sigma_i/2$, multiplication of Pauli matrices gives

$$\sum_{i=1}^{3} J_i^2 = \frac{3}{4}\mathbf{1}_2. \tag{IX.8.14}$$

To find the unbroken commutant, write a general complex matrix as $A = a_0\mathbf{1}_2 + \sum_i a_i\sigma_i$. The equations $[A, J_i] = 0$ for all three i set every a_i to zero, leaving only the identity. Restricting to the real Lie algebras therefore yields

$$\dim \mathrm{Comm}_{\mathfrak{u}(2)}(J) = 1, \qquad \dim \mathrm{Comm}_{\mathfrak{su}(2)}(J) = 0. \tag{IX.8.15}$$

The central $\mathfrak{u}(1)$ is not removed by solving the pole equation. Removing it would be a change in the bulk algebra, not another solution of the same commutant problem.

Table IX.8.5: Rank-two Nahm pole. The last column gives commutant dimensions in $\mathfrak{u}(2)$ and $\mathfrak{su}(2)$.

Row	Bulk algebra	Partition	$\sum_i J_i^2$	Commutants
N2	$\mathfrak{u}(2)$	[2]	$\frac{3}{4}\,\mathbf{1}_2$	1 / 0

IX.8.3.2 Reading the two T theories

In Chapter 4, $T[SU(N)]$ is the intrinsic three-dimensional theory appearing in a boundary duality. For the two entries here its quiver gives a particularly transparent dimension calculation. $T[SU(2)]$ is $U(1)$ with two fundamental hypers. At a regular quotient point,

$$n_H = 2, \qquad \dim G = 1, \qquad (\dim_{\mathbb{H}} \mathcal{H}, \dim_{\mathbb{H}} \mathcal{C}) = (1, 1). \tag{IX.8.16}$$

The $T[SU(3)]$ graph in Figure IX.8.2 has ranks $(1, 2)$, three fundamentals at the second node, and none at the first. Thus

$$n_H = (1)(2) + (2)(3) = 8, \qquad \dim G = 1^2 + 2^2 = 5, \tag{IX.8.17}$$

and its branch dimensions are

$$\dim_{\mathbb{H}} \mathcal{H} = 8 - 5 = 3, \qquad \dim_{\mathbb{H}} \mathcal{C} = 1 + 2 = 3. \tag{IX.8.18}$$

There is no continuously ineffective gauge center in these examples. For $T[SU(3)]$, a putative central gauge transformation that acts trivially on the three fundamentals must vanish at the rank-two node; the bifundamental then forces it to vanish at the rank-one node as well. This statement concerns the action on this matter representation. It does not choose every allowed background bundle or settle all global forms of the boundary symmetry.

Table IX.8.6: Intrinsic three-dimensional $T[SU(N)]$ theories at a four-dimensional half-space boundary, preserving eight real supercharges. Branch dimensions are quaternionic.

Row	Ranks	Framing	n_H	$\dim G$	$(\dim \mathcal{H}, \dim \mathcal{C})$
T2	(1)	(2)	2	1	$(1,1)$
T3	$(1,2)$	$(0,3)$	8	5	$(3,3)$

The $U(1)$ matter in T2 is the same local quiver as two-flavor SQED in S2. The extra content of T2 is its boundary coupling and physical role. Likewise, matching Higgs and Coulomb dimensions in T3 is not a derivation of four-dimensional S-duality. The direct exchange of boundary conditions, its infrared limit, and the distinction between a bulk center and an interacting boundary sector must be inherited from Chapter 4.

IX.8.4 From the M5 equation to periods and particles

A curve is useful for low-energy gauge theory only together with its physical identification. Chapter 5 starts from the IIA D4–NS5 system, lifts it to an M5 brane, and fixes a differential and period convention. We can reconstruct the algebra of the pure curves here while retaining the protected-continuation premise that relates their periods to the four-dimensional theory. The $SU(2)$ example also teaches why a primitive cycle need not carry the electric charge of the W boson.

IX.8.4.1 Eliminating the exponential coordinate

Let v be the mass-valued complex transverse coordinate of Chapter 5, with $[v] = [\Lambda] = 1$, and let the dimensionless exponential coordinate be $t = \exp(-s)$, with $s = x^6/R + ix^{10}$ and angular x^{10}. The normalized pure equations are

$$\Lambda^N(t^2+1) - 2P_N(v)t = 0, \qquad P_2(v) = v^2 - u, \quad P_3(v) = v^3 - u_2 v - u_3, \tag{IX.8.19}$$

only for $N = 2, 3$ in this atlas. To eliminate t, define

$$y = \Lambda^N t - P_N(v). \tag{IX.8.20}$$

Squaring this expression and using (IX.8.19) cancels the terms linear in t, leaving

$$y^2 = P_N(v)^2 - \Lambda^{2N}. \tag{IX.8.21}$$

The power of Λ is part of the normalization, not an optional constant. In particular the quadratic discriminant of the t equation is

$$\operatorname{disc}_t = 4\big(P_N(v)^2 - \Lambda^{2N}\big). \tag{IX.8.22}$$

For generic moduli the right side has $2N$ distinct roots in v. The double cover of the v sphere is branched there. Riemann–Hurwitz gives

$$2g - 2 = 2(-2) + 2N, \qquad g = N - 1. \tag{IX.8.23}$$

Thus the two curves have genus one and two, respectively; genus is stated at a smooth generic point, not at a degeneration.

Table IX.8.7: Pure M5 curves at generic smooth moduli. These four-dimensional setups preserve eight real supercharges.

Row	Theory	Hyperelliptic curve	Genus
C2	$SU(2)$	$y^2 = -\Lambda^4 + \left(u - v^2\right)^2$	1
C3	$SU(3)$	$y^2 = -\Lambda^6 + \left(u_2 v + u_3 - v^3\right)^2$	2

For $SU(2)$ the quartic discriminant supplies a further readout,

$$\mathrm{disc}_v\left[(v^2-u)^2 - \Lambda^4\right] = 256\Lambda^8(u^2 - \Lambda^4). \tag{IX.8.24}$$

At $\Lambda \neq 0$ the singular fibers occur at $u = \pm\Lambda^2$. Their particle interpretation still requires the differential and cycle normalization; the vanishing of this discriminant alone does not label an electric or magnetic charge.

IX.8.4.2 The factor of two in the SU(2) readout

Choose primitive cycles α_M, β_M with intersection one. The differential normalized in Chapter 5 gives their periods

$$\lambda_M = \frac{v\, d\log t}{2\sqrt{2}\pi i}, \qquad A_M = \oint_{\alpha_M} \lambda_M, \quad B_M = \oint_{\beta_M} \lambda_M, \qquad M_{\mathrm{BPS}} = \sqrt{2}|Z|. \tag{IX.8.25}$$

Its coefficient uses the membrane tension and the stated BPS mass convention, not just the polynomial. Chapter 5 fixes $B_M = a_D$ and $A_M = a/2$. The conversion to the field-theory periods is therefore

$$\begin{pmatrix} a_D \\ a \end{pmatrix} = \begin{bmatrix} 1 & 0 \\ 0 & 2 \end{bmatrix} \begin{pmatrix} B_M \\ A_M \end{pmatrix}, \qquad [H_1 : \langle \beta_M, 2\alpha_M \rangle] = 2. \tag{IX.8.26}$$

The determinant is two rather than one. This is not an integral symplectic change of primitive basis. It specifies the particle/electric normalization used to compare the two curve descriptions.

Use the ordered cycle coefficients (e, m) relative to (α_M, β_M). The three particles retained in the normalized example have

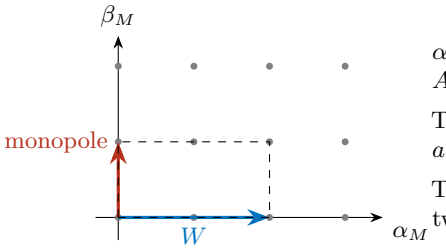
$$W = (2, 0), \qquad M = (0, 1), \qquad D = (-2, 1). \tag{IX.8.27}$$

Their normalized central charges are the period combinations

$$Z_W = 2A_M = a, \qquad Z_M = B_M = a_D, \qquad Z_D = B_M - 2A_M = a_D - a. \tag{IX.8.28}$$

The intersection convention gives the antisymmetric pairing $em' - me'$. For the W and monopole this equals two, consistently with the index in (IX.8.26). The primitive α_M

cycle is not therefore to be relabeled as the W particle. Nor does this list assert that every integral homology vector is populated by a stable particle in every chamber.



α_M is primitive but its period is $A_M = a/2$.

The particle normalization uses $a = 2A_M$, $a_D = B_M$.

The displayed cell has index two.

Figure IX.8.3: Primitive genus-one homology and the particle normalization. The horizontal W vector spans two primitive steps. The diagram describes the period/particle comparison, not the full lattice of genuine line operators.

One algebraic way to see why the curves require care is the map from the quartic to the cubic. Put $x = u - v^2$ and $y_c = ivy$. Then

$$y_c^2 = (x - u)(x^2 - \Lambda^4). \tag{IX.8.29}$$

This is the cubic with its three specified roots. The map is degree two, not a birational reparametrization at fixed u. The period normalization cannot be replaced by a claim that the two equations merely look alike. Chapter 5 supplies the differential and the selected period identification used in (IX.8.26). In particular its pullback differential and cycle images obey

$$\phi^*\lambda_C = 2\lambda_M, \qquad \phi_*\alpha_M = \alpha_C, \quad \phi_*\beta_M = 2\beta_C. \tag{IX.8.30}$$

Integrating these relations gives $a = 2A_M$ and $a_D = B_M$ separately.

The genuine-line lattice remains undetermined here. Specifying it would require global-form and line-operator information beyond a list of particle charges and a polarization map. This absence is not a statement that no line operators exist.

IX.8.4.3 What the SU(3) extension adds

The second curve extends the polynomial and genus calculation, not the rank-one particle chamber. For a concrete degeneration take $\Lambda = 1$, $u_2 = 3$, $u_3 = -3$. Then

$$P_3 = v^3 - 3v + 3, \qquad P_3 - 1 = (v - 1)^2(v + 2), \qquad P_3 + 1 = v^3 - 3v + 4. \tag{IX.8.31}$$

At $v = 1$ the second factor is two. Writing $v = 1 + \delta$ gives

$$y^2 = 6\delta^2 + O(\delta^3). \tag{IX.8.32}$$

The two distinct tangent directions give an ordinary node. Equivalently, the greatest common divisor of the hyperelliptic polynomial and its derivative is $v - 1$. This is a local degeneration calculation, not a construction of the complete $SU(3)$ BPS spectrum.

A smooth genus-two curve needs four primitive homology generators. No such explicit basis was constructed for this bounded extension in Chapter 5. Its primitive basis is therefore *not constructed here*, and its period conversion is *not determined here*. The particle chamber and genuine-line lattice are also not determined. In particular, the two genus-one cycle labels cannot be carried into the genus-two row as if they were a complete basis. The useful conclusion of C3 is the curve with its genus and local node, not an unperformed period calculation.

IX.8.5 Rotating fivebranes and comparing interacting sectors

Rotating one fivebrane changes the supersymmetry and the endpoint problem. The four-dimensional construction of Chapter 6 preserves four real supercharges. In its $(N_c, N_f) = (3, 5)$ example, crossing the five flavor branes creates one D4 segment for each flavor. Reconnection with the three original color segments leaves

$$N_c^{\mathrm{mag}} = N_f - N_c = 5 - 3 = 2, \qquad (n_1, \ldots, n_5) = (1, 1, 1, 1, 1). \tag{IX.8.33}$$

The endpoint construction retains five flavor edges. Its magnetic interaction is a holomorphic meson coupling $W = hM\widetilde{q}q$, with its coefficient depending on the chosen meson normalization. Brane creation, the allowed endpoint splitting, and infrared continuity along the move are physical inputs; the final subtraction does not replace them.

Table IX.8.8: The rotated fivebrane move, in four dimensions with four real supercharges. The groups retain their brane centers.

Row	Electric	Magnetic	N_f	Created D4 occupancies
R35	U(3)	U(2)	5	$(1, 1, 1, 1, 1)$

The finite-quartic brane groups are $U(3)$ and $U(2)$. We now make a separate comparison of undeformed $SU(3)$ and $SU(2)$ SQCD with five flavors, with the adjoint-induced quartic absent. This comparison tests the field-theory matter representations without deleting a brane center. The distinction matters for both the spectrum of gauge-invariant operators and the interpretation of abelian factors.

Let $SU(5)_L \times SU(5)_R$ be the nonabelian flavor symmetry. Normalize the quadratic index of a fundamental to $1/2$ and its cubic anomaly to $+1$. Electric Q is a left fundamental and $\widetilde{Q}$ a right antifundamental. Their baryon charges are $+1, -1$, respectively. The anomaly-free scalar R charge is $2/5$, so both fermions have charge

$$R_{Q,\mathrm{f}} = R_{\widetilde{Q},\mathrm{f}} = -\frac{3}{5}. \tag{IX.8.34}$$

The magnetic quarks have fermion R charge $-2/5$ and baryon charges $\pm 3/2$. The meson is a gauge singlet in $(\mathbf{5}, \overline{\mathbf{5}})$, with zero baryon charge and fermion R charge $-1/5$.

Its flavor multiplicities cannot be suppressed merely because it is neutral under the magnetic gauge group.

For the left cubic flavor anomaly, the electric colors give 3. The two magnetic anti-fundamentals give -2, while the five right-flavor copies of the meson give $+5$:

$$\mathcal{A}_L^{\text{electric}} = 3, \qquad \mathcal{A}_L^{\text{magnetic}} = -2 + 5 = 3. \tag{IX.8.35}$$

The mixed left-flavor R anomaly is sensitive to different information,

$$\mathcal{A}_{L^2R}^{\text{electric}} = 3\frac{1}{2}\left(-\frac{3}{5}\right) = -\frac{9}{10}, \qquad \mathcal{A}_{L^2R}^{\text{magnetic}} = 2\frac{1}{2}\left(-\frac{2}{5}\right) + 5\frac{1}{2}\left(-\frac{1}{5}\right) = -\frac{9}{10}. \tag{IX.8.36}$$

Here the antifundamental has the same quadratic index as the fundamental, although their cubic signs differ. The gauge-R anomalies also vanish on each side,

$$3 + 5\left(-\frac{3}{5}\right) = 0, \qquad 2 + 5\left(-\frac{2}{5}\right) = 0. \tag{IX.8.37}$$

Including the gaugino, of R charge one, gives the gravitational R trace

$$\text{Tr}\, R\big|_{\text{el}} = 8 + 30\left(-\frac{3}{5}\right) = -10, \qquad \text{Tr}\, R\big|_{\text{mag}} = 3 + 20\left(-\frac{2}{5}\right) + 25\left(-\frac{1}{5}\right) = -10. \tag{IX.8.38}$$

The cubic R trace checks all three fermion charges with different weights,

$$8 + 30\left(-\frac{3}{5}\right)^3 = 3 + 20\left(-\frac{2}{5}\right)^3 + 25\left(-\frac{1}{5}\right)^3 = \frac{38}{25}. \tag{IX.8.39}$$

Table IX.8.9: Selected anomaly traces of the separate interacting $SU(3)$ and $SU(2)$ sectors. All lines belong to the one comparison A35, not to additional brane setups.

Row	Anomaly	Electric	Magnetic
A35	$SU(5)_L^3$	3	3
	$SU(5)_L^2 B$	$\frac{3}{2}$	$\frac{3}{2}$
	$SU(5)_L^2 R$	$-\frac{9}{10}$	$-\frac{9}{10}$
	$\text{Tr}R$	-10	-10
	$\text{Tr}R^3$	$\frac{38}{25}$	$\frac{38}{25}$
	$\text{Tr}B^2R$	-18	-18

These equalities compare electric and magnetic traces, not each side with a separately chosen total. They are necessary anomaly-matching conditions for the stated interacting sectors. They do not prove the full infrared duality, nor do they establish an equivalence of the two brane U theories by ignoring their central gauge fields.

IX.8.6 Fixed ends and the MQCD winding

The fixed-end MQCD construction uses holomorphic information from a rotated M5 brane. Unlike the $\mathcal{N}=2$ curves above, it has four real supercharges in four dimensions. The decisive condition is that both asymptotic coefficients are held fixed. In the coordinates of Chapter 6, v, w are length coordinates and ζ has dimension length squared. The curve is parameterized by

$$v = z, \qquad w = \frac{\zeta}{z}, \qquad t = Az^n, \qquad t \sim Bw^{-n} \quad \text{at the other end.} \tag{IX.8.40}$$

Since $z = \zeta/w$, compatibility of the two ends requires

$$B = A\zeta^n, \qquad A\zeta^n - B = 0. \tag{IX.8.41}$$

When A and B are fixed and nonzero, the derivative $nA\zeta^{n-1}$ cannot vanish at a root. The polynomial is squarefree, and its n complex solutions are distinct. For the two chosen cases,

$$(n,A,B) = (2,2,8) \;\Rightarrow\; \zeta = \pm 2, \qquad (n,A,B) = (3,2,16) \;\Rightarrow\; \zeta = 2e^{2\pi i j/3},\; j = 0,1,2. \tag{IX.8.42}$$

These are two and three isolated holomorphic choices at the specified ends. If an end coefficient were allowed to vary, the conclusion about isolated choices would no longer follow from the same equation.

Orientation is equally important. Along a positively oriented small circle $z = re^{i\theta}$, the logarithmic differential gives

$$\frac{1}{2\pi i}\oint d\log t = \frac{1}{2\pi i}\oint n\frac{dz}{z} = n. \tag{IX.8.43}$$

But $t = \exp[-(x^6/R + ix^{10})]$ has argument $-x^{10}$. The physical angular winding is consequently

$$\frac{\Delta x^{10}}{2\pi} = -n. \tag{IX.8.44}$$

The positive holomorphic winding and negative physical winding refer to the same oriented curve, not to two alternative conventions left unspecified.

Table IX.8.10: Two fixed-end MQCD cases in the same setup card. The last columns are signed windings for positive z orientation, with $t = \exp(-s)$.

Row	n	(A,B)	End constraint	Roots	t	x^{10}
Q23	2	$(2,8)$	$2\zeta^2 - 8 = 0$	2	2	-2
Q23	3	$(2,16)$	$2\zeta^3 - 16 = 0$	3	3	-3

The fixed-end argument concerns protected holomorphic information. Transferring that information to the corresponding field-theory vacua uses the physical M-theory interpretation of Chapter 6. It does not determine a nonprotected mass spectrum, and

this atlas supplies no such spectrum. A root count and a signed winding are therefore the useful outputs of Q23; neither is a substitute for a calculation of massive excitations in ordinary Yang–Mills theory.

IX.8.7 Four-supercharge dualities in three dimensions

The three-dimensional $\mathcal{N} = 2$ examples use a spacetime circle x^3 in the four-dimensional parent. This circle is not the finite suspension direction x^6. Chapter 7 fixes the finite-radius duality, the real-mass deformation, and the magnetic vacuum before removing massive sectors. The atlas retains one Aharony example and both signs of one Giveon–Kutasov example. Their rank arithmetic is short; keeping the surviving interactions is the more informative task.

IX.8.7.1 Why the remote sectors cannot be discarded first

For the Aharony $(N_c, N_f) = (2, 5)$ pair, the finite-circle electric parent has $N_f + 2 = 7$ flavors. The magnetic parent has five colors. In the selected real-mass vacuum its Cartan expectation value is

$$\sigma_m = \mathrm{diag}(M, 0, 0, 0, -M), \qquad U(5) \longrightarrow U(1) \times U(3) \times U(1). \tag{IX.8.45}$$

Each remote abelian factor retains one vectorlike flavor. The central $U(3)$ factor retains the five light flavors. In the original heavy flavor labels, the massless pairs are crossed: at $+M$ they are $(q_a, \widetilde{q}_b)$ and at $-M$ they are $(q_b, \widetilde{q}_a)$. The diagonal drawing follows a permutation of the two heavy antiflavors, not a different spectrum. Chapter 7 explains this coordinate choice and the associated monopole signs.

To see what survives, use the abelian dual descriptions of the two remote sectors. Denote their mesons by N_1, N_2, their monopoles by p_i, n_i, and their meson flips by M_i. The central monopoles are v_+, v_-. With a nonzero renormalized coefficient μ, the relevant superpotential is

$$\begin{aligned} W_{\mathrm{rem}} = {} & N_1 p_1 n_1 + N_2 p_2 n_2 + M_1 N_1 + M_2 N_2 \\ & + v_+ n_1 + v_- p_2 + \mu p_1 n_2. \end{aligned} \tag{IX.8.46}$$

Differentiating with respect to the flips first sets $N_i = 0$. The N_i equations give $M_i = -p_i n_i$. The two fields paired by μ then satisfy

$$\partial_{p_1} W_{\mathrm{rem}} = \mu n_2 = 0, \qquad \partial_{n_2} W_{\mathrm{rem}} = \mu p_1 = 0. \tag{IX.8.47}$$

Thus $p_1 = n_2 = M_1 = M_2 = 0$, while n_1 and p_2 remain as singlets coupled to the central monopoles. Identifying $V_- = n_1$ and $V_+ = p_2$ leaves

$$W_{\mathrm{mag}} = M q \widetilde{q} + V_- v_+ + V_+ v_-. \tag{IX.8.48}$$

The light meson matrix has $5^2 = 25$ entries, and there are two electric-monopole singlets, not two additional meson matrices.

Table IX.8.11: Aharony pair with four real supercharges in three dimensions. Mesons and electric-monopole singlets are distinct sectors.

Row	Electric / magnetic	N_f	Blocks	Mesons	Monopoles
A25	U(2) / U(3)	5	$(1,3,1)$	25	2

This elimination is conditional on $\mu \neq 0$ and on the sourced abelian dual descriptions. Setting the interaction to zero before eliminating the remote fields retains unwanted light degrees of freedom. Likewise, simply removing a finite-radius monopole term at the start does not perform the controlled real-mass flow. The instanton zero-mode input, the finite-radius continuation, and the remote abelian duality are the physical ingredients behind the polynomial elimination.

IX.8.7.2 Keeping the sign of the Chern–Simons level

The Giveon–Kutasov entries have electric rank two, three flavors, and levels $k = +2$ and $k = -2$. These are bare supersymmetric levels, before any gaugino threshold shift to a bosonic description. In the resolved fivebrane move, the additional capacity depends on $|k|$. Hence both have

$$\widetilde{N}_c = N_f + |k| - N_c = 3 + 2 - 2 = 3. \tag{IX.8.49}$$

The magnetic level instead reverses the signed electric level,

$$(k_{\mathrm{el}}, k_{\mathrm{mag}}) = (+2, -2) \quad \text{or} \quad (-2, +2). \tag{IX.8.50}$$

These two operations cannot be merged into an unsigned formula. In the $U(N)$ trace convention, the central $U(1)$ level is Nk. Thus

$$(K_{\mathrm{el}}, K_{\mathrm{mag}}) = (2k, -3k) = \begin{cases} (4, -6), & k = 2, \\ (-4, 6), & k = -2. \end{cases} \tag{IX.8.51}$$

The group notation means

$$U(N)_k = \big[SU(N)_k \times U(1)_{Nk}\big]/\mathbb{Z}_N \tag{IX.8.52}$$

in the convention used here. A central trace level is not a second arbitrary level that can be chosen independently of the nonabelian factor and the quotient.

Table IX.8.12: Signed Giveon–Kutasov pairs. The last column gives the electric and magnetic central $U(1)$ trace levels; both pairs use the spacetime x^3 reduction circle.

Row	Electric	Magnetic	N_f	Central levels
G+	$U(2)_2$	$U(3)_{-2}$	3	$(4, -6)$
G-	$U(2)_{-2}$	$U(3)_2$	3	$(-4, 6)$

The magnetic mesons have the usual coupling $Mq\widetilde{q}$ in these entries. Their rank and signed-level consistency do not prove the infrared equivalence. The resolved creation and continuation premises remain those of Chapter 7. The two signs are retained because they answer different level questions even though their magnetic ranks coincide. No general chiral duality is inferred from these vectorlike examples.

IX.8.8 Two suspension-circle interfaces

We end with a geometric interface rather than another completed duality calculation. Compactifying the suspension direction x^6 allows a different T-duality from compactifying spacetime x^3. The T-dual description uses the isometric zero-mode approximation of Chapter 7. The subsequent M-theory description has an ordered torus basis $(\widetilde{x}^6, x^{10})$. The two examples use $k = 1$ and $k = 2$. At $\chi = 0$ and finite positive g_s^B, these nonzero-k equal-angle geometries inherit six real supercharges from the source analysis in Chapter 7. The parallel $k = 0$ geometry instead has eight. Counting torus cycles does not independently reproduce that statement.

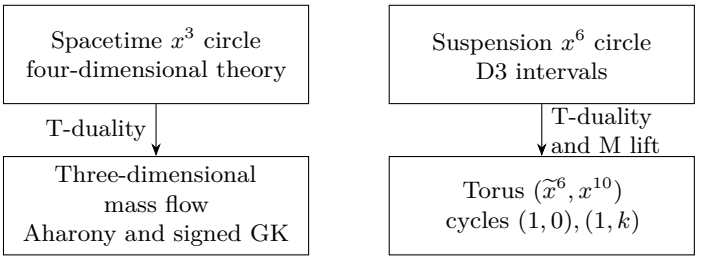


Figure IX.8.4: The two compactifications used by the atlas. The left route underlies the three-dimensional mass-flow examples. The right route supplies only the bounded suspension-circle and torus interface.

The order of fivebrane charges must be declared before computing anything. In source order (NS, D) the two vectors are $(1, 0)$ and $(1, k)$. In the (D, NS) order used for the brane readout they become

$$(0, 1),\ (k, 1), \qquad (k_1, k_2) = (k, -k). \tag{IX.8.53}$$

The ordered interval levels retain their signs. The torus degeneration cycles are a different pair of geometric vectors, in their own basis,

$$v_1 = (1, 0), \quad v_2 = (1, k), \qquad L = \begin{pmatrix} 1 & 1 \\ 0 & k \end{pmatrix}. \tag{IX.8.54}$$

Subtracting the first column from the second gives an integral diagonal form. The

primitive lattice quotient is therefore

$$\mathbb{Z}^2/\langle v_1, v_2\rangle \simeq \mathbb{Z}/|k|\mathbb{Z}, \qquad [\mathbb{Z}^2 : \langle v_1, v_2\rangle] = |\det L| = |k|. \tag{IX.8.55}$$

It is trivial for I1 and $\mathbb{Z}_2$ for I2. Each individual cycle is primitive even when the pair spans a proper sublattice. Neither primitivity nor the absolute determinant would distinguish all possible reversals of basis, charge order, or interval orientation; those choices were specified separately in (IX.8.53) and (IX.8.54).

Table IX.8.13: Suspension x^6 interfaces. Charges use (D, NS); cycles use $(\widetilde{x}^6, x^{10})$. The six real supercharges are an inherited geometric statement, not a lattice result.

Row	Fivebranes	Torus cycles	Levels	Index	Quotient
I1	$(0,1),(1,1)$	$(1,0),(1,1)$	$(1,-1)$	1	trivial
I2	$(0,1),(2,1)$	$(1,0),(1,2)$	$(2,-2)$	2	$\mathbb{Z}_2$

After the x^6 T-duality the D2 worldvolume occupies 012. The finite quotient above is a torus-lattice result. It does not specify an action on four complex coordinates, a moduli space of an ABJM theory, a resolved metric, or an infrared supersymmetry enhancement. Those quantities are not determined by either interface entry. In particular, the values $k = 1, 2$ do not license an enhancement claim in this chapter simply because they are familiar from other settings.

IX.8.9 Carrying a result to the next calculation

The atlas is most useful when its output is a well-specified next calculation. For a matter question, choose a setup and retain its ranks, framing, and centers. For a protected branch question, choose the complex structure and deformation parameters before reading its coordinate ring. For a boundary problem, state both the bulk algebra and the intrinsic boundary theory. For a period problem, carry the differential and charge normalization along with the curve. For a compactification, name the circle before naming the duality.

The worked reconstructions illustrate three different levels of information. A representation count fixes the ingredients of a quotient. A polynomial relation fixes a particular affine algebra. A physical transfer identifies that algebra, period, or endpoint configuration with a field-theory quantity. The first two can often be calculated directly in a few lines; the third may use a nonperturbative duality or an infrared-continuation premise. Repeating the direct calculation does not make the physical premise disappear.

Take-home message of this chapter

Choose a construction by the quantity it determines. Reconstruct its row from the appropriate endpoints, representations, equations, or cycles, and carry the physical assumptions with the result. A missing metric, line lattice, period map, or dynamical spectrum is an unanswered question, not a vanishing quantity. The twenty-two entries are a map of the worked examples in this volume, not a classification of all Hanany–Witten theories.

IX.8.10 Three reconstructions for the reader

The companion grades finite answers to the following exercises. Its fixed cards make the chosen representations, masses, curves, and circles explicit. The physical identification of a card with its field theory retains the premise stated beside that card; arithmetic does not establish the premise.

1. **Choose a branch card.** For one-flavor, two-flavor, or three-flavor $U(1)$ SQED, calculate the regular-locus electric and mirror branch dimensions. Give the mirror gauge ranks, framing, and charge matrix; check its integer kernel rather than guessing from the number of circles. For the separate asymmetric three-flavor card, use $m = (-4, 1, 3)$ to solve the complex moment maps for each t_i, multiply them into the full relation $V_+V_- = P(z)$, and calculate the discriminant. State why this affine calculation leaves the resolved metric undetermined. The three-flavor mirror and the framed two-node C11 interval are different objects.

2. **Read two M5 curves at their actual scope.** At $(u, \Lambda) = (2, 1)$ reconstruct the pure $SU(2)$ quartic from the t equation, and record the primitive-period to particle-period matrix and its index. Then take the pure $SU(3)$ card at $(u_2, u_3, \Lambda) = (3, -3, 1)$, calculate the sextic and the ordinary node at $v = 1$, and state exactly which period, particle, and genuine-line data remain absent. A genus-two curve requires four primitive cycles; no such basis is supplied by the local node calculation.

3. **Reconcile cards across constructions.** Starting from the $(N_c, N_f) = (3, 5)$ rotated move, retain its U groups while separately computing the undeformed, quartic-absent interacting SU anomaly comparison including the meson row. For the two fixed-end MQCD cases compute the signed t and x^{10} windings. For the Aharony $(2, 5)$ card retain both remote monopole couplings, and for GK at $k = \pm 2$ compute the rank using $|k|$ but the levels using signed k. Finally distinguish the spacetime x^3 circle from the suspension x^6 circle when computing the $k = 1, 2$ torus quotients. Name each upstream chapter and the physical premise that remains conditional.

See `benchmark/tasks.json` and `benchmark/PROTOCOL.md` for the public structured-answer format. These exercises use structured integers, rational anomaly coefficients and sparse polynomials for the selected objects. Their scope is limited to those quantities.

Status and sources

This atlas collects the finite comparisons of Chapters 1–7. The tables distinguish calculated quantities, supplied physical premises and quantities outside the stated scope.

§IX.8.1 and §IX.8.9. Scope and navigation. The tables collect examples from the preceding chapters. There are eight setup objects, seven dual pairs, two branch objects, three boundary objects, and two interfaces. The two rows are cases of one object, and the several anomaly lines of A35 are components of one comparison. Figures IX.8.1 and IX.8.4 are local teaching diagrams, not extra duality chains.

§IX.8.2. Intervals, mirrors, and affine rings. S1–S3 and F12 reuse IX.1/2. The interval and endpoint dictionary is supported by Hanany and Witten (1997), hep-th/9611230v3, §3, pp. 5–12, and §§6.1–6.2, pp. 29–38. F12 uses its Fig. 1, pp. 7–9, and the actual IX.1 two-node construction. Its bifundamental is an NS5-boundary prescription, not a new perturbative worldsheet derivation. M1–M3 additionally use Intriligator and Seiberg (1996), hep-th/9607207v1, §3, pp. 6–10. The direct counts in (IX.8.1) and (IX.8.11) are calculations; the mirror interpretation uses the Chapter 2 mirror route, including the IIB nonperturbative generator and the creation/continuity assumptions [NP,A].

B2 and B3 reuse IX.3's selected complex structure and its fixture, with the protected abelian Coulomb relation supported by Bullimore et al. (2017), 1503.04817v2, §3.1, pp. 8–10, (3.1)–(3.8). The mass sign is the book's $z-m_i$ convention. Equations (IX.8.5)–(IX.8.9) reconstruct the asymmetric moment-map elimination and discriminant. The identification with the electric Coulomb algebra is source-backed; the affine algebra is not a resolved metric. The full relation, including its monopole-product left side, is consumed by separate principal-ideal calculation in $\mathbb{Q}[V_+, V_-, z]$. Figure IX.8.2 uses the actual rank and framing vectors from IX.2/4. Conventions are inherited from Chapters 1–3, including the triplet projection and algebraic rescaling. The zero-FI and zero-primitive-mirror-mass hypotheses are those of IX.3.

§IX.8.3. Boundary objects. N2 is IX.4's irreducible rank-two pole. The relevant source is Gaiotto and Witten (2009b), 0804.2902v2, §2.4, (2.37)–(2.43), pp. 23–25. T2 and T3 instead use Gaiotto and Witten (2009a), 0807.3720v1, §3.3.1, Figs. 22–24, pp. 49–53; these are different papers and locators. The Pauli-matrix and commutant calculation in (IX.8.13) and the quiver count in (IX.8.17) are bounded calculations. Chapter 4 describes the direct S exchange, with its boundary infrared premise [NP]; no excluded rearrangement is added. Ambient dimension four, intrinsic dimension three, and eight preserved real supercharges are retained separately. The frame and global form are those of the examples in Chapter 4.

§IX.8.4. M5 curve, normalization, and absent SU(3) data. C2 and C3 reuse IX.5. The curve source is Witten (1997b), hep-th/9703166v1, *§2.4*, (2.19)–(2.21), printed p. 14. The heading order and equations are verified together in the pinned text; §2.3 is not the curve locator. The source's introduction and §§2–2.2 support the native eight-supercharge interpretation separately. The normalized t equation, hyperelliptic equation, elimination, genus, discriminant, and local node are calculated in IX.5 and recomputed against the displayed catalog fields. The pure $SU(2)$ construction uses the M-theory lift and protected low-energy continuation [NP], not a proof from the

polynomial alone.

The $SU(2)$ period/particle interpretation also uses Seiberg and Witten (1994), hep-th/9407087v1, §6, pp. 34–40, (6.1)–(6.28), and the explicit period normalization of Chapter 5. The populated period conversion (IX.8.26) has determinant and index two. Figure IX.8.3 illustrates this convention. C3 has no constructed four-cycle basis, period conversion, or particle chamber. Both genuine-line lattices remain uncomputed. The genus-two extension is not a rank-one particle-map reuse. The genus-two calculation uses its own stated conventions.

§IX.8.5 and §IX.8.6. Rotated and fixed-end constructions. R35 follows IX.6 and Elitzur et al. (1997), hep-th/9702014v2, §3, pp. 4–6, steps (a)–(d), (3.1). Its actual endpoint split, occupancies, and flavor edges are retained. The brane move requires separate creation and infrared-continuation assumptions [A]. A35 is the separately identified undeformed, quartic-absent interacting-SU comparator using the fermion representations and anomaly conventions of Volume I, Chapter 3. Its meson is a gauge singlet but a nontrivial flavor representation; the electric and magnetic traces are compared both with each other and with the specified target. The component trace convention is the one stated in IX.6 and Volume 0.3; entry 6 instead governs the superpotential and meson normalization. No brane center is silently removed.

Q23 follows Witten (1997a), hep-th/9706109v2, §2.2, (2.2)–(2.4), pp. 5–7; §3.1, (3.5)–(3.7), pp. 12–13; and §6, (6.3), p. 35. Fixed nonzero coefficients at both ends are essential to (IX.8.41). The logarithmic winding is calculated, while its physical sign uses $t = \exp(-s)$. The M5 lift has a protected MQCD interpretation [NP]; no nonprotected-spectrum transfer is made. The rotation and MQCD conventions are those of Chapter 6.

§IX.8.7. Three-dimensional pairs. A25 follows IX.7, Aharony (1997), hep-th/9703215v1, §3, (3.1)–(3.3), pp. 5–7; Amariti et al. (2015), 1501.06571v2, §§2.2, 3.2, pp. 5–7, 10–11; and Aharony, Razamat, et al. (2013), 1305.3924v2, §4.1, pp. 35–38. The remote elimination in (IX.8.46)–(IX.8.48) assumes the finite-radius, zero-mode, and abelian-duality premises and $\mu \neq 0$. The route uses the selected nonperturbative NS/D exchange for the remote abelian description.

G+ and G- follow Giveon and Kutasov (2009), 0808.0360v1, §3, pp. 4–7, Fig. 3 and (3.1)–(3.2), with the signed flow in 1501.06571v2, §4.1, p. 12. The field-theory comparison uses the creation and continuation premises and the charge, level and spacetime-circle conventions of Chapter 7.

§IX.8.8. Geometric interfaces. I1 and I2 index IX.7 alone. Their source is Aharony, Bergman, et al. (2008), 0806.1218v4, §3.1, (3.1), Fig. 4, pp. 15–18, for the charge/angle geometry; §3.2, p. 19, and Appendix B, (B.7)–(B.12), pp. 32–35, for the lift. The six-real-supercharge statement is explicitly *source-only*. The ordered charge and cycle conversions, signed levels, and integer lattice quotient are bounded calculations, not a supersymmetry proof. The comparison concerns the suspension circle of Chapter 7. The $\mathbb{C}^4$ action, ABJM moduli space, and enhancement remain uncomputed. Neither interface belongs to Volume VIII.

Scope of the calculations. The endpoint, worldvolume and polynomial identities use the hypotheses stated with each example. WS would require a separate untwisted-string physical-worldsheet derivation.

References

Aharony, O. (1997). "IR duality in d = 3 N=2 supersymmetric USp(2N(c)) and U(N(c)) gauge theories". In: *Phys. Lett. B* 404, pp. 71–76. DOI: 10.1016/S0370-2693(97)00530-3. arXiv: hep-th/9703215.

Aharony, O., O. Bergman, et al. (2008). "N=6 superconformal Chern-Simons-matter theories, M2-branes and their gravity duals". In: *JHEP* 10, p. 091. DOI: 10.1088/1126-6708/2008/10/091. arXiv: 0806.1218 [hep-th].

Aharony, O., S. S. Razamat, et al. (2013). "3d dualities from 4d dualities". In: *JHEP* 07, p. 149. DOI: 10.1007/JHEP07(2013)149. arXiv: 1305.3924 [hep-th].

Amariti, A. et al. (2015). "The braneology of 3D dualities". In: *J. Phys. A* 48.26, p. 265401. DOI: 10.1088/1751-8113/48/26/265401. arXiv: 1501.06571 [hep-th].

Bullimore, M., T. Dimofte, and D. Gaiotto (2017). "The Coulomb Branch of 3d $\mathcal{N} = 4$ Theories". In: *Commun. Math. Phys.* 354.2, pp. 671–751. DOI: 10.1007/s00220-017-2903-0. arXiv: 1503.04817 [hep-th].

Elitzur, S., A. Giveon, and D. Kutasov (1997). "Branes and N=1 duality in string theory". In: *Phys. Lett. B* 400, pp. 269–274. DOI: 10.1016/S0370-2693(97)00375-4. arXiv: hep-th/9702014.

Gaiotto, D. and E. Witten (2009a). "S-Duality of Boundary Conditions In N=4 Super Yang-Mills Theory". In: *Adv. Theor. Math. Phys.* 13.3, pp. 721–896. DOI: 10.4310/ATMP.2009.v13.n3.a5. arXiv: 0807.3720 [hep-th].

Gaiotto, D. and E. Witten (2009b). "Supersymmetric Boundary Conditions in N=4 Super Yang-Mills Theory". In: *J. Statist. Phys.* 135, pp. 789–855. DOI: 10.1007/s10955-009-9687-3. arXiv: 0804.2902 [hep-th].

Giveon, A. and D. Kutasov (2009). "Seiberg Duality in Chern-Simons Theory". In: *Nucl. Phys. B* 812, pp. 1–11. DOI: 10.1016/j.nuclphysb.2008.09.045. arXiv: 0808.0360 [hep-th].

Hanany, A. and E. Witten (1997). "Type IIB superstrings, BPS monopoles, and three-dimensional gauge dynamics". In: *Nucl. Phys. B* 492, pp. 152–190. DOI: 10.1016/S0550-3213(97)00157-0. arXiv: hep-th/9611230.

Intriligator, K. A. and N. Seiberg (1996). "Mirror symmetry in three-dimensional gauge theories". In: *Phys. Lett. B* 387, pp. 513–519. DOI: 10.1016/0370-2693(96)01088-X. arXiv: hep-th/9607207.

Seiberg, N. and E. Witten (1994). "Electric-magnetic duality, monopole condensation, and confinement in N=2 supersymmetric Yang-Mills theory". In: *Nucl. Phys. B* 426. [Erratum: Nucl.Phys.B 430, 485–486 (1994)], pp. 19–52. DOI: 10.1016/0550-3213(94)90124-4. arXiv: hep-th/9407087.

Witten, E. (1997a). "Branes and the dynamics of QCD". In: *Nucl. Phys. B* 507, pp. 658–690. DOI: 10.1016/S0550-3213(97)00648-2. arXiv: hep-th/9706109.

Witten, E. (1997b). "Solutions of four-dimensional field theories via M-theory". In: *Nucl. Phys. B* 500, pp. 3–42. DOI: 10.1016/S0550-3213(97)00416-1. arXiv: hep-th/9703166.